

# **The Immunomodulatory Effects of Methamphetamine**

*Thesis submitted in fulfilment of the requirements for the degree of Master of  
Science (Research).*

*Victoria University*

*Marco Papageorgiou*

*2020*

## **General abstract**

The psychostimulant, METH causes central nervous system damage, along with short and long-term changes to the innate and adaptive immune system. METH was investigated for its impact(s) across a range of physiological contexts. Specifically, crystal METH was investigated for its immune-modulatory effects, in cells of the innate immunity, as well as gene expression modifications in the mouse colon using open-source gene ontology programs. In this regard, changes in differential gene expression and subsequent enrichment in gene ontology groups allowed for a deeper understanding of how METH impacts ontological pathways. Metagenomics was also employed to track changes to colon bacteria upon an escalating dose, followed by a withdrawal period. Together, results indicated that METH causes changes to some genes involved in innate immunity, and minor shifts to abundant bacterial species in the colon. Moreover, gene ontology networks showed several significantly up- and down-differentially regulated genes across functional, molecular and biological processes according to open-source software. Overall, this work represents a significant milestone in the amalgamation of bioinformatics, next-generation sequencing technology and metagenomic diversity profiling. Lastly, this work can initiate further research into how chronic METH use, and withdrawal could help construct models on weaving the relationship between mental health outcomes in METH users.

## **VICTORIA UNIVERSITY STUDENT DECLARATION TEMPLATE**

### **Overview**

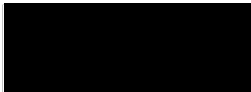
VU offers a number of research degrees for which a Thesis is the major component of assessment. These include Master degrees by Research, the Doctor of Philosophy degree (PhD) and professional doctorates (eg. the Doctor of Business Administration and the Doctor of Education). Research does not only take on the standard form of a Thesis, but may be submitted in alternative creative forms such as a dance performance, exhibition or a novel, or as a approved publications with linking and framing material with an analytical written component. VU also offers a coursework doctorate in Psychology/Applied Psychology.

### **Masters by Research Student Declaration**

#### **Master by Research Declaration**

"I, Marco Papageorgiou, declare that the Master by Research thesis entitled The immune-modulatory effects of Methamphetamine is no more than 60,000 words in length including quotes and exclusive of tables, figures, appendices, bibliography, references and footnotes. This thesis contains no material that has been submitted previously, in whole or in part, for the award of any other academic degree or diploma. Except where otherwise indicated, this thesis is my own work".

Signature



Date 21/11/19

#### **Master by Research Declaration (by performance / exhibition)**

"I, Marco Papageorgiou, declare that the Master by Research exegesis entitled The immune-modulatory effects of Methamphetamine is no more than 60,000 words in length including quotes and exclusive of tables, figures, appendices, bibliography, references and footnotes. This exegesis contains no material that has been submitted previously, in whole or in part, for the award of any other academic degree or diploma. Except where otherwise indicated, this exegesis is my own work".

Signature



Date 21/11/19

# Chapter 1 – Literature Review

Maturitas 121 (2019) 13–2



Contents lists available at ScienceDirect

Maturitas

journal homepage: [www.elsevier.com/locate/](http://www.elsevier.com/locate/)



Review

## Methamphetamine and its immune-modulating effects

Marco Papageorgiou<sup>a</sup>, Ali Raza<sup>a</sup>, Sarah Fraser<sup>a</sup>, Kulmira Nurgali<sup>a,b,1,2,3</sup>, Vasso Apostolopoulos<sup>a,\*,1</sup>

<sup>a</sup> Institute for Health and Sport, Victoria University, Melbourne, VIC, Australia

<sup>b</sup> Department of Medicine, The University of Melbourne, Regenerative Medicine and StemCells Program, Australian Institute of Musculoskeletal Science (AIMSS), Melbourne, VIC, Australia



### ARTICLE INFO

#### Keywords:

Methamphetamine

METH

Ice

Drug addiction

Inflammation

Signaling pathways

### ABSTRACT

The recreational use of methamphetamine (METH, or ice) is a global burden. It pervades and plagues contemporary society; it has been estimated that there are up to 35 million users worldwide. METH is a highly addictive psychotropic compound which acts on the central nervous system, and chronic use can induce psychotic behaviour. METH has the capacity to modulate immune cells, giving the drug long-term effects which may manifest as neuropsychiatric disorders, and that increase susceptibility to communicable diseases, such as HIV. In addition, changes to the cytokine balance have been associated with compromise of the blood–brain barrier, resulting to alterations to brain plasticity, creating lasting neurotoxicity. Immune-related signaling pathways are key to further evaluating how METH impacts host immunity through these neurological and peripheral modifications. Combining this knowledge with current data on inflammatory responses will improve understanding of how the adaptive and innate immunity responds to METH, how this can activate premature-ageing processes and how METH exacerbates disturbances that lead to non-communicable age-related diseases, including cardiovascular disease, stroke, depression and dementia.

<sup>1</sup> Corresponding authors at: Institute for Health and Sport, Victoria University, Melbourne, VIC, Australia.

E-mail addresses: [kulmira.nurgali@vu.edu.au](mailto:kulmira.nurgali@vu.edu.au) (K. Nurgali), [vasso.apostolopoulos@vu.edu.au](mailto:vasso.apostolopoulos@vu.edu.au) (V. Apostolopoulos).

<sup>2</sup> These authors have equal contribution to this work.

<https://doi.org/10.1016/j.maturitas.2018.12.003>

Received 9 November 2018; Received in revised form 29 November 2018; Accepted 4 December 2018

<sup>3</sup> -5122/ © 2018 Elsevier B.V. All rights reserved.

## **List of tables and figure**

**Table 1.** Effects of METH on immune cells.

**Table 2.** METH causes changes in expression to several known pathways.

**Figure 1.** METH elicits changes to the innate and adaptive immune response, causing changes to pro-inflammatory cytokines and related oxidative stress molecules

## Table of contents

1.0	Introduction .....	1-2
2.0	Methodology.....	3
3.0	Effects of METH on immune cells.....	3-10
3.1	Monocytes and macrophages.....	4
3.2	Dendritic cells.....	6-7
3.3	T cells .....	8-9
3.4	Natural killer cells .....	9
3.5	Astrocytes .....	9-10
4.0	METH and inflammation.....	10-15
4.1	Tumor necrosis factor-alpha.....	10-11
4.2	Interleukin-1 beta.....	11-12
4.3	IL-10 .....	12
4.4	IL-12 .....	12-13
4.5	IL-6 .....	13-14
4.6	IL-2 .....	14
4.7	IL-8 .....	14-15
5.0	Other inflammatory responses to METH .....	15-17
5.1	Cyclooxygenase-2 .....	15
5.2	CXCR4 .....	16
5.3	CXCL10.....	16
5.4	CXCL5.....	16-17
5.5	CXCR3 .....	17
6.0	Immune pathways activated in the presence of METH.....	17 - 22
6.1	NF- $\kappa$ B signalling .....	18-19
6.2	MAPK/ERK and JNK signalling.....	19-20
6.3	AKT-PI3K pathway signalling.....	21
6.4	JAK/STAT signalling.....	21-22
7.0	METH and its relationship to ageing.....	22-27
7.1	METH contributes to age-related diseases, such as cardiovascular pathology, stroke and Alzheimer's Disease .....	23-24
7.2	Effect of METH on adolescence and adulthood, our learnings from animal models.....	24
7.3	Impacts of METH on mental health .....	25
7.4	METH-induced inflammation and link to ageing.....	26-27
8.0	Conclusion and future prospects.....	27-28
	References .....	29-38

## 1.0 Introduction

Methamphetamine (METH, also known as ice), is the second most popular recreational drug of choice worldwide [1]. In the 2014 United Nations office on drugs and crime, world drug report indicated that METH accounted for 80% of all amphetamine-type stimulant seizures [2]. In the 2017 World drug report, METH was reported to be used by around 37 million people across the globe, with other reports indicating between 14–53 million METH users globally [2]. Worrying, is the trafficking of METH around the world with data suggesting expanding METH markets in South East Asia, Oceania, along with growing concerns about METH use in North America, parts of Europe and China [130;131]. In Australia, an increase of high purity crystalline METH has been documented since 2010. As a result, METH-related hospital admissions have been on the rise, from just under 2000 hospital admissions - from 2009 to 2010 - to just over 10,000 cases from 2014 to 2015 [3]. Three forms of METH are currently found in Australia; powder methamphetamine, also known as speed; base METH, a damp oily form characterized by its yellow or brownish hue [1] and crystal METH, also known as ice, a crystalline and highly pure form of METH [4]. Crystal METH in its smoked form is the most popular choice of METH use in recreational and social settings; however, due to the attached health risks and high dependence of smoking METH there has been a substantial increase for METH treatment [5]. METH use disorders have been previously attributed to those subgroups, such as rural persons who are more likely to use METH in comparison to those residing in metropolitan areas [6]. This has been supported by reports that young people living in rural areas are twice as likely

to use METH in comparison to those living in urban areas [3,6]. Comparing the patterns and prevalence of METH users in rural and metropolitan areas, shows statistically significant differences in METH use, particularly crystal METH, in those living in rural locations [5]. These results were supported by the fact that rural men and employed rural Australians were more likely to use METH, with prevalence being mostly between the ages of 18–24 and 25–29 years – reported as higher than Australians residing in cities [5,7]. In addition, previous data has reported that older people who are HIV seronegative who have a high level of METH use are at risk of contracting the illness [8]. In assessing the oral health and quality of life, out of 545 METH users, the majority comprised older males – median age of 45 years – with a greater degree of worsening oral health [9]. The recent statistics show that out of 390 METH users, 24.36% were aged 35–49, with 8.72% aged 50–64 [10]. METH’s ease of manufacture stems from its easily obtainable ingredients, which contribute to the final METH product. This ease of manufacture has led to the prevalence of local “METH” laboratories, along with “super-labs” operated by larger organizations [11]. Overall, a lack of well-rounded knowledge and perception is available on how this drug impacts the immune system, in the long-term. This long-term impact currently remains to be fully explored, and understanding this aspect of METH use in addiction and withdrawal scenarios can inform and guide public policy, and communicate communicable and non-communicable disease prevalence and risk. Moreover, long-term knowledge could inform METH’s relationship in the ageing process.

## **2.0 Methodology**

Searches were conducted through NCBI PUBMED using the following search terms: Methamphetamine OR METH AND population AND age, Methamphetamine OR METH AND immune system, methamphetamine OR METH AND immune dysregulation, methamphetamine OR METH AND cytokines OR chemokines, methamphetamine OR METH AND addiction, methamphetamine OR METH AND monocytes, methamphetamine OR METH AND macrophages, methamphetamine OR METH AND dendritic cells, methamphetamine OR METH AND T-cells, methamphetamine OR METH and natural killer cells, methamphetamine OR METH AND astrocytes, methamphetamine OR METH AND inflammation, methamphetamine OR METH AND immune pathways, methamphetamine OR METH AND Australia, methamphetamine OR METH AND global use, methamphetamine OR METH AND cell signalling. Articles included mainly those post-2000; and, within the reviewed articles other articles were assessed for suitability for this review. Inclusion criteria was based on peer-reviewed articles denoting experimental studies, both in vitro and in vivo, of methamphetamine and its impacts on the immune system and its constituents. Non-English language articles were excluded from being included in this review.

## **3.0 Effects of METH on the immune system**

The effects of METH on the immune response have yet to be fully determined, however, there is growing evidence that METH suppresses and modulates the immune system (Fig. 1) [12,13]. Consequently, immune dysregulation through METH abuse could lead to lasting neuropsychiatric conditions [14]. METH has

significant effects on both the innate and adaptive immune responses [12,15], with reported reductions in the numbers of natural killer (NK) cells and leukocytes [16]. In addition, macrophages stimulated by METH show increased levels of the pro-inflammatory cytokine TNF- $\alpha$  [17–19]. METH causes decreased levels of dendritic cells (DCs) [20], impacting the adaptive immune system and rendering individuals susceptible to certain diseases and infections [16]. Furthermore, there is growing evidence that mood disorders are related to the changing levels of pro-inflammatory cytokines and their influence on the level of monoamines; along with the dysregulation of the hypothalamic pituitary adrenal (HPA) axis, activation of microglial cells, and changes in the neuroplasticity of the brain [21] (Tables 1 and 2; Fig 2).

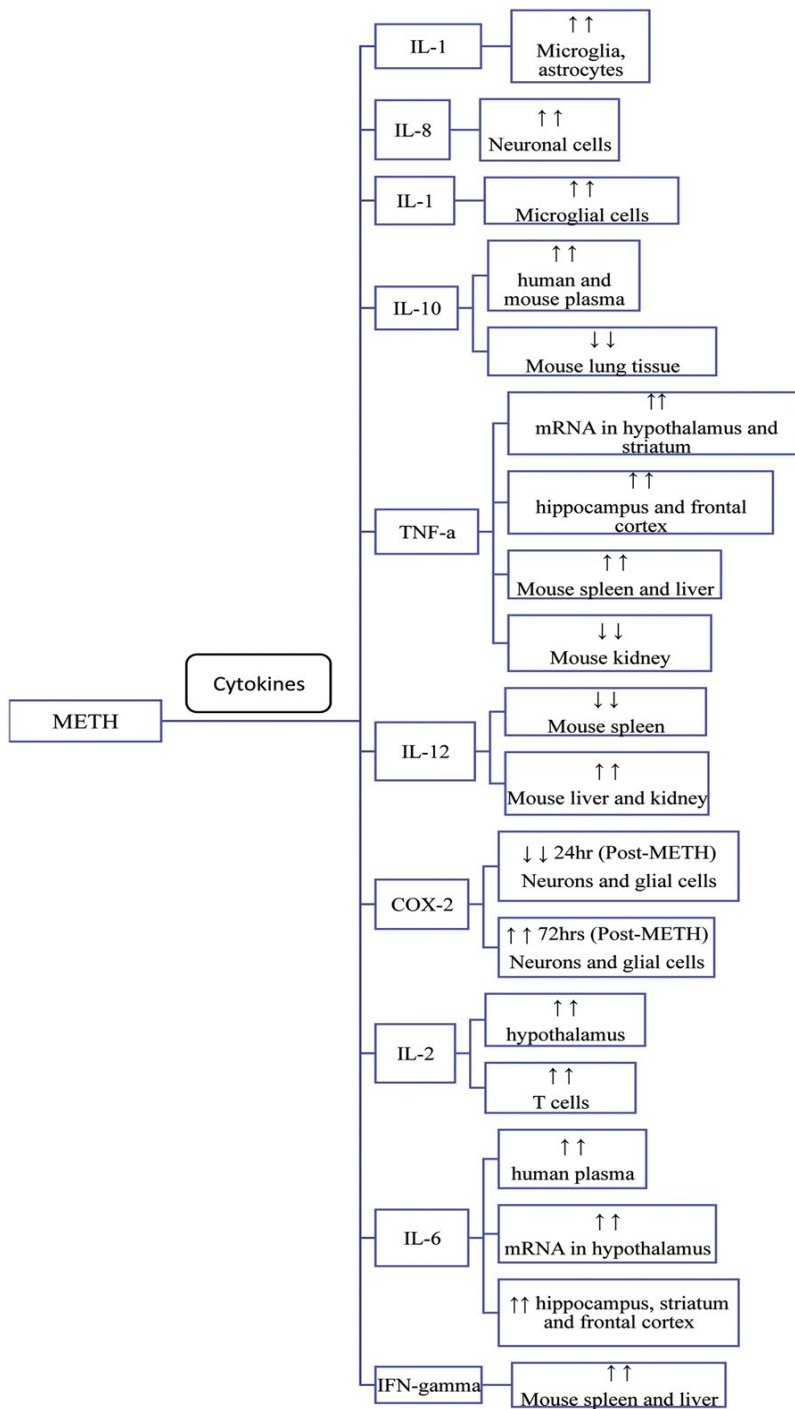


**Figure. 1. METH elicits changes to the innate and adaptive immune response, causing changes to pro-inflammatory cytokines and related oxidative stress molecules. METH also impacts frequencies of T cell subsets (CD4+ and CD8+) along with proliferation.**

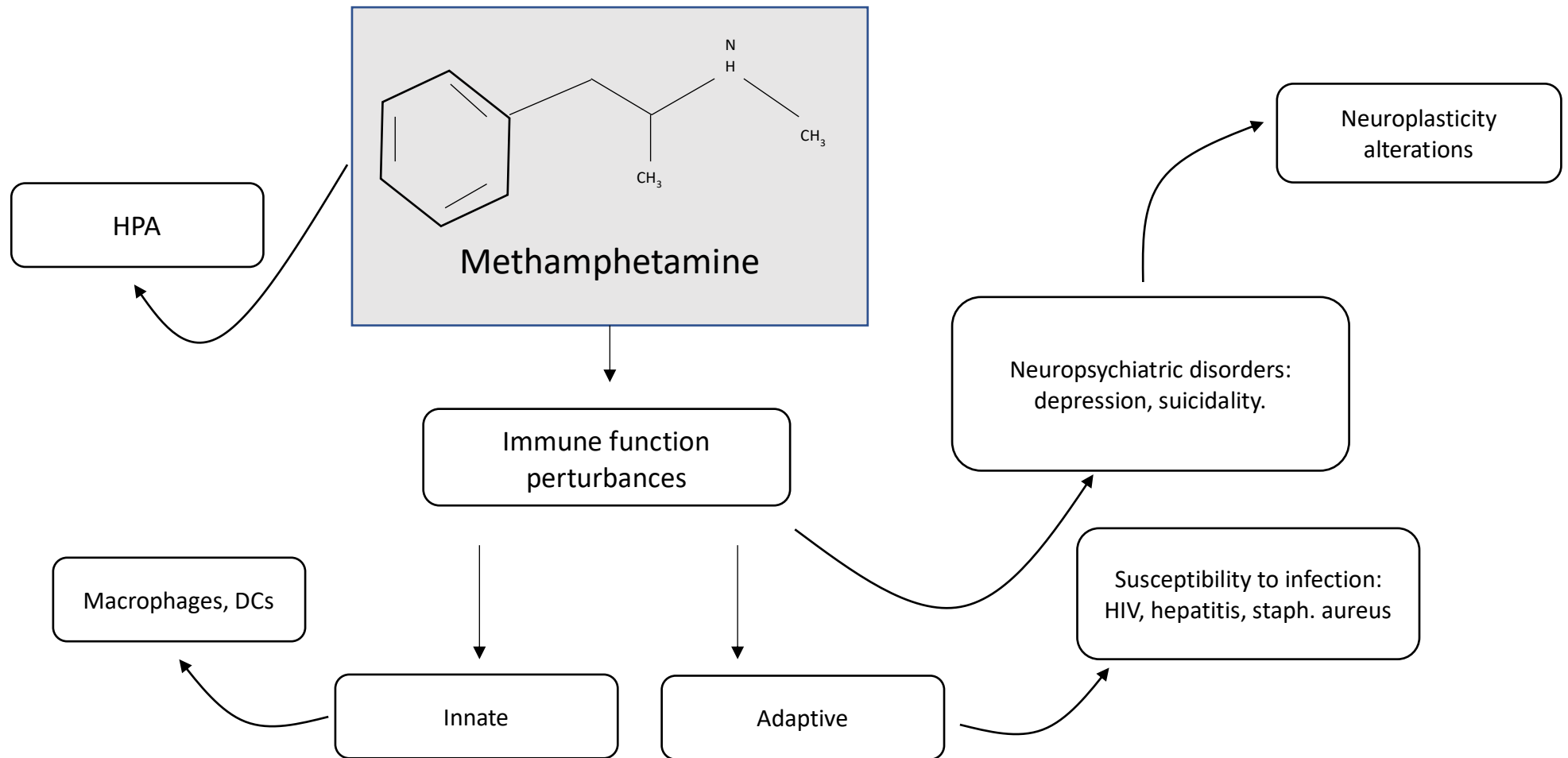


**Figure 2. Overall effects and disturbances caused by METH use over time.** Key features of METH use include changes to inflammatory cytokines, immune cells, and disturbances to the brain.

### 3.1. Monocytes and macrophages

Monocytes differentiate into both macrophages and DC as they circulate to sites of inflammation. Monocytes represent immune effector cells, in which chemokine receptors and adhesion receptors allow them to migrate from blood to sites of infection [22]. In healthy individuals, 90–95% of circulating monocytes are CD14+CD16-, whilst 5–10% are CD14+/CD16+ [23]. Macrophages secrete cytokines in response to external stimuli, which are involved in the recruitment of other immune cells to initiate a cascade of innate and adaptive immune responses [17]. In the presence of METH, macrophages secrete pro-inflammatory cytokines, interleukin-1 (IL-1) beta, IL-2, IL-6 and IL-8 [24] with IL-1 $\beta$  and IL-6 being significantly upregulated in the co-presence of bacterial lipopolysaccharide (LPS) [25]. Likewise, co-stimulation of macrophages with LPS and METH results in a significant increase in IL-1 $\beta$ , IL-8 and TNF- $\alpha$  [26]. Furthermore, the number of monocytes and macrophages are reduced in the presence of METH, and their cell surface marker expression are altered with the upregulation of CD80 and down-regulation of CD11b whilst there are no effects on GR-1(high) monocyte/ macrophage cells [20]. In the context of human immunodeficiency virus (HIV-1) - METH increases expression of levels of galectin-1 which is involved in HIV-1 viral absorption [27].

### 3.2. Dendritic cells

DCs express a diverse range of cell surface receptors in order to sense their environment and activate immune-related functions [28]. Amongst these receptors are toll like receptors (TLRs), surface pattern recognition receptors (PRRs) and NOD-like receptors which assist in detecting signals such as those associated with pathogen-associated molecular patterns (PAMPs) or damage-associated molecular patterns (DAMPs) [28]. DC are also professional antigen presenting cells, where they efficiently activate the adaptive immune system. Stimulation of DCs with METH results in altered chemokines, chemokine receptors, cytokines, G-protein signalling, cell cycle regulation and cell transcriptional regulation [16]. Specifically, METH was shown to increase HIV-1 co-receptors CXCR4 and CCR5 in human monocyte-derived DC [29]. Similar work investigating METH use and HIV-1 infection, demonstrated the differential expression of the chemokine receptor CXCR3 in immature DCs (IDC) [30]. More broadly, METH has been shown to decrease the overall abundance of splenic DCs, which renders the effectiveness of the adaptive immune response [20]. Moreover, a highthroughput investigation study of genomic changes to mature DCs noted significant increased levels of CCR5, CCR2, IL-1 $\beta$  TNF- $\alpha$  and IL8; in addition, to decreases in IL-IR3 and TGF- $\beta$  [16].

**Table 1: Effects of METH on immune cells.**

Cell type	Impacts by METH	Reference
Monocytes	↑↑ Dose escalation mouse model assessing immune subsets ↓↓ THP-1 cell viability (after 24 hrs) Cytotoxicity on LPS-stimulated IL-1β THP-1 monocytes	[20] [125]
Macrophages	↑↑ IL-8, IL-1β and TNF-α in LPS-treated macrophages ↑↑ Activated brain macrophages	[25] [36]
T cells	↓ CD4 ↑ CD8 Effect of METH on systemic immune system ↓ CD4 In vivo lymphocytic choriomeningitis virus infection model CD8+ and CD4+ cell cycle progression disrupted (in vitro) ↓↓ frequency of CD4+ ↓↓ frequency of CD8+ Dysfunction of primary human T cells (mitochondrial oxidative damage.) Inhibition of T cell proliferation	[126] [30] [32] [126] [34] [15]
Dendritic cells	Dose escalation mouse model assessing immune subsets ↑↑ infectivity of human immunodeficiency virus-1 in monocyte-derived DC Modulation of genes in pathogenesis of human immunodeficiency virus-1.	[20] [29] [16]
Natural killer cells	↑↑ Activation of NK cells ↓↓ Splenic NK lymphocytes	[36] [127]

**Table 2: METH causes changes in expression to several known pathways.**

Pathway	METH-induction	METH dose	Study period	Study type	Reference
JAK-STAT	↑ TNF-α and IL-6 ↓ Bax/Bcl-2 ratio (microglial cells)	0.1-4mM	24hours	<i>In vitro</i>	[58]
JNK	Activation of Src-JNK-Jun signalling cascade Activation via METH-induced oxidative stress	-	-	<i>In vivo</i>	[89] [88]
AKT-PI3K	Activation by pro-inflammatory cytokines and chemokines	250-1000μM 500μM	24 hours 48 hours	<i>In vitro</i>	[62] [25]
MAPK/ERK	Mediation of IL-8 and IL-1β ↑ METH-induced HO-1 Activation of p38 MAPK pathway (METH toxicity) Changes in MAPK pathways in mouse striatum and frontal cortex	0.1-10mM 1mg/kg-6mg/kg	24 hours 5 days	<i>In vivo/In vitro</i> <i>In vivo</i>	[84] [81]
NF-κB	ERK1/2 activation via D1 and D2 receptors Pro-inflammatory cytokine and chemokine activation Inflammation, apoptosis, cell survival, gene expression: immune and inflammatory response	250-1000μM 0.1mg/kg-20mg/kg	24 hours 24hours/8-10 days	<i>In vitro</i> <i>In vivo/in vitro</i>	[62] [129]

### **3.3. T cells**

T cells play an important role in the orchestration of immune responses [30]. There are few studies that document the effects of METH on T cells. In mice, chronic METH administration reduces the number of CD4 and CD8 T cells in the spleen [20]. In addition, METH significantly increases expression of the inflammatory chemokine receptor CXCR3, suggesting that METH contributes to effector T cell function and migration [12,31]. METH also prolongs the transition from G1 to S phase of T cells [32]. In particular, METH alters gene expression by suppressing the CDK-cyclin E complex, a critical limiting factor which is suppressed in CD4 and CD8 T-cell subsets and disrupts cell cycle progression [32]. This finding was also consistent with changes in other cell cycle genes, such as E2F1, responsible for normal cell cycle regulation [32]. Similarly, METH causes down-regulation of cell-cycle genes and proteins involved in apoptosis in a rat study addressing acute hepatic injury from METH [33]. METH also alters intracellular calcium concentrations in T cells via reactive oxygen species (ROS) production, leading to mitochondrial injury [34].

### **3.4. Natural killer cells**

NK cells are primarily involved in the destruction of virally infected cells [35], and any dysfunction or numbers of NK cells, results to overall suppressed immunity [20]. METH has been shown to markedly increase the activation of NK cells [36] through an increase in simian immunodeficiency viral load and CNS damage in simian immunodeficiency virus-infected macaques. The

increase in NK cells were primarily present in the brain and in peripheral sites [36]. In addition, the cell surface marker, CD107a or lysosome-associated membrane protein-1, is increased in the presence of METH [37]. However, splenic NK cells have been shown to be significantly reduced in METH treated mice [20]. These results also showed a marked reduction in CD27 and killer cell lectin-like receptor expression [20]. CD27 is an important cell surface marker of NK cells as it is involved in its cytotoxic function [38]. Thus, METH induces a dysregulated NK cell profile, one that indicates a suppressed state.

### **3.5. Astrocytes**

Primary astrocyte cell cultures cultured in the presence of METH for 24 h, significantly upregulates CXCL5, MAP2K5 and GPR65 as core gene network components with both neuroprotective and neuropathological roles [39]. MAP2K5 belongs to the MAP kinase family; CXCL5 has been implicated in the activation of the PI3K/AKT, MAP kinase and  $\beta$ -catenin pathway, and GPR65 has been described as a GCPR activated through extracellular acidic pH via protonation of histidine residues, regulating cell behaviour [40]. In addition, METH increases expression of Caspase-11 and TLR4 of primary astrocyte cell cultures [39]. This study also reported the downstream expression of nuclear factor kappa B (NF- $\kappa$ B) through the MyD88 independent pathway and MyD88 dependent pathway, from expression of TLR4. Consequently, increased transcription of inflammatory cytokines is found in the nucleus [39].

## **4.0 METH and inflammation**

METH abuse leads to severe dysregulation in the peripheral immune response, leading to an imbalanced expression in cytokines, chemokines and other molecular factors. In addition, expression of pro- and anti-inflammatory cytokines and chemokines have been implicated in METH-related neuronal injury which may also be related to METH addiction [41]. Further, METH-induced immune dysfunction has potential to augment HIV replication [42]. Interestingly, inflammatory responses have the ability to pass through the blood brain barrier (BBB) which can relay messages responsible for inducing changes to motor function and motivation [43].

### **4.1. Tumour necrosis factor-alpha (TNF- $\alpha$ )**

Tumour necrosis factor alpha (TNF- $\alpha$ ) is a pro-inflammatory cytokine which has cell signalling functions and can cause chronic and acute inflammatory responses along with having a central role in the pathophysiology of autoimmune diseases such as ulcerative colitis, rheumatoid arthritis and multiple sclerosis. TNF- $\alpha$  can either be membrane bound or in soluble form, with roles in apoptosis, immunity development and tumour cell necrosis. It is primarily produced by macrophages and is encoded by the TNF- $\alpha$  gene present on chromosome 6 and 17 (Figure 2) [44]. TNF- $\alpha$  is known to be involved in activation of transcription factors such as AP-1 and NF- $\kappa$ B which can lead to a number of other physiological and pathological mechanisms [45]. In addition, METH stimulation of BV2 cells and primary microglial cells pre-treated with LPS, causes the expression of TNF- $\alpha$  via the cAMP/PKA/CREB signalling

pathways [33]. Based on these findings, further studies are required that target the TNF- $\alpha$  cytokine pathway. Seeking to better define the role of METH in HIV-1 pathogenesis, gene and protein expression of TNF- $\alpha$  was markedly increased by DCs [16]. Better understanding of this pathway can help to inhibit the harmful effects caused by METH abuse.

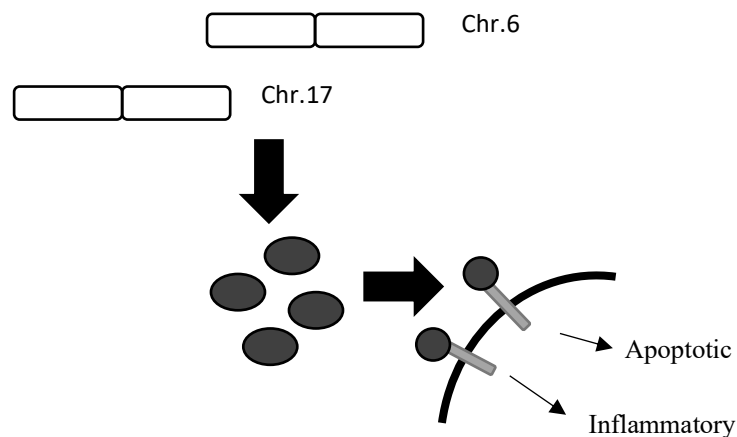


**Figure 2. Summary of TNF- $\alpha$  pathways.** Chromosomes 6 and 17 produce TNF- $\alpha$ , and are directed to either inflammatory or apoptotic pathways. METH has been shown to express TNF- $\alpha$  across select *in vitro* cell lines.

#### 4.2. Interleukin-1 beta

IL-1 $\beta$  induces catabolic effects and inflammatory reactions and is encoded by the IL-1 $\beta$  gene [46]. Maturation of IL-1 $\beta$  requires the action of enzyme caspase-1, converting it into active its IL-1 $\beta$  form [47]. Activation of NF- $\kappa$ B results in increased expression of other cytokines and chemokines [48]. The effects of IL-1 $\beta$  has a significant effect on the metabolism and on the extracellular matrix of the cells as seen in patients with osteoarthritis [49]. Since NF- $\kappa$ B is activated

both in METH treatments and as a result of IL-1 $\beta$  stimuli, it is plausible to assume that METH may cause change in expression of IL-1 $\beta$ . In fact, METH stimulation of monocytic cell lines differentiated to macrophages resulted in elevated expression of IL-1 $\beta$  [33]. It was proposed that the pathways involved in such stimulation included NF- $\kappa$ B and mitogen-activation protein kinase (MAPK). Recently, in mice, METH-induced T-cell alterations of IL-1 $\beta$  profiles [12].

### **4.3. IL-10**

IL-10, is an anti-inflammatory cytokine that has a role in preventing inflammatory and autoimmune pathologies [50], and is secreted by a variety of activated immune cells [39]], having pleiotropic effects on T and B cells, long with myeloid cells [51]. In addition, IL-10 has been described as a soluble factor released by type-2 T helper cells, in which also inhibits the secretion of type-1 T helper cytokines [51]. Upregulation of IL-10 has previously been reported in mice [32]. Recently, IL10 was shown to prevent metabolic programming induced, in macrophages, by inflammatory stimuli [39]. METH has been shown to increase IL-10 in human plasma [14]. Similarly, the evaluation of METH in microglial cell (ESdM) activation showed an increased IL-10 production following 48-hr METH treatment [52]. In a comprehensive gene array overview, macrophages stimulated over a time-dependent METH dose showed considerable upregulation of IL-10 at 6 h post METH exposure [17].

#### 4.4. IL-12

The IL-12 family, comprising IL-12, IL-23, IL-27, and IL-35 are key players in the pathophysiology of immune responses in various disease conditions [53]. IL-12 family cytokines have been central targets in a number of inflammatory diseases, such as multiple sclerosis; along with rheumatoid arthritis and Crohn's disease (CD) [Sun et al., 2015; Stetsko et al., 2008]. Monocytes, macrophages, DC and B-cells are able to secrete IL-12 [54]. In mouse spleen, IL-12 was shown to decrease; conversely, mouse liver and kidney revealed significantly increased expression of IL-12 [15]. Moreover, IL-12, in conjunction with other cytokines also function to inhibit HIV-1 expression and infectivity in macrophages [54].

#### 4.5. IL-6

IL-6 is a multipotent cytokine secreted by various immune cells, such as monocytes, macrophages, fibroblasts, mesenchymal cells, endothelial cells and fibroblasts [55; 134]. Additionally, the IL-6 receptor (IL-6R) system and signal transduction mechanism has importance in immune regulation and inflammation [56]. IL-6 has been implicated in Alzheimer's disease, and may be used as a useful biomarker in determining the extent of cognitive impairment [57]. mRNA IL-6 expression is increased in mice in the hypothalamus, hippocampus, striatum, cortex and cerebellum following METH injection compared to saline treated mice [26]. In an astrocytic cell line cultured with METH for 3 days, IL-6 RNA levels increase 4-fold. In addition, METH exposure for 24 h increases both mRNA and protein expression of IL-6 [57]. In the same study, IL-6 expression found to be overridden by the IKK-b inhibitor SC415 [57]. Coelho-Santos et al. found that microglial cells exposed to METH

caused an increase in IL-6 expression and also upregulated IL-6 receptor (IL-6R-a) after 24 h [58]. Interestingly, exogenous IL-6 expression was shown to have an antiapoptotic effect through activation of the JAK-STAT3 pathway [58]. Assessing the anti-neurotoxic agent asiatic acid, it was noted that METH-induced neuronal cells treated with asiatic acid inhibited IL-6 secretion [59]. In addition, BV2 cells and primary glial cells treated with METH, showed an elevated expression in the levels of IL-6 along with TNF- $\alpha$  [60]. Likewise, an early increase in the levels of IL-6 expression in hippocampus and striatum in mouse brains is noted within 1.5 h post METH injection [19].

#### **4.6. IL-2**

IL-2 is reported as having specific function in T cell homeostasis and memory differentiation [61]. The addition of METH to T cells in vitro increases IL-2 secretion by 3-fold [34]. Furthermore, when METH was conjugated to lymphocytic choriomeningitis virus promoter, it further exacerbated IL-2 secretion by splenocyte CD4 and CD8 T cells [30]. Likewise, METH-treated mice were found to exhibit an increased expression of IL-2 in the hippocampus [14]. Additionally, METH was shown to increase the IL-2RG system and IL-2 ligand in an HIV-1 model, with the authors noting that this IL-2RG/IL-2 expression representing an important mechanism contributing to neuro-inflammation [61].

#### **4.7. IL-8**

IL-8 is a chemokine known to be associated with an inflammatory response in several neurological disorders, including Parkinson's disease [62]. In astrocytes, METH was shown to increase IL-8 in a dose-dependent manner [62]. Other work has described a moderate IL-8 upregulation in the presence of METH on macrophages [17]. Similarly, macrophages treated with METH at 48–72 hours resulted in significant increase in IL-8; these findings, compared to macrophages treated with LPS alone showed higher IL-8 expression [25]. Huckans et al., through hypothesising the relationship between METH, immune factors and neuropsychiatric symptoms were able to show IL-8 to be a significant marker of anxiety and depression [63].

### **5.0 Other inflammatory responses to METH**

#### **5.1. Cyclooxygenase-2**

Cyclooxygenase-2 (COX-2) is expressed by stimulation from an assortment of pro-inflammatory agents, with its expression in the brain signaling physical and psychological stress [64]. METH has been shown to increase striatal expression of COX-2 protein [65,66]. Induction of COX-2 through the NF- $\kappa$ B pathway results in nitric oxide, prostaglandins and inflammatory cytokine production [67]; and, induction of COX-2 might suggest drug-induced neurodegeneration [67]. METH significantly increases COX-2 protein expression in the striatum within 72 h after METH administration to mice with no changes in COX-2 expression in the hippocampus and cerebral cortex. Interestingly, a relationship between depleted dopamine and a delay in COX-2 expression was observed.

Similarly in an acute METH dose, significant reduction in COX-2 positive cells are noted in the striatum after 24 hours. In addition, upregulation of COX-2, with co-expression of NF- $\kappa$ B is noted after 72 h, and this is marked by reductions in dopamine in the striatum. Reports of COX-2 expression in METH models, suggests its targeting in early METH-related neurotoxicity during METH use. Increased COX-2 expression is noted in a METH-CUS (chronic unpredictable stress) model, and this has been suggested to enhance monoaminergic depletions in both the hippocampus and striatum [64].

## **5.2. CXCR4**

METH enhances expression of chemokine receptor CXCR4 in the brain [24]. In HIV-1 infection, METH in a dose-dependent manner caused an increase of CXCR4 expression by DCs [68]. Due to the involvement of the CXCR4 receptor, being a major co-receptor, along with CCR5 in HIV-1 infection, CXCR4 may be a likely candidate for targeting in the development of therapeutic prevention of HIV-1 entry into cells in METH addiction [27].

## **5.3. CXCL10**

CXCL10, known also as IFN- $\gamma$ -induced protein 10, is a chemoattractant for immune cells such as T-cells and monocytes [59]. In response to IFN- $\gamma$ , in an appropriate inflammatory environment, CXCL10 is secreted from the host's immune cells upon activation of its receptor CXCR3 [59]. METH has been shown to significantly increase CXCL10 in astrocyte cells and is involved in the activation of the innate immune system [69].

#### **5.4. CXCL5**

CXC chemokine ligand 5 (CXCL5) is a cytokine expressed in a range of cell types, including monocytes [70] and endothelial cells, along with several organs including the brain [70] and lung [71]. In the lung, and in response to microbial infection, CXCL5 orchestrates neutrophil trafficking by activating G-protein and arrestin signaling pathways [71]. Interestingly, through pro-inflammatory cytokines, CXCL5 is activated via activation of NF- $\kappa$ B, and produced by immune and vascular endothelial cells [70]. Additionally, tumor suppressors and oncogenes work to regulate CXCL5 expression. In astrocyte cell cultures, low to high concentrations of METH over 24-hour exposure significantly upregulates CXCL5 gene expression [39].

#### **5.5. CXCR3**

The chemokine receptor, CXCR3 is the receptor for the IFN-inducible chemokines CXCL9, CXCL10 and CXCL11 and its expression on activated T cells. In addition, CXCR3 is crucial for amplifying IFN- $\gamma$ dependent recruitment of cells in peripheral sites of infection [31]. METH has been shown to significantly differentially regulate CXCR3 protein expression in immature-DCs [72]. In addition, chronic METH exposure strongly increases CXCR3, which is important in CD8 T cell recruitment, in order to provide modulation of T cell memory [12]. CXCR3 is known to have roles in migrating T cells into the microenvironment of peripheral tissues, aiding in their interaction with antigen presenting cells leading to effector and memory T cells [31].

## **6.0 Immune pathways activated in the presence of METH**

Immune pathways relating to drug addiction have been documented as falling into two categories: those pathways involved in upstream events of drug addiction, i.e., MAPK signaling and calcium signaling. The second are pathways involved in downstream effects, including those regulating glycolysis metabolisms, regulation of the actin cytoskeleton and apoptosis [37]. Pathways which are impacted upon by METH, and which increase the inflammatory response have been described as the AKT-PI3K, NF- $\kappa$ B, MAPK [25,62], along with the JAKSTAT pathway [58].

### **6.1. NF- $\kappa$ B signalling**

The NF- $\kappa$ B family of inducible transcription factor proteins exist as inactive cytoplasmic complexes, in which activation of NF- $\kappa$ B occurs via two main signalling pathways: canonical and non-canonical [73,74]. NF- $\kappa$ B proteins involve a cascade of events which begin outside the cell, converging in the nucleus [75], promoting immunity through controlling expression inflammatory genes [73,76,77]. Through the action of cytokines and PAMPs, receptors such as TLRs are consequently stimulated, resulting in a cascade that activates the NF- $\kappa$ B [76]. The NF- $\kappa$ B pathway is important in activation of naive T-cells through TCR signalling and is necessary for both the generation and maintenance of effector and memory T cells [76]. In B-cells, the NF- $\kappa$ B pathway mediates survival of naive B cells as well as influencing immunoglobulin class switching [74]. In METH, increases in the production of pro-inflammatory cytokines and chemokines has been attributed to dependence

on the NF- $\kappa$ B pathway [62]. Upon the expression of pro-inflammatory cytokines and chemokines, due to extracellular signals, NF $\kappa$ B is activated in which subsequent processes and regulation can include inflammation, apoptosis, cell survival, and inducing gene expression pertinent to immune and inflammatory responses [75]. Further data suggests that the NF- $\kappa$ B signalling pathway induces inflammatory cytokines in METH-treated macrophages. The NF- $\kappa$ B pathway has also been thoroughly described as influencing and being a mediator of reward following long-term drug abuse [78], having a role in learning and memory, and increasing expression of opioid receptors and neuropeptides [78]. In neuronal cells, asiatic acid was shown to inhibit METH-induced NF- $\kappa$ B translocation, thus exhibiting an anti-neurotoxic effect [59]. Further, cytoplasmic and nuclear fractions of METH-exposed astrocytes showed an increased protein expression of NF- $\kappa$ B [39]. Heightened expression of NF- $\kappa$ B upregulated caspase-11 subsequently upregulating the NLRP3 inflammasome and inducing IL1 $\beta$  and IL-8 expression [33]. In humans, METH induces the production of TNF- $\alpha$  which is involved in the BBB dysfunction. Animal and in vitro work using endothelial cells showed that METH initiated endothelial dysfunction, through activation of the NF- $\kappa$ B pathway [18]. This finding revealed the role of the NF- $\kappa$ B pathway in decreasing tight junction stabilization and increasing the permeability of the BBB. Conversely, blocking of the NF- $\kappa$ B pathway inhibits BBB dysfunction [18].

## 6.2. MAPK/ERK and JNK signalling

Extracellular signalling regulated kinase (ERK) and mitogen-activated protein kinase (MAPKs) pathways have been reported to play a role in METH-mediated signalling [79,80]. MAPK signal cascades are important intracellular signalling pathways which transmit signals from cell membrane to nucleus [81], and possess a regulatory role of proinflammatory cytokines [82]. ERK contained in the nucleus is known as a target of stimulants [83]. Confirmatory experiments, determining the involvement of heme-oxygenase-1 (HO-1) – a crucial cellular mechanism mitigating oxidative damage - in METH-induced toxicity, showed that the p38 MAPK pathway was involved in upregulating METH-induced HO-1 [84]. Authors of this study support the role of the p38 MAPK pathway in cellular defence against METH toxicity [84]. Single and multiple METH injections in mice revealed complex changes in MAPK-related pathways mouse striatum and frontal cortex [81]. More specifically, MAPK-related pathways significantly impacted, through repeated METH administration, included map kinase I, Erk1, Erk2 and MAP kinase 7; these MAPK-related pathways have been implicated in substance abuse [81]. Evidence supports the involvement and role of the nuclear and cytoplasmic trafficking of ERK1/2 in learning and memory and cell death [85] along with behavioural modifications in brain specific ERK pathway expression from drug abuse [86]. Similarly, assessments and the involvement of the sigma-1 receptor found downstream activation of ERK MAPK pathway was necessary for promoting the activation of astrocytes upon stimulation via METH [87]. The c-Jun NH2-terminal kinase (JNK) signalling pathway is an evolutionary conserved group of mitogen-activated protein kinases (MAPKs) [88]. This signalling pathway has been previously

implicated in its ability to respond due to activation of cytokines and exposure to extracellular signals [88]. METH has been reported to activate the SrcJNK-Jun signalling cascade [89]. In line with METH addiction, and possible neurodegeneration, the JNK signalling pathway has been suggested to possibly mediate neurodegeneration in METH addiction [90]. A further report outlines the activation of the JNK signalling pathway via METH-induced oxidative stress' ultimately, this leads to signal transduction into the nucleus through the activation of transcription factors, such as activator protein-1 (AP1) – a major target of JNK signalling [88] NF- $\kappa$ B and cAMP-responsive element binding protein (CREB) [91].

### **6.3. AKT-PI3K pathway signalling**

The protein kinase B (AKT) and phosphatidylinositol-3-kinase (PI3K) pathway is vital for many aspects of cell growth and survival [92] and is triggered through the result of growth factors and regulators [92]. This signal transduction cascade also supports a role in protein synthesis, metabolism and angiogenesis, with prevention of apoptotic events [93]. METH triggers cell survival-signalling events which involve dopamine receptors, PI3K and AKT [93]. Activation of the AKT/PI3K cascade was demonstrated through pro-inflammatory cytokine and chemokine expression by METH-induced astrocytes, in which METH caused alteration of mGluR5 receptor. In turn, this was shown to activate the Akt/PI3K pathway [62]. These results were in the context of METH-mediated, NF- $\kappa$ B dependent increases of cytokine and chemokine expression [62]. Similarly, the AKT/PI3K signalling pathway was also found to mediate METH-induced IL-8 and IL-1 $\beta$  [25]. Using topiramate (TPM) as a potential treatment

for METH dependence, Niu et al. were able to elucidate enrichment of PI2K-AKT signalling pathway amongst seven biologically relevant pathways [94]. Moreover, TPM's effects on METH addiction further showed a decrease in oxidative stress and increased neuroplasticity, consistent with METH's ability to increase oxidative stress through a perturbation of the PI3K-AKT pathway [94].

#### **6.4. JAK/STAT signalling**

The JAK/STAT signalling pathway is utilized by several diverse cytokines, chemokines, interferons and growth factors. The simplicity of the JAK/STAT pathway allows for direct communication from transmembrane receptors to the nucleus, and cytokine receptor stimulation leads to phosphorylation events that ultimately recruit STAT, translocating to the nucleus and binding specific sequences to initiate gene expression [95]. METH has been shown to increase the Bax/Bcl-2 ratio, with the cytokine IL-6 being able to prevent this effect in microglial cells [58]. METH-induced microglial cells showed that IL-6 expression served to disrupt this pro and anti-apoptotic protein ratio level [58]. The bcl-2 family of apoptotic regulators are related to cell death and survival, in which these regulators can either suppress or activate apoptosis programming. Expression of Bax proteins is correlated to pro-apoptosis, whereas Bcl-2 is related to anti-apoptosis events [96]. In addition, the same study reported that low concentration expression of TNF- $\alpha$ , which, with IL-6, had a protective effect – through activation of JAK/STAT signalling - on microglial cells from the toxic effects elicited from METH.

## **7.0 METH and its relationship to ageing**

METH use leads to a number of cellular changes, disrupting normal cell function which trigger events related to inflammation, oxidative stress and ageing [97]. METH abuse is also associated with neurotoxicity of the fronto-striatal region, along with morphometric alterations in the hippocampus and cortex [98]. In particular, the hippocampus remains sensitive to drug abuse from adolescence years to adulthood, as it ensures structural and functional changes crucial for hippocampus maturation and function [99]. Adult METH users also experience cognitive impairments which impact on adaptive decision making, which also has long-term effects on reversal learning [100]. Long-term METH use on the brain neuro-biochemistry have been associated to age-related cognitive decline and neurochemical alterations [98]. Also, METH causes obvious changes to inflammatory immune responses leading to significant long-term alternations. Chronic inflammatory modifications in immune response have been linked to the ‘inflamm-ageing’ phenomena [101].

### **7.1. METH contributes to age-related diseases, such as cardiovascular pathology, stroke and Alzheimer’s Disease**

Acute and chronic METH use has been attributed to stroke [102]. Binge METH doses have been shown to significantly alter cardiovascular function leading to cardiac pathology [103]. In addition, heart rate variability (HRV) measured across a cohort of abstinent individuals with a known history of METH dependence showed impairments in several parameters of HRV in comparison to drug-free individuals [104]. A decreased HRV has been associated with

cardiovascular pathology, along with psychiatric disorders such schizophrenia and bipolar disorder, and an impairment in social functioning and cognition [104]. Importantly, HRV is generally thought to decline as an individual age [105]. Other reports have assessed METH-associated cardiomyopathy (MACM) in which METH has been attributed to negative effects on the myocardium [106]. Changes to the myocardium at a structural, molecular, cellular and functional level are all related to cardiac ageing [107]. In assessing the link between METH exposure and the development of Alzheimer's Disease (AD)-like changes, the formation of amyloid- $\beta$  ( $A\beta$ ) was used as a measurement to evaluate this relationship [108]. In an *in vitro* cell model, results indicated that, in a dose-dependent manner, METH increased the levels of the  $A\beta$  precursor protein (APP) [108].  $A\beta$  accumulation is a crucial indicator of AD pathogenesis [109], in which neuroimmune cells such as astrocytes, neurons and microglia respond by upregulating NADH, COX-2 and proinflammatory cytokines [110].

## **7.2. Effect of METH on adolescence and adulthood, our learnings from animal models**

The development of drug seeking, and addiction behaviour is largely shaped at the adolescent stage of life [111], governed by the chronic exposure to the neurotoxic effects of several drugs of abuse. METH use in early-life increases risk of developing Parkinson-like symptoms [112]. In fact, in adult male rats, chronic binge METH dose revealed similar impairments in metabolites within the striatum, prefrontal cortex and hippocampus. In addition, METH impacts on neurotransmitters – dopamine and serotonin in adult rats [98]. In adolescent rats,

METH was modelled to assess reversal learning and the likelihood of continued METH use through to adulthood [100]. Results of this study indicated a positive correlation between METH taken at adolescent stages – specifically in the late adolescent period – to adult METH use [100]. METH was also found to have a discriminatory effect in adolescent and adult rat developmental age [99], with METH exhibiting impairments in hippocampal cell proliferation and survival in young adult rats [99].

### **7.3. Impacts of METH on mental health**

Other than the common withdrawal symptoms associated with METH use, such as excessive sleeping and severe cravings, METH also triggers depressive-like symptoms chronic METH users experiencing withdrawal [113], usually lasting for longer than two weeks of abstinence [114]. This is in stark contrast to the euphoric and elevated mood effects which METH brings on when initially consumed [115]. In a cross-sectional study using a self-reporting tool and comparing active adult METH users with early ex-users and no history of METH users, it was noted that METH-dependent users had greater anxiety and depressive symptoms; with 10 plasma immune factors being associated with, and contributing to neuropsychiatric function [63]. Another cross-sectional study evaluating the pervasiveness of major depression among 400 people accessing treatment for METH use, reported a higher proportion of individuals with depression upon entering treatment facilities [116]. Furthermore, authors noted that the high prevalence of substance-induced depression manifested greatly in symptoms associated with appetite, sleep perturbations, trouble focusing, fatigue and feelings of sadness and emptiness [116]. Comparisons

between regional volumes of cortical grey matter in adults with a history of METH showed age-related grey matter loss in several regions of the brain [117]. This finding is particularly important as it suggests that adult METH-users may be at higher risk of developing neurodegenerative disorders and cognitive decline at a younger age when compared with healthy non-METH users.

#### **7.4. METH-induced inflammation and link to ageing**

METH creates an immune imbalance where changes in immune cell function, inflammatory cytokines and chemokines are apparent. METH creates an environment which disturbs the balance between oxidative stress and antioxidant defence [118]. IL-6 is over-expressed in METH addicted individuals and has been linked to the ageing process [119]. Moreover, IL-6 has been described as a central aspect of ‘inflamm-ageing’ [120], with an increase of this cytokine in serum is characteristic of ageing [121]. IL-6 has also been implicated in poor physical performance, with loss of muscle strength. Similarly, TNF- $\alpha$ , a cytokine impacted upon by METH, has also been associated with the ageing process [121]. Post-mortem analysis from human tissues have aligned METH with diseases characteristic of old age [122]. It was noted that METH fast-tracked cellular senescence and activated genes involved in the cell cycle and inflammation [122]. Moreover, METH caused an increase in ceramide biosynthesis, a process known to play a role in cellular replicative senescence, which led to the expression of senescent-associated biomarkers, IL-6 and TNF- $\alpha$ . Results of this study indicated that METH initiated a cascade of genetic changes observed in rapid health decline, characteristic of chronic inflammation and ageing [122]. Indeed, the immune changes from chronic and

acute METH (increased inflammation and oxidative stress) have been suggested to lead towards a reduction in telomere length [123]. Shortened telomere length is associated to increased cellular ageing as well as a range of non-communicable age-related diseases, including hypertension, cardiovascular disease, stroke, diabetes and dementia. In fact, drug abusers on METH, heroin or diazepam have shorter telomere length and accelerates cellular senescence [122,124].

## **8.0 Conclusion and future prospects**

METH carries out its immunomodulatory effects via a number of key changes to both pro- and anti-inflammatory cytokines, leading to a cascade of signalling responses in both innate and adaptive immune cells. Alterations to IL-6, TNF- $\alpha$ , IL-10, COX-2 and IL-1 $\beta$  all play a vital role in METH-induced neurotoxicity. Although knowledge relevant to the effects of METH on several human cell types and in *in vitro* models has been well-established, there lacks a well-described, accumulated understanding of METH's immune-modulatory and immune-metabolomic effects. In addition, human peripheral immune cells have gained attention in recent years for their potential in being a valuable source for discovering biomarkers. Data supports the case that METH lowers an effective immune response in humans, leading to susceptibility of transmitting sexually transmitted diseases and infections. In addition, METH may contribute to the pathophysiology of inflammatory diseases through its association with inflammatory cytokine production. However, data is limited on the immune and oxidative-related pathways activated and maintained from changes in immune cell metabolism – glycolytic fluxes, mitochondrial respiration and reactive

oxygen species generation, which are disturbed through METH use. In particular, the Nod-like receptor pyrin containing 3 inflammasome (NLRP3), a multiprotein complex related to infection and inflammation, and its activation, could be relevant in METH abuse. The NLRP3 pathway ties immunity to cell metabolism, which holds significance in assessing the pathogenesis of psychiatric disorders and further research in this inflammasome complex might uncover peripheral markers associated with METH use for assessing major depressive disorders. Furthermore, a better understanding of the link between METH use in the younger years, and its consequence to health outcomes in the long term (after METH has been stopped) in regard to increased risk of communicable and non-communicable diseases and accelerating the ageing process are required.

### **Contributors**

Marco Papageorgiou wrote the article under the guidance of the other four authors.

All authors edited and reviewed the article.

### **Conflict of interest**

The authors declare they have no conflict of interest.

#### **Funding**

General financial support was provided by Victoria University.

#### **Ethical approval**

No ethics was required for this review article.

#### **Provenance and peer review**

This article has undergone peer review.

## References

- [1] C.C. Cruickshank, K.R. Dyer, A review of the clinical pharmacology of methamphetamine, *Addiction* 104 (2009) 1085–1099.
- [2] R. McKetin, D.I. Lubman, J.M. Najman, S. Dawe, P. Butterworth, A.L. Baker, Does methamphetamine use increase violent behaviour? Evidence from a prospective longitudinal study, *Addiction* 109 (2014) 798–806.
- [3] R. McKetin, O.M. Dean, A.L. Baker, G. Carter, A. Turner, P.J. Kelly, et al., A potential role for N-acetylcysteine in the management of methamphetamine dependence, *Drug Alcohol Rev.* 36 (2017) 153–159.
- [4] L. Degenhardt, A. Roxburgh, E. Black, R. Bruno, G. Campbell, S. Kinner, et al., The epidemiology of methamphetamine use and harm in Australia, *Drug Alcohol Rev.* 27 (2008) 243–252.
- [5] A.V. Rebecca McKetin, Richard Burns, *Research into Methamphetamine Use in the Australian Capital Territory*, National Drug Research Institute, Curtin University, Perth, Western Australia, 2017.
- [6] K.M. Grant, T.D. LeVan, S.M. Wells, M. Li, S.F. Stoltenberg, H.E. Gendelman, et al., Methamphetamine-associated psychosis, *J. Neuroimmune Pharmacol.* 7 (2012) 113–139.
- [7] A. Roche, A. McEntee, Ice and the outback: patterns and prevalence of methamphetamine use in rural Australia, *Aust. J. Rural Health* 25 (2017) 200–209.
- [8] J.L. Montoya, J. Cattie, E. Morgan, S.P. Woods, M. Cherner, D.J. Moore, et al., The impact of age, HIV serostatus and seroconversion on methamphetamine use, *Am. J. Drug Alcohol Abuse* 42 (2016) 168–177.
- [9] A. Mukherjee, B.A. Dye, J. Clague, T.R. Belin, V. Shetty, Methamphetamine use and oral health-related quality of life, *Qual. Life Res.* 27 (12) (2018) 3179–3190.
- [10] S.A. Larson, R. Desai, F.R. Kates, Concerns about heroin, cocaine and methamphetamine: prevalence and correlates of at-risk users from 2015 National Survey on Drug Use and Health, *J. Subst. Use* (2018) 1–6.
- [11] Alasdair M. Barr, G. William MacEwan, Allen E. Thornton, William G. Honer, Tania Lecomte, The need for speed: an update on methamphetamine addiction, *J. Psychiatry Neurosci.* 31 (2006) 301–313.
- [12] U. Sriram, B. Haldar, J.M. Cenna, L. Gofman, R. Potula, Methamphetamine mediates immune dysregulation in a murine model of chronic viral infection, *Front. Microbiol.* (2015) 6.
- [13] G.A. Cabral, Drugs of abuse, immune modulation, and AIDS, *J. Neuroimmune Pharmacol.* 1 (2006) 280–295.
- [14] J.M. Loftis, D. Choi, W. Hoffman, M.S. Huckans, Methamphetamine causes persistent immune dysregulation: a cross-species, translational report, *Neurotox. Res.* 20 (2010) 59–68.

- [15] H. Peerzada, J.A. Gandhi, A.J. Guimaraes, J.D. Nosanchuk, L.R. Martinez, Methamphetamine administration modifies leukocyte proliferation and cytokine production in murine tissues, *Immunobiology*. 218 (2013) 1063–1068.
- [16] Supriya D. Mahajan, Z. Hu, Jessica L. Reynolds, Ravikumar Aalinkeel, Stanley A. Schwartz, Madhavan P.N. Nair, Methamphetamine modulates gene expression patterns in monocyte derived mature dendritic cells, *Mo. Diagn. Ther.* 10 (2006) 257–269.
- [17] A. Burns, P. Ciborowski, Acute exposure to methamphetamine alters TLR9-mediated cytokine expression in human macrophage, *Immunobiology* 221 (2016) 199–207.
- [18] V. Coelho-Santos, R.A. Leitão, F.L. Cardoso, I. Palmela, M. Rito, M. Barbosa, et al., The TNF- $\alpha$ /Nf- $\kappa$ B signaling pathway has a key role in methamphetamine-induced blood-brain barrier dysfunction, *J. Cereb. Blood Flow Metabol.* 35 (2015) 1260–1271.
- [19] J. Gonçalves, T. Martins, R. Ferreira, N. Milhazes, F. Borges, C.F. Ribeiro, et al., Methamphetamine-induced early increase of IL-6 and TNF- $\alpha$  mRNA expression in the mouse brain, *Ann. New York Acad. Sci.* 1139 (2008) 103–111.
- [20] R. Harms, B. Morsey, C.W. Boyer, H.S. Fox, N. Sarvetnick, Methamphetamine administration targets multiple immune subsets and induces phenotypic alterations suggestive of immunosuppression, *PLoS One* 7 (2012) e49897.
- [21] Joshua D. Rosenblat, Rodrigo B. Mansur, Roger S. McIntyre, Inflamed moods: a review of the interactions between inflammation and mood disorders, *Progress Neuro-Psychopharmacol. Biol. Psychiatry* 53 (2014) 23–34.
- [22] Frederic Geissmann, Steffen Jung, Michael H. Sieweke, Miriam Merad, Klaus Ley, Development of monocytes, macrophages, and dendritic cells, *Science* 327 (2010) 656–661.
- [23] P.J. Gaskill, T.M. Calderon, J.S. Coley, J.W. Berman, Drug induced increases in CNS dopamine alter monocyte, macrophage and t cell functions: implications for HAND, *J. Neuroimm. Pharmacol.* 8 (2013) 621–642.
- [24] M.D. Prakash, K. Tangalakis, J. Antonipillai, L. Stojanovska, K. Nurgali, V. Apostolopoulos, Methamphetamine: effects on the brain, gut and immune system, *Pharmacol. Res.* 120 (2017) 60–67.
- [25] X. Liu, P.S. Silverstein, V. Singh, A. Shah, N. Qureshi, A. Kumar, Methamphetamine increases LPS-mediated expression of IL-8, TNF-alpha and IL1beta in human macrophages through common signaling pathways, *PLoS One* 7 (2012) e33822.
- [26] Jessica B. Buchanan, Rodney W. Johnson, A neurotoxic regimen of methamphetamine exacerbates the febrile and neuroinflammatory response to a subsequent peripheral immune stimulus, *J. Neuroinflamm.* 7 (2010).
- [27] J.L. Reynolds, W.C. Law, S.D. Mahajan, R. Aalinkeel, B. Nair, D.E. Sykes, et al., Nanoparticle based galectin-1 gene silencing, implications in

- methamphetamine regulation of HIV-1 infection in monocyte derived macrophages, *J. Neuroimm. Pharmacol.* 7 (2012) 673–685.
- [28] A.M. Dudek, S. Martin, A.D. Garg, P. Agostinis, Immature, semi-mature, and fully mature dendritic cells: toward a DC-Cancer cells interface that augments anticancer immunity, *Front. Immunol.* 4 (2013).
- [29] M.P.N. Nair, Z.M. Saiyed, N. Nair, N.H. Gandhi, J.W. Rodriguez, N. Boukli, et al., Methamphetamine enhances HIV-1 infectivity in monocyte derived dendritic cells, *J. Neuroimm. Pharmacol.* 4 (2008) 129–139.
- [30] A.K. Ankit Shah, Methamphetamine-mediated endoplasmic reticulum (ER) stress induces type-1 programmed cell death in astrocytes via ATF6, IRE1a and PERK pathways, *Oncotarget* 7 (2016).
- [31] R. Groom Joanna, J. Richmond, T. Murooka Thomas, W. Sorensen Elizabeth, H. Sung Jung, K. Bankert, et al., CXCR3 chemokine receptor-ligand interactions in the lymph node optimize CD4+ t helper 1 cell differentiation, *Immunity* 37 (2012) 1091–1103.
- [32] R. Potula, B. Halder, J.M. Cenna, U. Sriram, S. Fan, Methamphetamine alters T cell cycle entry and progression: role in immune dysfunction, *Cell Death Discov.* 4 (2018).
- [33] Qiao D.-F. Du S-H, C.-X. Chen, S. Chen, C. Liu, Z. Lin, et al., Toll-like receptor 4 mediates methamphetamine-induced neuroinflammation through Caspase-11 signaling pathway in astrocytes, *Front. Mol. Neurosci.* 10 (2017).
- [34] R. Potula, B.J. Hawkins, J.M. Cenna, S. Fan, H. Dykstra, S.H. Ramirez, et al., Methamphetamine causes mitochondrial oxidative damage in human t lymphocytes leading to functional impairment, *J. Immunol.* 185 (2010) 2867–2876.
- [35] C. Tomescu, F.-M. Duh, M.A. Lanier, A. Kapalko, K.C. Mounzer, M.P. Martin, et al., Increased plasmacytoid dendritic cell maturation and natural killer cell activation in HIV-1 exposed, uninfected intravenous drug users, *Aids* 24 (2010) 2151–2160.
- [36] M.C.G. Marcondes, C. Flynn, D.D. Watry, M. Zandonatti, H.S. Fox, Methamphetamine increases brain viral load and activates natural killer cells in simian immunodeficiency virus-infected monkeys, *Am. J. Pathol.* 177 (2010) 355–361.
- [37] E. Aktas, U.C. Kucuksezer, S. Bilgic, G. Erten, G. Deniz, Relationship between CD107a expression and cytotoxic activity, *Cell Immunol.* 254 (2009) 149–154.
- [38] F.C. YANG, K. AGEMATSU, T. Nakazawa, T. MORI, S.I.T.O.T. KOBATA, C. Morimotoj, A. Komiyama, CD27/CD70 interaction directly induces natural killer cell killing activity, *Immunology* 88 (1996) 289–293.
- [39] N. Bortell, L. Basova, S. Semenova, H.S. Fox, T. Ravasi, M.C. Marcondes, Astrocytespecific overexpressed gene signatures in response to methamphetamine exposure in vitro, *J. Neuroinflamm.* 14 (2017) 49.

- [40] E.J. Sanderlin, N.R. Leffler, K. Lertpiriyapong, Q. Cai, H. Hong, V. Bakthavatchalu, et al., GPR4 deficiency alleviates intestinal inflammation in a mouse model of acute experimental colitis, *Biochim. Biophys. Acta (BBA) – Mol. Basis Dis.* 1863 (2017) 569–584.
- [41] T.-V. Tran, E.-J. Shin, L.T.T. Nguyen, Y. Lee, D.-J. Kim, J.H. Jeong, et al., Protein kinase C $\delta$  gene depletion protects against methamphetamine-induced impairments in recognition memory and ERK1/2 signaling via upregulation of glutathione Peroxidase-1 gene, *Mol. Neurobiol.* 55 (5) (2018) 4136–4159.
- [42] V. Soontornniyomkij, J.P. Kesby, E.E. Morgan, A. Bischoff-Grethe, A. Minassian, G.G. Brown, et al., Effects of HIV and methamphetamine on brain and behavior: evidence from human studies and animal models, *J. Neuroimm. Pharmacol.* 11 (2016) 495–510.
- [43] Treadway JCFaMT, Inflammation effects on motivation and motor activity: role of dopamine, *Neuropsychopharmacology* 42 (2017) 216–241.
- [44] T. Horiuchi, H. Mitoma, Harashima Si, H. Tsukamoto, T. Shimoda, Transmembrane TNF-: structure, function and interaction with anti-TNF agents, *Rheumatology* 49 (2010) 1215–1228.
- [45] W.M. Chu, Tumor necrosis factor, *Cancer Lett.* 328 (2013) 222–225.
- [46] C.A. Dinarello, Overview of the IL-1 family in innate inflammation and acquired immunity, *Immunol. Rev.* 281 (2018) 8–27.
- [47] T. Kawai, S. Akira, Signaling to NF- $\kappa$ B by toll-like receptors, *Trends Mol. Med.* 13 (2007) 460–469.
- [48] J.A. Roman-Blas, S.A. Jimenez, NF-kappaB as a potential therapeutic target in osteoarthritis and rheumatoid arthritis, *Osteoarthr. Cartil.* 14 (2006) 839–848.
- [49] Kenneth B. Marcu, M. Otero, Eleonora Olivotto, Rosa Maria Borzi, B. Mary, Goldring. NF- $\kappa$ B signaling: multiple angles to target OA, *Curr Drug Targets* 11 (2010) 599–613.
- [50] Cheng SSIaG, Role of interleukin 10 transcriptional regulation in inflammation and autoimmune disease, *Crit. Rev. Immunol.* 32 (2012) 23–63.
- [51] E.O. Glocker, D. Kotlarz, K. Boztug, E.M. Gertz, A.A. Schaffer, F. Noyan, et al., Inflammatory bowel disease and mutations affecting the interleukin-10 receptor, *N. Engl. J. Med.* 361 (2009) 2033–2045.
- [52] Nicole C. Fernandes, U. Sriram, Larisa Gofman, Jonathan M. Cenna, Servio H. Ramirez, Raghava Potula, Methamphetamine alters microglial immune function through P2X7R signaling, *J. Neuroinflamm.* 13 (2016).
- [53] J. Yan, M.J. Smyth, M.W.L. Teng, Interleukin (IL)-12 and IL-23 and their conflicting roles in Cancer, *Cold Spring Harb. Perspect. Biol.* 10 (2018).
- [54] Katrina Gee, C. Guzzo, Nor Fazila Che Mat, Wei Ma, Ashok Kumar, The IL-12 family of cytokines in infection, inflammation and autoimmune disorders, *Inflamm. Allergy - Drug Targets* 8 (2009) 40–52.
- [55] V.V. Pop, A. Seicean, I. Lupan, G. Samasca, C.C. Burz, IL-6 roles - molecular pathway and clinical implication in pancreatic cancer - a systemic review, *Immunol. Lett.* 181 (2017) 45–50.
- [56] H. Ghasemi, Roles of IL-6 in ocular inflammation: a review, *Ocular Immunol.*

- Inflamm. 26 (2017) 37–50.
- [57]K.S.P. Lai, C.S. Liu, A. Rau, K.L. Lanctot, C.A. Kohler, M. Pakosh, et al., Peripheral inflammatory markers in Alzheimer’s disease: a systematic review and metaanalysis of 175 studies, *J. Neurol. Neurosurg. Psychiatry* 88 (2017) 876–882.
- [58]J.Ga Vanessa Coelho-Santos, Carlos Fontes-Ribeiro, Ana Paula Silva, Prevention of methamphetamine-induced microglial cell death by TNF- $\alpha$  and IL-6 through activation of the JAK-STAT pathway, *J. Neuroinflamm.* 9 (2012).
- [59]W.J. Jin, B. Kim, D. Kim, H.Y. Park Choo, H.H. Kim, H. Ha, et al., NF-kappaB signaling regulates cell-autonomous regulation of CXCL10 in breast cancer 4T1 cells, *Exp. Mol. Med.* 49 (2017) e295.
- [60]Q. Wang, L.W. Wei, H.Q. Xiao, Y. Xue, Liu Y.G. Du SH, et al., Methamphetamine induces hepatotoxicity via inhibiting cell division, arresting cell cycle and activating apoptosis: in vivo and in vitro studies, *Food Chem. Toxicol.* 105 (2017) 61–72.
- [61]N. Bortell, B. Morsey, L. Basova, H.S. Fox, M.C. Marcondes, Phenotypic changes in the brain of SIV-infected macaques exposed to methamphetamine parallel macrophage activation patterns induced by the common gamma-chain cytokine system, *Front. Microbiol.* 6 (2015) 900.
- [62]P.S.S. Ankit Shah, Dharendra P. Singh, Anil Kumar, Involvement of metabotropic glutamate receptor 5, AKT/PI3K Signaling and NF- $\kappa$ B pathway in methamphetamine-mediated increase in IL-6 and IL-8 expression in astrocytes, *J. Neuroinflamm.* 9 (2012).
- [63]M. Huckans, B.E. Fuller, A.L. Chalker, M. Adams, J.M. Loftis, Plasma inflammatory factors are associated with anxiety, depression, and cognitive problems in adults with and without methamphetamine dependence: an exploratory protein array study, *Front. Psychiatry* 6 (2015) 178.
- [64]N.A. Northrop, B.K. Yamamoto, Cyclooxygenase activity contributes to the monoaminergic damage caused by serial exposure to stress and methamphetamine, *Neuropharmacology* 72 (2013) 96–105.
- [65]D.M. Thomas, D.M. Kuhn, MK-801 and dextromethorphan block microglial activation and protect against methamphetamine-induced neurotoxicity, *Brain Res.* 1050 (2005) 190–198.
- [66]K. Permpoonputtana, P. Govitrapong, The anti-inflammatory effect of melatonin on methamphetamine-induced proinflammatory mediators in human neuroblastoma dopamine SH-SY5Y cell lines, *Neurotox. Res.* 23 (2013) 189–199.
- [67]M. Asanuma, Methamphetamine-induced neurotoxicity in mouse brain is attenuated by ketoprofen, a non-steroidal anti-inflammatory drug, *Neurosci. Lett.* (2003).
- [68]P.S. Silverstein, A. Shah, R. Gupte, X. Liu, R.W. Piepho, S. Kumar, et al., Methamphetamine toxicity and its implications during HIV-1 infection, *J.*

- NeuroVirol. 17 (2011) 401–415.
- [69] A.R. Jackson, A. Shah, A. Kumar, Methamphetamine alters the normal progression by inducing cell cycle arrest in astrocytes, *PLoS One* 9 (2014) e109603.
- [70] G. Pendyala, R. Zhu, T. Yang, F. Kobeissy, T.H. Mouhieddine, M. Raad, et al., The effect of chronic methamphetamine exposure on the hippocampal and olfactory bulb neuroproteomes of rats, *PLoS One* 11 (2016).
- [71] K.M. Sepuru, K.M. Poluri, K. Rajarathnam, Solution structure of CXCL5—a novel chemokine and adipokine implicated in inflammation and obesity, *PLoS One* 9 (2014) e93228.
- [72] J.L. Reynolds, S.D. Mahajan, D.E. Sykes, S.A. Schwartz, M.P.N. Nair, Proteomic analyses of methamphetamine (METH)-induced differential protein expression by immature dendritic cells (IDC), *Biochim. Biophys. Acta (BBA) - Proteins Proteom.* 1774 (2007) 433–442.
- [73] M. Serasanambati, S.R. Chilakapati, Function of nuclear factor kappa B (NF- $\kappa$ B) in human diseases—a review, *South Indian J. Biolog. Sci.* 2 (2016).
- [74] S.-C. Sun, The non-canonical NF- $\kappa$ B pathway in immunity and inflammation, *Nat. Rev. Immunol.* 17 (2017) 545–558.
- [75] T. Shabab, R. Khanabdali, S.Z. Moghadamtousi, H.A. Kadir, G. Mohan, Neuroinflammation pathways: a general review, *Int. J. Neurosci.* 127 (2016) 624–633.
- [76] R.G. Baker, M.S. Hayden, S. Ghosh, NF- $\kappa$ B, inflammation, and metabolic disease, *Cell Metab.* 13 (2011) 11–22.
- [77] F.C. Li, J.C. Yen, S.H. Chan, A.Y. Chang, Bioenergetics failure and oxidative stress in brain stem mediates cardiovascular collapse associated with fatal methamphetamine intoxication, *PLoS One* 7 (2012) e30589.
- [78] S.E. Nennig, J.R. Schank, The role of NF $\kappa$ B in drug addiction: beyond inflammation, *Alcohol Alcohol.* (2017).
- [79] B.H. Yong Woo Lee, Jin Yao, Michal Toborek, Methamphetamine induces AP-1 and NF- $\kappa$ B binding and transactivation in human brain endothelial cells, *J. of Neurosci. Res.* 66 (2001) 583–591.
- [80] Y. Zhang, G. Shu, Y. Bai, J. Chao, X. Chen, H. Yao, Effect of methamphetamine on the fasting blood glucose in methamphetamine abusers, *Metab. Brain Dis.* (2018).
- [81] B.P. Sokolov, J.L. Cadet, Methamphetamine causes alterations in the MAP kinase-related pathways in the brains of mice that display increased aggressiveness, *Neuropsychopharmacology* 31 (2005) 956–966.
- [82] J.-H. Park, Y.H. Seo, J.-H. Jang, C.-H. Jeong, S. Lee, B. Park, Asiatic acid attenuates methamphetamine-induced neuroinflammation and neurotoxicity through blocking of NF- $\kappa$ B/STAT3/ERK and mitochondria-mediated apoptosis pathway, *J. Neuroinflamm.* 14 (2017).

- [83]L.-M. Mao, J.M. Reusch, E.E. Fibuch, Z. Liu, J.Q. Wang, Amphetamine increases phosphorylation of MAPK/ERK at synaptic sites in the rat striatum and medial prefrontal cortex, *Brain Res.* 1494 (2013) 101–108.
- [84]Y.-N. Huang, C.-H. Wu, T.-C. Lin, J.-Y. Wang, Methamphetamine induces heme oxygenase-1 expression in cortical neurons and glia to prevent its toxicity, *Toxicol. Appl. Pharmacol.* 240 (2009) 315–326.
- [85]P.W. Chu, K.S. Seferian, E. Birdsall, J.G. Truong, J.A. Riordan, C.S. Metcalf, et al., Differential regional effects of methamphetamine on dopamine transport, *Eur. J. Pharmacol.* 590 (2008) 105–110.
- [86]E. Valjent, J.C. Corvol, J.M. Trzaskos, J.A. Girault, D. Herve, Role of the ERK pathway in psychostimulant-induced locomotor sensitization, *BMC Neurosci.* 7 (2006) 20.
- [87]J. Dan Dunn, L.A.J. Alvarez, X. Zhang, T. Soldati, Reactive oxygen species and mitochondria: a nexus of cellular homeostasis, *Redox Biol.* 6 (2015) 472–485.
- [88]C.R. Weston, R.J. Davis, The JNK signal transduction pathway, *Curr. Opin. Cell Biol.* 19 (2007) 142–149.
- [89]Subramaniam Jayanthi, M.T. McCoy, B. Ladenheim, JeanLud Cadet, Methamphetamine causes coordinate regulation of Src, Cas, Crk, and the jun Nterminal kinase–Jun pathway, *Mol. Pharmacol.* 61 (2002) 1124–1131.
- [90]T. Yan, L. Li, B. Sun, F. Liu, P. Yang, T. Chen, et al., Luteolin inhibits behavioral sensitization by blocking methamphetamine-induced MAPK pathway activation in the caudate putamen in mice, *PLoS One* 9 (2014) e98981.
- [91]Jiraporn Tocharus, C. Khonthun, Sukumal Chongthammakun, Piyarat Govitrapong, Melatonin attenuates methamphetamine-induced overexpression of pro-inflammatory cytokines in microglial cell lines, *J. Pineal Res.* 48 (2010) 347–352.
- [92]B.T. Hennessy, D.L. Smith, P.T. Ram, Y. Lu, G.B. Mills, Exploiting the PI3K/AKT pathway for cancer drug discovery, *Nat. Rev. Drug Discov.* 4 (2005) 988–1004.
- [93]T.F. Rau, A. Kothiwala, L. Zhang, S. Ulatowski, S. Jacobson, D.M. Brooks, et al., Low dose methamphetamine mediates neuroprotection through a PI3K-AKT pathway, *Neuropharmacology* 61 (2011) 677–686.
- [94]T. Niu, J. Li, J. Wang, J.Z. Ma, M.D. Li, Identification of novel signal transduction, immune function, and oxidative stress genes and pathways by topiramate for treatment of methamphetamine dependence based on secondary outcomes, *Front. Psychiatry* 8 (2017).
- [95]P.J. Murray, The JAK-STAT signaling pathway: input and output integration, *J. Immunol.* 178 (2007) 2623–2629.
- [96]J. Vier, M. Groth, M. Sochalska, S. Kirschnek, The anti-apoptotic Bcl-2 family protein A1/Bfl-1 regulates neutrophil survival and homeostasis and is controlled via PI3K and JAK/STAT signaling, *Cell Death Dis.* 7 (2016) e2103-e..

- [97] S.A. Najafi Khadije, Mahdi Rahpeyma, Habibolah Khazaie, Asad Vaisi-Raygani, Ali Moini, Amir Kiani, Study of serum malondialdehyde level in opioid and methamphetamine dependent patients, *Acta Med. Iran.* 55 (2017).
- [98] P. Melo, A. Magalhaes, C.J. Alves, M.A. Tavares, L. de Sousa, T. Summavielle, et al., Methamphetamine mimics the neurochemical profile of aging in rats and impairs recognition memory, *Neurotoxicology* 33 (2012) 491–499.
- [99] R. García-Cabrerizo, M.J. García-Fuster, Comparative effects of amphetamine-like psychostimulants on rat hippocampal cell genesis at different developmental ages, *NeuroToxicology* 56 (2016) 29–39.
- [100] T. Ye, H. Pozos, T.J. Phillips, A. Izquierdo, Long-term effects of exposure to methamphetamine in adolescent rats, *Drug Alcohol Depend.* 138 (2014) 17–23.
- [101] C. Franceschi, J. Campisi, Chronic inflammation (inflammaging) and its potential contribution to age-associated diseases, *J. Gerontol. A Biol. Sci. Med. Sci.* 69 (Suppl. 1) (2014) S4–S9.
- [102] B.T. Winslow, K.I. Voorhees, K.A. Pehl, Methamphetamine abuse, *Am. Family Phys.* 76 (2007) 1169–1174.
- [103] K.J. Varner, B.A. Ogden, J. Delcarpio, S. Meleg-Smith, Cardiovascular responses elicited by the "binge" administration of methamphetamine, *J. Pharmacol. Exp. Ther.* 301 (2002) 152–159.
- [104] B.L. Henry, A. Minassian, W. Perry, Effect of methamphetamine dependence on heart rate variability, *Addict. Biol.* 17 (2012) 648–658.
- [105] J.P.H. Tan, J.E. Beilharz, U. Vollmer-Conna, E. Cvejic, Heart rate variability as a marker of healthy ageing, *Int. J. Cardiol.* 5273 (18) (2018) 31925–31929.
- [106] S. Schurer, K. Klingel, M. Sandri, N. Majunke, C. Besler, R. Kandolf, et al., Clinical characteristics, histopathological features, and clinical outcome of methamphetamine-associated cardiomyopathy, *JACC Heart Fail.* 5 (2017) 435–445.
- [107] E.S. Nakou, F.I. Parthenakis, E.M. Kallergis, M.E. Marketou, K.S. Nakos, P.E. Vardas, Healthy aging and myocardium: a complicated process with various effects in cardiac structure and physiology, *Int. J. Cardiol.* 209 (2016) 167–175.
- [108] L. Chen, P. Yu, L. Zhang, Y. Zou, Y. Zhang, L. Jiang, et al., Methamphetamine exposure induces neuropathic protein beta-Amyloid expression, *Toxicol. Vitro: Int. J. Publ. Assoc. BIBRA* 54 (2018) 304–309.
- [109] K.J. Wirth, Role of noradrenergic brain nuclei in the regulation of carotid artery blood flow: pharmacological evidence from anesthetized pigs with Alpha-2 adrenergic receptor modulator drugs, *J. Alzheimer's Dis.: JAD* 66 (2018) 407–419.
- [110] R. Hardeland, Recent findings in melatonin research and their relevance to the CNS, *Centr. Nerv. Syst. Agents Med. Chem.* 18 (2018) 102–114.

- [111] R.L. Good, R.A. Radcliffe, Methamphetamine-induced locomotor changes are dependent on age, dose and genotype, *Pharmacol. Biochem. Behav.* 98 (2011) 101–111.
- [112] Butler B. JG-G, P. Prins, A. North, J.T. Clarke, H. Khoshbouei, Chronic methamphetamine increases alpha-synuclein protein levels in the striatum and Hippocampus but not in the cortex of juvenile mice, *J. Addict. Prev.* 2 (2014).
- [113] B. Thrash, K. Thiruchelvan, M. Ahuja, V. Suppiramaniam, M. Dhanasekaran, Methamphetamine-induced neurotoxicity: the road to Parkinson's disease, *Pharmacol. Rep.* 61 (2009) 966–977.
- [114] C. Evren, M. Bozkurt, Update on methamphetamine: an old problem that we have recently encountered, *Dusunen Adam: J. Psychiatry Neurol. Sci.* 31 (2018) 1–10.
- [115] W.J. Panenka, R.M. Procyshyn, T. Lecomte, G.W. MacEwan, S.W. Flynn, W.G. Honer, et al., Methamphetamine use: a comprehensive review of molecular, preclinical and clinical findings, *Drug Alcohol Depend.* 129 (2013) 167–179.
- [116] Rebecca McKetin, D.I. Lubman, Nicole M. Lee, Joanne E. Ross, Tim N. Slade, Major depression among methamphetamine users entering drug treatment programs, *MJA* 195 (2011).
- [117] H. Nakama, L. Chang, G. Fein, R. Shimotsu, C.S. Jiang, T. Ernst, Methamphetamine users show greater than normal age-related cortical gray matter loss, *Addiction* 106 (2011) 1474–1483.
- [118] K. McDonnell-Dowling, J.P. Kelly, The role of oxidative stress in methamphetamine-induced toxicity and sources of variation in the design of animal studies, *Curr. Neuropharmacol.* 15 (2017) 300–314.
- [119] J.E. Morley, Richard N. Baumgartner, Cytokine-related aging process, *J. Gerontol.* 59A (2004) 924–929.
- [120] C.R. Gomez, J. Karavitis, J.L. Palmer, D.E. Faunce, L. Ramirez, V. Nomellini, et al., Interleukin-6 contributes to age-related alteration of cytokine production by macrophages, *Mediat. Inflamm.* 2010 (2010) 1–7.
- [121] S. Xia, X. Zhang, S. Zheng, R. Khanabdali, B. Kalionis, J. Wu, et al., An update on inflamm-aging: mechanisms, prevention, and treatment, *J. Immunol. Res.* 2016 (2016) 8426874.
- [122] G. Astarita, A. Avanesian, B. Grimaldi, N. Realini, Z. Justinova, L.V. Panlilio, et al., Methamphetamine accelerates cellular senescence through stimulation of de novo ceramide biosynthesis, *PLoS One* 10 (2015) e0116961.
- [123] K. Bachi, S. Sierra, N.D. Volkow, R.Z. Goldstein, N. Alia-Klein, Is biological aging accelerated in drug addiction? *Curr. Opin. Behav. Sci.* 13 (2017) 34–39.
- [124] Z. Yang, J. Ye, C. Li, D. Zhou, Q. Shen, J. Wu, et al., Drug addiction is associated with leukocyte telomere length, *Sci. Rep.* 3 (2013) 1542.
- [125] D.A. Tipton, Z.T. Legan, M.K. Dabbous, Methamphetamine cytotoxicity and effect on LPS-stimulated IL-1 $\beta$  production by human monocytes, *Toxicol. Vitro* 24 (2010) 921–927.

- [126] M.M. Mata, T.C. Napier, S.M. Graves, F. Mahmood, S. Raeisi, L.L. Baum, Methamphetamine decreases CD4 T cell frequency and alters pro-inflammatory cytokine production in a model of drug abuse, *Eur. J. Pharmacol.* 752 (2015) 26–33.
- [127] Masayoshi Saito, M. Terada, Tetsuya Kawata, Hisao, Naoyuki Shigematsu, Pudcharaporn Kromkhun, Makoto Yokosuka, Toru R. Saito, Effects of single or repeated administrations of methamphetamine on immune response in mice, *Exp. Anim.* 57 (2008) 35–43.
- [128] K.Y. Hiroyuki Mizoguchi, Makoto Mizuno, Tomoko Mizuno, Atsumi Nitta, a T.N. Yukihiro Noda, Regulations of methamphetamine reward by extracellular signal-regulated kinase 1/2/ets-Like Gene-1 signaling pathway via the activation of dopamine receptors, *Mol. Pharmacol.* 65 (2004) 1293–1301.
- [129] J.L. Cadet, Epigenetics of stress, addiction, and resilience: therapeutic implications, *Mol. Neurobiol.* 53 (2014) 545–560.
- [130] Galbraith N. (2015). The methamphetamine problem: Commentary on ... Psychiatric morbidity and socio-occupational dysfunction in residents of a drug rehabilitation centre. *BJPsych bulletin*, 39(5), 218–220. <https://doi.org/10.1192/pb.bp.115.050930>
- [131] McKetin R, Kozel N, Douglas J, et al. The rise of methamphetamine in Southeast and East Asia. *Drug Alcohol Rev.* 2008;27(3):220-228. doi:10.1080/09595230801923710
- [132] Sun, L., He, C., Nair, L., Yeung, J., & Egwuagu, C. E. (2015). Interleukin 12 (IL-12) family cytokines: Role in immune pathogenesis and treatment of CNS autoimmune disease. *Cytokine*, 75(2), 249–255. <https://doi.org/10.1016/j.cyto.2015.01.030>
- [133] Croxford, Andrew & Kulig, Paulina & Becher, Burkhard. (2014). IL-12- and IL-23 in health and disease. *Cytokine & growth factor reviews*. 25. 10.1016/j.cytogfr.2014.07.017.
- [134] Tanaka, T., Narazaki, M., & Kishimoto, T. (2014). IL-6 in inflammation, immunity, and disease. *Cold Spring Harbor perspectives in biology*, 6(10), a016295. <https://doi.org/10.1101/cshperspect.a016295>

## Chapter 2

### Chronic Methamphetamine (METH) and withdrawal effects on distal colon tissue in an escalating-dose mouse model

---

#### Abstract

Methamphetamine (METH) is a powerful drug which causes considerable body, brain and behavioural alterations. Further, METH acts on a variety of systems within the body which are yet to be fully described. Research in the effects of METH on the gastrointestinal tract, gut-brain axis and immune system is still unclear and in early stages. This study sought to determine the effects of an escalating METH dose on C57BL/6 mice over a three-week period, followed by a withdrawal period of three days. Distal mouse colon was extracted and RNA-Seq data, via gene ontological software programs: DAVID, Gorilla and Amigo, showed a number of gene changes across several processes. The largest genes changes observed were traced to carboxylic acid metabolism, biological process, and response to bacterium gene ontologies. Moderate and minor fold gene changes were observed in neuropeptide signalling, and exogenous catabolic processing. More specifically, significantly upregulated, differentially expressed genes (DEG) included Leptin (*Lep*), caudal type homobox 2 (*cdx2*), gamma-glutamyltransferase 1 (*Ggt1*), adiponectin (*adipoq*), cytochrome P450 Family 2 Subfamily E member 1 (*cyp2e1*), angiopoietin (*Ang4*) and resistin like beta (*retnlb*). Significantly down-regulated DEG included actinin alpha 2 (*actn2*) (-30-fold) and myosin light chain, phosphorylatable, fast skeletal muscle (*mylpf*) (-81-fold). Fold-change genes, from this escalating METH mouse model indicates that METH plays a role across several ontological systems.

## Table of contents

<b>1.0 Introduction</b> .....	40-42
<b>2.0 Materials and Methods</b> .....	42-47
2.1 Chronic METH mouse model.....	42
2.2 RNA extraction.....	43-44
2.3 RNA concentrations and quality control .....	44-45
2.4 High throughput RNA-Sequencing of mRNA .....	45-47
<b>3.0 Results</b> .....	48-88
3.1 Differentially expressed tight junction and leukocyte trans-endothelial migration (LTM) genes are altered by METH in the distal colon.....	64
3.2 METH causes gene expression changes in serotonergic synapses.....	67
3.3 Gene ontology of METH shows genes enriched in cytokine-cytokine receptor interactions .....	69
3.4 Genes associated with METH are enriched across several ontological terms in Gorilla.....	74
3.5 METH induces changes to genes enriched in the molecular function GO:0004497 monooxygenase activity category.....	82
3.6 METH induces changes to receptor regulatory, receptor ligand and hormone activity .....	85
3.7 Genes involved in placenta development are differentially expressed in a chronic METH withdrawal mouse model.....	86
3.8 METH effects genes involved in the neuropeptide signalling pathway (GO: 0007218).....	87
<b>4.0 Discussion</b> .....	89-101
4.1 Tight junctions and METH.....	91
4.2 METH involvement in Serotonergic synapses .....	92
4.3 Cytokine-cytokine receptor interactions caused by METH .....	93
4.4 Placental and blood vessel development .....	96
4.5 Neuropeptide signalling.....	97
4.6 Bacterial responses to METH.....	99
<b>Conclusion</b> .....	102-103
<b>References</b> .....	104-112

## Tables and Figures

### 2.1 Chronic METH mouse model

**Table 1.** Chronic methamphetamine administration protocol.

### 2.4 High throughput RNA-Sequencing of mRNA

**Figure 1.** Illustrative summary of RNA extraction and subsequent RNA purification, and bioinformational analysis.

## 3.0 Results

**Figure 2.** Workflow of NGS data filtering to gene ontologies

**Table 2.** Summary of 560 genes reported by DAVID Bioinformatics Resource 6.8 against a *mus musculus* background reference gene set.

**Figure 3.** Figure 3. Diagrammatic representation of the colon and gene ontological processes.

**Table 3.** KEGG pathway annotation

**Table 4.** Functional Annotation of functional categories.

**Figure 4:** Frequency of genes enriched in the functional gene ontology

**Table 5.** Functional annotation of Gene Ontology as annotated by reference to Goterms\_CC\_Direct

**Figure 5.** Frequency of genes enriched in functional gene ontology from Goterms\_CC\_Direct.

### 3.1 Differentially expressed tight junction and leukocyte trans-endothelial migration (LTM) genes are altered by METH in the distal colon.

**Figure 6.** Tight junction genes.

**Figure 7.** Leukocyte trans-endothelial migration (LTM).

### 3.2 METH causes differential gene expression changes in serotonergic synapses.

**Figure 8.** KEGG pathway of serotonergic synapses.

### **3.3 Gene ontology of METH shows genes enriched in cytokine-cytokine receptor interactions.**

**Table 6.** Summary of differentially expressed genes (DEG) from METH gene set.

**Figure 9A.** Cytokine-cytokine receptor interaction map, highlighting the chemokine subfamilies: CC, and CX

**Figure 9B.** Class II helical cytokines.

**Figure 9C.** TNF family-related genes

### **3.4 Genes associated with METH are enriched across several ontological terms in Gorilla**

**Table 7.** Biological process as retrieved from the Gorilla GO

**Figure 10.** GO term response to bacterium

**Figure 11.** Go term fatty acid metabolic process.

**Figure 12.** GO term neuropeptide signalling pathway.

**Figure 13.** Go term monocarboxylic acid metabolic process

**Figure 14.** GO term blood vessel development.

**Figure 15.** GO term placenta development.

**Figure 16.** GO term exogenous drug catabolic process.

**Figure 17.** Flow chart and heat map indicating biological process.

**Table 8.** Molecular function as annotated by Gorilla.

**Figure 18A.** Flow chart and heat map indicating molecular function.

**Figure 18B.** Overlapping genes from DEG list

### **3.5 METH induces changes to genes enriched in the molecular function GO:0004497 monooxygenase activity category.**

**Table 9.** Gorilla GO terms associated to cytochrome P450

**Figure 19.** KEGG pathway map of metabolism of xenobiotics via cytochrome P450

**3.8 METH effects genes involved in the neuropeptide signalling pathway (GO: 0007218)**

**Table 10.** GO terms of enriched genes in the neuropeptide signalling network

## 1.0 Introduction

The highly addictive, and illicit psychostimulant and psychoactive drug, Methamphetamine (METH), has impacted society economically, socially and increased the burden of disease [Chen et al., 2019; Zhang et al., 2019], with an estimated 37 million users worldwide [Droutman et al., 2019]. METH is characterised by an aromatic ring and nitrogen along the aryl sidechain, which defines its agonistic behaviour, as it shares structural similarity to most monoamine neurotransmitters, such as dopamine (DA) and serotonin (5-HT) [Ferrucci et al., 2019]. Apart from its severe neurotoxic effects on the central nervous system (CNS), high METH doses, taken over a long-term, leads to the interference of presynaptic and synaptic processes [Wen et al., 2019; Zoubkova et al., 2019]. Moreover, over time METH leads to brain alterations as a result of ongoing neurotoxicity, via the degradation of dopaminergic terminals in the striatum, or from constant epigenetic changes in some brain regions [Shaerzadeh et al., 2018; Ferrucci et al., 2019]. Further, METH abuse has potential to lead to METH-related psychosis, better known as psychotic disorder methamphetamine-associated psychosis (MAP) [Vuletic et al., 2018]. Psychosis in some is characterised by delusions, auditory and visual hallucinations and thought broadcasting [Su et al., 2018], with other psychiatric behaviours related to mood, sleep, cognition and violence tendencies [Khalkhali et al., 2018]. In the body, METH exposure can also affect the male reproductive system, with impacts on testis (expression reduction of progesterone and estrogen receptors), quality of sperm and endocrine disruption [Kaewman et al., 2018]. METHs neurotoxicity is triggered by inflammation, which, in studies of METH, involve an increased production of inflammatory cytokines, T-cell proliferation,

perturbations to cytokine signalling and an increase in blood brain barrier (BBB) permeability [Cook et al., 2019]. METH also causes changes to gut wall integrity, increasing intestinal permeability which shifts the body's microbiota leading to chronic inflammation [Cook et al., 2019]. Recent work investigating the impacts of METH on intestinal barrier integrity has shun a light on the involvement of major tight junction proteins [Persons, et al., 2018]. Two tight junction proteins, colon claudin-1 and zonula occludens-1 (ZO-1), which play a role in gut permeability, were shown to increase colon permeability after moderate METH doses were administered to transgenic and non-transgenic rats [Persons, et al., 2018]. Further, immunofluorescence data showed a reduction in claudin-1 and ZO-1 proteins, decreasing tight junction immunofluorescence in non-transgenic rats [Persons, et al., 2018]. Ning et al (2017) investigated the role of METH addiction and its possible modifications in the intestinal microbiota, supporting their hypothesis that CNS disorders are linked to alterations in gut microbiota [Ning et al., 2017]. Results of this work showed that METH caused significant gut dysbiosis, including repression of *Phascolarctobacterium* [Ning et al., 2017]. Indeed, there is a bidirectional flow of communication between the gut microbiome and brain, known as the gut-brain axis [Temko et al., 2017]. This study sought to investigate gene expression changes in gene expression in the distal colon, after the administration of an escalating METH dose in mice. Little is known about the impacts of METH on the colon, along with how this perturbation may be linked to the gut-brain axis. Using a systematic gene ontological approach, incorporating established open-source ontological software, and a stringent screening pipeline, this study

mapped several up and down differentially regulated genes to various gene ontological terms, against a *mus musculus* background.

## **2.0 Materials and Methods**

### **2.1 Chronic METH mouse model**

C57BL/6 mice (5-9 weeks old; n=14) were obtained from the Australian Research council (ARC, Perth, Australia). Mice had free access to food, water and were kept under a 12-hour light/ dark cycle in a well-ventilated room and at an appropriate temperature of 22 °C. Mice acclimatized for up to 1 week prior to the onset of treatment cycle of METH / sham for 14 days. Mice were separated into two groups: sham treatment and METH treatment administered via daily intraperitoneal (i.p) injections in the morning and late evening (10-13 hours apart). SHAM group received 100µl of saline water, whilst the METH group received METH beginning at 0.5mg/kg diluted in 100µl of saline water with an increment of METH concentration every two days (equivalent to the human dosage as per body surface area) (Table 1). This administrative regime was incorporated to overcome drug resistance and maintain a constant high for 14 days. The mice were kept under observation for 3 days after their last treatment injection (withdrawal) after which mice were culled using lethobarb (pentobarbitone) and colon tissues collected. All procedures and protocols performed within this study were approved by the Victoria University Animal Experimentation Ethics committee (AEETH 15/010) and were conducted according to the guidelines of the Australian National Health and Medical Research Council.

**Table 1: Chronic methamphetamine administration protocol.** C57BL/6 mice were administered two METH doses (morning and afternoon) over a seven-day period, lasting for two weeks. Week three, indicated by days 15, 16, and 17, allowed time for mice to experience withdrawal from METH.

WEEK 1	Schedule	Day 1 (mg/kg)	Day 2 (mg/kg)	Day 3 (mg/kg)	Day 4 (mg/kg)	Day 5 (mg/kg)	Day 6 (mg/kg)	Day 7 (mg/kg)
WEEK 2	<i>Morning</i>	0.5	1	1	2	2	3	3
	<i>Afternoon</i>	0.5	1	1	2	2	3	3
		Day 8 (mg/kg)	Day 9 (mg/kg)	Day 10 (mg/kg)	Day 11 (mg/kg)	Day 12 (mg/kg)	Day 13 (mg/kg)	Day 14 (mg/kg)
WEEK 3	<i>Morning</i>	4	4	5	5	6	6	7
	<i>Afternoon</i>	4	4	5	5	6	6	7
		Day 15 withdrawal	Day 16 withdrawal	Day 17 withdrawal	Day 18 Cull, collection of colon tissues			

## 2.2 RNA extraction

The distal colon was collected from mice, and colon was flushed with saline to removed faecal contents. Colon was then flash frozen in liquid nitrogen immediately after culling and stored at -80°C until RNA was extracted. RNA extraction was carried out according to ThermoFisher® RNA isolation and purification reference guidelines. Tissues were placed in separate tubes containing 1000µL of TRIzol® reagent at 4°C (Thermo Fisher Scientific, Australia) and two metallic beads each. Tubes were then placed in a homogenising bead beater and was pulsed at 50 oscillations per second for 2x5 minutes with a 1 min break in between to dissociate the tissue. To perform phase separation of RNA, the TRIzol tissue homogenate solution was removed from homogenisation tubes and 200µL of chloroform was added. Solutions were

mixed by shaking for 15s, were incubated for 3 min at room temperature and were centrifuged at 12000 x g for 15 min at 4°C. From this solution the aqueous phase containing RNA was removed and incubated with 500µL of absolute isopropanol at room temperature for 10 min before centrifugation at 12000 x g for 10 min at 4°C to obtain RNA pellets. The RNA pellets were washed in 500 µL of 75% ethanol and spun at 5000 x g for 5 min to remove contaminating phenols and recollect the pellet. Pellets were dissolved in 100 µL of pure nucleotide free H<sub>2</sub>O for processing using the RNeasy Mini Kit (Qiagen, Australia). Briefly, a mixture of 350µL RLT containing 1% 2-mercaptoethanol and 250 µL of absolute ethanol were added to the resuspended RNA which was then transferred to silica-membrane RNeasy spin columns and spun at 8000 x g for 15s to bind RNA. Samples were washed by spinning samples with 350µL of RW1 buffer at 8000 x g for 15s either side of an on-column DNA denaturing step with DNase (Qiagen, Melbourne Australia) incubated for 15 min at room temperature. Samples were then washed by two spins with 500µL RPE buffer for 15s at 8000 x g and spun dry at 8000 x g for 1 min. Purified RNA was collected in 36µL of nuclease-free water spun at 8000 x g for 1 min and frozen at -80°C for use in experiments.

### **2.3 RNA concentrations and quality control**

The concentration of RNA in each sample was quantified by a Qubit 1.0 fluorometer (Invitrogen, Thermofisher, Australia) using the Qubit® RNA Broad Range Assay Kit (Life Technologies, Thermofisher, Australia) as of manufacturers protocol. Briefly, 10µL of supplied standards and 10µL of sample RNA diluted 1:2 in nuclease-free water was added to 190 µL of Qubit®

RNA working solution containing an RNA-specific fluorometric dye in clear PCR tubes which were incubated for 2 min at room temperature before readings were taken for fluorometric quantitation of only RNA in the samples. Contaminates (such as phenol) were evaluated in RNA samples using a Nanodrop spectrophotometer. Absorbance (A) scores for all samples were between 1.8 – 2.0 for A260/A280 ratios. and 2.0-2.2 for A260/A230 ratios, suggesting that nucleotide purity was high. The quality of RNA was assessed using a 2100 Bioanalyzer (Agilent Technologies, Australia) microfluidics platform with the RNA 6000 Nano Kit (Agilent Technologies) as of manufacturer's instructions. All sample were free from contamination of genomic DNA and 16S ribosomal RNA from bacteria. All samples were of very high quality and had minimal degradation with RNA integrity number (RIN) values between 9.9-10/10.

#### **2.4 High throughput RNA-Sequencing of mRNA**

An experimental design similar to Seaman et al. (2015) was employed for RNA-sequencing experiments. Samples of RNA (n=7) from C57Bl/6 and *Winnie* mice treated with either sham or MSC enemas were pooled into groups containing equal concentrations of RNA totalling at least 3 µg of RNA at 100ng/µL in nuclease-free water with concentrations and RIN verified (Figure 1). Samples were submitted to the Australian Genome Research Facility (AGRF) for polyA purification of mRNA from total RNA samples, RNA-Seq library preparation and read high-throughput sequencing using a 100bp single-end read protocol on the Illumina HiSeq 2500 System. A data yield of approximately 2.5-3.2 Gb were acquired per sample. Base calling was

performed using HiSeq Control Software (HCS) v2.2.68 and Real Time Analysis (RTA) v1.18.66.3. Sequencing data was generated using the Illumina bcl2fastq 2.20 pipeline. The quality of raw reads was assessed by FASTQC at a kmer size of 7. In addition, 1000 raw reads were randomly selected for alignment to the NCBI nonredundant nucleotide database using Blast+ v2.7.1, To map raw reads, the program STAR v2.6.0c was used to align to the mouse reference genome (GRCm38), Optical duplicates were removed, and the alignment file was sorted by coordinates using Sequence Alignment/Map (SAM)tools v1.8.0, Read summarisation of the raw counts per gene was determined using featureCounts v1.6.2 program of the software package subread. Differentially expressed genes (DEG) from raw mapped reads were evaluated by the R package DEGseq v 1.34.0 (Wang et al., 2009). DEGs were identified with a P value of  $<0.001$  using the Benjamini-Hochberg correction. Resulting datasets were additionally cleaned by cut-offs for lowly expressed genes with  $<10$  counts in a group and low changes in expression of between  $\pm 0.5\text{LogFC}$ . Up and downregulated DEGs were analysed for enriched gene ontology (GO) terms associated with biological processes, molecular function and cellular components using a rank-based method with a  $P < 0.001$  threshold by the web-based tool GOrilla. Selected, enriched gene ontologies identified using GOrilla were visualised as interaction map.

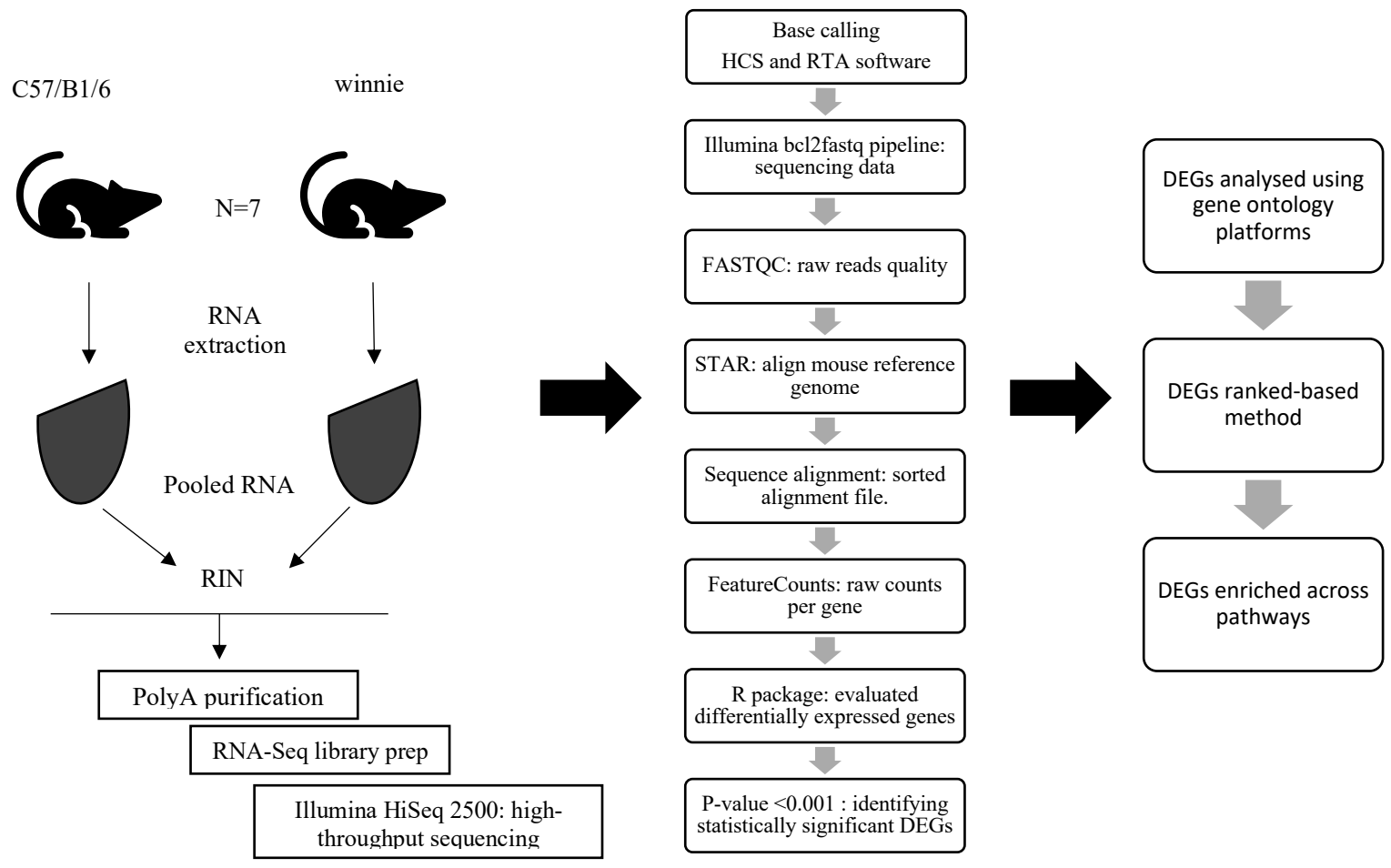


**Figure 1.** Illustrative summary of RNA extraction and subsequent RNA purification, and bioinformatical analysis.

### 3.0 Results

From the gene list, only those genes with a (+/-) 2-fold change (fold change criteria) and p-value cut-off (p-value criteria of  $p=0.003$ ) were selected for enrichment analysis using gene ontology tools, namely DAVID (<https://david.ncifcrf.gov/geneReport.jsp>) and Gorilla. Based on this criterion, a total of 602 genes were preselected for further GO analysis. Out of these selected 602 genes, DAVID Gene Ontology defined 560 genes aligned to *mus musculus*. *Table 1* summarises alignments to Functional Categories, Gene Ontology, Pathways and Protein\_domains. Another gene ontological program, Gorilla recognised 598 genes out of the 601 genes. All downstream analysis in the following sub-sections were derived from both exploratory analysis of DAVID and gorilla GO.

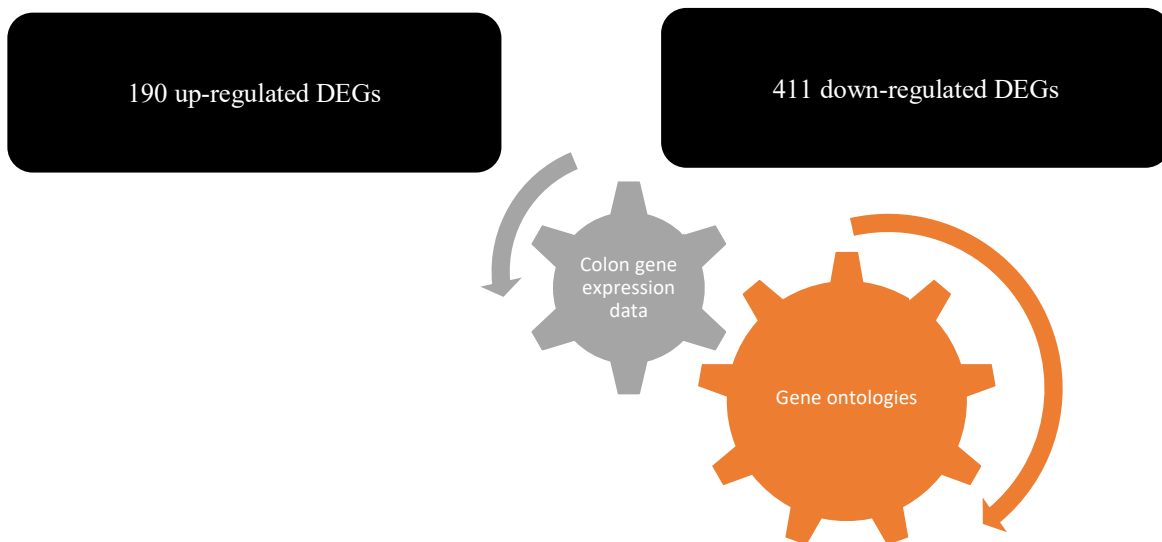


**Figure 2. Workflow of NGS data filtering to gene ontologies.** Process of filtering a large set of differentially expressed genes (DEGs) from distal colon tissue.

**Table 2. Summary of 560 genes reported by DAVID Bioinformatics Resource 6.8 against a *mus musculus* background reference gene set.** DAVID bioinformatics tool uses novel algorithms that allow for a gene-annotation enrichment analysis of a set of genes, also permitting the reduction in size of large gene lists into functionally related groups of genes.

<b>Category</b>	<b>Database/reference</b>	<b>Genes involved in annotation category</b>	<b>% Overall genes</b>
Functional	Up keywords	541	96.6
Gene ontology	GOTERM_CC_DIRECT	508	90.7
Pathways	KEGG PATHWAY	210	37.5
Protein domains	INTERPRO	515	92.0

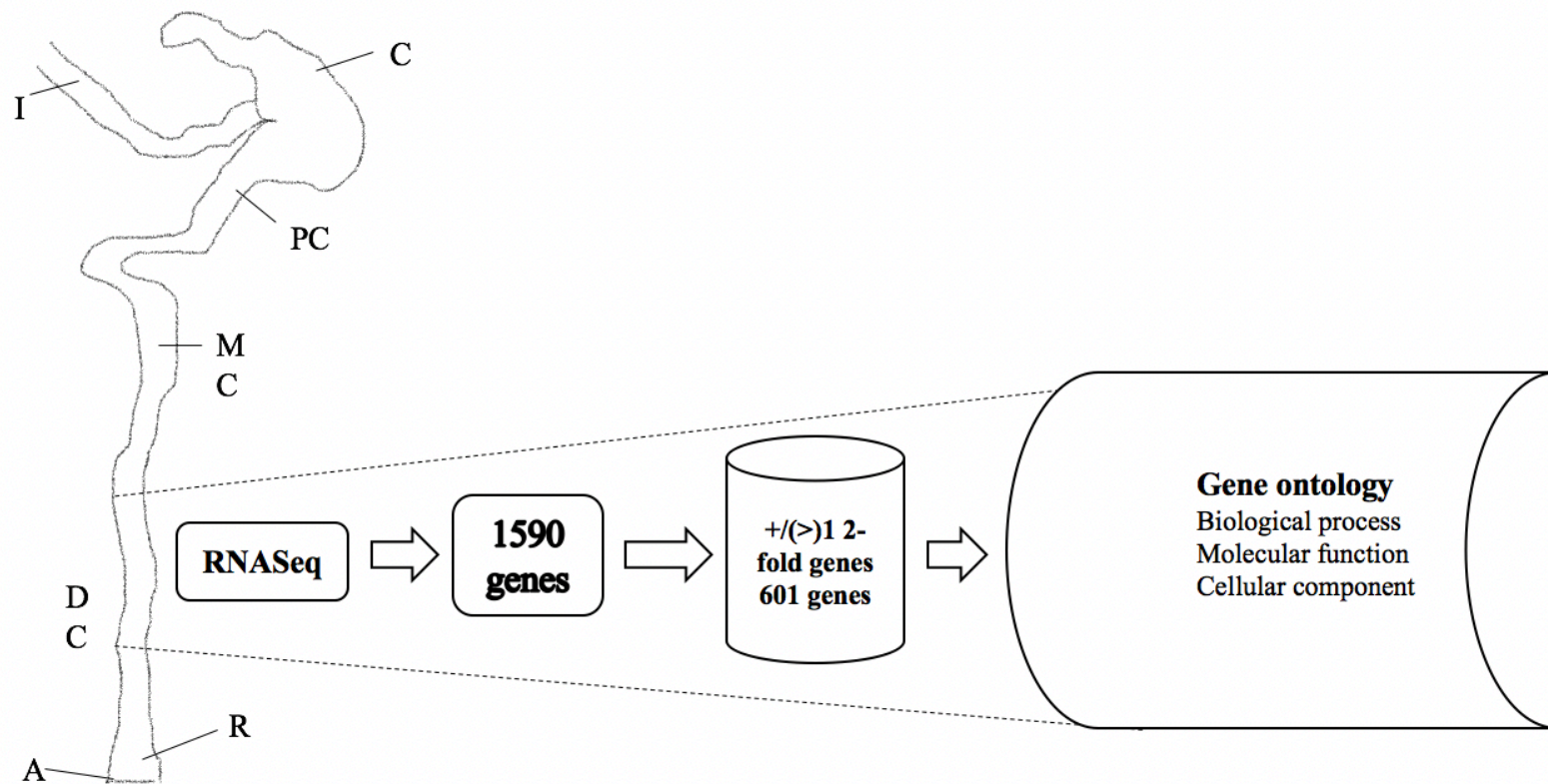


**Figure 3. Diagrammatic representation of the colon and gene ontological processes.** Distal colon (left), abbreviated as DC, was found to have 601 genes up- or down-regulated by METH. The distal colon includes the descending colon and the sigmoid colon which connects to the rectum. Ontological processing of RNA-Seq data from DC showed a number of changes associated with intracellular molecular functioning, components and biological processing. DC: Distal colon, I: Ileum, M: medial colon, C: colon, P: proximal colon, R: rectum, A: anus.

**Table 3. KEGG pathway annotation.** 210 out of 560 genes were associated with *mus musculus*. Orange highlighted rows indicate ontological terms that were further investigated, as they contained genes with fold-changes that were considered significant for this study.

<i>Term</i>	<i>p-value</i>	<i>Genes</i>	<i>%</i>
Metabolic pathways	3.5E-3	51	9.1
Calcium signalling	1.2E-3	14	2.5
Hypertrophic cardiomyopathy (HCM)	4.8E-5	11	2.0
PPAR signalling	5.4E-5	11	2.0
Proteoglycans in cancer	4.9E-2	11	2.0
Focal adhesion	5.5E-2	11	2.0
Dilated cardiomyopathy	3.8E-4	10	1.8
Serotonergic synapse	9.4E-3	10	1.8
Tight junction	1.3E-2	10	1.8
Arrhythmogenic right ventricular cardiomyopathy (ARVC)	6.2E-4	9	1.6
Bile secretion	6.2E-4	9	1.6
Wnt signalling	3.7E-2	9	1.6

Adipocytokine signalling	3.2E-3	8	1.4
Arachidonic acid metabolism	1.0E-2	8	1.4
Leukocyte trans-endothelial migration	4.6E-2	8	1.4
Inflammatory mediator regulation of TRP channels	5.5E-2	8	1.4
Glycolysis/gluconeogenesis	8.6E-3	7	1.2
Steroid hormone biosynthesis	3.0E-2	7	1.2
Chemical carcinogenesis	3.8E-2	7	1.2
Glucagon signalling	5.4E-2	7	1.2
Amoebiasis	9.7E-2	7	1.2
Metabolism of xenobiotics by cytochrome P450	2.9E-2	6	1.1
Hematopoietic Cell lineage	7.7E-2	6	1.1
Aldosterone synthesis and secretion	8.3E-2	6	1.1
ECM-receptor interaction	9.0E-2	6	1.1

Protein digestion and absorption	9.0E-2	6	1.1
Retinol metabolism	9.3E-2	6	1.1
ABC transporters	3.5E-2	5	0.9
Tyrosine metabolism	8.8E-2	4	0.7
Mineral absorption	9.9E-2	4	0.7
Nitrogen metabolism	7.6E-2	3	0.5
Arginine biosynthesis	9.2E-2	3	0.5
Cytokine-cytokine receptor interaction	6.6E-2	12	2.1

**Table 4. Functional Annotation of functional categories.** A total of 541 genes were annotated using the Up\_keywords database/reference. The majority of genes taken from the input gene list were mapped to membrane functional annotation.

Term	Genes	P-value
Membrane	230	2.6E-2
Phosphoprotein	199	6.9E-2
Glycoprotein	193	1.0E-26
Signal	176	5.0E-12
Disulfide bond	153	4.4E-19
Cytoplasm	124	2.8E-2
Cell membrane	102	9.9E-2
Secreted	101	7.2E-18
Metal-binding	99	2.3E-2
Transport	63	7.0E-3
Hydrolase	51	4.5E-2
Calcium	42	8.7E-6
Developmental protein	37	6.5E-3
ER	37	9.0E-3
Lipoprotein	31	7.2E-3

Oxidoreductase	30	7.4E-4
Ion transport	29	9.7E-4
<b>Cell junction</b>	<b>25</b>	<b>3.0E-4</b>
Extracellular matrix	21	9.9E-7
Iron	21	7.3E-4
Immunoglobulin domain	20	2.3E-2
Protease	20	6.2E-2
Signal-anchor	19	1.9E-2
Cleavage on pair of basic residues	18	1.0E-4
Lipid metabolism	18	2.3E-2
Heme	14	2.4E-4
Ion channel	14	6.1E-2
Actin-binding	13	1.8E-2
Muscle protein	12	3.1E-8
Monoxygenase	12	3.5E-4
GPI-anchor	12	5.4E-4

Inflammatory response	12	1.7E-3
Hormone	11	2.6E-4
Zymogen	11	3.2E-2
Microsome	10	4.4E-3
Wnt signalling pathway	10	2.5E-2
NAD	10	3.2E-2
Lipid-binding	10	4.6E-2
Glycosyltransferase	10	9.0E-2
Pyrrolidone carboxylic acid	9	7.5E-5
Symport	9	5.1E-3
Sodium transport	9	5.7E-3
Sodium	9	8.1E-3
Calmodulin-binding	9	1.8E-2
NADP	9	5.9E-2

Sarcoplasmic reticulum	8	2.8E-5
LIM domain	8	1.9E-3
Carbohydrate metabolism	8	6.4E-3
Protease inhibitor	8	2.6E-2
Growth factor	8	3.2E-2
Metalloprotease	8	5.5E-2
Heparin-binding	7	6.9E-3
Intermediate filament	7	8.9E-3
Collagen	7	1.6E-2
Hydroxylation	7	1.9E-2
Keratin	7	8.8E-2
Integrin	6	8.4E-3
Lipid degradation	6	9.1E-2
Mysosin	5	2.7E-2
Chloride	5	7.6E-2
Keratinization	4	2.3E-2

Lipid droplet	4	3.7E-2
Serine esterase	4	5.0E-2
Antiport	4	5.4E-2
Amino-acid transport	4	5.7E-2
Amidation	4	7.4E-2
Diabetes mellitus	3	5.4E-3
Urea cycle	3	1.1E-2
Thick filament	3	3.2E-2
Oxygen transport	3	5.4E-2
Oxidation	3	6.1E-2

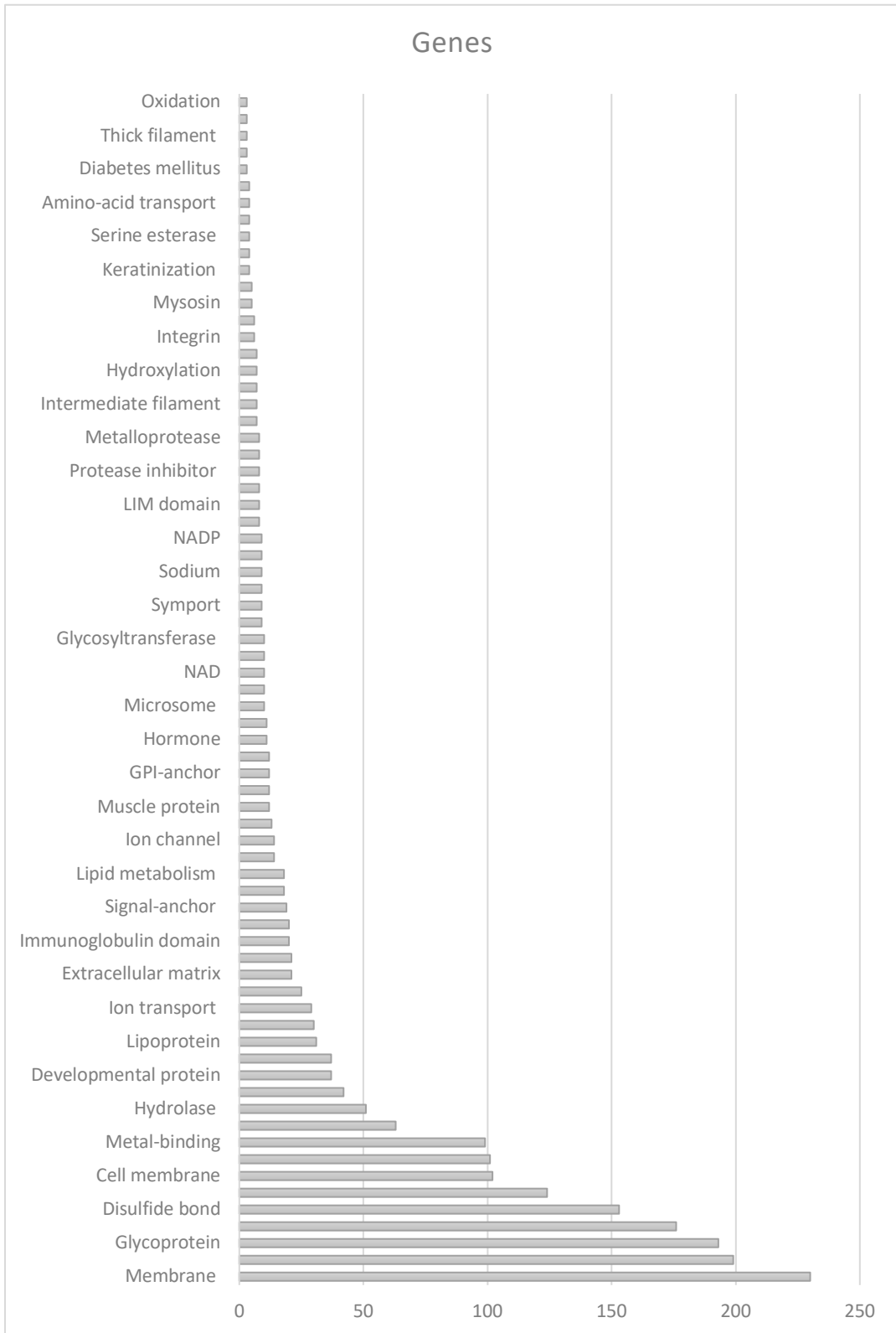


**Figure 4. Frequency of genes enriched in the functional gene ontology.** Bar chart representation of functional categories as indicated by Up\_keywords

**Table 5. Functional annotation of Gene Ontology as annotated by reference to Goterms\_CC\_Direct.** A total of 508 genes were mapped to the 560 gene reference list in DAVID.

Term	Genes	P-value
Membrane	228	9.9E-6
Cytoplasm	188	7.1E-2
Plasma membrane	140	9.2E-2
Extracellular exosome	118	3.3E-9
Extracellular region	105	3.4E-16
Extracellular space	97	4.1E-17
Integral component of plasma membrane	47	1.4E-3
ER	45	5.0E-2
Cell surface	29	3.7E-3
Proteinaceous Extracellular matrix	28	5.9E-8
<b>Cell junction</b>	<b>28</b>	<b>3.3E-2</b>
Extracellular matrix	25	7.4E-7
Neuronal cell body	22	3.8E-2
Dendrite	20	5.2E-2
Apical plasma membrane	19	2.3E-3
Z disc	17	1.3E-7

Neuron projection	17	7.9E-2
Sarcolemma	16	3.8E-7
Anchored component of membrane	12	1.1E-3
Myofibril	10	6.3E-7
Sarcoplasmic reticulum	10	1.6E-5
Sacromere	9	3.7E-6
Vesicle	9	6.3E-2
T-tubule	8	6.3E-4
Collagen trimer	8	5.6E-3
Receptor complex	8	5.9E-2
Perikaryon	8	9.4E-2
Striated muscle thin filament	7	7.2E-7
I band	7	2.6E-5
Cell periphery	7	9.9E-3
Lateral plasma membrane	6	1.3E-2
Lipid particle	6	2.8E-2
Brush border membrane	6	3.4E-2
Organelle membrane	6	9.6E-2
M band	5	2.2E-3

Sarcoplasmic reticulum membrane	5	9.9E-3
Neuromuscular junction	5	8.3E-2
Sarcoplasmic reticulum lumen	3	6.3E-3
Muscle myosin complex	3	9.3E-3
Junctional membrane complex	3	1.7E-2
Membrane-bounded vesicle	3	4.3E-2
Myosin filament	3	4.3E-2
Interstitial matrix	3	7.0E-2
Inhibin B complex	2	5.1E-2
ATP-binding cassette (ABC) transporter complex	2	5.1E-2
Chromaffin granule	2	7.5E-2



**Figure 5. Frequency of genes enriched in functional gene ontology from Goterms\_CC\_Direct.** Majority enriched genes belonged to membrane, cytoplasm, plasma membrane and extracellular exosome.

### **3.1 Differentially expressed tight junction and leukocyte trans-endothelial migration (LTM) genes are altered by METH in the distal colon.**

Tight junction, along with leukocyte trans-endothelial migration proteins play a key role in intestinal barrier integrity in METH use [Persons et al., 2018; Sajja et al., 2016]. To assess the role of tight junctions in the colon, a total of 10 tight junction genes were analysed, along with GO terms derived from KEGG pathway annotation: leukocyte trans-endothelial migration (LTM), and Inflammatory mediator regulation of TRP channels. Tight junction (TJ) genes (Figure 4) were found to be differentially expressed by METH. Actinin alpha 2 (*actn2*) showed a 30-fold decrease, whereas *Mylpf* was found at (-) 81-fold. Also, *Ctnna3*, a gene classified within the LTM category (DAVID gene ontology) was found to be significantly upregulated in the colon tissue.

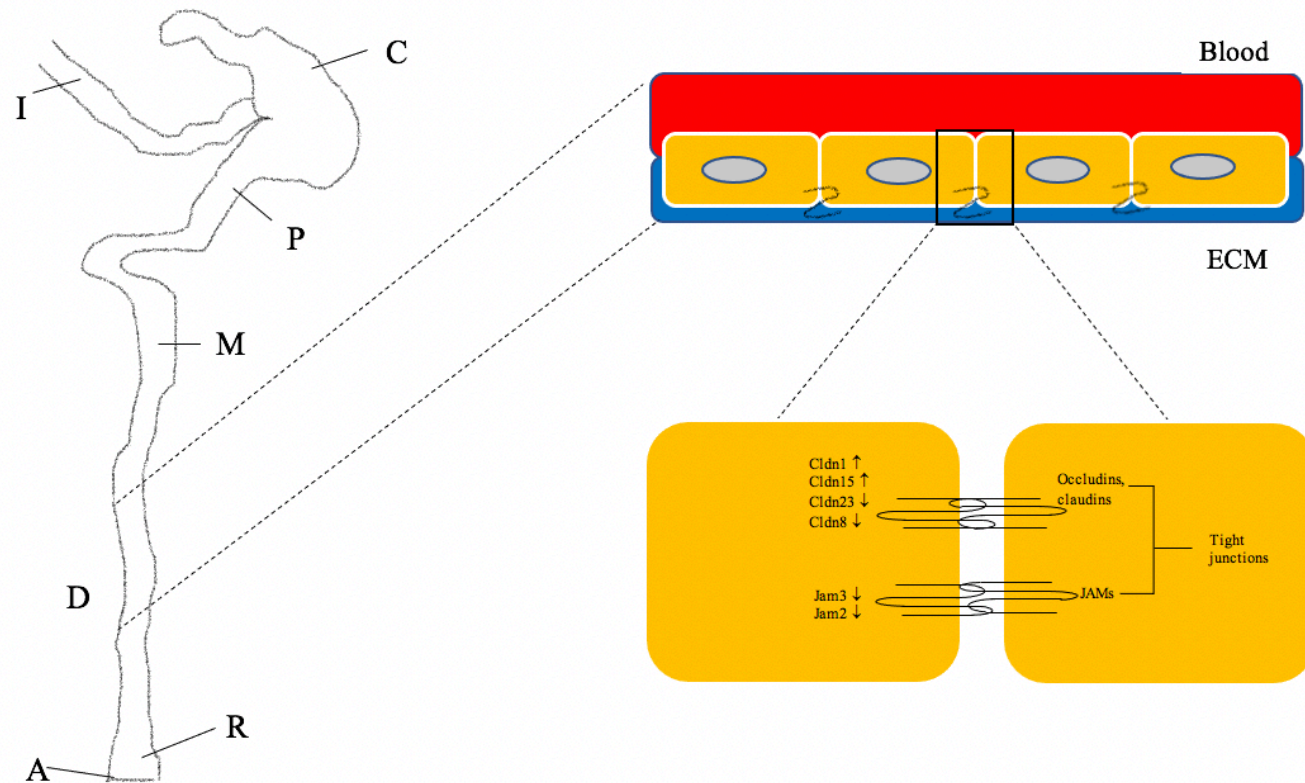


**Figure 6. Tight junction genes.** Diagram of the relationship between tight junction proteins and cell-cell adhesion. Claudins, occludins and JAMs are responsible for inhibiting permeability from the extracellular matrix (ECM) into the blood stream. D: Distal colon, I: Ileum, M: medial colon, P: proximal colon, R: rectum, A: anus.

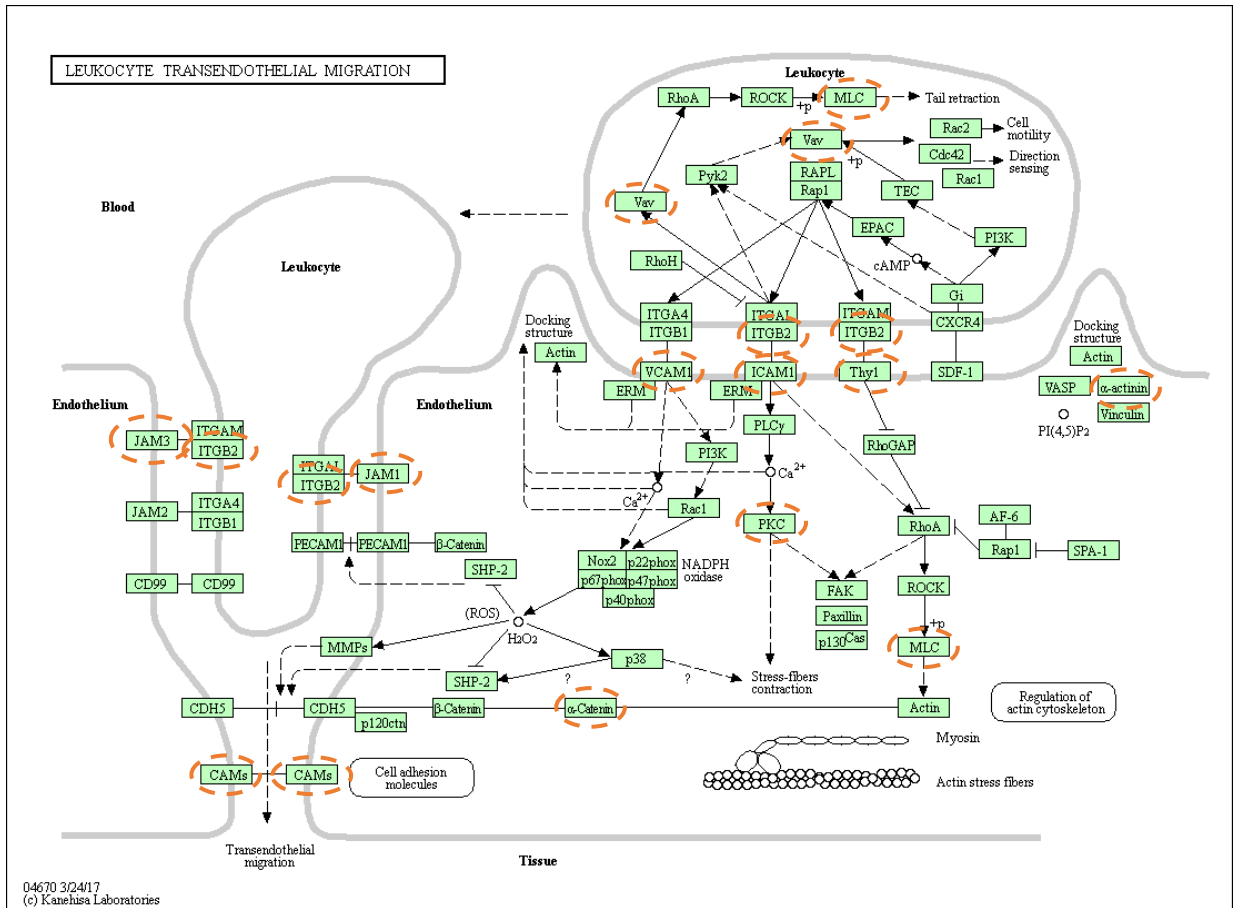


**Figure 7. Leukocyte trans-endothelial migration (LTM).** The perturbation of tight junctions is intrinsic to the collaboration between leukocytes and endothelium [Schimmel et al., 2017]. Several tight junction genes, claudin-1 and claudin-15, along with a myosin gene (Mylpf), were shown to be enriched in the LTM pathway from input gene list. Broken orange circles refer to genes found to be enriched within gene ontologies.

### **3.2 METH causes differential gene expression changes in serotonergic synapses.**

Serotonergic systems are known to contribute to a range of disorders and diseases, including insomnia, anxiety, depression, Parkinson's disease and Alzheimer's disease [Charnay et al., 2010]. METH has previously been reported to play a role in neurotoxicity of serotonergic axon arbours [Sekine et al., 2006] of mature neurons. Several genes, indicated by KEGG, including *Alox12 (Lox)*, *Alox15*, *Cacna1s (VGCC)*, *Plcb4 (PLC)*, *Prkcb (PKC)* and *Tph1* were shown to be associated with serotonergic synapses. In addition, four cytochrome P450 genes were enriched to the serotonergic synapse pathway. *Cacna1s*, calcium voltage-gated channel subunit alpha 1S, is involved in excitation-contraction coupling in skeletal muscle. In this KEGG pathway, *Cacna1s* was found to be involved in the post-synaptic neuron. *Plcb4*, known as phospholipase C beta 4, plays a role in the selective serotonin reuptake inhibitor pathway, and also is known to be a circadian gene which has been shown to be involved in alcohol dependence [Kovanen et al., 2010]. *Prkcb* was also found to be attributed to the repression of caspase 3, which leads to neuroprotection.



### **3.3 Gene ontology of METH shows genes enriched in cytokine-cytokine receptor interactions.**

Cytokine-cytokine receptor interactions, and their networks, play crucial roles in inflammation [Dong et al., 2017]. Interestingly, this cytokine and chemokine response might lead to neuroinflammation, and also psychiatric manifestations. This is important to understand in the context of METH, since METH is known to lead to changes in psychiatric behaviour and immune modulation in the brain. Enriched in the gene list include, *Ccl8*, *Ccr10*, *Cxcl5*, *Cxcl9*, *IL1b*, *IL2* receptor, beta chain, *IL20* receptor beta and tumour necrosis factor receptor superfamily, member 19 (*Tnfrsf19*). Genes were assessed in KEGG pathway. Specifically, KEGG pathways breaks down each subfamily within the cytokine-cytokine receptor interaction map as:

- Chemokine – CC and CXC subfamilies,
- Class I and II helical cytokines,
- IL-1-like cytokines
- TNF family, and,
- TGF- $\beta$  family

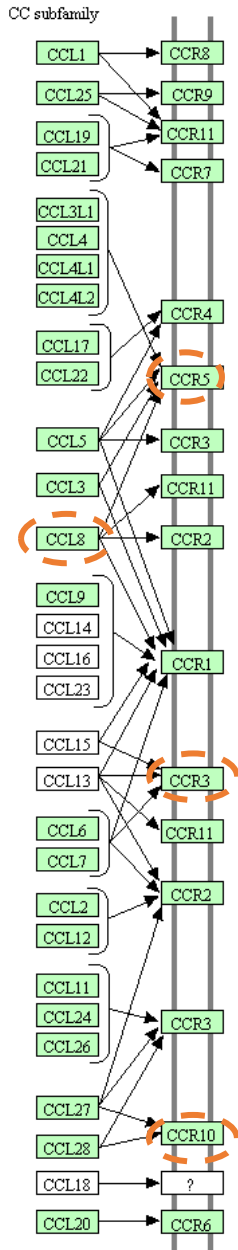
KEGG cytokine-cytokine receptor term brought back a total of 12 genes (Table 6) associated to this pathway, with a p-value calculation of  $6.6 \times 10^2$ .

**Table 6. Summary of differentially expressed genes (DEG) from METH gene set.** DEGs are shown along with fold change corresponding to unique pathway and subfamily class as mapped by DAVID bioinformatics resource.

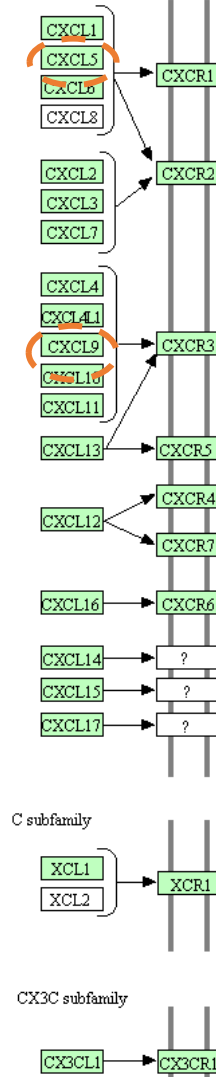
Pathway	Sub-type	Gene	Fold-change
Chemokines	CC subfamily	CCL8	-1.50
		CCR10	+1.95
	CXC subfamily	CXCL5	-3.95
		CXCL9	+1.61
Class I helical cytokines	$\gamma$ chain utilising	IL2RB	-1.03
	IL4-like	CSF2RB	-0.63
	Prolactin family	CSF3R	-1.65
		LEP	+2.92
Class II helical cytokines	IL10/28-like	IL20RB	-1.03
IL-1-like cytokines	-	IL1B	-1.71
TNF family	-	TROY (tnfrsf19)	-1.69
TGF- $\beta$ family		INHBA (inha)	-1.35

CYTOKINE-CYTOKINE RECEPTOR INTERACTION

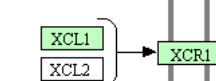
Chemokines



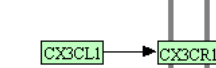
CXC subfamily



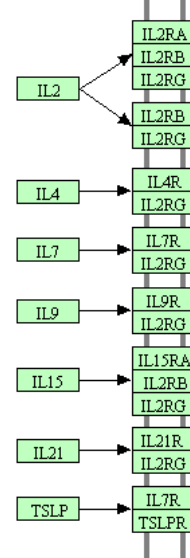
C subfamily



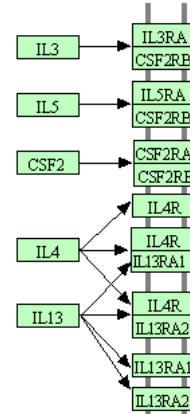
CX3C subfamily



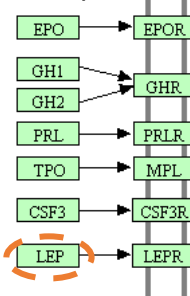
The class I helical cytokines  
γ-chain utilising



IL4-like



Prolactin family



14060 5/25/18  
c) Kanehisa Laboratories

**Figure 9A.** Cytokine-cytokine receptor interaction map, highlighting the chemokine subfamilies: CC, and CX. In addition, class I helical cytokines (prolactin family) indicates Leptin (LEP) in this gene set. KEGG pathways were generated from DAVID Bioinformatics Resource, 6.8. Broken orange circles represent genes differentially regulated in this study.

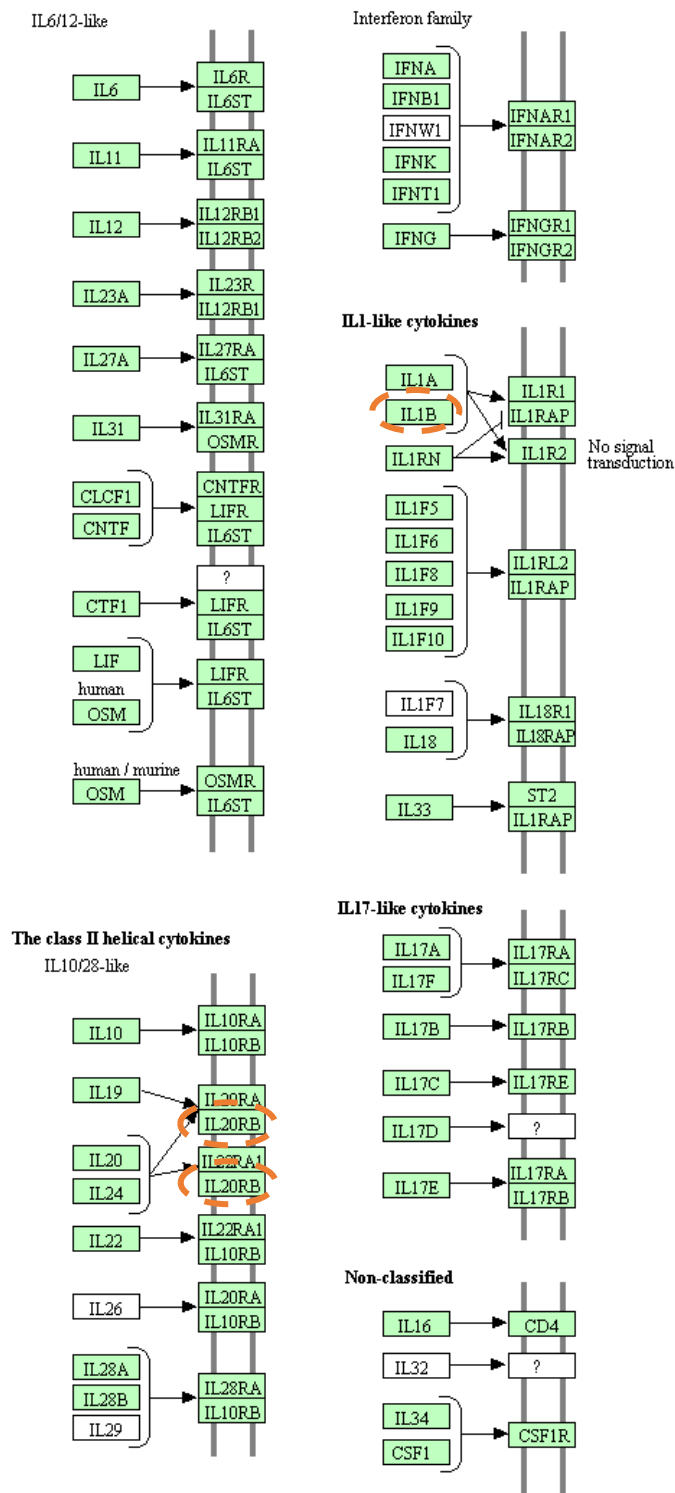


**Figure 9B.** Class II helical cytokines (IL20, and IL-1-like cytokines (IL1B and IL1R2) were shown to be enriched in the overall DEG set. Broken orange circles represent genes differentially regulated in this study.

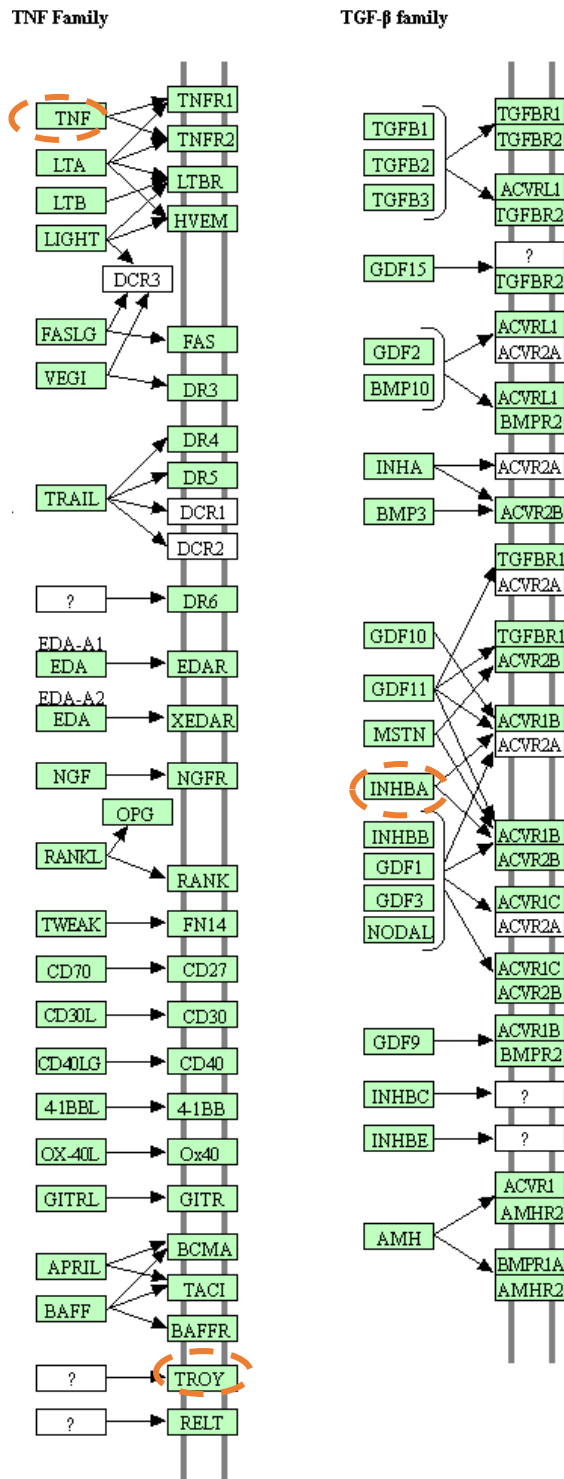


**Figure 9C. TNF family-related genes.** The TNF family and TGF- $\beta$  family genes are indicated in broken orange circles. TNF: tumour necrosis factor; TROY: tumour necrosis factor receptor superfamily, member 19 (tnfrsf19); INHBA: inhibin beta-A (inha). Broken orange circles represent genes differentially regulated in this study.

### 3.4 Genes associated with METH are enriched across several ontological terms in Gorilla

Using Gorilla gene ontology software, results indicated that the majority of genes belonged to the metabolic process (Table 3). In addition, significant gene enrichment was seen in response to bacterium (GO: 0009617), fatty acid metabolic process (GO: 0006631), neuropeptide signalling pathway (GO:0007218), and blood vessel development (GO:0001568). Within each ontological term described by Gorilla, a significant proportion of genes was concentrated in the fatty acid metabolic process (19 genes), response to bacterium (22 genes), and monocarboxylic acid metabolic process pathways (22 genes).

**Table 6. Biological process as retrieved from the Gorilla GO.** Gene expression using set criteria using Gorilla, showing the major biological processes with Gorilla's recognition of 598 genes

GO Term	Description	P-value	FDR q-value	N	b
GO:0006631	fatty acid metabolic process	1.45E-04	7.33E-01	580	19
GO:0001568	Blood vessel development	9.72E-5	4.97E-1	580	3
GO:0001890	placenta development	4.30E-04	1.00E+00	580	2
GO:0009617	response to bacterium	4.73E-04	7.95E-01	580	22
GO:0007218	neuropeptide signalling pathway	6.60E-04	6.65E-01	580	5
GO:0032787	monocarboxylic acid metabolic process	9.68E-04	8.14E-01	580	22
GO:0042738	Exogenous drug catabolic process	9.58E-4	7.0E-1	580	6
FDR q-value: correction of the p-value for multiple testing using Benjamini and Hochberg method					
N: total number of genes					
b: total number of genes associated with specific GO term					

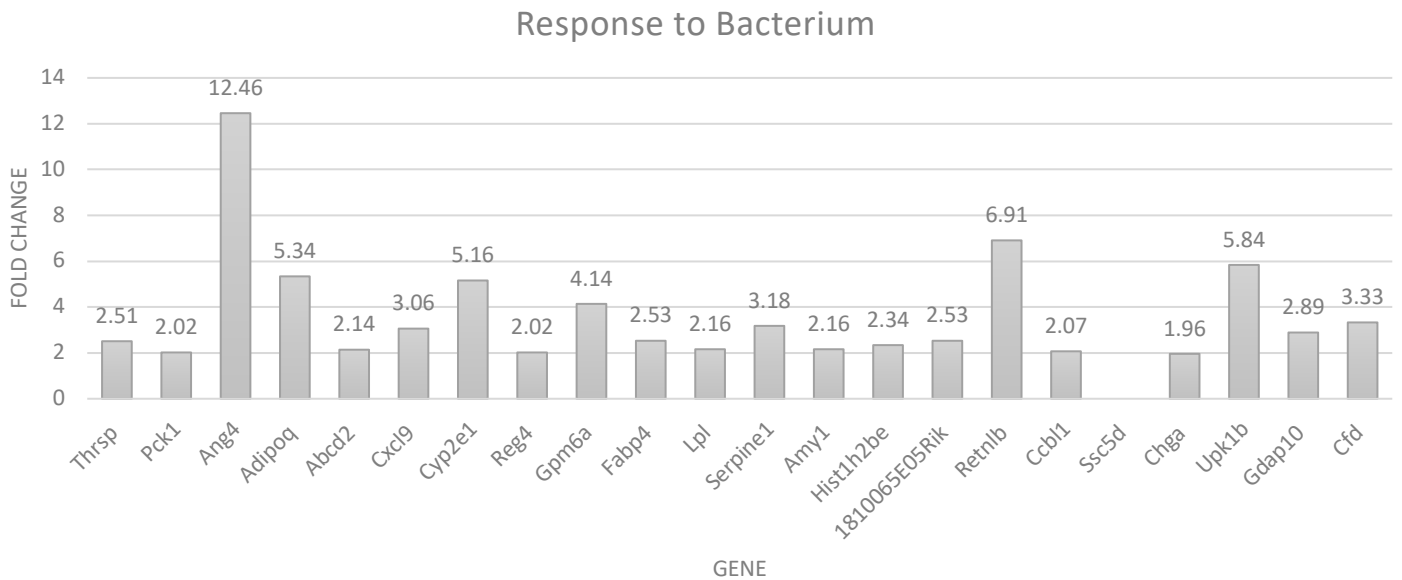


**Figure 10. GO term response to bacterium.** Bar chart of GO term response to bacterium and enriched genes containing fold-change values. *Corresponding table available in Appendix 1.*

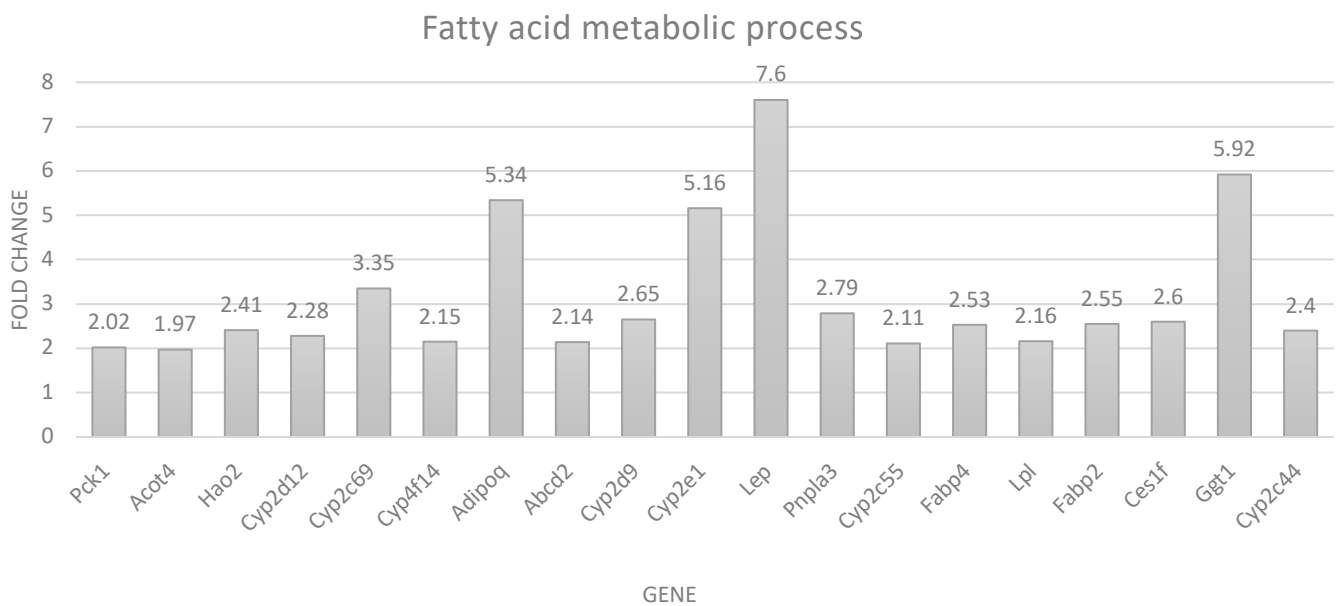


**Figure 11. Go term fatty acid metabolic process.** Bar chart of GO term Fatty acid metabolism process and enriched genes containing fold-change values. *Corresponding table available in Appendix 1*

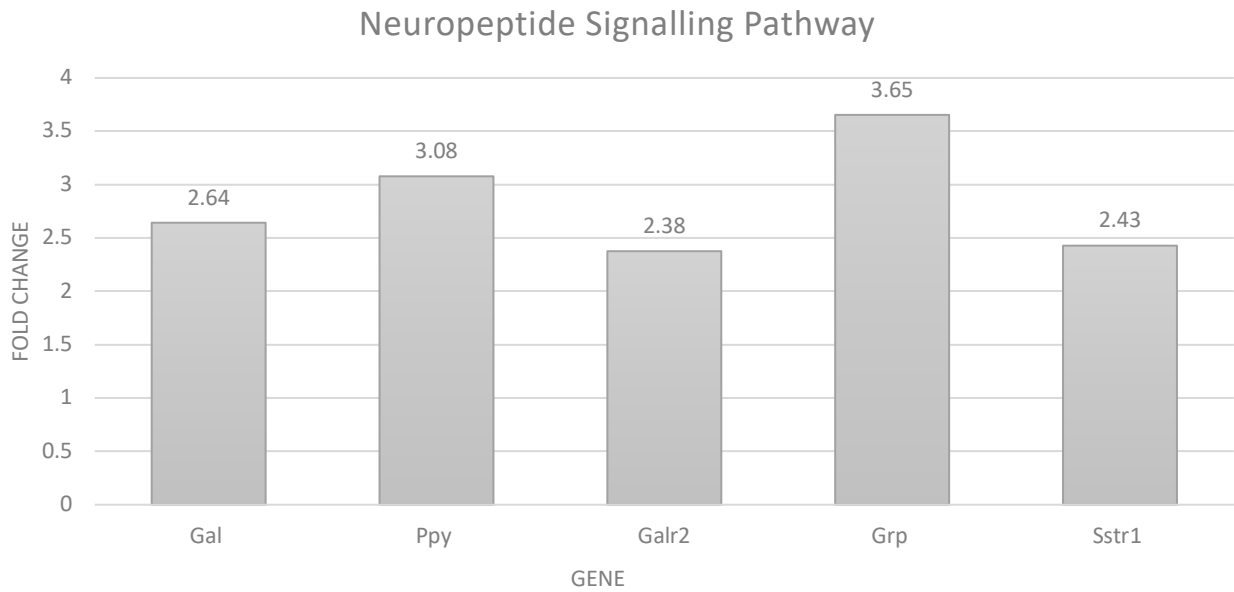


**Figure 12. GO term neuropeptide signalling pathway.** Bar chart of GO term Neuropeptide signalling pathway and enriched genes containing fold-change values. *Corresponding table available in Appendix 1*

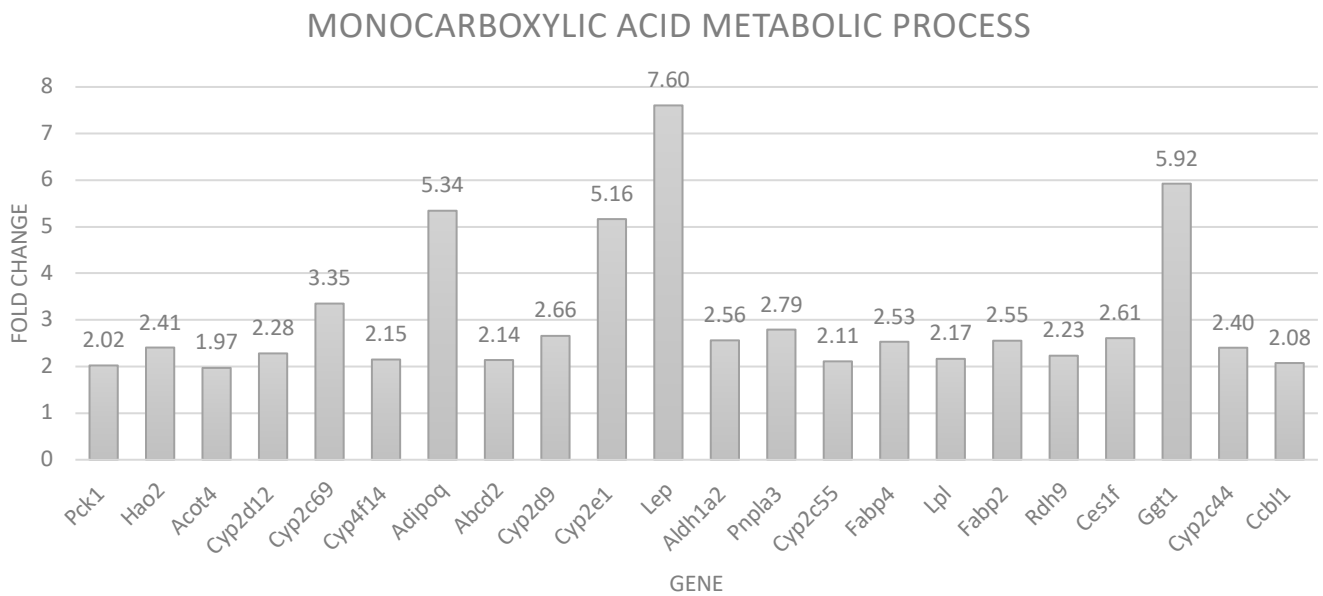


**Figure 13. Go term monocarboxylic acid metabolic process.** Bar chart of GO term monocarboxylic acid metabolic process and enriched genes containing fold-change values. *Corresponding table available in Appendix 1*

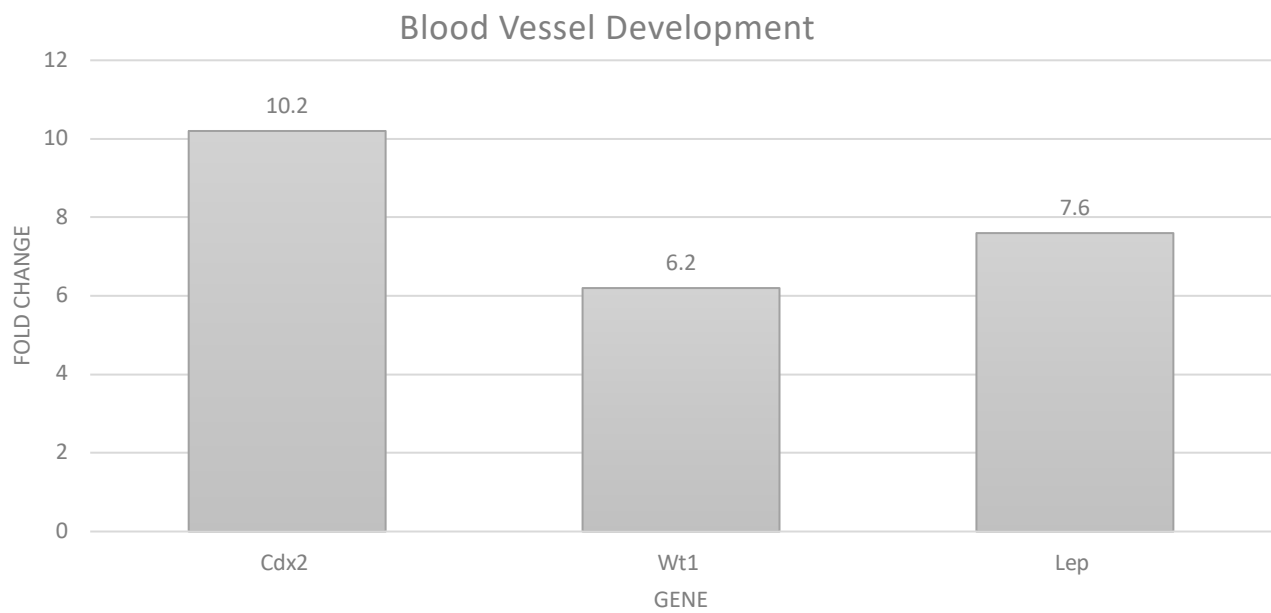


**Figure 14. GO term blood vessel development.** Bar chart of GO term blood vessel development and enriched genes containing fold-change values. *Corresponding table available in Appendix 1*

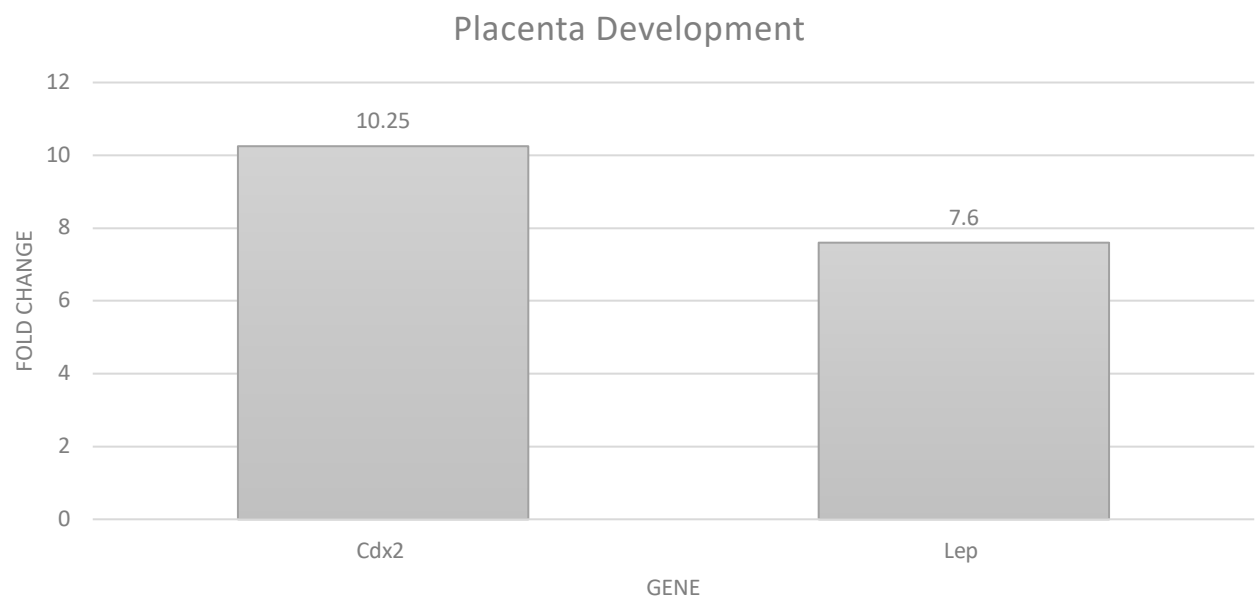


**Figure 15. GO term placenta development.** Bar chart of GO term placenta development and enriched genes containing fold-change values. *Corresponding table available in Appendix 1*

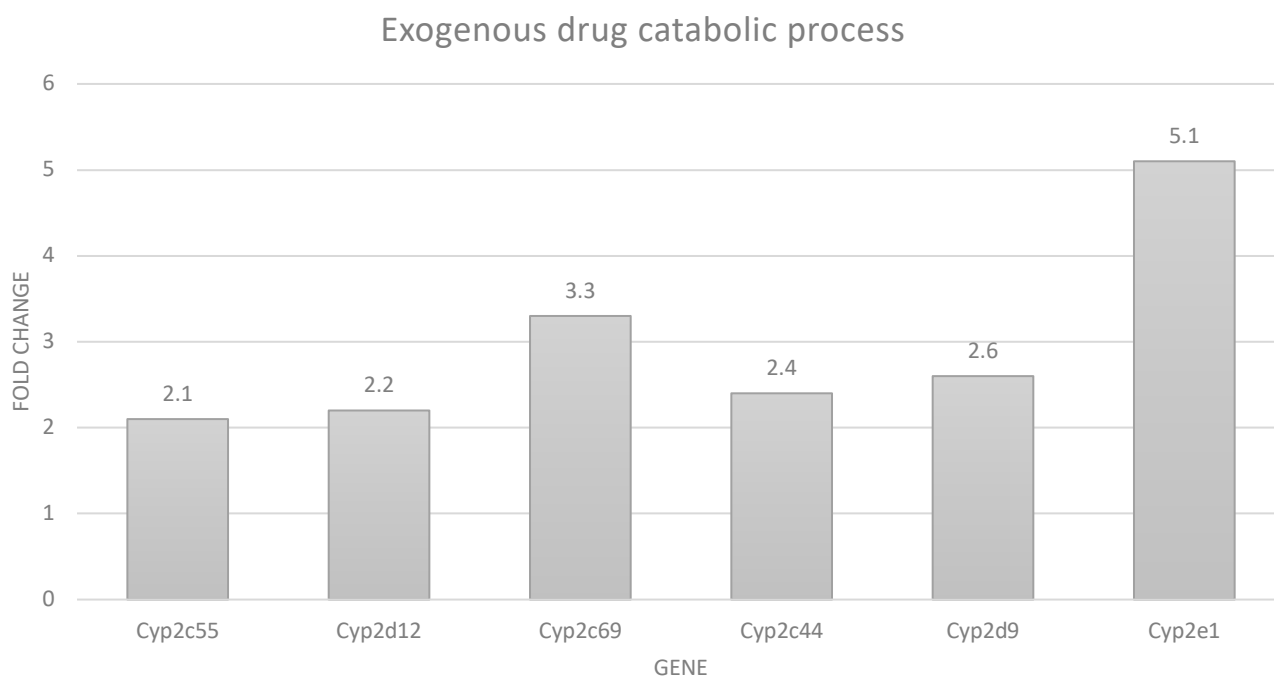


**Figure 16. GO term exogenous drug catabolic process.** Bar chart of GO term exogenous drug catabolic process and enriched genes containing fold-change values. *Corresponding table available in Appendix 1*



**Table 7. Molecular function as annotated by Gorilla.** GO terms associated to hormone activity, receptor activity and monooxygenase activity showed genes enriched in these categories. Genes associated with each GO term are listed below each description in a separate row.

GO term	Description	P-value
GO:0005179	hormone activity	2.30E-06
Insl5, Gal, Ppy, Retn, Fndc5, Retnlb, Sst, Adipoq, Grp, Lep		
GO:0048018	receptor ligand activity	1.37E-04
Gal, Klk1b4, Ppy, Adipoq, Cxcl9, Cmtm8, Lep, Insl5, Fgf10, Sectm1a, Nov, Fndc5, Retn, Gdf15, Retnlb, Sst, Nenf, Grp		
GO:0004497	monooxygenase activity	2.90E-04
Cyp2c55, Cyp2d12, Cyp2c69, Cyp2c44, Cyp2d9, Cyp2e1		
GO:0030545	receptor regulator activity	7.72E-04
Gal, Klk1b4, Adipoq, Cxcl9, Cmtm8, Lep, Insl5, Fgf10, Sectm1a, Nov, Retn, Fndc5, Retnlb, Gdf15, Sst, Mrap, Nenf, Grp		

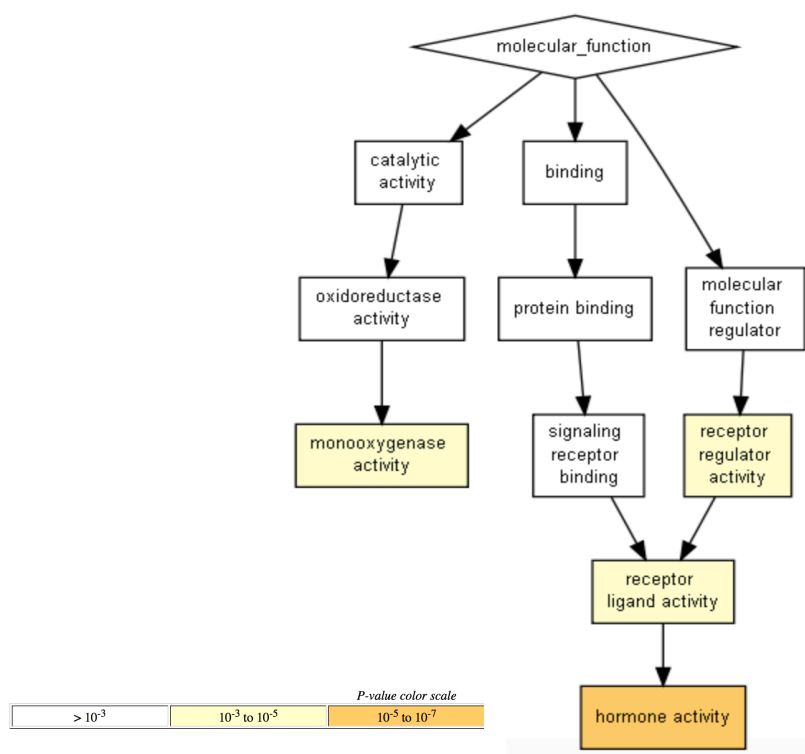
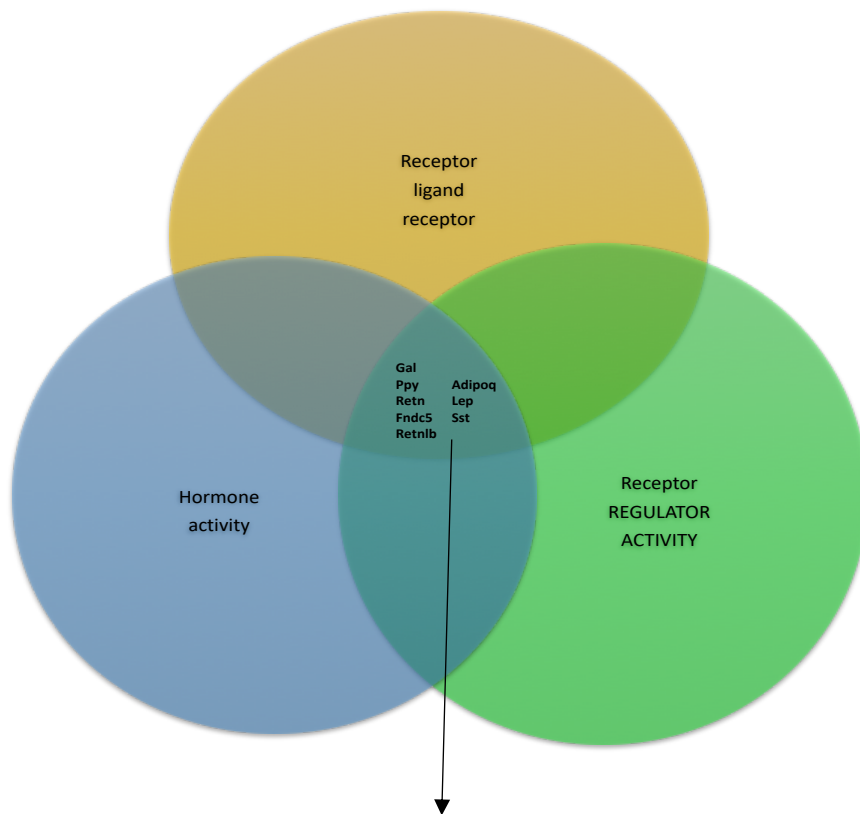


**Figure 18A. Flow chart and heat map indicating molecular function.** Left: Enriched genes in Gorilla associated to molecular function gene ontology.



**Galnin:** Gal  
**Pancreatic polypeptide:** Ppy  
**Resistin:** Retn  
**Fibronectin type III domain containing 5:** Fndc5  
**Resistin-like beta:** Retnlb  
**Adiponectin, C1Q and collagen domain containing:** Adipoq  
**Leptin:** Lep  
**Somatostatin:** Sst

**Figure 18B. Overlapping genes from DEG list.** Venn diagram showing common genes found between hormone activity, receptor ligand activity and receptor regulatory activity gene ontology terms. A total of 8 genes were found to have overlapping roles across (1) receptor ligand activity, (2) hormone activity, and (3) receptor regulator activity.

### 3.5 METH induces changes to genes enriched in the molecular function

#### GO:0004497 monooxygenase activity category.

Gorilla Gene Ontology and KEGG pathways mapped a total of seven genes (Table 7 and 8; figure 16 and 19) to the monooxygenase activity category. By definition, the monooxygenase activity gene ontology category is marked by the catalysis of the incorporation of one atom from molecular oxygen into a compound, and the subsequent reduction of a second oxygen atom to water.

**Table 8. Gorilla GO terms associated to cytochrome P450.** Derived from Gorilla gene ontology, seven genes were enriched in the monooxygenase activity category.

Cyp sub-family	Gene	Fold change
Cyp2	C55	+2.1
	C69	+3.3
	C44	+2.4
Cyp2d	D12	+2.2
	D9	+2.6
Cyp4f	F14	+2.1
Cyp2e	E1	+5.1

Three genes were related to the CYP2C sub-family, two genes to the CYP2D sub-family, one gene within the CYP4F subfamily, and one gene to the CYP2E sub-family. Within the mouse genome, and genome organisation, 15 functional CYP2C genes account for this cluster, whereas only 4 are defined in humans; making it futile to compare orthologs between these two species [Scheer et al., 2012]. In addition, two genes, *Cyp2d12* (>2-fold) and *Cyp2d9* (>2-fold), belonged to the *Cyp2d* gene cluster. In mice, nine *Cyp2d* homologs exist: *Cyp2d9*, *2d10*, *2d11*, *2d12*, *2d13*, *2d22*, *2d26*, *2d34* and *2d40* [Ning et al., 2015]. *Cyp2d12* possess a trans-membrane topology and is expressed in

adult colon. Furthermore, DAVID (KEGG pathway gene enrichment), mapped to the *metabolism of xenobiotics by cytochrome P450*, indicated Cytochrome P450, family 2, subfamily e, polypeptide 1, *Cyp2e1*, also known as cytochrome P450 2E1, throughout a series of xenobiotic pathways. Other cytochrome P450 molecules were not mapped onto the KEGG pathway. *Cyp2e1* is a major enzyme that catalyses ethanol oxidation in the CNS [Heit et al., 2013]. In addition, *Cyp2e1* is acted upon by inflammation and is highly conserved across species which signifies its relevance [Heit et al., 2013].

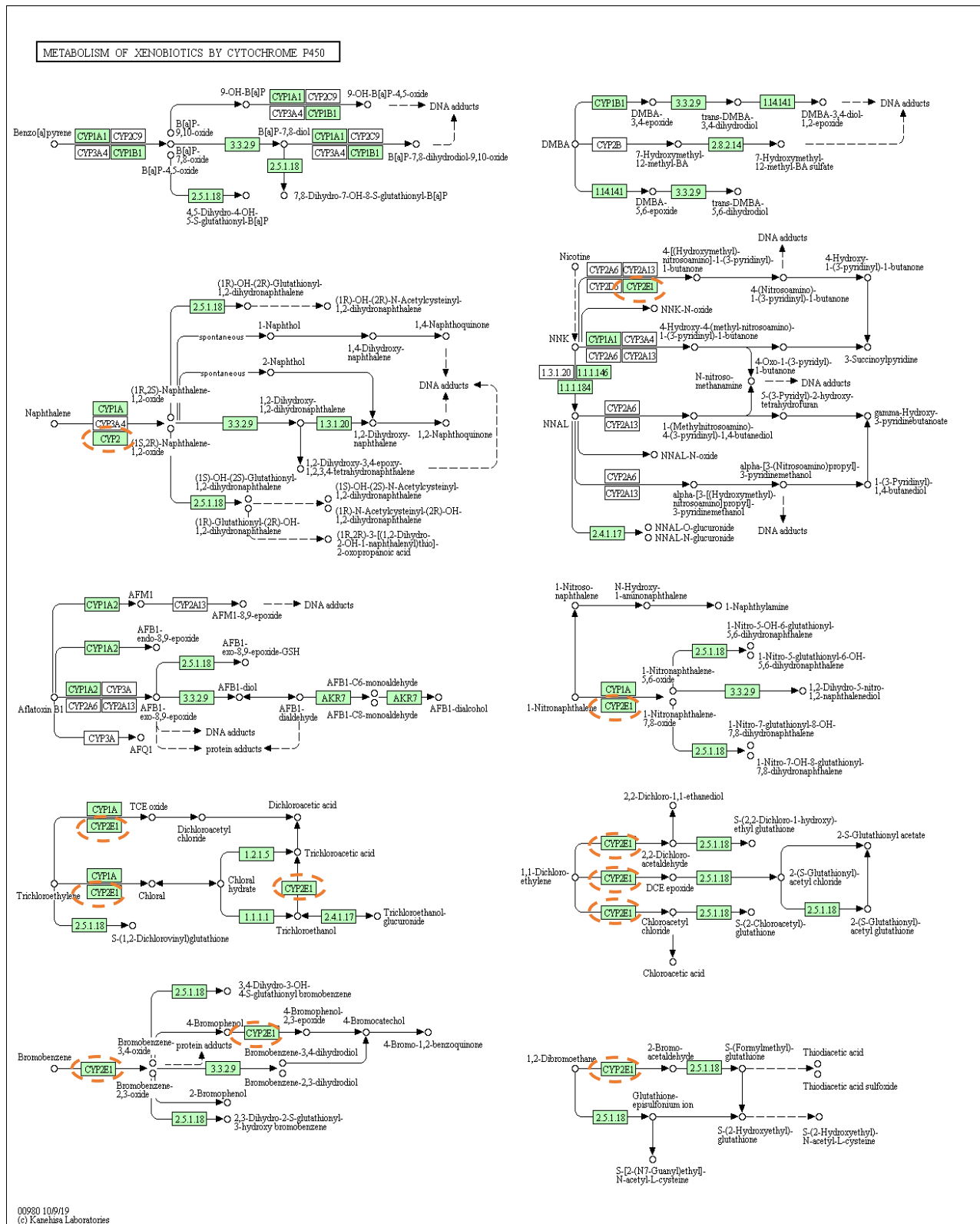


**Figure 19. KEGG pathway map of metabolism of xenobiotics via cytochrome P450.** *Cyp2e1*, known as cytochrome P450 2E1, was found to be associated to a number of metabolised xenobiotics. Broken orange circles refer to those enriched genes found in this study.

### **3.6 METH induces changes to receptor regulatory, receptor ligand and hormone activity.**

Hormone activity and levels can be significantly altered in chronic drug abuse, which can also lead to changes in the HPA axis [Zuloaga et al., 2015]. Moreover, galanin (*gal*), and galanin receptor-1 (*GalR1*) genes are upregulated in the locus coeruleus (LC) following opiate withdrawal [Picciotto et al., 2008]. Leptin, considered a hormone, is involved in regulating food and also drug-related behaviour [Cota et al., 2006]. In addition, leptin has been shown to play a role in appetite reduction or induction, and also serves a dual role as a hormone and cytokine thus, linking the immune and neuroendocrine systems [Gruzdeva et al., 2018]. A total of 8 genes were found to be expressed across three GO categories: receptor regulation, receptor ligand and hormone activity (Table 2) *Gal* (>2 fold), encoding a neuroendocrine peptide - a gene with known expression in the CNS, PNS, along with the gastrointestinal tract, adrenal gland and pancreas. *Retn*, resistin, (>4 fold) is a gene that plays several roles in inflammation, glucose homeostasis, and cardiovascular disease [Park et al., 2013]. In addition, *Retnlb* (resistin like beta) (>6 fold) encodes a colon and small intestine-specific cysteine rich protein which has a relation to the IL-4 mediated signalling pathway, along with microglia activation during neuroinflammatory events. *Lep*, leptin, was found to be highly expressed (>7 fold) in colon tissue. *Ppy* (pancreatic peptide) was also found to be expressed in colon tissue. *Ppy* encodes a member of the neuropeptide Y (NPY) family of peptides. This gene encodes for a preproprotein which is synthesised in the pancreatic islets of Langerhans and are subsequently proteolytically processed to two peptides. Fibronectin type II domain-containing 5 (*Fndc5*) was also

significantly upregulated (>2 fold) in mouse colon, along with *Adipoq* (>5 fold), known as adiponectin, clq and collagen domain containing.

Somatostatin, *Sst*, was found to be upregulated (>2 fold) in colon tissue.

### **3.7 Genes involved in placenta and blood vessel development are differentially expressed in a chronic METH withdrawal mouse model.**

Placenta development and simultaneous drug use can impact both the developing fetus and newborn. In addition, birth defects can occur with illicit drug use in females, and cocaine is known to cross the placenta, constricting blood vessels, and subsequently reducing blood flow to the fetus [Sachdeva et al., 2009]. The implications of METH and its abuse by pregnant individuals may lead to fetus development deficiencies, exemplified by a growing evidence of literature which suggests that amphetamines, like METH, target both norepinephrine and serotonin transporters located in the placental syncytiotrophoblast [Ganapathy et al., 2011; Sachdeva et al., 2009]. In this work, colon tissue was analysed for DEG changes, and the involvement of a dysregulated colon and placental development in a chronic METH withdrawal mouse model is yet to be fully described. Gorilla GO placenta development (GO:0001890) biological process also showed two DEGs; *Cdx2* (+10.2-fold-change) and *Lep* (+7.6-fold-change). *Cdx2* encodes a caudal type homeobox 2 transcription factor, which is involved in allantoic development, The *Cdx2* homeobox gene has multiple functions, including trophoctoderm specification, antero-posterior patterning and determination of intestinal identity [Benahmed et al., 2008]. In addition, *Cdx2* is the first homeobox protein to be expressed extra-embryonically in order to specify the trophoctoderm [Benahmed et al.,

2008], and is considered the ‘master gene’ to initiate intestinal identity

[Benahmed et al., 2008].

### **3.8 METH effects genes involved in the neuropeptide signalling pathway**

**(GO: 0007218)**

The neuropeptide signalling pathway is described as a series of molecular signals which are generated in response to a peptide neurotransmitter binding a cell surface receptor. Moreover, neuropeptides are signalling molecules that serve to regulate physiological processes in animals [Elphick et al., 2018].

Neuropeptide signalling pathway might be important in METH use since this particular pathway, and associated neuropeptides, may be linked to drug relapse, and drug taking behaviour. The secondary importance of better understanding this pathway in METH abuse is how to develop therapeutic outcomes for METH addicts, utilising neuropeptide pathways. The highest fold-change gene throughout the set of genes enriched in the neuropeptide signalling pathway was gastrin releasing peptide (*Grp*), with a fold-change of +3.6. Galanin, *Gal*, (+2.6) Pancreatic peptide, *Ppy*, (+3.0) and galanin receptor 2, *Galr2*, (+2.3) showed a slightly lower expression from the overall genes enriched in this ontology term.

**Table 9. GO terms of enriched genes in the neuropeptide signalling network.**  
Summary and description of neuropeptides and fold-change.

<b>Gene</b>	<b>Full name</b>	<b>Function</b>	<b>Expression (fold)</b>
Gal	Galanin	Modulation of processes: cognition, memory, sensing, pain processing, neurotransmission, hormone secretion and feeding behaviour [Kim et al., 2007].	+2.6
Ppy	Pancreatic polypeptide	Expressed by endocrine cells of the digestive system [Holzer et al., 2012].	+3.0
Galr2	Galanin receptor-2	Mainly mediates stimulatory effects of galanin on neurotransmitter release; coupled to the phospholipase C pathway, intracellular calcium mobilisation and calcium – dependent Cl <sup>-</sup> channel activation [Ogren et al., 2010].	+2.3
Grp	Gastrin-releasing peptide	Gastrin releasing peptide, along with its receptor, is expressed in epithelial cell lining in the colon during gut development [Tell et al., 2011]. GRP and its receptor are upregulated in colon cancer [Ruginis et al., 2006]. GRP is known to regulate numerous physiological processes/responses in the GI tract including altering smooth muscle contractility, regulating secretion of the exocrine pancreas, and influencing release of other GI peptide hormones [Carroll et al., 2002].	+3.6

## 4.0 Discussion

The obvious strength of gene ontologies (GO) rests within its capability to access around 40,000 terms across three broad ontologies: 1) molecular function, 2) biological process and 3) cellular component [Huntley et al., 2014]. Gene expression data require careful analysis in order to provide output that is both relevant and powerful [Dalman et al., 2012]. The incorporation of Gene Ontology (GO) annotation, p-value and fold change cut-offs and Bonferroni corrections [Dalman et al., 2012] all lead to a decrease in expression data, enriching and empowering search criteria. The aim of this work was to determine associated gene expression changes in the mouse distal colon from the chronic administration of a psychoactive drug – METH – followed by a withdrawal period. The purpose of understanding how METH affects colon gene expression is more specifically linked to how disruption to the colon may be linked to communication with the brain, from a chronic METH dose, and how this might lead to heightened neuro-inflammation. This study sought to interpret NGS colon data which could help better understand the role of the colon, impacted by a chronic METH dose, might play in a chronic drug model; and, how this role could be linked to alterations in neurological behaviour, such as the relationship between the gut-brain axis (GBA). Furthermore, gene ontological software assisted in building several informative ‘maps’ indicating the enrichment of groups of genes specific to one, or more, biological, functional and/or molecular function processes (Table 3; Table 4; Table 5; Table 8; Figure 4; Figure 5).

In this study, a stringent criterion was utilised in order to study only genes with a differential expression of  $\geq 2$ -fold for analysis (Figure 3). Further, p-values were set at  $p = 0.003$  to reduce gene list size, ensuring that the data analysis represented genes with significant associations with the research in question. To our knowledge, these results are the first to report the effects of METH on a multitude of differentially expressed genes (DEG) in the mouse distal colon. We found the majority of significantly expressed gene changes in processes associated with various cytochrome P450 genes and several metabolic processes (Figure 19; Figure 13; Table 9). A total of 34 genes:  $\geq 2$ -fold, 32 genes  $\geq 3$ -fold, 11 genes  $\geq 4$ -fold, 9 genes  $\geq 5$ -fold, 4 genes  $\geq 6$ -fold, 2 genes  $\geq 7$ -fold, 1 gene  $\geq 8$ -fold and 4 genes above 10-fold were mapped to various gene ontological terms using, namely, DAVID bioinformatics and Gorilla gene ontology. The METH dose chosen for this animal model (0.5mg/kg-7mg/kg) reflects an escalating dose pattern that is usually observed in human METH addicts. In our model, escalating METH dose was administered in order for mice to acclimatize to the dose, wherein a three-day withdrawal period would allow time for withdrawal experience.

Furthermore, a search within NCBI using 'Methamphetamine AND colon' brought back 11 PubMed results. To our knowledge, this study represents the first critical analysis of understanding how METH impacts the colon, specifically the distal colon, using NGS coupled with a gene ontological bioinformatics approach. However, a more holistic experimental approach to METH will be required in order to specify any significant connections between the colon and CNS in a mouse model. Moreover, gene expression profiles across several organs, including the brain, might provide invaluable data as to the role

of chronic METH in neuro-inflammation, as well as how this may impact behaviour.

#### 4.1 Tight junctions and METH

Our data also suggests the involvement of tight junction genes in this chronic METH model (Figure 6). Previous data on the effects of METH on mouse colon has shown that self-administration of METH saw a reduction of protein *claudin-1* and *ZO-1*, indicating an increase in colon permeability. From our input of 602 genes, we found a significant increase in *claudin-15* ( $\geq 2$ -fold), whilst observing a significant decrease in *claudin-1* (-3.7-fold). This supports previous findings that have shown a marked reduction of protein *claudin-1*. *Claudin-1* is a major tight junction protein (TJ) which is important for the correct maintenance of epithelial cell polarity [Huo et al., 2009], along with being involved in various cancers and inflammatory states [Forster, 2008]. We also found insignificant expression patterns with other tight junction genes such as *Cldn23* (+0.73-fold) and *Cldn-8* (-0.62-fold). The significance of tight junction proteins in endothelial cells is their necessary function to create a physical barrier that not only maintains adhesion of ECs, but also control leukocyte migration through striking a balance between several signalling molecules [Cerutti et al., 2017]. In general, claudins are major tight junction components [Samanta et al., 2018]. METH, in this escalating dose mouse model may alter tight junctions, during the withdrawal period. The apparent fold-increase of *claudin-15* could be associated with the repair of tight junction permeability, as the chronic METH dose period was followed by three days of drug withdrawal.  $\alpha$ -T-catenin (*ctnna3*) was found to be upregulated in our study and related to the KEGG pathway leukocyte trans-endothelial migration (Figure 7). Recently,  $\alpha$ -T-catenin was described as being expressed in the cerebellum, heart and skeletal

muscle and testis [Vite et al., 2015], with a role in cell adhesion [Ramoni et al., 2009]. Interestingly,  $\alpha$ -T-catenin is associated to the cadherin catenin complex, which makes up the core of the adherens junction (AJ) [Wickline et al., 2016]. Prior work has shown the role of  $\alpha$ -T-catenin as an actin-binding  $\alpha$ -catenin which couples the adherens junction to the actin cytoskeleton [Wickline et al., 2016]. Our results confirm that METH plays a role in regulating  $\alpha$ -T-catenin. This increased expression in our chronic METH model could serve as preliminary data which suggests  $\alpha$ -T-catenin, along with tight junctions, play important roles in adhesion of epithelial cells. Furthermore, the upregulation of  $\alpha$ -T-catenin could be a response to a 'leaky gut', from colonic bacteria. Collectively, METH does play a role in altering several tight junction genes in the colon. However, obtaining protein expression profiles, juxtaposed to gene expression profiling in not only colon, but also brain tissue would serve as a robust comparison with other METH studies, along with providing vital information as to the relationship between tight junction expression, the CNS, and psychiatric behaviour. These should be studied in the context of both acute and chronic METH use, followed by drug withdrawal, as to ascertain the degree of similarity and/or difference in tight junction expression in inflammation.

#### **4.2 METH involvement in Serotonergic synapses**

Serotonergic systems contribute to several disorders and diseases, including insomnia, anxiety, depression, Parkinson's disease and Alzheimer's disease [Charnay et al., 2010]. In this study, *alox12* (-1.15-fold), *alox15* (-1.20-fold), *cacl1s* (-3.60-fold), *plcb4* (-1.13-fold), *prkcb* (-1.62-fold) and *tph1* (+1.04-fold) showed differential gene expression (Figure 8). *Alox12* and *alox15* are both lipooxygenases, enzymes that are involved in oxidase polyunsaturated fatty acids and also which play roles in inflammation and oxidation [Singh et al.,

2019]. In humans, *alox12* is the predominant isoform of lipoxygenases, and produces 12-(S)-hydroxyeicosatetraenoic acid from arachidonic acid [Imai et al., 2017]. Significantly over-expressed, *cacna1s* (-3.60-fold) is involved in excitation and contraction in skeletal muscle. Little is known of *cacna1s* in METH studies, however previous work assessed METH and its impact on voltage-gated Calcium channels in an SH-SY5Y cell line which modelled dopaminergic neurons [Andres et al., 2015]. This work found that that a prolonged exposure of SH-SY5Y cells to METH led to up-regulation of the *cacna1s* gene. As a result, increases in L-type  $Ca^{2+}$  channels were observed. The long-term effects of this *cacna1s* upregulation has been attributed to neuronal death [Andres et al., 2015]. Our results of the *cacna1s* gene expression support this view, however, cannot be adequately compared due to differences in METH dose, study design and cell type being investigated. However, the over 3-fold expression of the *cacna1s* gene in this study might suggest that a chronic METH plays a role in neuronal damage. *Plcb4* (-1.13-fold), known as phospholipase C Beta 4, was shown, according to KEGG pathways, to be involved in calcium signalling. Little is known about *Plcb4* and its role in METH, however due its ability to act as a second messenger and assist in the regulation of intracellular calcium stores, *Plcb4*, and its downregulation may be involved in calcium signalling processes.

### 4.3 Cytokine-cytokine receptor interactions caused by METH

Our results show that distal colon *cxcl9* ( $\geq 3$ -fold) and *cxcl5* ( $\leq 15$ -fold) were significantly impacted upon by chronic METH withdrawal in our mouse model (Table 6). Highest expression was seen with *slc9a3* (88.50-fold), sodium/hydrogen exchanger 3 – also known as NHE3. *Slc9a3* deficient mice have previously been reported to develop spontaneous colitis [Johansson et al., 2014]. In addition, *Slc9a3* has also been demonstrated to have a critical role in both sodium ( $\text{Na}^+$ ) and fluid absorption in the intestine, evident from  $\text{NH}_3^{-/-}$  (nullified) mice experiencing chronic diarrhoea [Engevik et al., 2013]. The high *Slc9a3* gene expression could be due to an impaired expression caused by proinflammatory cytokines and/or bacteria [Laubitz et al., 2008]. *Slc9a3* knock-out mice showed a vast shift in colon gene expression. Furthermore, genes associated with this mouse knock-out were largely attributed to an exacerbated innate, adaptive immune and inflammatory response [Laubitz et al., 2008]. Another possibility for the high gene expression of *Slc9a3* could be attributed to the action of short-chain fatty acids (SCFA) on colonic epithelial cell functioning [Musch et al., 2001]. Indeed, it has been shown that *Slc9a3* was shown to be regulated by luminal SCFAs, which in turn was found to modulate *Slc9a3* activity, and overall sodium (Na) absorption [Musch et al., 2001]. Other work has found that METH self-administration in mice elevated  $\alpha$ -synuclein whilst reducing production of parkin, tyrosine hydroxylase (TH) and D $\beta$ H (dopamine- $\beta$ -hydroxylase) in the myenteric plexus of the distal colon [Flack et al., 2017]. Interestingly, a period of forced abstinence returned of all three METH biomarkers to control levels [Flack et al., 2017]. In this work, however, *dbh* was only over expressed slightly by +1.5-fold. *Dbh* is involved in

converting dopamine into norepinephrine in noradrenergic neurons [Gaval-Cruz et al., 2012], and this enzyme plays as central role in the regulation of ration of dopamine and norepinephrine [Okahisa et al., 2014]. The +1.5-fold change seen in this chronic METH model may be due to the increased concentration of neurotransmitters such as dopamine, serotonin and norepinephrine, from the presence of METH. An increase in dopamine- $\beta$ -hydroxylase could signify an increased conversion of dopamine to norepinephrine in the colon tissue. The CXCR3 ligand, *Cxcl9*, plays a role in Ulcerative Colitis (UC) [Chen et al., 2017; Elia et al., 2018]. In this work, *Cxcl9* was upregulated (above +3-fold). *Cxcl9*, in the colon, is increased in response to inflammation [Trivedi et al., 2018]. Its role in chronic METH use has yet to be understood. Under normal physiological conditions, the colon epithelium expresses basal levels of *Cxcl9*, and its chemokine receptor, CXCR3, has an important role to play during leukocyte recruitment to an inflamed intestine [Trivedi et al., 2018]. The increased expression of *Cxcl9* could be a consequence of local inflammation in the distal colon, which may be caused by the chronic METH dose used in this model (Figure 9A). Moreover, *Cxcl5* (CXC chemokine ligand 5), also known as epithelial neutrophil-activating peptide-78 [Wang et al., 2016], revealed an expression of  $\leq 15$ -fold, and is a chemokine which is known to bind to the chemokine receptor, CXCR2 [Koltsova et al., 2010]. *Cxcl5* is known to be produced by immune (neutrophils and monocytes) and vascular endothelial cells via NK- $\kappa$ B activation [Li et al., 2011; Wang et al., 2016]. The high gene fold-change could be attributed to one of several explanations. Firstly, its expression may be a response to microbial killing or tissue repair [Sepuru et al., 2014]. Secondly, *Cxcl5* has been shown to be overexpressed in colon cancer, along with gastric and pancreatic cancer [Li et al., 2011]. Previous work has indicated that *Cxcl5* was upregulated (above 27-fold) at a METH dose of 100 $\mu$ l

[Bortell et al., 2017]. This overexpression of *Cxcl5* was associated with several gene networks involved in inflammation, and neuroactive ligand-receptor interactions [Bortell et al., 2017]. Furthermore, *Cxcl5*, along with *MAP2K5* and *GPR65*, might play a role in neurological disease, from astrocytes exposed to a high METH dose [Bortell et al., 2017]. METH, after a chronic period, followed by drug withdrawal (this study) may induce *Cxcl5* expression in the colon due to inflammation brought on by an escalating METH dose. However, further analysis on protein expression studies is required to determine its role *in vivo*.

#### **4.4 Placental and blood vessel development**

Placental and blood vessel development (Table 7) and drug abuse use can have harmful effects both the developing fetus and newborn. Further, birth defects can occur with illicit drug use in pregnant females. The illicit drug, cocaine is known to cross the placenta, constricting blood vessels, and subsequently reducing blood flow to the fetus [Sachdeva et al., 2009]. In this study three genes were differentially expressed – *cdx2* (+3.35-fold), *wt1*(+2.65-fold), and *lep* (+2.92) (Figure 14; Figure 15). *Cdx2*, claudal-type homeobox-2, is involved in trophoblast development, and is also significant in the self-renewal of trophoblast stem cells which form the placenta [Vadakke-Madathil et al., 2019]. Moreover, *cdx2* is known as the master regulator of murine trophoblast development and is also expressed in human trophoblasts [Knofler et al., 2019]. In this work, *cdx2* was observed as significantly differentially expressed, and, according to gene ontologies mapped to placental and blood vessel development. *Wt1*, known as Wilms tumour 1 gene, functions as an instruction to make a zinc-finger transcription factor protein required for kidney and gonad development [Ambu et al., 2015], along with prenatal development of other organs, such as adrenal glands, heart and spleen [Ferretti et al., 2005]. Moreover,

wt1 gene is also necessary for correct embryogenesis [Scholz et al., 2011]. Lep, leptin gene, also known as placental leptin in this context, is also hypothesized to play a role in fetal growth and development [Tsai et al., 2015]. It has also been suggested that leptin levels might have an effect on fetal brain development, through the activation of pro-inflammatory cytokines [Valleau et al., 2014]. The implications of METH and its abuse by pregnant individuals may lead to fetus development deficiencies, exemplified by a growing evidence of literature which suggests that amphetamines, like METH, target both norepinephrine and serotonin transporters located in the placental syncytiotrophoblast [Ganapathy et al., 2011; Sachdeva et al., 2009]. However, in this work, the collective over expression of cdx2, wt1 and lep is yet to be clearly defined in METH animal models. It might be that the chronic METH dose, followed by a withdrawal period could impact a range of genes, including those studied here, which may lead to the proper development of the fetus. However, this would require further METH research in animal models, investigating a wider spectrum of genes involved in placental and blood vessel development.

#### **4.5 Neuropeptide signalling**

Our data also showed significantly high expression of the neuropeptide galanin (gal: +2.6-fold) (Figure 12; Table 10), a 29-amino acid highly conserved neuroendocrine peptide found in both the brain and gut [Kim et al., 2007]; which, apart from being distributed and expressed in the CNS is also present in the gastrointestinal (GI) tract [Benya et al., 1999]. In addition, galanin is secreted by enteric nerves which function to inhibit pancreatic exocrine and endocrine secretions, enable smooth muscle contraction and relaxation, and to modulate other peptide hormones [Benya et al., 1999]. In the rat gastrointestinal

tract, galanin, *Gal*, serves multiple roles such as regulating transmitter release, secretion and motility [Anselmi et al., 2005]. In this work, Gal expression was observed (+1.4-fold). However, little has been reported on the role of galanin in METH research. Galanin may be involved in the gut-brain communication during METH consumption, along with a potential role in neuroinflammation. Further, galanin might also serve a role in neuromodulation in drug addiction, however this has yet to be fully uncovered [Genders et al., 2020]. Interestingly, galanin receptor-2 (*galr2*) gene expression was observed as +2.3-fold change. *Galr2* is found primarily in peripheral tissues, such as the gastrointestinal tract, skeletal muscle, heart, kidneys, and also in the CNS. Activation of *Galr2* receptor leads to both anti-depressant and anxiolytic effects [Genders et al., 2020]. With both *gal* and *galr2* showing a similar gene expression profile, their involvement in chronic METH administration in this study may be linked to both mood and neuromodulation. Gastrin-releasing protein (GRP), fold-change of +3.6 in this study, is known to mediate gastric acid secretion in the gut [Shirey et al., 2019]. Gastric-releasing protein (or peptide) bind to G-protein coupled receptors [Pendharkar et al., 2017]. Moreover, this 27-amino acid peptide is involved in a number of cellular responses, including cell growth, proliferation, inflammation and angiogenesis [Park et al., 2017]. *Grp* has also been shown to improve intestinal barrier function, along with decreasing inflammation [Pendharkar et al., 2017]. In METH, the increased gene expression of *grp* might be involved in brain function, through its gut-brain axis relationship. Moreover, since *grp* is also reported to regulate emotions, memory and feeding behaviour, it may play a role in these processes in chronic METH. Ppy, (MAAACRCLSLLLLSTCVALLL) pancreatic polypeptide, belongs to the neuropeptide Y family [Hoyle, 2008]. Furthermore, Ppy is a hormone and is known to have communication between the gut and the brain, influencing the

gut microbiota whilst also regulating the CNS [Li et al., 2019]. As an expression of +3.0-fold was observed in this study, Ppy may be another molecule which maintains communication between the gut and brain during chronic METH and chronic METH withdrawal models. Overall, the involvement of neuropeptides – ppy, grp, gal, and galr2 - in METH may all contribute physiological functions in the colon. Expanding this view, it could also be that there is considerable cross-communication between the peripheral (PNS) and central nervous (CNS) systems via the expression of these neuropeptides and neuropeptide receptors. Further work should focus on a better understanding of this particular signalling pathway in METH.

#### **4.6 Bacterial responses to METH**

Our results processed in GO Gene Ontology Enrichment analysis and visualisation tool (Gorilla) database also revealed genes associated with bacterial response. We found 23 genes related to the GO:0009617: Response to bacterium (Figure 10; Figure 17). Interestingly, *ang4*, known as angiogenin 4, and whose product encodes a bactericidal/antimicrobial gut protein [Hooper et al., 2003] was found to be highly expressed in distal colon tissue ( $\geq 12$ -fold). Angiogenin-4 expression is induced by the gut microflora bacteria, *Bacteroides thetaiotaomicron* [Hooper et al., 2003], and is expressed in Paneth cells in which *Ang4* product mediates epithelial host defence against *L. monocytogenes* and *E. faecalis* [Nelson et al., 2005]. In mice, five ANG genes sit on chromosome 14, whereas only one ANG gene (chromosome 14) is present in humans [Sheng et al., 2015]. Resistin-like molecule beta (*Retnlb*:  $\geq 6$ -fold), represents the gene name for RELM- $\beta$ , which is synthesised and secreted by goblet cells, as a homodimer [Bhatia et al., 2015]. RELM- $\beta$  is induced by enteric bacterial colonisation and helminth infection [Bhatia et al., 2015]. Goblet cells are known

to secrete a range of molecules, including mucins, and resistin-like molecule beta and are highly expressed in several disease settings such as inflammatory bowel syndrome (IBS) [Nair et al., 2008]. The presence of increased *Retnlb* gene expression in this mouse model could suggest defence against gram-negative bacteria, thereby enabling protection of host tissues [Propheter et al., 2017]. Lesser expression, above 2-fold, however below 4-fold, was observed for *Thrsp*, *Gpm6a*, *Fabp4*, *Serpine1*, *Hist1h2be* and *Gdap10*. *Thrsp*, known as thyroid hormone responsive, is regulated and controlled by nutritional and hormonal factors. A genomics-based approach research on non-alcoholic fatty liver disease (NAFLD), chronic liver disease, showed *Thrsp* to be one gene, along with *Fasn*, *Pklr* and *Chchd6*, to have an involvement as a potential regulator of the NAFLD processes [Krishnan et al., 2018]. *Gpm6a*, known as stress-responsive neuronal membrane glycoprotein M6a, plays several roles in brain functioning, including synaptogenesis [Monteleone et al., 2014], and is primarily expressed in neurons [Fuchsova et al., 2015]. Its expression (+4.1-fold) in distal colon tissue, in a chronic METH dose context, has yet to be fully described in the literature. One main finding of *Gpm6a* is its role in stress response in animals [Fuchsova et al., 2015]. Given that *Gpm6a* is expressed across multiple regions in the central nervous system (CNS), one likely explanation could be the presence of gut-brain communication instigated by chronic METH dose in mice. *Fabp4* (+2.5-fold change), fatty acid binding protein 4, was differentially expressed in the mouse colon NGS data (Figure 11). Fatty acid-binding proteins are low-molecular weight molecules which assist in transporting long-chain fatty acids in cells [Zhang et al., 2019]. *Fabp4* is expressed in differentiated adipocytes and macrophages [Zhang et al., 2019], and has been found to be expressed in intestinal epithelial cells and the colon [Mosinska et al., 2019]. Moreover, *Fabp4* has roles in inflammation and

metabolism and may also regulate cyclooxygenase 2 (COX2) which in turn affect macrophage function [Qiao et al., 2019]. Its potential expression in chronic METH mice models could a response to inflammation. Little is known about *Serpine1*, Serpin family E member 1, and its role in chronic METH. Previously, *Serpine1* has been linked to prognosis of patients with the colorectal cancer type known as colon adenocarcinoma [Zeng et al., 2019]. In addition, *serpine1* was found to have a higher expression in gastric tumour tissues [Liao et al., 2018]. Although no data is currently available linking *Serpine1* expression to METH, its expression (+3.1-fold change) in this study requires further investigation to better elucidate its role in chronic METH mice models. *Hist1h2be*, histone cluster 1 H2B family member E, is a unique homomorphic variant of H2B [Nayak et al., 2015]. Its expression (+2.3-fold) was observed in this work, and this may be related to several biological processes, as indicated by gene ontology studies, such as antibacterial humoral response, defence against gram-positive bacteria and innate immune response in mucosa. Overall, the genes related to bacterial responses in this chronic METH withdrawal model could play a significant role in responding to bacterial threats in the colon. In addition, inflammation in the colon might lead to changes in gene expression which could impact the gut-brain axis, upon METH administration.

## Conclusion(s)

Overall, this work represents the first NGS study that has investigated the role of chronic METH and its effects on mouse colon gene expression. Specifically, several ontological processes allowed for a closer investigation as to which genes were enriched in each process. This enrichment aspect of gene ontologies can lead to a more focused study on gene groups which can be further analysed in a drug abuse context, and subsequently compared to the literature.

Changes in gene expression were observed across several ontological processes, including monooxygenase activity, responses to bacteria, tight junction and cell-cell adherence, and neuropeptide signalling. Overlapping genes (Figure 18A and 18B) were noted in three molecular functions: hormone activity, receptor ligand activity and receptor regulator activity. Expression of these genes were hypothesised to serve a role in stress during METH withdrawal in mice, however this hypothesis requires further behavioural studies of animals, in a chronic METH context. Of particular interest is the finding of neuropeptide signalling, in which minimal data exists in METH studies. Neuropeptide signalling is becoming increasingly discussed in its role in mental health – depression, motivation, reward. This is an important aspect of METH abuse, since METH causes profound changes in mood following drug withdrawal. Although further METH-related *in vivo* and *in vitro* studies should incorporate more detailed study designs to assess the role of neuropeptides, such as pancreatic polypeptide (ppy), our work provides a glimpse into the possible role of neuropeptide signalling in a chronic drug model, and how this may influence certain neurological processes which are linked to the gut. The colon is home to around between 1000-1,150 bacteria. The perturbation of these microbial communities can have downstream effects which greatly influence and can

cause conditions such as depression and immune system disorders. Since a part of this study found an enrichment of genes belonging to the gene ontology term, response to bacteria, this may indicate that chronic METH, in a mouse model, causes changes to genes responsible for regulating the defence against bacteria. Furthermore, this [bacterial] response, evidenced by the upregulation of the bactericidal/antimicrobial protein, angiogenin 4, could have severe implications that affect mood, and may lead to behavioural and mental health issues in chronic METH users. This data suggests that understanding gut homeostasis, or the presence of dysbiosis of gut microbiota is crucial to better understanding how METH might impact the gut-brain axis. More work regarding the elucidation and role of certain bacterial species in the gut, in an acute and chronic METH mouse model, would help build a case for how inflammatory states in the colon are communicative pathways across the gut and brain. Lastly, the role of genes involved in placental and blood vessel development in this work highlights, for the first time, the role of METH in these developmental processes. In order to gauge a stronger conclusion of these data, more exclusive *in vivo* work of METH with closer investigation of *cdx2*, *wt1* and *lep* genes, could provide strengthened insights into how METH impacts fetal development.

## References

- Ambu, R., Vinci, L., Gerosa, C., Fanni, D., Obinu, E., Faa, A., & Fanos, V. (2015). WT1 expression in the human fetus during development. *European journal of histochemistry : EJH*, 59(2), 2499. <https://doi.org/10.4081/ejh.2015.2499>
- Andres, M. A., Cooke, I. M., Bellinger, F. P., Berry, M. J., Zaportez, M. M., Rueli, R. H., Barayuga, S. M., & Chang, L. (2015). Methamphetamine acutely inhibits voltage-gated calcium channels but chronically up-regulates L-type channels. *Journal of neurochemistry*, 134(1), 56–65. <https://doi.org/10.1111/jnc.13110>
- Anselmi, L., Stella, S. L., Jr, Lakhter, A., Hirano, A., Tonini, M., & Sternini, C. (2005). Galanin receptors in the rat gastrointestinal tract. *Neuropeptides*, 39(3), 349–352. doi:10.1016/j.npep.2004.12.023
- Benahmed, Fairouz & Gross, Isabelle & Gaunt, Stephen & Felix, Beck & Jehan, Frédéric & Domon-Dell, Claire & Martin, Elisabeth & Kedinger, Michèle & Freund, Jean-Noel & Duluc, Isabelle. (2008). Multiple Regulatory Regions Control the Complex Expression Pattern of the Mouse Cdx2 Homeobox Gene. *Gastroenterology*. 135. 1238-1247, 1247.e1. 10.1053/j.gastro.2008.06.045.
- Benya, Richard & Marrero, Jorge & Ostrovskiy, Denis & Koutsouris, Athanasia & Hecht, Gail. (1999). Human colonic epithelial cells express galanin-1 receptors, which when activated cause Cl<sup>-</sup> secretion. *The American journal of physiology*. 276. G64-72. 10.1152/ajpgi.1999.276.1.G64.
- Bhatia, Shikha & Ponnuraj, Nagendra Prabhu & Benefiel, Ann & Miller, Michael & Chow, Jomay & Davis, Steven & Gaskins, Rex. (2015). Galacto-oligosaccharides may directly enhance intestinal barrier function through the modulation of goblet cells. *Molecular Nutrition & Food Research*. 59. 10.1002/mnfr.201400639.
- Bortell, N., Basova, L., Semenova, S., Fox, H. S., Ravasi, T., & Marcondes, M. C. (2017). Astrocyte-specific overexpressed gene signatures in response to methamphetamine exposure in vitro. *Journal of neuroinflammation*, 14(1), 49. doi:10.1186/s12974-017-0825-6
- Carroll, Robert & Matkowskyj, Kristina & Sauntharajah, Yogen & Sekosan, Marin & Battey, James & Benya, Richard. (2002). Contribution of gastrin-releasing peptide and its receptor to villus development in the murine and human gastrointestinal tract. *Mechanisms of development*. 113. 121-30. 10.1016/S0925-4773(02)00032-1.
- Cerutti, C., & Ridley, A. J. (2017). Endothelial cell-cell adhesion and signaling. *Experimental cell research*, 358(1), 31–38. doi:10.1016/j.yexcr.2017.06.003
- Charnay, Y., & Léger, L. (2010). Brain serotonergic circuitries. *Dialogues in clinical neuroscience*, 12(4), 471–487.

- Chella Krishnan, K., Kurt, Z., Barrere-Cain, R., Sabir, S., Das, A., Floyd, R., ... Yang, X. (2018). Integration of Multi-omics Data from Mouse Diversity Panel Highlights Mitochondrial Dysfunction in Non-alcoholic Fatty Liver Disease. *Cell systems*, 6(1), 103–115.e7. doi:10.1016/j.cels.2017.12.006
- Chen, W., Edington, C., Suter, E., Yu, J., Velazquez, J. J., Velazquez, J. G., ... Lauffenburger, D. A. (2017). Integrated gut/liver microphysiological systems elucidates inflammatory inter-tissue crosstalk. *Biotechnology and bioengineering*, 114(11), 2648–2659. doi:10.1002/bit.26370
- Chen, X., Lu, J., Zhao, X., Chen, C., Qiao, D., Wang, H., & Yue, X. (2019). Role of C/EBP- $\beta$  in Methamphetamine-Mediated Microglial Apoptosis. *Frontiers in cellular neuroscience*, 13, 366. doi:10.3389/fncel.2019.00366
- Cook, R. R., Fulcher, J. A., Tobin, N. H., Li, F., Lee, D. J., Woodward, C., ... Gorbach, P. M. (2019). Alterations to the Gastrointestinal Microbiome Associated with Methamphetamine Use among Young Men who have Sex with Men. *Scientific reports*, 9(1), 14840. doi:10.1038/s41598-019-51142-8
- Cota, Daniela & Barrera, Jason & Seeley, Randy. (2006). Leptin in Energy Balance and Reward: Two Faces of the Same Coin?. *Neuron*. 51. 678-80. 10.1016/j.neuron.2006.09.009.
- Dalman, Mark & Deeter, Anthony & N, Ga & Duan, Zhong-Hui. (2012). Fold change and p-value cutoffs significantly alter microarray interpretations. *BMC bioinformatics*. 13 Suppl 2. S11. 10.1186/1471-2105-13-S2-S11.
- Dong, C. & Wang, X. & Xu, H. & Zhan, Xiaohui & Ren, H. & Liu, Z. & Liu, G. & Liu, L.. (2017). Identification of a cytokine-cytokine receptor interaction gene signature for predicting clinical outcomes in patients with colorectal cancer. *International Journal of Clinical and Experimental Medicine*. 10. 9009-9018.
- Droutman, V., Xue, F., Barkley-Levenson, E., Lam, H. Y., Bechara, A., Smith, B., ... Read, S. J. (2019). Neurocognitive decision-making processes of casual methamphetamine users. *NeuroImage. Clinical*, 21, 101643. doi:10.1016/j.nicl.2018.101643
- Elia, G & Guglielmi, G. (2018). CXCL9 chemokine in ulcerative colitis. *La Clinica terapeutica*. 169. e235-e241. 10.7417/CT.2018.2085.
- Elphick, M. R., Mirabeau, O., & Larhammar, D. (2018). Evolution of neuropeptide signalling systems. *The Journal of experimental biology*, 221(Pt 3), jeb151092. doi:10.1242/jeb.151092
- Engevik, M. A., Aihara, E., Montrose, M. H., Shull, G. E., Hassett, D. J., & Worrell, R. T. (2013). Loss of NHE3 alters gut microbiota composition and influences *Bacteroides thetaiotaomicron* growth. *American journal of physiology. Gastrointestinal and liver physiology*, 305(10), G697–G711. doi:10.1152/ajpgi.00184.2013
- Ferretti, Elisabetta & Arturi, Franco & Mattei, Tiziana & Scipioni, Angela & Tell, Gianluca & Tosi, Emanuele & Presta, Ivan & Morisi, Roberta & Lacroix, Ludovic & Gulino, Alberto & Russo, Diego & Damante, Giuseppe & Filetti, Sebastiano. (2005). Expression, Regulation, and Function of Paired-Box Gene

8 in the Human Placenta and Placental Cancer Cell Lines. *Endocrinology*. 146. 4009-15. 10.1210/en.2005-0084.

- Ferrucci, M., Limanaqi, F., Ryskalin, L., Biagioni, F., Busceti, C. L., & Fornai, F. (2019). The Effects of Amphetamine and Methamphetamine on the Release of Norepinephrine, Dopamine and Acetylcholine From the Brainstem Reticular Formation. *Frontiers in neuroanatomy*, 13, 48. doi:10.3389/fnana.2019.00048
- Flack, A., Persons, A. L., Kousik, S. M., Celeste Napier, T., & Moszczynska, A. (2017). Self-administration of methamphetamine alters gut biomarkers of toxicity. *The European journal of neuroscience*, 46(3), 1918–1932. doi:10.1111/ejn.13630
- Förster, C., Burek, M., Romero, I. A., Weksler, B., Couraud, P. O., & Drenckhahn, D. (2008). Differential effects of hydrocortisone and TNFalpha on tight junction proteins in an in vitro model of the human blood-brain barrier. *The Journal of physiology*, 586(7), 1937–1949. doi:10.1113/jphysiol.2007.146852
- Fuchsova, B., Alvarez Juliá, A., Rizavi, H. S., Frasch, A. C., & Pandey, G. N. (2015). Altered expression of neuroplasticity-related genes in the brain of depressed suicides. *Neuroscience*, 299, 1–17. doi:10.1016/j.neuroscience.2015.04.057
- Ganapathy V. (2011). Drugs of abuse and human placenta. *Life sciences*, 88(21-22), 926–930. <https://doi.org/10.1016/j.lfs.2010.09.015>
- Gaval-Cruz, M., Liles, L. C., Iuvone, P. M., & Weinshenker, D. (2012). Chronic inhibition of dopamine  $\beta$ -hydroxylase facilitates behavioral responses to cocaine in mice. *PloS one*, 7(11), e50583. <https://doi.org/10.1371/journal.pone.0050583>
- Genders SG, Scheller KJ, Djouma E. Neuropeptide modulation of addiction: Focus on galanin. *Neurosci Biobehav Rev*. 2020;110:133-149. doi:10.1016/j.neubiorev.2018.06.021
- Gruzdeva, O., Borodkina, D., Uchasova, E., Dyleva, Y., & Barbarash, O. (2019). Leptin resistance: underlying mechanisms and diagnosis. *Diabetes, metabolic syndrome and obesity : targets and therapy*, 12, 191–198. <https://doi.org/10.2147/DMSO.S182406>
- Heit, C., Dong, H., Chen, Y., Thompson, D. C., Deitrich, R. A., & Vasiliou, V. K. (2013). The role of CYP2E1 in alcohol metabolism and sensitivity in the central nervous system. *Sub-cellular biochemistry*, 67, 235–247. doi:10.1007/978-94-007-5881-0\_8
- Holzer, P., Reichmann, F., & Farzi, A. (2012). Neuropeptide Y, peptide YY and pancreatic polypeptide in the gut-brain axis. *Neuropeptides*, 46(6), 261–274. doi:10.1016/j.npep.2012.08.005
- Hooper, Lora & Stappenbeck, Thaddeus & Hong, Chieu & Gordon, Jeffrey. (2003). Angiogenins: A new class of microbicidal proteins involved in innate immunity. *Nature immunology*. 4. 269-73. 10.1038/ni888.
- Hoyle, Charles. (2008). Neuropeptides and their Receptors: Evolution. 10.1002/9780470015902.a0006150.pub2.

- Huntley, R. P., Sawford, T., Martin, M. J., & O'Donovan, C. (2014). Understanding how and why the Gene Ontology and its annotations evolve: the GO within UniProt. *GigaScience*, 3(1), 4. doi:10.1186/2047-217X-3-4
- Huo, Qun & Kinugasa, Tetsushi & Wang, Lin & Huang, Jian & Zhao, Jun & Shibaguchi, Hiroto & Kuroki, Motomu & Tanaka, Toshihiro & Yamashita, Yuichi & Nabeshima, Kazuki & Iwasaki, Hiroshi & Kuroki, Masahide. (2009). Claudin-1 protein is a major factor involved in the tumorigenesis of colorectal cancer. *Anticancer research*. 29. 851-7.
- Imai, Y., Dobrian, A. D., Morris, M. A., Taylor-Fishwick, D. A., & Nadler, J. L. (2016). Lipids and immunoinflammatory pathways of beta cell destruction. *Diabetologia*, 59(4), 673–678. <https://doi.org/10.1007/s00125-016-3890-y>
- Johansson, M. E., Gustafsson, J. K., Holmén-Larsson, J., Jabbar, K. S., Xia, L., Xu, H., ... Hansson, G. C. (2014). Bacteria penetrate the normally impenetrable inner colon mucus layer in both murine colitis models and patients with ulcerative colitis. *Gut*, 63(2), 281–291. doi:10.1136/gutjnl-2012-303207
- Kaewman, P., Nudmamud-Thanoi, S., & Thanoi, S. (2018). GABAergic Alterations in the Rat Testis after Methamphetamine Exposure. *International journal of medical sciences*, 15(12), 1349–1354. doi:10.7150/ijms.27609
- Khalkhali, M., Golshahi, M., Hasandokht, T., Kafie, M., & Zare, R. (2018). Cognitive Functioning in Schizophrenia, Methamphetamine-induced Psychotic Disorder, and Healthy People: A Comparative Study. *Advanced biomedical research*, 7, 123. doi:10.4103/abr.abr\_14\_18
- Kim, Kye & Kee, Mee & Chong, Seon & Nam, Myeong. (2007). Galanin Is Up-Regulated in Colon Adenocarcinoma. *Cancer epidemiology, biomarkers & prevention : a publication of the American Association for Cancer Research, cosponsored by the American Society of Preventive Oncology*. 16. 2373-8. 10.1158/1055-9965.EPI-06-0740.
- Knöfler M, Haider S, Saleh L, Pollheimer J, Gamage TKJB, James J. Human placenta and trophoblast development: key molecular mechanisms and model systems. *Cell Mol Life Sci*. 2019;76(18):3479-3496. doi:10.1007/s00018-019-03104-6
- Koltsova, Ekaterina & Ley, Klaus. (2010). The mysterious ways of the chemokine CXCL5. *Immunity*. 33. 7-9. 10.1016/j.immuni.2010.07.012.
- Laubitz, D., Larmonier, C. B., Bai, A., Midura-Kiela, M. T., Lipko, M. A., Thurston, R. D., ... Ghishan, F. K. (2008). Colonic gene expression profile in NHE3-deficient mice: evidence for spontaneous distal colitis. *American journal of physiology. Gastrointestinal and liver physiology*, 295(1), G63–G77. doi:10.1152/ajpgi.90207.2008
- Li, A., King, J., Moro, A., Sugi, M. D., Dawson, D. W., Kaplan, J., ... Hines, O. J. (2011). Overexpression of CXCL5 is associated with poor survival in patients with pancreatic cancer. *The American journal of pathology*, 178(3), 1340–1349. doi:10.1016/j.ajpath.2010.11.058

- Li, Jin-Wang & Fang, Bing & Pang, Guo-Fang & Zhang, Ming & Ren, Fa-Zheng. (2019). Age- and diet-specific effects of chronic exposure to chlorpyrifos on hormones, inflammation and gut microbiota in rats. *Pesticide Biochemistry and Physiology*. 159. 10.1016/j.pestbp.2019.05.018.
- Liao, P., Li, W., Liu, R., Teer, J. K., Xu, B., Zhang, W., ... He, Y. (2018). Genome-scale analysis identifies SERPINE1 and SPARC as diagnostic and prognostic biomarkers in gastric cancer. *OncoTargets and therapy*, 11, 6969–6980. doi:10.2147/OTT.S173934
- Monteleone, M. C., Adrover, E., Pallarés, M. E., Antonelli, M. C., Frasc, A. C., & Brocco, M. A. (2014). Prenatal stress changes the glycoprotein GPM6A gene expression and induces epigenetic changes in rat offspring brain. *Epigenetics*, 9(1), 152–160. doi:10.4161/epi.25925
- Mosinska, Paula & Jacenik, Damian & Sałaga, Maciej & Wasilewski, Andrzej & Cygankiewicz, Adam & Sibaev, Andrei & Małeczka-Panas, Ewa & Pintelon, I. & Storr, M. & Timmermans, Jean-Pierre & Krajewska, Wanda & Fichna, J.. (2017). FABP4 blocker attenuates colonic hypomotility and modulates white adipose tissue-derived hormone levels in mouse models mimicking constipation-predominant IBS. *Neurogastroenterology & Motility*. 30. e13272. 10.1111/nmo.13272.
- Musch, Mark & Bookstein, Cres & Xie, Yue & Sellin, Joseph & Chang, Eugene. (2001). SCFA increase intestinal Na absorption by induction of NHE3 in rat colon and human intestinal C2/bbe cells. *American journal of physiology. Gastrointestinal and liver physiology*. 280. G687-93. 10.1152/ajpgi.2001.280.4.G687.
- Nair, M. G., Guild, K. J., Du, Y., Zaph, C., Yancopoulos, G. D., Valenzuela, D. M., ... Artis, D. (2008). Goblet cell-derived resistin-like molecule beta augments CD4+ T cell production of IFN-gamma and infection-induced intestinal inflammation. *Journal of immunology (Baltimore, Md. : 1950)*, 181(7), 4709–4715. doi:10.4049/jimmunol.181.7.4709
- Nayak, S. R., Harrington, E., Boone, D., Hartmaier, R., Chen, J., Pathiraja, T. N., ... Oesterreich, S. (2015). A Role for Histone H2B Variants in Endocrine-Resistant Breast Cancer. *Hormones & cancer*, 6(5-6), 214–224. doi:10.1007/s12672-015-0230-5
- Nelson, Aaron & Barasch, Jonathan & Bunte, Ralph & Weiser, Jeffrey. (2005). Bacterial colonization of nasal mucosa induces expression of siderocalin, an iron-sequestering component of innate immunity. *Cellular microbiology*. 7. 1404-17. 10.1111/j.1462-5822.2005.00566.x.
- Ning, T., Gong, X., Xie, L., & Ma, B. (2017). Gut Microbiota Analysis in Rats with Methamphetamine-Induced Conditioned Place Preference. *Frontiers in microbiology*, 8, 1620. doi:10.3389/fmicb.2017.01620
- Ning, T., Gong, X., Xie, L., & Ma, B. (2017). Gut Microbiota Analysis in Rats with Methamphetamine-Induced Conditioned Place Preference. *Frontiers in microbiology*, 8, 1620. doi:10.3389/fmicb.2017.01620

- Ogren, Sven & Kuteeva, Eugenia & Elvander-Tottie, Elin & Hokfelt, Tomas. (2009). Neuropeptides in learning and memory processes with focus on galanin. *European journal of pharmacology*, 626, 9-17. 10.1016/j.ejphar.2009.09.070.
- Park, H. J., Kim, M. K., Kim, Y., Bae, S. S., Kim, H. J., Bae, S. K., & Bae, M. K. (2017). Gastrin-releasing peptide promotes the migration of vascular smooth muscle cells through upregulation of matrix metalloproteinase-2 and -9. *BMB reports*, 50(12), 628–633. doi:10.5483/bmbrep.2017.50.12.158
- Park, H. K., & Ahima, R. S. (2013). Resistin in rodents and humans. *Diabetes & metabolism journal*, 37(6), 404–414. doi:10.4093/dmj.2013.37.6.404
- Pendharkar, S. A., Drury, M., Walia, M., Korc, M., & Petrov, M. S. (2017). Gastrin-Releasing Peptide and Glucose Metabolism Following Pancreatitis. *Gastroenterology research*, 10(4), 224–234. doi:10.14740/gr890w
- Persons, A. L., Bradaric, B. D., Dodiya, H. B., Ohene-Nyako, M., Forsyth, C. B., Keshavarzian, A., ... Napier, T. C. (2018). Colon dysregulation in methamphetamine self-administering HIV-1 transgenic rats. *PloS one*, 13(1), e0190078. doi:10.1371/journal.pone.0190078
- Propheter, Daniel & Chara, Andrew & Harris, Tamia & Ruhn, Kelly & Hooper, Lora. (2017). Resistin-like molecule  $\beta$  is a bactericidal protein that promotes spatial segregation of the microbiota and the colonic epithelium. *Proceedings of the National Academy of Sciences*. 114. 201711395. 10.1073/pnas.1711395114.
- Qiao, Y., Liu, L., Yin, L., Xu, L., Tang, Z., Qi, Y., ... Peng, J. (2019). FABP4 contributes to renal interstitial fibrosis via mediating inflammation and lipid metabolism. *Cell death & disease*, 10(6), 382. doi:10.1038/s41419-019-1610-5
- Ramoni, R. B., Saccone, N. L., Hatsukami, D. K., Bierut, L. J., & Ramoni, M. F. (2009). A testable prognostic model of nicotine dependence. *Journal of neurogenetics*, 23(3), 283–292. doi:10.1080/01677060802572911
- Ruginis, Tom & Taglia, Lauren & Matusiak, Damien & Lee, Bob & Benya, Richard. (2006). Consequence of Gastrin-Releasing Peptide Receptor Activation in a Human Colon Cancer Cell Line: A Proteomic Approach. *Journal of proteome research*. 5. 1460-8. 10.1021/pr060005g.
- Sachdeva, P., Patel, B. G., & Patel, B. K. (2009). Drug use in pregnancy; a point to ponder!. *Indian journal of pharmaceutical sciences*, 71(1), 1–7. <https://doi.org/10.4103/0250-474X.51941>
- Sajja, R. K., Rahman, S., & Cucullo, L. (2016). Drugs of abuse and blood-brain barrier endothelial dysfunction: A focus on the role of oxidative stress. *Journal of cerebral blood flow and metabolism : official journal of the International Society of Cerebral Blood Flow and Metabolism*, 36(3), 539–554. <https://doi.org/10.1177/0271678X15616978>

- Samanta, P., Wang, Y., Fuladi, S., Zou, J., Li, Y., Shen, L., ... Khalili-Araghi, F. (2018). Molecular determination of claudin-15 organization and channel selectivity. *The Journal of general physiology*, *150*(7), 949–968. doi:10.1085/jgp.201711868
- Scheer, Nico & Kapelyukh, Yury & Chatham, Lynsey & Rode, Anja & Buechel, Sandra & Wolf, Charles. (2012). Generation and Characterization of Novel Cytochrome P450 Cyp2c Gene Cluster Knockout and CYP2C9 Humanized Mouse Lines. *Molecular pharmacology*. 82. 10.1124/mol.112.080036.
- Scholz, H., & Kirschner, K. M. (2011). Oxygen-Dependent Gene Expression in Development and Cancer: Lessons Learned from the Wilms' Tumor Gene, WT1. *Frontiers in molecular neuroscience*, *4*, 4. <https://doi.org/10.3389/fnmol.2011.00004>
- Sekine Y, Ouchi Y, Takei N, et al. Brain Serotonin Transporter Density and Aggression in Abstinent Methamphetamine Abusers. *Arch Gen Psychiatry*. 2006;63(1):90–100. doi:10.1001/archpsyc.63.1.90
- Sepuru, K. M., Poluri, K. M., & Rajarathnam, K. (2014). Solution structure of CXCL5--a novel chemokine and adipokine implicated in inflammation and obesity. *PloS one*, *9*(4), e93228. doi:10.1371/journal.pone.0093228
- Shaerzadeh, F., Streit, W. J., Heysieattalab, S., & Khoshbouei, H. (2018). Methamphetamine neurotoxicity, microglia, and neuroinflammation. *Journal of neuroinflammation*, *15*(1), 341. doi:10.1186/s12974-018-1385-0
- Sheng, Jinghao & Xu, Zhengping. (2015). Three decades of research on angiogenin: A review and perspective. *Acta Biochimica et Biophysica Sinica*. 48. gmv131. 10.1093/abbs/gmv131.
- Shirey, K. A., Sunday, M. E., Lai, W., Patel, M. C., Blanco, J., Cuttitta, F., & Vogel, S. N. (2019). Novel role of gastrin releasing peptide-mediated signaling in the host response to influenza infection. *Mucosal immunology*, *12*(1), 223–231. doi:10.1038/s41385-018-0081-9
- Singh, N. K., & Rao, G. N. (2019). Emerging role of 12/15-Lipoxygenase (ALOX15) in human pathologies. *Progress in lipid research*, *73*, 28–45. <https://doi.org/10.1016/j.plipres.2018.11.001>
- Su, M. F., Liu, M. X., Li, J. Q., Lappin, J. M., Li, S. X., Wu, P., ... Bao, Y. (2018). Epidemiological Characteristics and Risk Factors of Methamphetamine-Associated Psychotic Symptoms. *Frontiers in psychiatry*, *9*, 489. doi:10.3389/fpsyt.2018.00489
- Tell, R., Rivera, C. A., Eskra, J., Taglia, L. N., Blunier, A., Wang, Q. T., & Benya, R. V. (2011). Gastrin-releasing peptide signaling alters colon cancer invasiveness via heterochromatin protein 1Hsβ. *The American journal of pathology*, *178*(2), 672–678. doi:10.1016/j.ajpath.2010.10.017
- Temko, J. E., Bouhlal, S., Farokhnia, M., Lee, M. R., Cryan, J. F., & Leggio, L. (2017). The Microbiota, the Gut and the Brain in Eating and Alcohol Use

Disorders: A 'Ménage à Trois'?. *Alcohol and alcoholism (Oxford, Oxfordshire)*, 52(4), 403–413. doi:10.1093/alcalc/agx024

- Trivedi, P. J., & Adams, D. H. (2018). Chemokines and Chemokine Receptors as Therapeutic Targets in Inflammatory Bowel Disease; Pitfalls and Promise. *Journal of Crohn's & colitis*, 12(12), 1508. doi:10.1093/ecco-jcc/jjy130
- Tsai, P. J., Davis, J., & Bryant-Greenwood, G. (2015). Systemic and placental leptin and its receptors in pregnancies associated with obesity. *Reproductive sciences (Thousand Oaks, Calif.)*, 22(2), 189–197. <https://doi.org/10.1177/1933719114537718>
- Vadakke-Madathil S, LaRocca G, Raedschelders K, et al. Multipotent fetal-derived Cdx2 cells from placenta regenerate the heart. *Proc Natl Acad Sci U S A*. 2019;116(24):11786-11795. doi:10.1073/pnas.1811827116
- Vite, A., Li, J., & Radice, G. L. (2015). New functions for alpha-catenins in health and disease: from cancer to heart regeneration. *Cell and tissue research*, 360(3), 773–783. doi:10.1007/s00441-015-2123-x
- Vuletic, D., Dupont, P., Robertson, F., Warwick, J., Zeevaart, J. R., & Stein, D. J. (2018). Methamphetamine dependence with and without psychotic symptoms: A multi-modal brain imaging study. *NeuroImage. Clinical*, 20, 1157–1162. doi:10.1016/j.nicl.2018.10.023
- Wang, L. Y., Tu, Y. F., Lin, Y. C., & Huang, C. C. (2016). CXCL5 signaling is a shared pathway of neuroinflammation and blood-brain barrier injury contributing to white matter injury in the immature brain. *Journal of neuroinflammation*, 13, 6. doi:10.1186/s12974-015-0474-6
- Wen, D., Hui, R., Wang, J., Shen, X., Xie, B., Gong, M., ... Ma, C. (2019). Effects of Molecular Hydrogen on Methamphetamine-Induced Neurotoxicity and Spatial Memory Impairment. *Frontiers in pharmacology*, 10, 823. doi:10.3389/fphar.2019.00823
- Wickline, E. D., Dale, I. W., Merkel, C. D., Heier, J. A., Stolz, D. B., & Kwiatkowski, A. V. (2016).  $\alpha$ T-Catenin Is a Constitutive Actin-binding  $\alpha$ -Catenin That Directly Couples the Cadherin·Catenin Complex to Actin Filaments. *The Journal of biological chemistry*, 291(30), 15687–15699. doi:10.1074/jbc.M116.735423
- Zeng, C., & Chen, Y. (2019). HTR1D, TIMP1, SERPINE1, MMP3 and CNR2 affect the survival of patients with colon adenocarcinoma. *Oncology letters*, 18(3), 2448–2454. doi:10.3892/ol.2019.10545
- Zhang, M., Zhao, D., Zhang, Z., Cao, X., Yin, L., Liu, Y., ... Luo, W. (2019). Time perception deficits and its dose-dependent effect in methamphetamine dependents with short-term abstinence. *Science advances*, 5(10), eaax6916. doi:10.1126/sciadv.aax6916
- Zhang, M., Zhao, D., Zhang, Z., Cao, X., Yin, L., Liu, Y., ... Luo, W. (2019). Time perception deficits and its dose-dependent effect in methamphetamine

dependents with short-term abstinence. *Science advances*, 5(10), eaax6916.  
doi:10.1126/sciadv.aax6916

Zoubková, H., Tomášková, A., Nohejlová, K., Černá, M., & Šlamberová, R. (2019). Prenatal Exposure to Methamphetamine: Up-Regulation of Brain Receptor Genes. *Frontiers in neuroscience*, 13, 771. doi:10.3389/fnins.2019.0077

Zuloaga, D. G., Jacobskind, J. S., & Raber, J. (2015). Methamphetamine and the hypothalamic-pituitary-adrenal axis. *Frontiers in neuroscience*, 9, 178. <https://doi.org/10.3389/fnins.2015.00178>

## Chapter 3

### **Microbial diversity within the colon from a chronic METH withdrawal mouse model**

---

#### **Abstract**

Metagenomic diversity, resulting from the advancement in high-throughput metabolomics technology, can now provide comprehensive coverage of microbial communities. The investigation of microbial populations in the gut is important since the established gut-brain axis paradigm is crucial for better understanding the impacts of gut perturbations on brain functioning. Drugs of abuse, such as METH, can lead to major depressive disorder (MDD) with symptomology ranging from anxiety, to poor appetite and suicidal thoughts. Little is known regarding the effects of METH on the gut microbiota. In this study, faecal samples from METH withdrawal mice, and control mice, were collected and analysed using a metagenomic analysis pipeline. Microbiome data was analysed using open-source available software, notably METAGENassist, MicrobiomeAnalyst and MG-RAST, using a range of parametric, non-parametric and supervised/unsupervised statistical methods. Microbial communities between METH and Sham were similar in their composition, however several significant differences were observed in *Faecalibacterium*, *Dehalobacterium*, *Coprococcus*, *Anaerotruncus*, *Ruminococcus* and *Prevotella*. Moreover, at a functional level alteration in METH faecal microbial samples based on metabolic phenotype showed lower abundances in cellulose degradation, aromatic hydrocarbon degradation, nitrogen fixation, chitin degradation, and sulphide oxidation metabolic categories. Taken together, METH causes several changes in microbial composition and abundance which may then trigger changes to several metabolic processes across a range of

bacteria. These findings could potentially be associated with changes in brain behaviour, following along the gut-brain axis (GBA) hypothesis, via possible reductions to key microbial metabolites necessary for proper immune functioning and brain health.

## Table of contents

<b>1.0 Introduction</b> .....	118-123
<b>2.0 Methods</b> .....	124-142
2.1 Sampling and DNA processing.....	124
2.1.1 Chronic METH mouse model .....	124
2.1.2 DNA isolation.....	126
2.1.3 DNA storage.....	128
2.1.4 DNA yield .....	128
2.2 Diversity profiling.....	130
2.2.1 AGRF: Diversity profiling and NGS report .....	130
2.2.2 Raw data.....	130
2.2.3 Bioinformatics method .....	131
2.2.4 Results format.....	132
2.3 FastQC sequence analysis.....	133
2.3.1 MG-RAST .....	133
2.3.2 GALAXY sequence analysis.....	134
2.4 MicrobiomeAnalyst pipeline .....	135
2.4.1 MicrobiomeAnalyst rarefaction curve	
2.5 METAGENassist pipeline .....	138
2.5.1 METAGENassist data processing .....	140
2.5.2 Data filtering.....	140
2.5.3 Data normalisation .....	141
<b>3.0 Results</b> .....	143-188
3.1 Summary analysis statistics (MG-RAST).....	143
3.2 Galaxy fastqc analysis.....	144
3.3 Diversity of microbial communities across METH – and Sham groups.....	146
3.4 Significant fold-change differences in OTUs was observed in – METH and Sham samples .....	148
3.5 Alpha diversity indices of METH and Sham samples .....	154
3.6 Beta diversity indices of METH and Sham groups .....	157
3.7 Hierarchical clustering revealed clusters based on – distance measure methods .....	160
3.8 Multivariate analysis revealed distinct clusters across - METH and Sham samples .....	167
3.9 Heatmap visualisation and pattern search reveals taxonomic – differences between METH and Sham groups .....	176
3.10 Functional metabolic phenotype analysis of – METH and Sham diversity .....	180
<b>4.0 Discussion</b> .....	189-210
<b>Conclusion</b> .....	211-212
<b>References</b> .....	213-222

## List of tables and figures

**Table 1.** Chronic methamphetamine administration protocol

**Table 2. Treatment and control (sham) groups**

**Table 3.** Outline indicating yielded DNA from treatment and sham samples.

**Table 4.** Paired ends and data yield from processed samples

**Table 5.** Forward and reverse primers used to amplify DNA

**Table 6.** Summary statistics of fastqc sequences from MG-RAST

**Table 7.** Cross validation of metabolic phenotype (LOOCV).

**Table 8.** VIP scores of PLS-DA across five components

**Figure 1.** Workflow of DNA isolation from faecal samples.

**Figure 2.** DNA bands indicating successful DNA yield

**Figure 3.** Flowchart of metagenomic tools used for this study.

**Figure 4.** MG-RAST sequence processing pipeline

**Figure 5.** Confirmation of sequence quality

**Figure 6.** Library size of total read counts across METH and Sham samples

**Figure 7.** Rarefaction curve of filtered samples

**Figure 8.** METAGENassist pipeline of samples.

**Figure 9.** Pareto scaling equation

**Figure 10.** Normalisation of variables and samples

**Figure 11** Quality reads from Galaxy FastQC algorithm

**Figure 12a.** Pie chart visualisation of Phylum level abundances.

**Figure 12b.** Pie chart visualisation of Genus level abundances

**Figure 13a.** Fold Change (FC) plot of OTU features at the genus level

**Figure 13b.** Box and whisker plots of OTU fold-changes across METH and Sham samples

**Figure 13c.** Fold-change and t-test scores for OTU Genus-level features.

**Figure 14.** MetagenomeSeq boxplots of significant microbes

**Figure 15a.** OTU-level alpha diversity boxplots of METH and Sham groups

**Figure 15b.** Genus-level alpha diversity boxplots of METH and Sham groups.

**Figure 16a.** Bray-Curtis 2D and 3D PCoA plots.

**Figure 16b.** PCoA plot of Jensen-Shannon Divergence beta diversity index

**Figure 16c.** Jaccard Index of beta diversity PCoA plots

**Figure 17a.** Average-linkage distance measure dendrogram

**Figure 17b.** Complete-linkage distance measure dendrogram

**Figure 17c.** Single-linkage distance measure dendrogram

**Figure 17d.** Ward-linkage distance measure dendrogram.

**Figure 18a.** Unsupervised clustering of METH and sham samples.

**Figure 18b.** Scree plot of Principal Components

**Figure 18c.** Bar chart of loading scores

**Figure 19a.** K-means line graphs representing group clusters.

**Figure 19b.** SOM clustering plots

**Figure 20a.** Feature-level random forest classification plots

**Figure 20b.** RF variance of importance and outlier plots.

**Figure 21a.** Heatmaps representation of taxonomic level abundance and clusters

**Figure 21b.** Heat map visualisation of sample group clustering

**Figure 21c.** Heat map visualisation of sample group clustering

**Figure 22.** METH and Sham metabolic phenotype profile of abundant bacteria

**Figure 23a.** Univariate statistical analysis of metabolic phenotype

**Figure 23b.** Loading score boxplots for metabolic phenotype categories

**Figure 24.** Multivariate statistics summary of metabolic phenotype

**Figure 25.** PLS-DA model measures of accuracy and importance

## 1.0 Introduction

The dopaminergic stimulant, Methamphetamine, known as METH, is a public health concern across the world [Kish et al., 2017; Courtney et al., 2014], as its misuse has been on the rise globally [Luo et al., 2018]. METH exists in two stereoisomers, D- and L- form, with the D-methamphetamine having a potency 3-5 times higher than that of L-methamphetamine [Courtney et al., 2014]. Chronic METH use has been attributed to causing serious neurotoxicity in both rodents and humans [Thanos et al., 2017]. Furthermore, after administration METH is readily taken up by the lungs, liver, brain, stomach, kidneys and pancreas, where it is eventually cleared [Thanos et al., 2017]. Also, after administration of the drug, METH initiates intense, often euphoric feelings, which are often accompanied by auditory and visual hallucinations [Zarrabi et al., 2016]. Interestingly, METH also causes hyperthermia [Matsumoto et al., 2014]. Also, METH use has previously been associated with an increase in hospital admissions and arrests [Hart et al., 2012]. The very nature of METH addiction and misuse often includes many confounding variables which can often complicate experimental studies in human subjects [Szumlinski et al., 2017]. In the brain, METH harbours the ability to affect behavioural performance through the alteration of the plasticity of the motor cortex [Huang et al., 2017]. Moreover, chronic METH use leads to long-term neuronal damage, with neuroimaging data showing modifications to prefrontotemporal and frontostriatal areas of the brain [Lyoo et al., 2015]. High METH doses can also result in severe physiological changes including weight loss, muscular wasting, along with impairments in attention and memory [Marshall et al., 2012]. More recently, links have been made between METH use and gut microbiota

dysbiosis [Ning et al., 2017]. The relevance of understanding how gut microbiota behaves in drug addiction studies has been reported in cocaine, since cocaine reduces blood flow to the gastrointestinal (GI) tract, possibly impacting gut barrier function [Chivero et al., 2019]. However, no supporting knowledge is available that can link chronic, long-term METH use to changes in gut microbial composition. An emerging paradigm reinforcing bidirectional communication between gut microbiota and the brain can help understand if the dysbiosis of gut flora from METH use, along with other drugs of abuse, plays a crucial role in not only causing psychiatric disorders, but also developing drug addiction [Ning et al., 2017]. The structure of the gut microbiome also has a significant impact on drug metabolism, which falls under the growing field of pharmaco-microbiomics, which describes the interplay of gut microbiota on drug pharmacokinetics and pharmacodynamics [Li et al., 2017]. Importantly, short-chain fatty acids (SCFAs) – main SCFAs being acetate, propionate and butyrate – are metabolised in different ways, and contribute to particular signalling pathways. Butyrate is by far the most dominant SCFA in the human gut, in which is produced mainly by the phylum Firmicutes, and the genus *Roseburia* [Chenard et al., 2020; Shin et al., 2019]. Moreover, SCFAs such as butyrate can influence tight junctions, with diminished levels disrupting barrier function [Chenard et al., 2020]. SCFA composition and abundance is influenced by several factors, including dietary intake, along with the microbial composition of the gut [Zhang et al., 2020]. Also, SCFA's are vital for proper host physiology, with these molecules being required for a number of processes relating to gut hormone production, epigenetic regulation and redox balance [Skonieczna-Zydecka et al., 2018]. Without doubt, SCFAs play a crucial role in maintaining adequate gut health and can be perturbed via extraneous influences. The SCFA propionate was found in decreased amounts in faecal samples of

mice who were administered METH [Ning et al., 2017]. The full effect of METH on other SCFAs, from METHs impact on gut physiology and composition is yet to be fully realised. However, links between SCFA depletions and negative alterations in neuropathology have been linked to depressive-like symptoms [Caspani et al., 2019].

Metagenomics is a rapidly growing area of research which aims to determine the many microbial communities within environmental samples [Garrido-Cardenas et al., 2017]. Currently, the addition of several high-throughput sequencing technologies has allowed for an inexpensive way to define bacterial communities in a given human sample. Indeed, one of the main challenges currently facing this field is the assembly of bacterial genomes within a single sample, which contains greater diversity [Ghurye et al., 2016]. The genome assembly process, usually achieved via 16S sequencing of variable regions, is further complicated by varying levels of microbial abundance (evenness and unevenness) and relatedness. To complement this growing need for metagenomic data analysis, several well-established pipelines have been developed, which are still being optimised, along with their algorithms, to better analyse highly complex metagenomic data [Dudhagara et al., 2015]. Along with this problem of greater complexity, several freely available, online software tools have been created to address metagenomics studies which provide user-friendly, graphical interfaces that can be readily adapted to research questions. Examples of these tools include, MG-RAST, MicrobiomeAnalyst and METAGENassist. The latter of these online metagenomic analysis tools can carry out multivariate statistical analyses on input sample data and is one of a handful of webservers that maps taxonomy to phenotype, across a range of functional [metabolic] categories. Output is in the form of graphs and plots –

describing uni- and multi-variate data analyses -, which can be readily downloaded and explored.

The aim of this study was to determine and evaluate changes to mouse faecal microbiota composition structure and diversity richness and evenness, upon the administration of a chronic METH dose over a period of time, followed by METH withdrawal. Faecal samples were processed, and DNA extracted using an established protocol. 16S Illumina sequencing was carried out, followed by a metagenomic analysis pipeline that addressed microbial communities in both METH treated mice and control mice (Sham) samples. Prior to statistical analyses, sequence reads were processed in MG-RAST and Galaxy where reads were confirmed for their integrity and quality. Statistical analysis was performed – via METAGENassist, MicrobiomeAnalyst and MG-RAST - across METH and Sham groups to understand alpha and beta diversity between and across samples, respectively. Principle coordinate analysis (PCoA), PCA, and partial least squares – discriminant analysis (PLS-DA) plots were also generated to visualise plotted variances. PCoA and PLS-DA are both multivariate analysis methods, in which PLS-DA is a supervised method, and PCoA is unsupervised [Cao et al., 2016; Worley et al., 2013]. The main goal of PCA (unsupervised) and PLS-DA (supervised) analysis is to distinguish class (group) differences from a multivariate set of data. With an array of data, and with the transfer of multidimensional data onto a 2-dimensional space, without the loss of variance in the original data set, PCA and PLS-DA can then identify these variables (in this case, OTUs, or taxa labels) that can explain this class/group separation. In addition, dendrogram and heatmaps were generated to visualise and observe taxa abundance across several taxonomic levels. Other univariate measures such as fold change, t-tests (parametric and non-parametric) and volcano plots (based

on two group analysis) were utilised. In summary, both univariate and multivariate analysis tools were employed to predict and measure taxonomic changes across METH (experimental) and Sham (control) groups. Unsupervised and supervised data output explained the group similarities and dissimilarities, based on significance scoring and loading scores. Moreover, species composition and structure abundance were determined, which allowed for the characterisation of metabolism phenotype microbial identity. Overall, abundances varied between the METH and control groups, with several fold-change and statistically significant abundance changes found in the METH group. In particular, lower abundances of Firmicutes and Verrucomicrobia were found in the METH group, Further, higher abundances of Akkermansia, Turibacter and Allobaculum were observed in the METH group. Results were confirmed by employing a series of well-established (supervised and unsupervised) ordination methods in order to reinforce that there were indeed distinct clusters that could explain the changes in microbial abundances. In addition to clustering and classification, metabolic phenotype, representing functional analysis, was carried out for both METH and control groups. Overall, the most important metabolic processes were, dehalogenation, cellulose degradation, and sulphide oxidation. Through substantial univariate and multivariate analysis, the METH group (and corresponding samples) had a much lower abundances of metabolic phenotypes associated with cellulose degradation, aromatic hydrocarbon degradation, nitrogen fixation, chitin degradation and sulphide oxidation, compared to control group. Overall, this analysis of microbial diversity and abundance, along with functional categorisation found changes in microbial composition in a chronic METH mouse model. METH may induce long-lasting impacts in the microbial communities residing in the colon, which could also create shifts in healthy

colon metabolism via the dampening of several important signalling metabolites, such as SCFAs – butyrate, propionate – and gut-derived serotonin. Alterations in microbial communities responsible for maintaining a homeostatic environment in the colon could also cause perturbations to other organs such as the brain, where pathologies associated with depression might develop.

## **2.0 Methods**

### **2.1 Sampling and DNA processing**

#### **2.1.1 Chronic METH mouse model**

C57BL/6 mice (5-9 weeks old; n=14) were obtained from the Australian Research council (ARC, Perth, Australia). Mice had free access to food, water and were kept under a 12-hour light/ dark cycle in a well-ventilated room and at an appropriate temperature of 22 °C. Mice acclimatized for up to 1 week prior to the onset of treatment cycle of METH / sham for 14 days. Mice were separated into two groups: sham treatment and METH treatment administered via daily intraperitoneal (i.p) injections in the morning and late evening (10-13 hours apart). SHAM group received 100µl of saline water, whilst the METH group received METH beginning at 0.5mg/kg diluted in 100µl of saline water with an increment of METH concentration every two days (equivalent to the human dosage as per body surface area) (Table 1). This administrative regime was incorporated to overcome drug resistance and maintain a constant high for 14 days. The mice were kept under observation for 3 days after their last treatment injection (withdrawal) after which mice were culled using lethobarb (pentobarbitone) and colon tissues collected. All procedures and protocols performed within this study were approved by the Victoria University Animal Experimentation Ethics committee (AEETH 15/010) and were conducted according to the guidelines of the Australian National Health and Medical Research Council.

**Table 1: Chronic methamphetamine administration protocol.** C57BL/6 mice were administered two METH doses (morning and afternoon) over a seven-day period, lasting for two weeks. Week three, indicated by days 15, 16, and 17, allowed time for mice to experience withdrawal from METH.

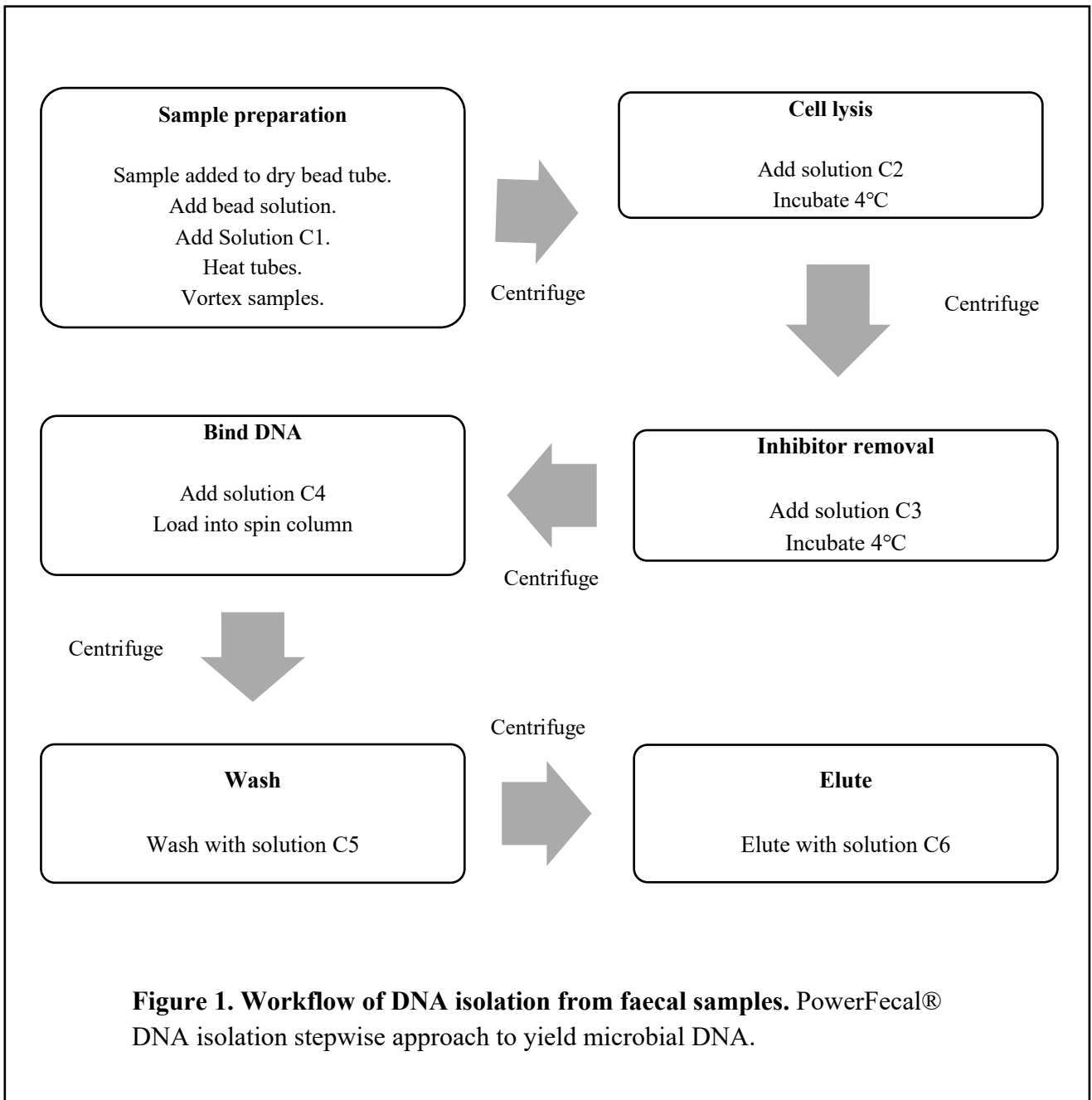
<b>WEEK 1</b>	<b>Schedule</b>	<b>Day 1 (mg/kg)</b>	<b>Day 2 (mg/kg)</b>	<b>Day 3 (mg/kg)</b>	<b>Day 4 (mg/kg)</b>	<b>Day 5 (mg/kg)</b>	<b>Day 6 (mg/kg)</b>	<b>Day 7 (mg/kg)</b>
<b>WEEK 2</b>	<i>Morning</i>	0.5	1	1	2	2	3	3
	<i>Afternoon</i>	0.5	1	1	2	2	3	3
		Day 8 (mg/kg)	Day 9 (mg/kg)	Day 10 (mg/kg)	Day 11 (mg/kg)	Day 12 (mg/kg)	Day 13 (mg/kg)	Day 14 (mg/kg)
<b>WEEK 3</b>	<i>Morning</i>	4	4	5	5	6	6	7
	<i>Afternoon</i>	4	4	5	5	6	6	7
		Day 15 withdrawal	Day 16 withdrawal	Day 17 withdrawal	Day 18 Cull, collection of colon tissues			

### 2.1.2 DNA isolation

DNA isolation of faecal samples was performed using the PowerFecal DNA isolation kit (according to the manufacturers specifications). Figure 1 indicates, diagrammatically, the steps taken to achieve purification of microbial genomic DNA. Briefly, between 0.10 and 0.25 grams of faecal sample was used for the downstream protocol. Importantly, due to the wet nature of the samples each faecal sample was added to a dry bead tube and centrifuged at room temperature for 30 seconds at 10,000 x g. Carefully, a pipette tip was used to draw away as much liquid as possible.

**Table 2. Treatment and control (sham) groups.** Two groups, chronic withdrawal and sham (control) indicated as A1-A8 (METH) and B1-B8 (Sham).

<b>Group 1 (Chronic Withdrawal)</b>	<b>Group 2 (Sham Withdrawal)</b>
A1	B1
A2	B2
A3	B3
A4	B4
A5	B5
A6	B6
A7	B7
A8	B8



### 2.1.3 DNA storage

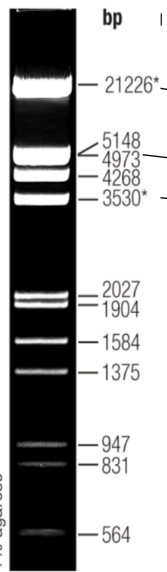
To ensure DNA was protected from degradation, and to store until further analysis, DNA samples were eluted in 10mM Tris buffer and stored at -20 degrees Celsius.

### 2.1.4 DNA Yield

DNA samples were assessed for yield. Briefly, 10 $\mu$ L DNA extracted from DNA isolation kit protocol was mixed with 2 $\mu$ L Loading Dye. Approximately 10 $\mu$ L of DNA-loading dye mix was loaded into an 8-well agarose gel, filled with 1xTAE buffer. 7 $\mu$ L of DNA ladder was loaded into well 1, followed by remaining DNA samples. Gel images (figure 2) indicate DNA bands from all samples.

**Table 3. Outline indicating yielded DNA from treatment and sham samples.** Gel electrophoresis plan, covering three separate gels, of chronic and sham withdrawal groups. Gel labels correspond to those labelled on Figure 2.

Lane No.	Gel 1	Gel labels according to image 2
1	L*	1
2	A1	2
3	A2	3
4	A3	4
5	A4	5
6	A5	6
7	A6	7
8	A7	8
Lane No.	Gel 2	-
1	L	9
2	A8	10
3	B1	11
4	B2	12
5	B3	13
6	B4	14
7	B5	15
8	B6	16
Lane No.	Gel 3	-
1	L	17
2	B7	18
3	B8	19



ThermoScientific Lambda  
DNA/Eco/RI + HindIII  
Marker, 3.  
Final DNA concentration of  
0.1 μg/μL.

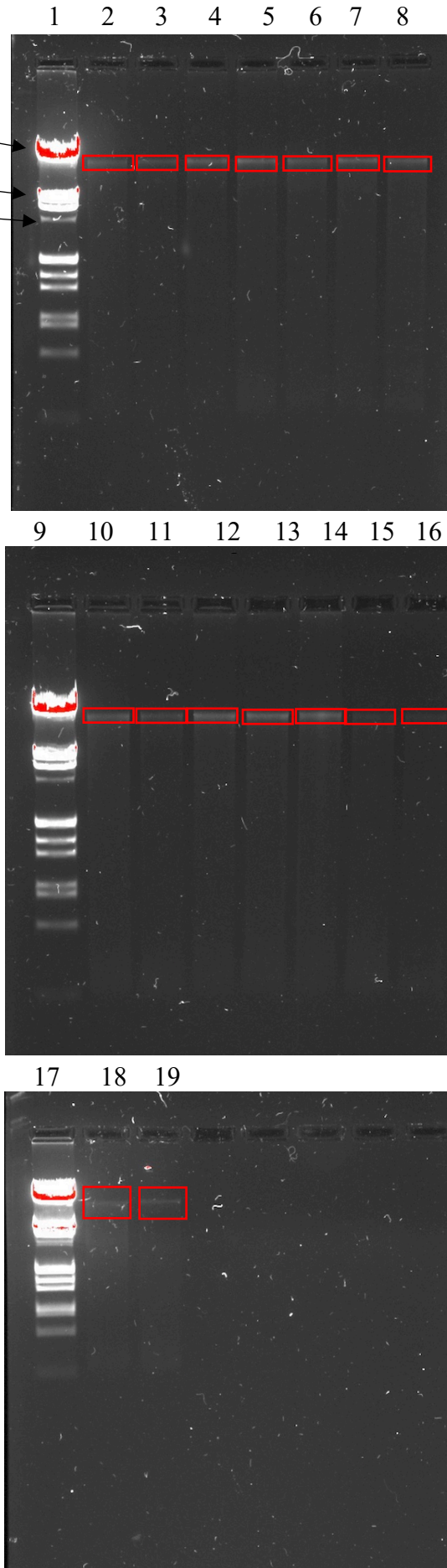


**Figure 2. DNA bands indicating successful DNA yield.** Gel electrophoresis of genomic DNA bands indicating DNA yield from both groups. L: ladder. All DNA samples were mixed with 2 μl 6x DNA loading dye and added to each corresponding wells. Red rectangles highlight DNA bands in both Meth and sham groups.

## 2.2 Diversity profiling

### 2.2.1 AGRF: Diversity profiling and Next-generation sequencing report.

DNA samples were removed from the -20-degree freezer and placed on dry ice. Samples were then transported to Australian Genomics Research Facility (AGRF) for diversity sequencing and profiling. Primary analysis of samples was performed in real time using the MiSeq Control Software (MCS) v2.6.2.1 and Real Time Analysis (RTA) v1.18.54. Then, the Illumina bcl2fastq 2.20.0.422 pipeline was utilised to generate sequence data. Regions V3 and V4 were amplified.

**Table 4. Paired ends and data yield from processed samples.** A total of 215,490 paired ends were generated.

Lane	Sample name	Paired end	Data Yield (bp)
1	A4-16S_V3-V4	215,490	0.13Gb
Total		215,490	0.13Gb

### 2.2.2 Raw data

Raw data was provided in the following format:

*<Sample\_name>\_<flowcell\_ID>\_<index\_lane>\_<readNum>.fastq.gz* – compressed FastQ sequence files contained untrimmed reads; *<readNum>* specified the first or second read of the pair. Raw data files consisted of read sequence output using the Illumina quality scores. Quality scores were encoded in symbolic ASCII format. Sequencing details were as follows:

**Table 5. Forward and reverse primers used to amplify DNA.** 341F and 806R were used as primers to amplify DNA in samples.

<b>Target</b>	<b>341F-806R</b>
Forward Primer (341F)	CCTAYGGGRBGCASCAG
ReversePrimer (806R)	GGACTACNNGGGTATCTAAT
Application	Amplicon sequencing
ReadLength	300bpPE

### **2.2.3 Bioinformatics Method**

Paired end reads were assembled by aligning the forward and reverse reads using PEAR (version0.9.5). Primers were identified and trimmed. Trimmed sequences were processed using Quantitative Insights into Microbial Ecology (QIIME 1.8) USEARCH (version 8.0.1623) and UPARSE software. Using usearch tools sequences were quality filtered, full length duplicate sequences were removed and sorted by abundance. Singletons or unique reads in the data set were discarded. Sequences were clustered followed by chimera filtered using “rdp\_gold” database as reference. A total of 170,082 reads were finalised from original raw read pre-processing of 215,40 reads. To obtain number of reads in each OTU, reads were mapped back to OTUs with a minimum identity of 97%. Using QIIME taxonomy was assigned using Greengenes database (Version 13\_8, Aug 2013).

## 2.2.4 Results Format

The diversity profiling results were provided in various files contained within folder name “Diversity\_profiling”. Results include bar and area charts, showing the breakdown of taxonomy by given levels. Formats included: OTU tables, Charts, Mg\_blast, otu\_table\_taxa.biom, and absolutea\_bundance.xlsx.

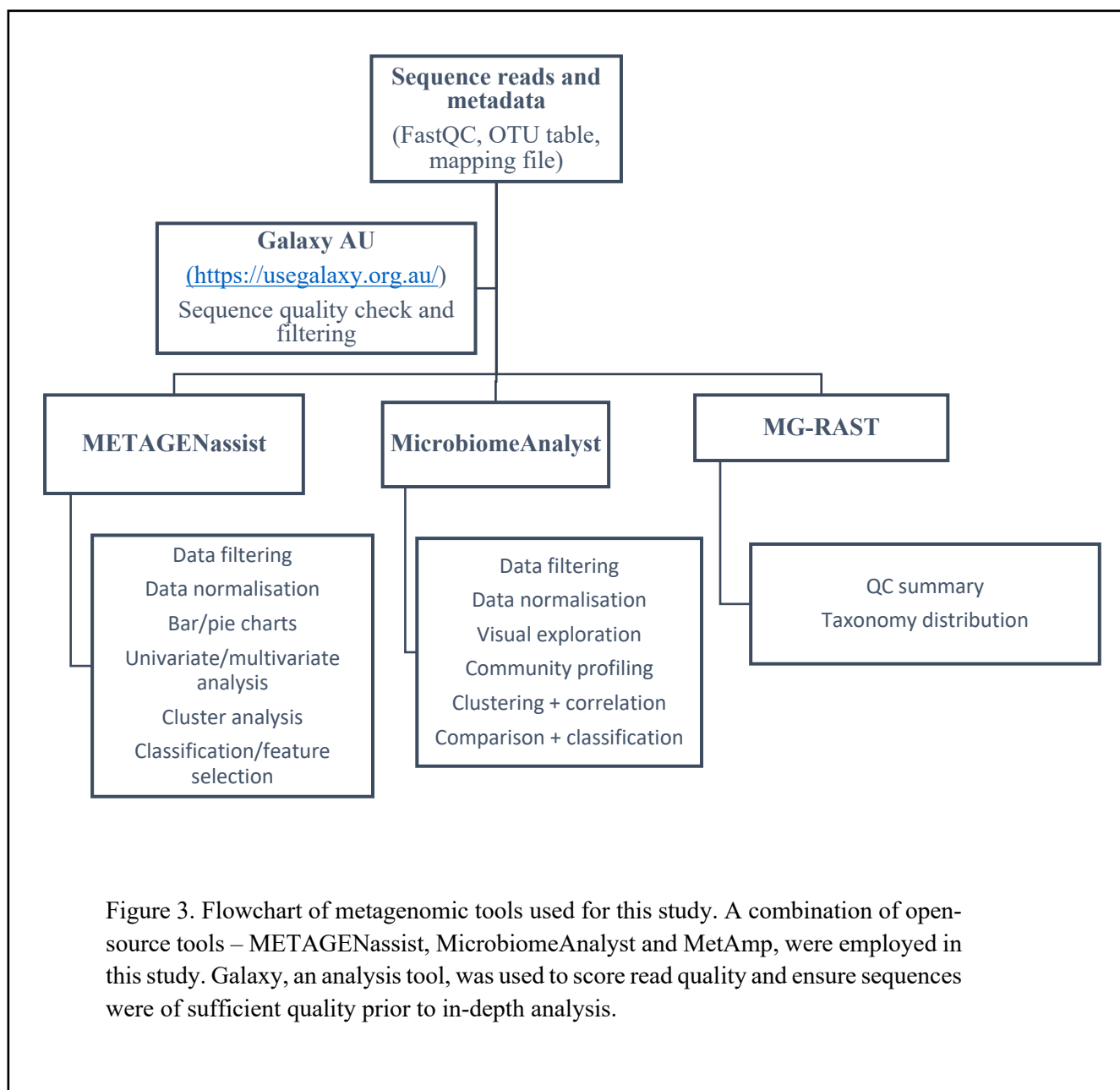
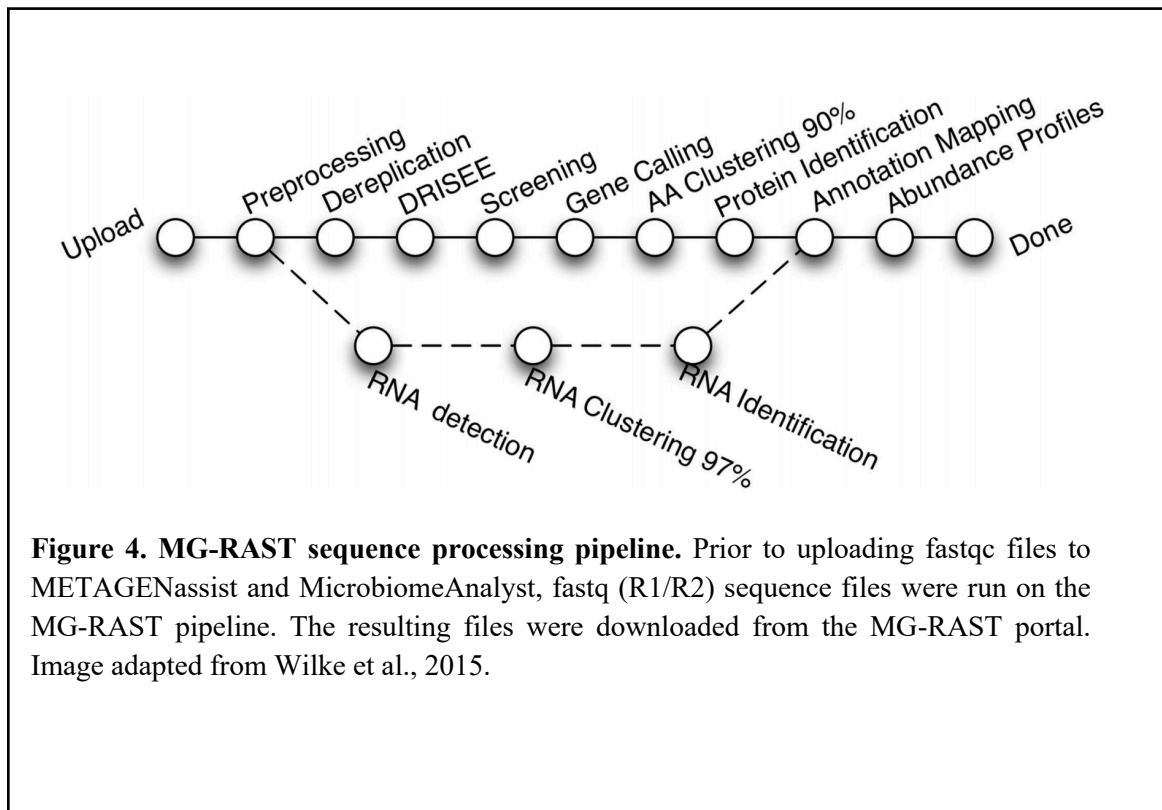


Figure 3. Flowchart of metagenomic tools used for this study. A combination of open-source tools – METAGENassist, MicrobiomeAnalyst and MetAmp, were employed in this study. Galaxy, an analysis tool, was used to score read quality and ensure sequences were of sufficient quality prior to in-depth analysis.

## 2.3 FastQC sequence analysis

### 2.3.1 MG-RAST

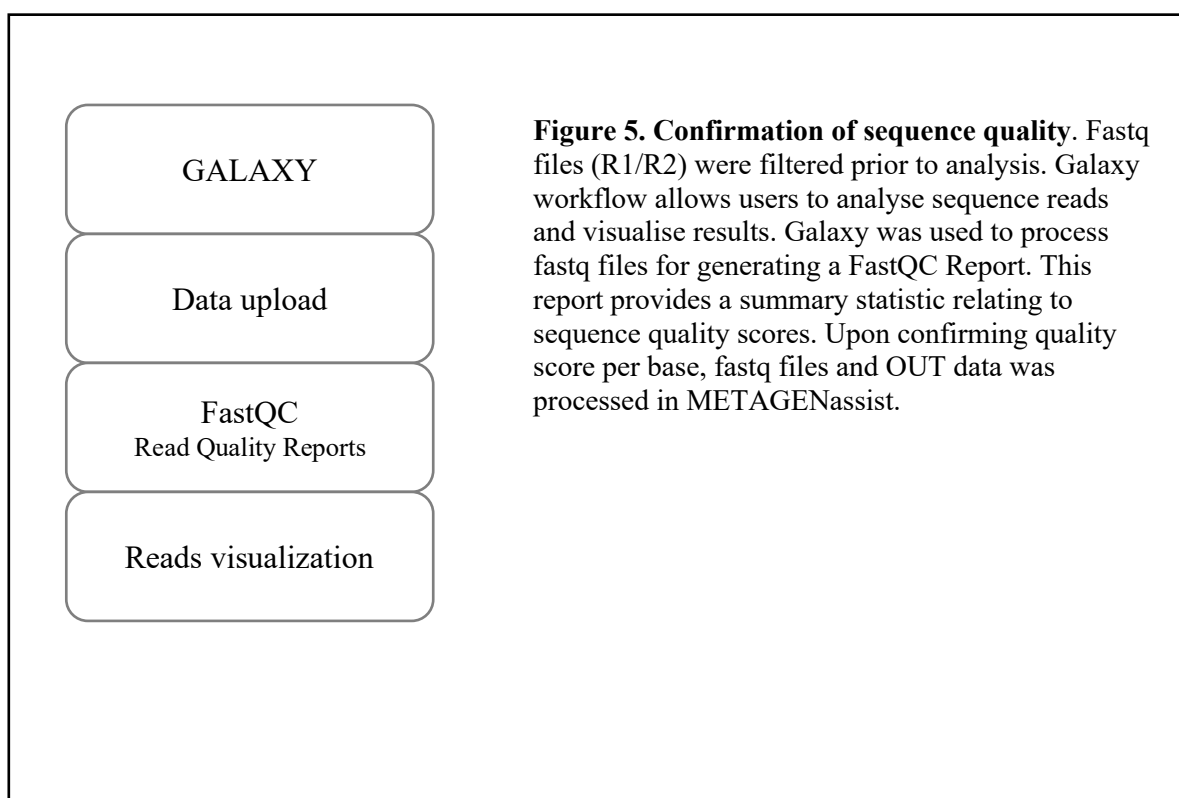
MG-RAST is a public resource that allows annotation and analysis of metagenomic sequence data. MG-RAST makes it possible to upload raw sequence reads (via fastq, fasta file format). Fastq files (R1 and R2) were uploaded to MG-RAST and submitted. The MG-RAST pipeline (Figure 4) provides an in-depth process from raw reads to results analysis/statistics.



**Figure 4. MG-RAST sequence processing pipeline.** Prior to uploading fastqc files to METAGENassist and MicrobiomeAnalyst, fastq (R1/R2) sequence files were run on the MG-RAST pipeline. The resulting files were downloaded from the MG-RAST portal. Image adapted from Wilke et al., 2015.

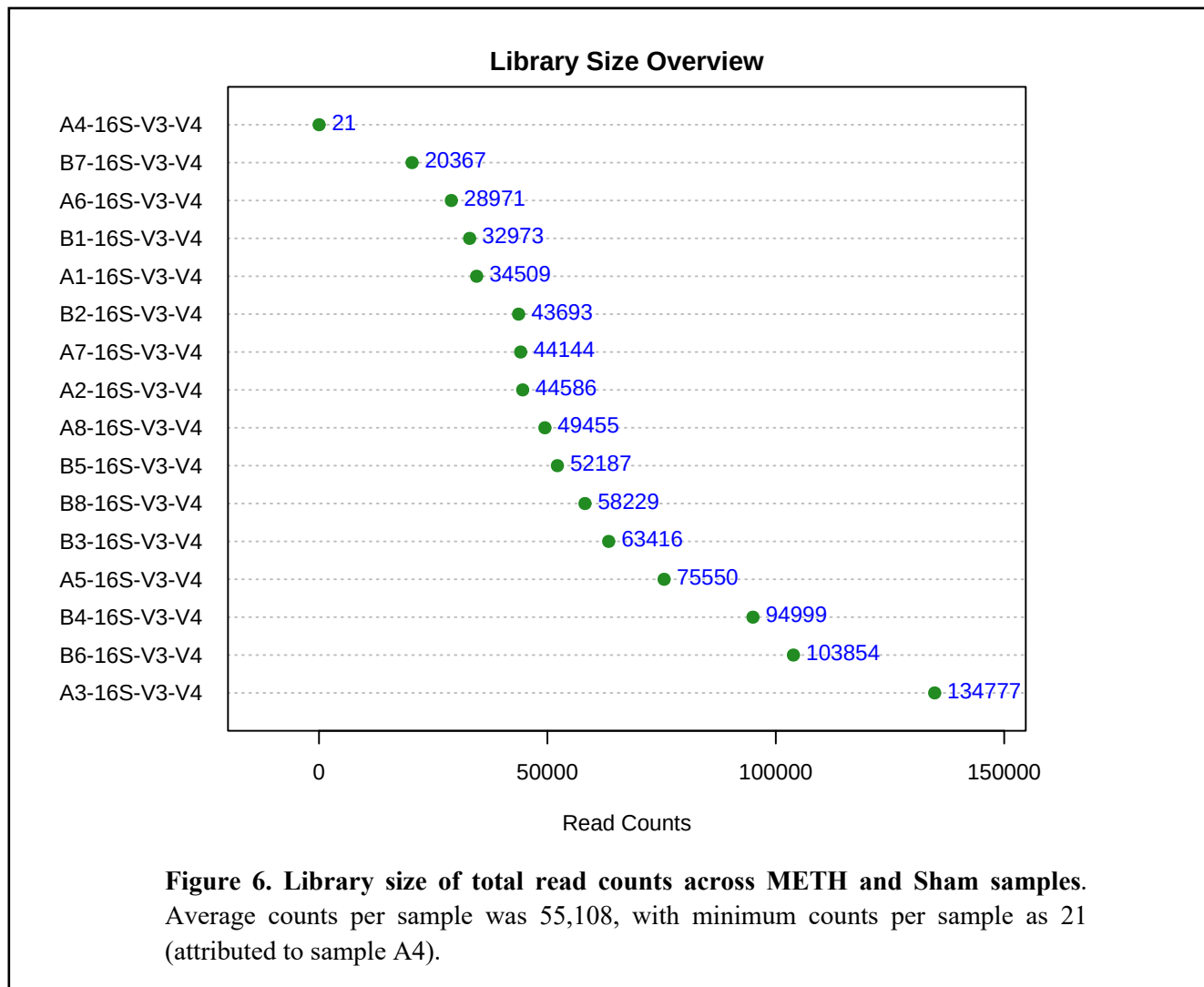
### 2.3.2 GALAXY sequence analysis

Galaxy Australia (<https://usegalaxy.org.au/>) was used to determine basic statistical analysis of sequence quality using fastq files from post-processing achieved in MG-RAST. Quality checking was previously carried out in USEARCH (AGRF), where adaptors were removed, and full-length duplicate sequences and singletons were removed. Illumina input reads were trimmed in QIIME 1.8 (USEARCH). In addition, per sequence quality scores, sequence duplication levels and adapter content were assessed in Galaxy, prior to further analysis in METAGENassist (Figure 5). The Galaxy pipeline described here served to ensure reads were re-checked for quality.



## 2.4 MicrobiomeAnalyst pipeline

MicrobiomeAnalyst is a web-based tool that is made up of four modules, which can use taxonomic data, mainly in the form of OTU tables, BIOM and/or Mothur files. In addition, MicrobiomeAnalyst allows users to select parameters associated with quality, filtering and normalisation, prior to exploratory analysis and subsequent visualisations via PCoA plots, heatmaps, dendrograms and box/bar plots [Dhariwal et al., 2017]. BIOM and metadata (mapping) files were uploaded to MicrobiomeAnalyst and 'Data Inspection' step matched all 16 samples from both BIOM and metadata files. Average, maximum, minimum, and total counts were recorded, and library size overview plot was generated. Data integrity step found 554 OTUs. Data filtering was performed to removed low counts and low variance counts. For low count filtering, a 20% prevalence filter (default) was set (20% of each samples' reads should contain four counts). For low variance count filtering, coefficient of variance was chosen (this was also consistent with a data filtering step in METAGENassist). Coefficient of variance was chosen for low variance filtering. 228 low abundance features were removed from the initial 554 OTUs, based on prevalence. Moreover, 33 low variance features were removed based on coefficient of variance filtering. Data normalisation was performed by rarefying and scaling. MicrobiomeAnalyst also performs alpha (within) and beta (between) diversity calculations supporting six and five diversity measures, respectively. For this study, diversity across METH and Sham samples was calculated using all diversity measures, and then compared. Results of diversity analysis were visualised as PCoA and non-metric multidimensional scaling (NMDS). Lastly, statistical significance was assessed using three statistical measures.

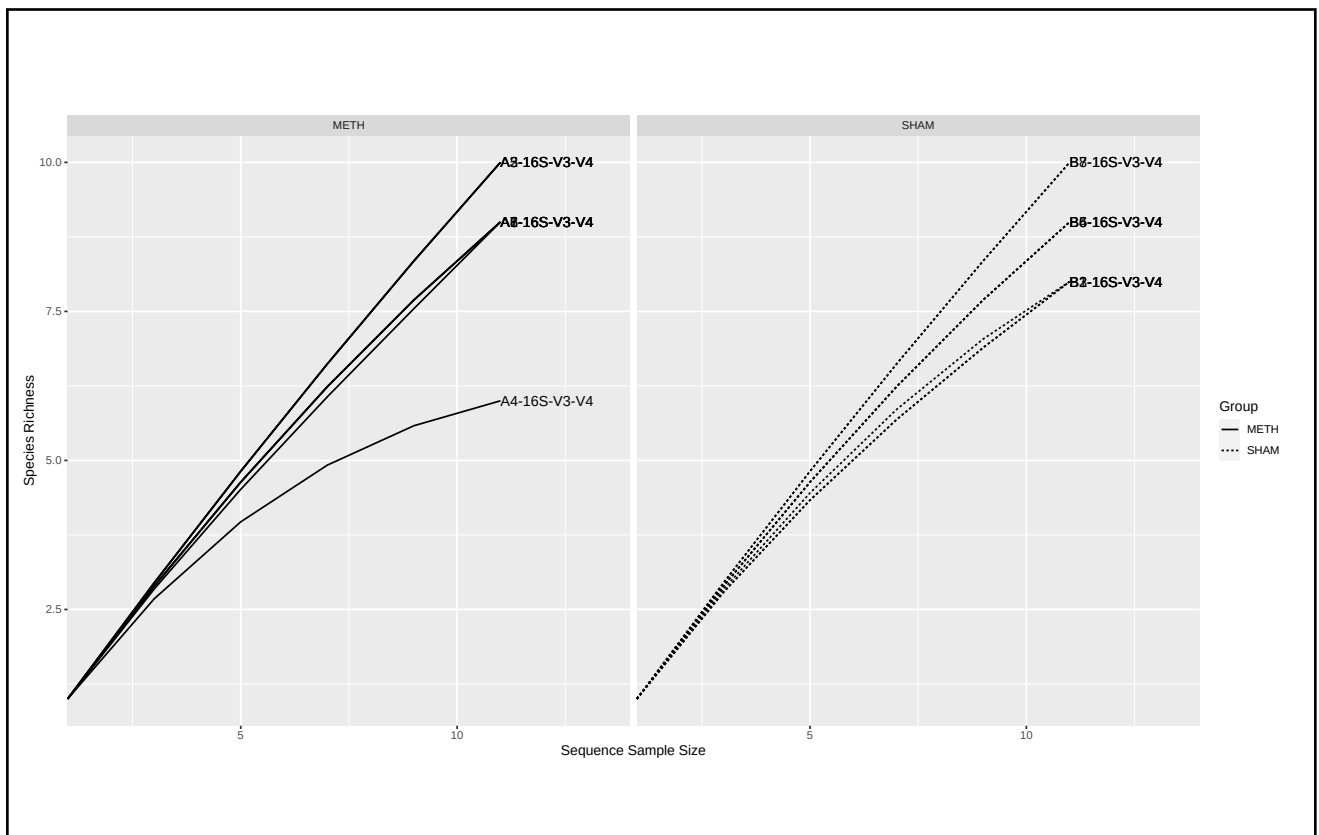


### 2.4.1 MicrobiomeAnalyst rarefaction curve

Rarefaction is a method used to standardise samples and involves randomly sub-sampling the pool of accumulated samples/species ( $N$ ), arriving at a subset size ( $m$ ), and finally calculating the phylogenetic diversity (DV) of the subset ( $PD_m$ ). Selecting rarefaction as a method of normalisation ensures a standardisation across samples, as phylogenetic evenness, beta-diversity and dispersion can then be measured [Nipperess, 2016]. In general terms, a rarefaction curve is generated in order to determine if sequencing of a particular sample, or group of samples is efficient enough to warrant true species diversity. Rarefaction curves were constructed for each sample (A1-A8 | B1-B8). Shape of rarefaction curve for METH and Sham samples indicated that species richness was similar

(based on distribution). Sequencing depth was also calculated using Good's coverage scores. METH samples ranged from between 18.8 – 81.8%; whereas Sham samples were significantly lower, ranging from between 54.4-18.1%.

**Figure 7. Rarefaction curve of filtered samples.** Vertical (y) axis shows species richness; horizontal (x) axis indicates sample size.



## **2.5 METAGENassist pipeline**

METAGENassist is a comprehensive comparative tool that utilises high-level statistical analysis methods to assess bacterial diversity samples. In this a logical flow of steps were taken – from data upload, to statistical analysis – to interpret output (Figure 8). The benefits of using METAGENassist analysis is that it combines pre-processing steps, and data analysis all in one package. Moreover, statistical analysis can be univariate, multivariate, clustering, and supervised classification [Arndt et al., 2012]. One immediate advantage of the METAGENassist platform is its ability to perform all standard analysis featured on other packages, such as QIIME, Mothur, MG-RAST, MEGAN and STAMP; however, provides additional features such as, interactive normalisation, metadata overlay and taxonomy-to-phenotype mapping [Arndt et al., 2012]. Visualisations were obtained from METAGENassist, along with construction of diversity plots and graphs.

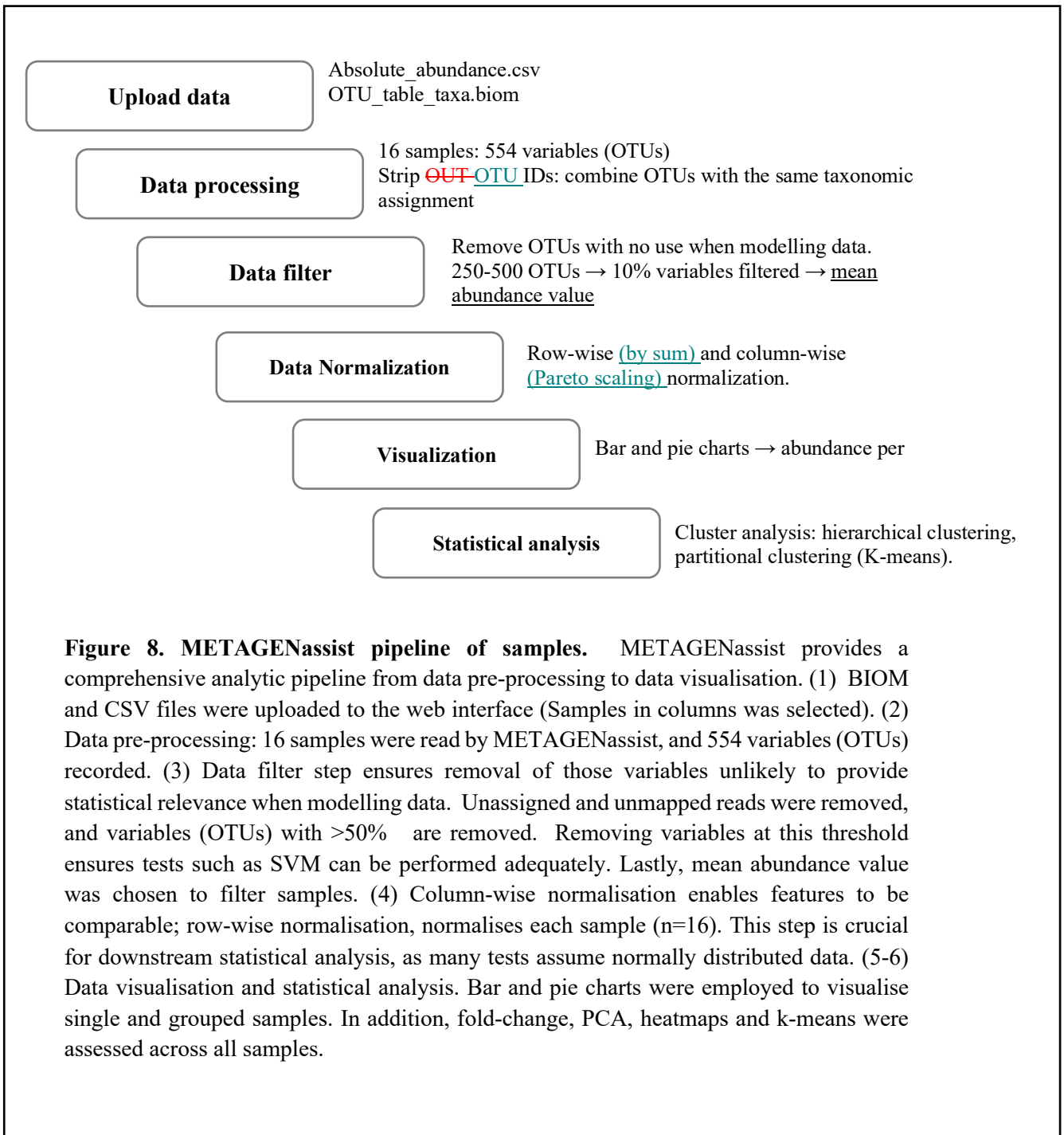


**Figure 8. METAGENassist pipeline of samples.** METAGENassist provides a comprehensive analytic pipeline from data pre-processing to data visualisation. (1) BIOM and CSV files were uploaded to the web interface (Samples in columns was selected). (2) Data pre-processing: 16 samples were read by METAGENassist, and 554 variables (OTUs) recorded. (3) Data filter step ensures removal of those variables unlikely to provide statistical relevance when modelling data. Unassigned and unmapped reads were removed, and variables (OTUs) with >50% are removed. Removing variables at this threshold ensures tests such as SVM can be performed adequately. Lastly, mean abundance value was chosen to filter samples. (4) Column-wise normalisation enables features to be comparable; row-wise normalisation, normalises each sample (n=16). This step is crucial for downstream statistical analysis, as many tests assume normally distributed data. (5-6) Data visualisation and statistical analysis. Bar and pie charts were employed to visualise single and grouped samples. In addition, fold-change, PCA, heatmaps and k-means were assessed across all samples.

### 2.5.1 METAGENassist Data processing

BIOM and mapping file (metadata) files were uploaded into METAGENassist, with 16 sample recognised (n=16: 8 METH, 8 Sham), and 554 OTUs (taxa) recognised. In addition, numbered OTU IDs (which is contained in this data) with low-read counts across matching taxonomic assignments were removed. Finally, OUT IDs were stripped and combined with OTUs with the same taxonomic assignment.

 Help

**Data processing information:**

Checking data content ...passed

16 samples and 554 variables were detected in the taxonomic profile.

Some labels under some columns ( OTU\_3, OTU\_1 and 552 others ) in the metadata file occur for fewer than 3 samples. They will be replaced by NA in some analyses.

Taxon-to-phenotype mapping initiated...

### 2.5.2 Data filtering

Data filtering was performed to remove low-quality reads. Unclassified and unmapped reads were removed. Secondly, an option to remove variables (taxa) with >50% zeros was chosen This was to ensure that abundance OTU reads with null values could not interfere with modelling, such as SVM and PCA methods.

**Main taxonomy table:**

Before filtering: 72 variables in dataset.

No variables were found with unassigned reads.

Removed 16 variables with over 50 percent zeroes.

Filtered out 2 variables (5%) based on Coefficient of Variation.

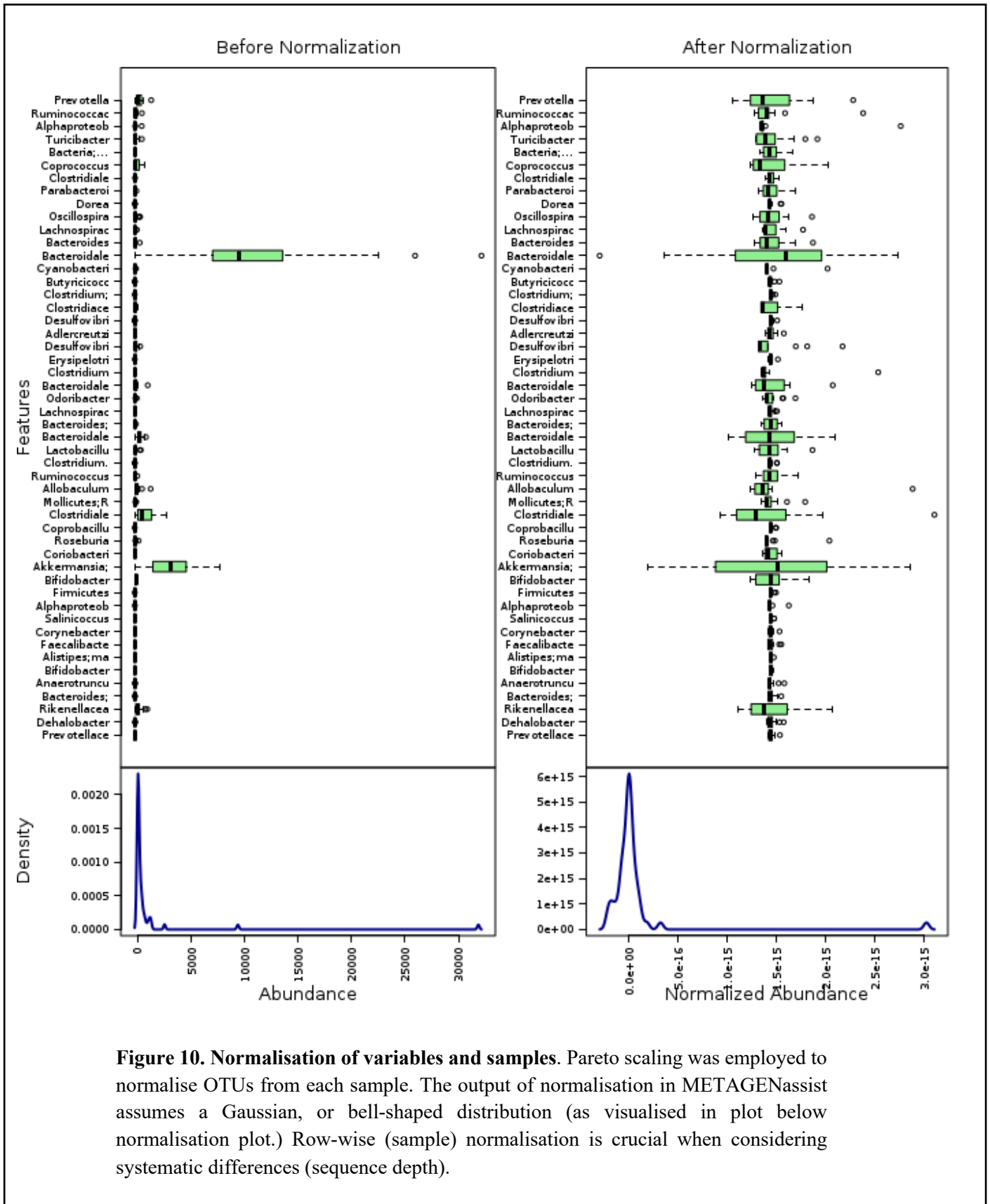
54 variables remain in the dataset.

### 2.5.3 Data normalisation

Data was normalised row-wise and column-wise. Normalisation for row-wise was carried out by normalisation by sums, whereas column-wise was normalised using Pareto scaling. METAGENassist first transforms the internal data structure, by assigning samples to rows, and variables (taxon) to columns. Normalisation by sum adjusts for differences in abundance coverage by normalising to the same total abundance for each sample. This normalisation is necessary to compare samples. The transformed OTU reads allows for comparisons between magnitude of each (OTU) to one another. Density curves showed normalised abundance (Figure 10). Pareto scaling (Figure 9) uses the square root of the standard deviation as the main scaling factor. In this way, large fold bacterial abundances are factored in, and thus reduced in comparison to small fold bacterial abundances; this rules out any dominance of large abundance readings that may skew overall samples. Moreover, Pareto scaling is one normalisation method considered a ‘stable’ pre-treatment method [Berg et al., 2006]. Lastly, Pareto scaling/normalisation remains as close to original data measurement as possible [Worley et al., 2015].

$$\tilde{x}_{ij} = \frac{x_{ij} - \bar{x}_i}{\sqrt{s_i}}$$

**Figure 9. Pareto scaling equation.** Scaling samples is a pre-treatment method. Pareto scaling, similar to autoscaling, which uses standard deviation as the scaling factor. However, in Pareto scaling, the square root of the standard deviation is used for scaling. Importantly, original data does not lose its dimensionality upon scaling [Berg et al., 2006].



### 3.0 Results

#### 3.1 Summary analysis statistics (MG-RAST)

Based on the stringent pipeline from MG-RAST (Figure 4), 13 sequences (~0.01%) did not pass the QC pipeline. 213,029 sequences contained ribosomal RNA genes.

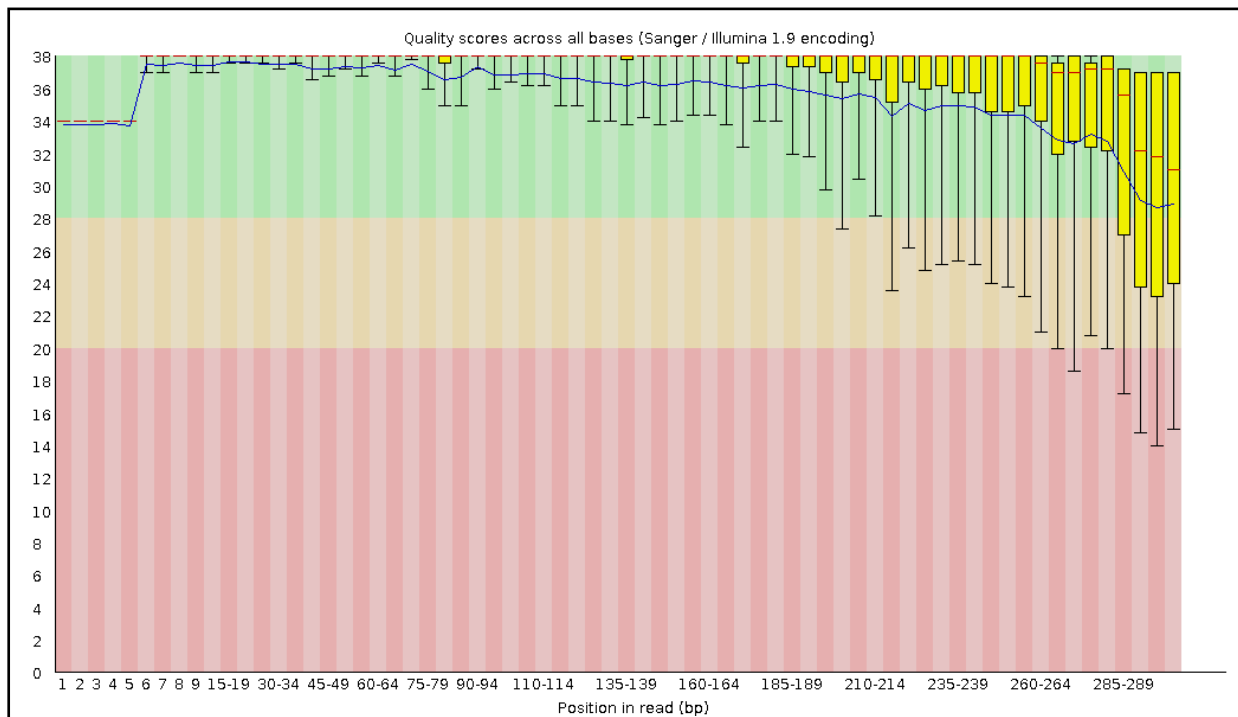
MG-RAST, based on fastqc files, summarises and ranks abundances from most abundant to least abundant. Summary abundance pie charts show MG-RAST taxonomic hits distribution, which uses the contigLCA algorithm. Analysis statistics (Table 6) summarises sequence information pertaining to sequence filtering through MG-RAST's pipeline.

**Table 6. Summary statistics of fastqc sequences from MG-RAST.**

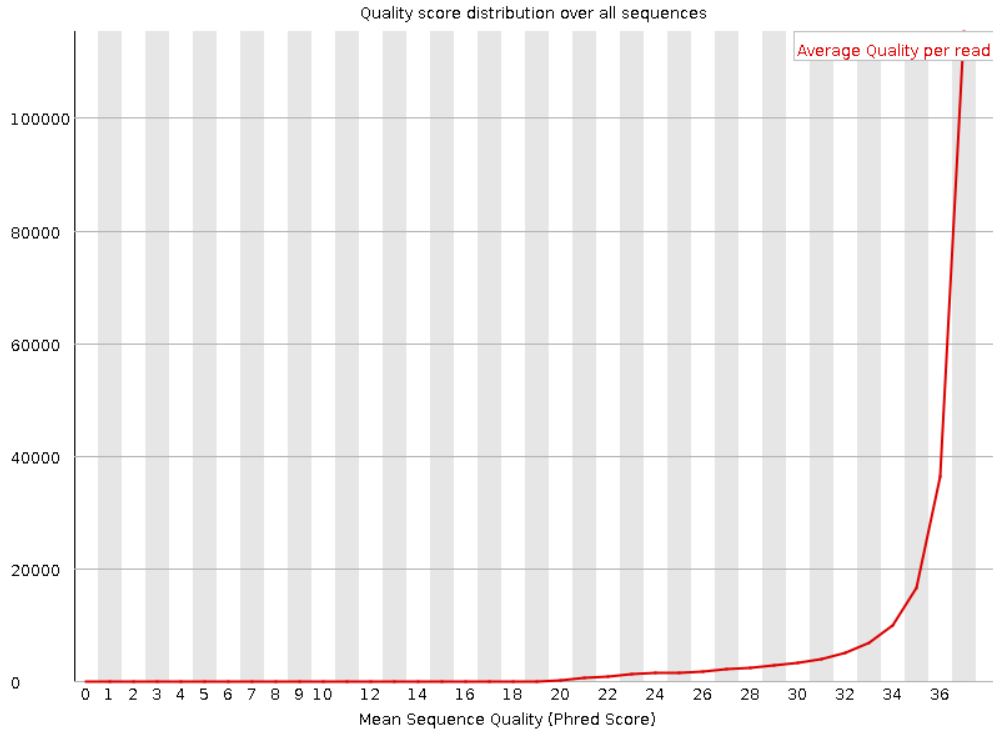
<b>Upload: bp Count</b>	<b>64,647,000 bp</b>
<b>Upload: Sequences Count</b>	215,490
<b>Upload: Mean Sequence Length</b>	300 ± 0 bp
<b>Upload: Mean GC percent</b>	56 ± 4 %
<b>Artificial Duplicate Reads:</b>	195,434
<b>Sequence Count</b>	
<b>Post QC: bp Count</b>	5,617,409 bp
<b>Post QC: Sequences Count</b>	20,043
<b>Post QC: Mean Sequence Length</b>	280 ± 28 bp
<b>Post QC: Mean GC percent</b>	55 ± 5 %
<b>Processed: Predicted Protein</b>	86
<b>Features</b>	
<b>Processed: Predicted rRNA</b>	39,275
<b>Features</b>	
<b>Alignment: Identified Protein</b>	6
<b>Features</b>	
<b>Alignment: Identified rRNA</b>	38,971
<b>Features</b>	
<b>Annotation: Identified Functional Categories</b>	undefined

### 3.2 Galaxy FastQC analysis

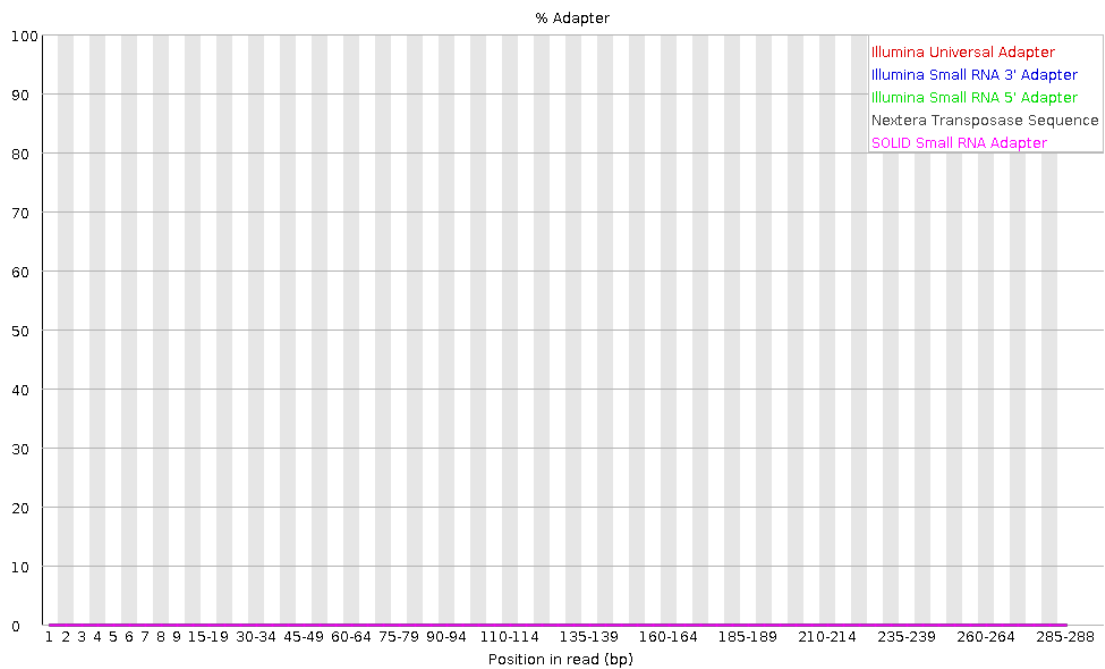
The purpose of fastqc analysis in Galaxy was to confirm quality assessment prior to statistical analysis. A total of 211,362 sequences were identified in the fastq file, with sequence length of 236-300 bases. GC content was confirmed as 55%. Moreover, Galaxy confirmed the Sanger/Illumina 1.9 encoding, which is based on the pred-like quality score +33. Quality scores across all bases (Figure 11a), with box-whisker plots describing central red line (median), yellow box (interquartile range), upper and lower whiskers (representing the 10% and 90% points), and, blue line (mean quality). Y-axis represents quality scores, where the higher the score, the higher the base quality. Further, the backdrop of the y-axis provides: green (very good quality), orange (moderate/reasonable quality), and red (poor base quality). Quality of bases towards the end of an Illumina run will typically see a degradation of base quality. Also, per sequence quality score and adaptor content graphs showed a pass in quality (Figure 11b, 11c).



**Figure 11a Quality reads from Galaxy FastQC algorithm.** Sequence quality scores per base was processed in Galaxy AU. MG-RAST was used to generate fastqc file after a series of pipeline steps were carried out.



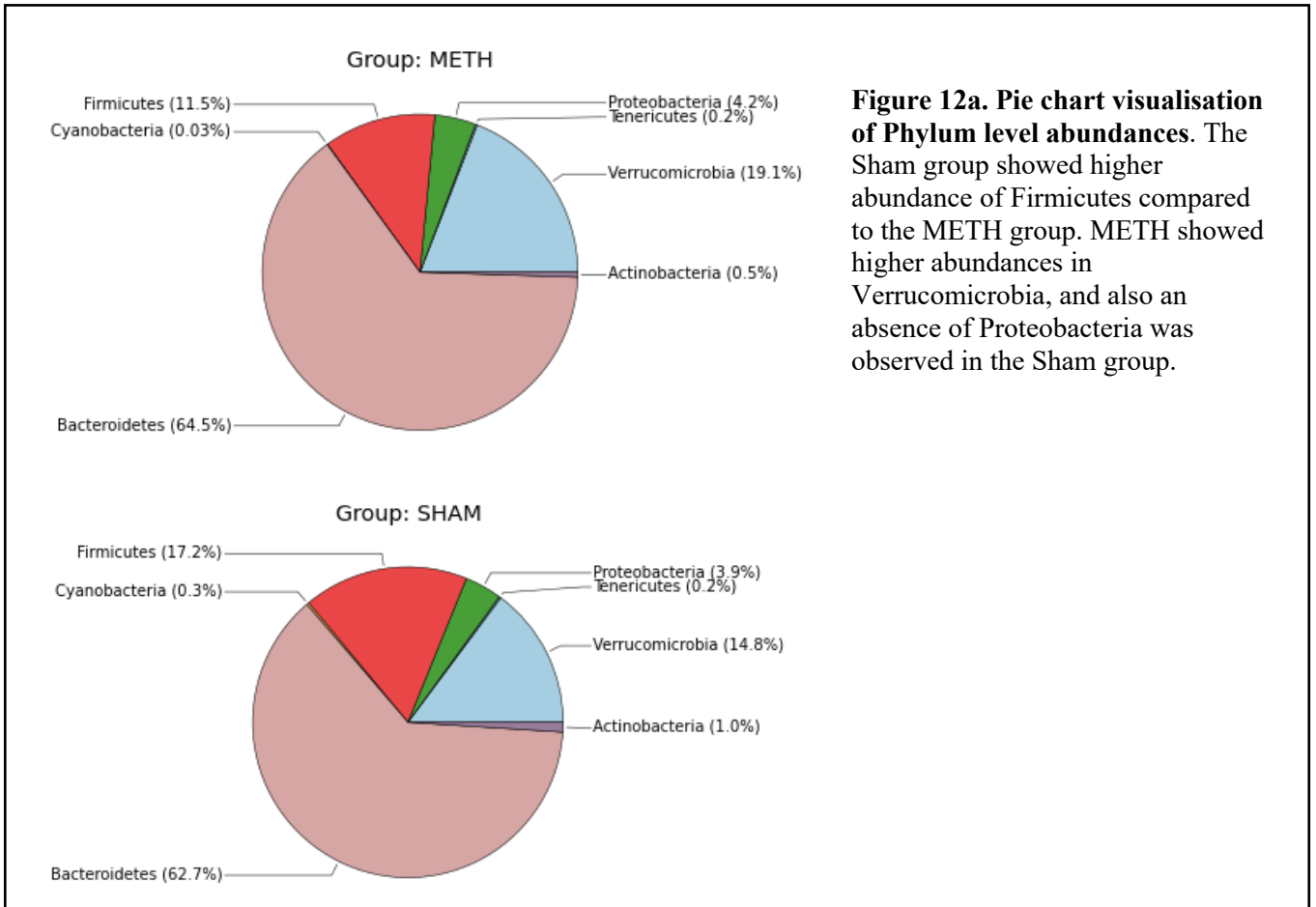
**Figure 11b. Per sequence quality score.** Mean sequence quality (x-axis) with total number of reads on the y-axis plotted. The distribution of average read quality usually takes a characteristic peak in the upper range of the plot (as seen here).



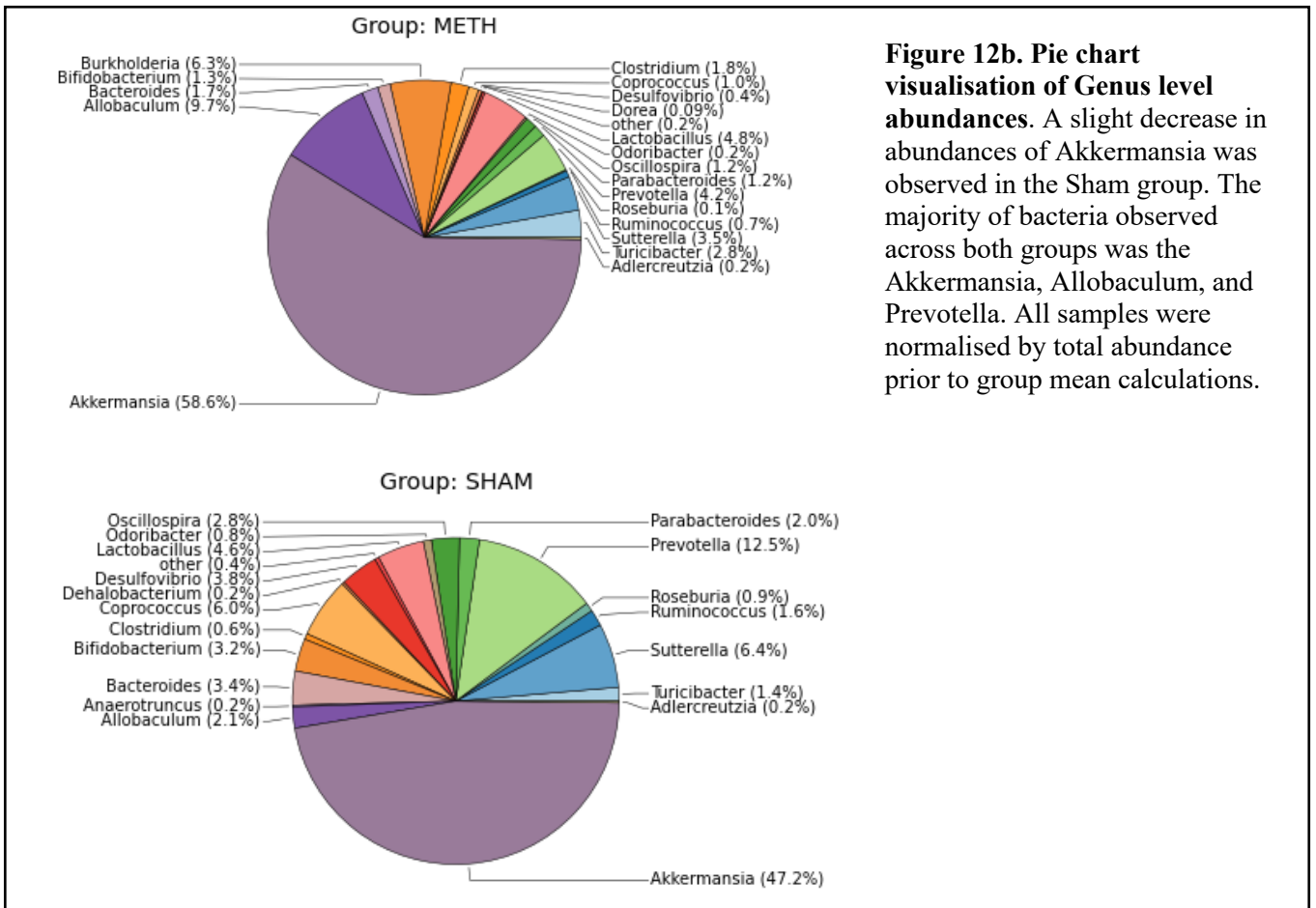
**Figure 11c. Galaxy adapter content plot.** No adapters were identified across the input sequences.

### 3.3 Diversity of microbial communities across METH and Sham groups

By analysing ‘genus’ and ‘phylum’ – *Domain* – ***Phylum*** – *Class* – *Order* – *Family* – ***Genus*** - at the perspective level, individual samples (A1-A8 [METH] and B1-B8 [Sham]) could be visualised and OTU mean abundances estimated and plotted. The richness of species within samples relates to the number of OTUs that have been mapped to bacterial species. The majority of taxonomies were mapped to Bacteriodes, Firmicutes and Verucomicrobia; whereas minor bacteria were Tenericutes, Cyanobacteria, Proteobacteria and Actinobacteria. At the phylum level, pie charts of METH and Sham diversity (Figure 12a) showed several minor differences, including a higher abundance of Firmicutes in the Sham group compared to the METH group. In addition, METH was shown to have a higher abundance of Verrucomicrobia compared to Sham group. At the genus level, around 10% increase in Akkermansia bacteria, in the METH group was observed (Figure 12b). In addition, a 2-fold increase in Turibacter was observed in the METH group (2.8%) compared to the Sham group (1.4%). In contrast, the Sham group contained a doubling of Ruminococcus (1.6%), compared to the METH group Ruminococcus (0.7%). No distinct abundance changes were observed in Lactobacillus across the METH and Sham groups. An almost 3-fold difference was observed in Prevotella between both groups, with the METH group containing 3-fold less Prevotella than the Sham group. Another significant difference in abundance was observed in Allobaculum, with the METH group containing ~4-fold increased abundance in this bacterium compared to the Sham group. METH group also showed a much lower abundance in Coprococcus (1.0%) than Sham group (6.0%). One particular bacterium, Burkholderia was not present in the Sham group, however had a presence in the METH group (6.3%). Lastly, major abundance difference was noted in Desulfovibrio, with Sham containing a three-fold higher abundance (3.8%), compared to METH group (0.4%).



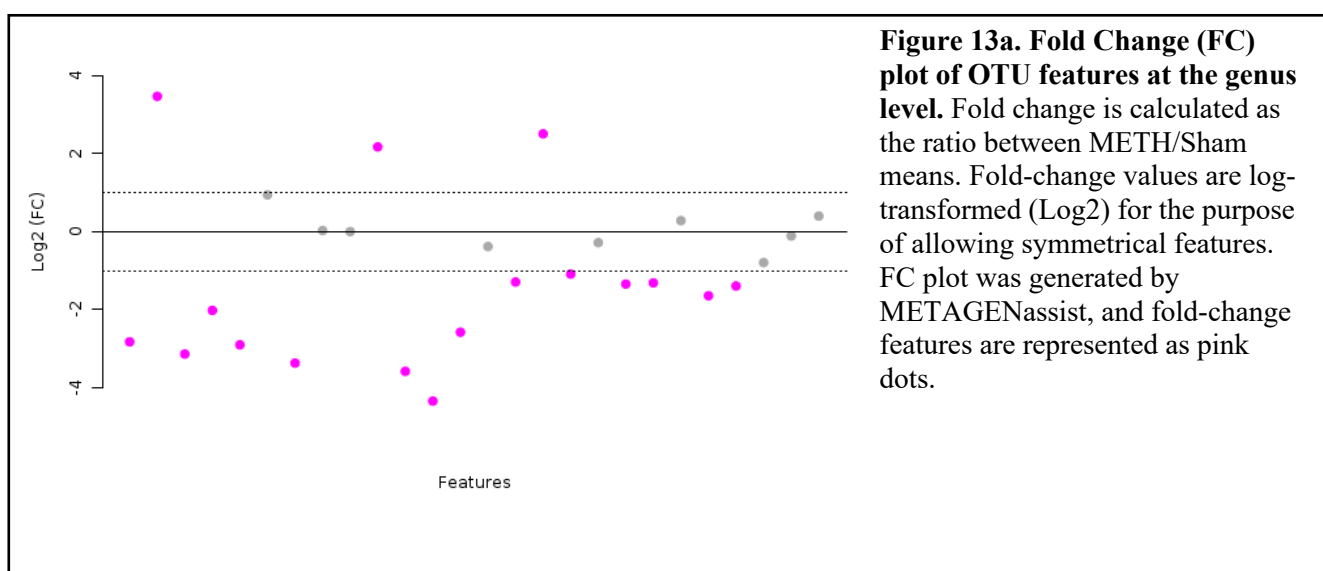
**Figure 12a. Pie chart visualisation of Phylum level abundances.** The Sham group showed higher abundance of Firmicutes compared to the METH group. METH showed higher abundances in Verrucomicrobia, and also an absence of Proteobacteria was observed in the Sham group.

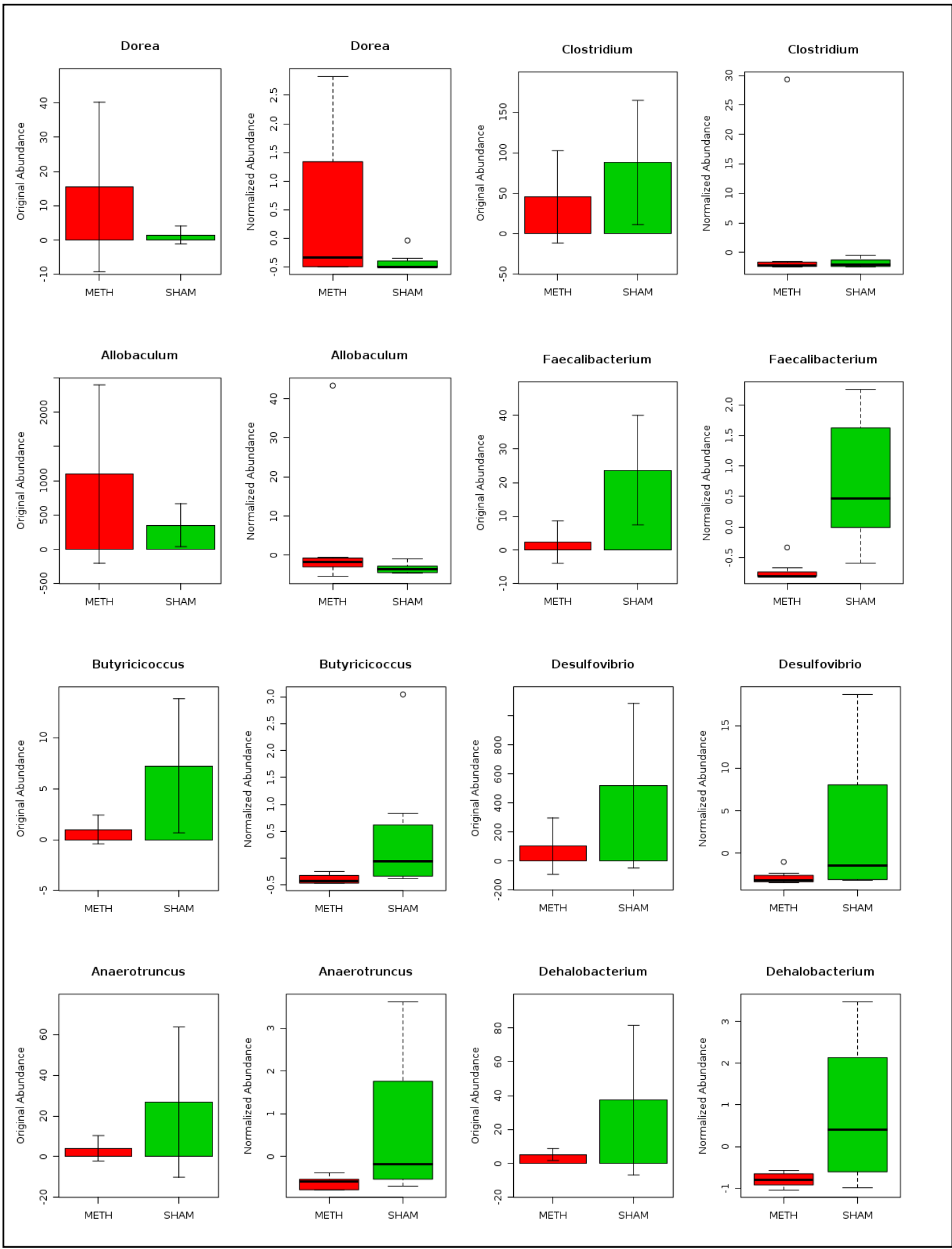


**Figure 12b. Pie chart visualisation of Genus level abundances.** A slight decrease in abundances of Akkermansia was observed in the Sham group. The majority of bacteria observed across both groups was the Akkermansia, Allobaculum, and Prevotella. All samples were normalised by total abundance prior to group mean calculations.

### 3.4 Significant fold-change differences in OTUs was observed in METH and Sham samples.

Filtered and normalised OTU abundances at the genus level were investigated for significant fold-change. A +/-2-fold change was set as a threshold for OTUs. Overall, three OTUs had a fold-change above 2-fold; 14 OTUs had a significantly below 2-fold change (Figure 13a). Specifically, Dorea (+3.47) and Allobaculum (+2.17), were significantly higher in METH compared to Sham samples. In contrast, Faecalibacterium (-4.34), Butyricicoccus (-3.58), Desulfovibrio (-3.37), Anaerotruncus (-3.14), Dehalobacterium (-2.90), Roseburia (-2.82), Coprococcus (-2.58), Clostridium (+2.51), and Odoribacter (-2.02) were significantly downregulated. In addition to fold-change, univariate volcano plot was constructed and features that passed both thresholds (fold-change and student's t-test) were highlighted (Figure 13c). Faecalibacterium ( $p=0.002$ ), Coprococcus ( $p=0.016$ ), Dehalobacterium ( $p=0.020$ ), Prevotella ( $p=0.027$ ), Ruminococcus ( $p=0.030$ ), and Anaerotruncus ( $p=0.046$ ) were found to pass both p-value and fold-change thresholds.





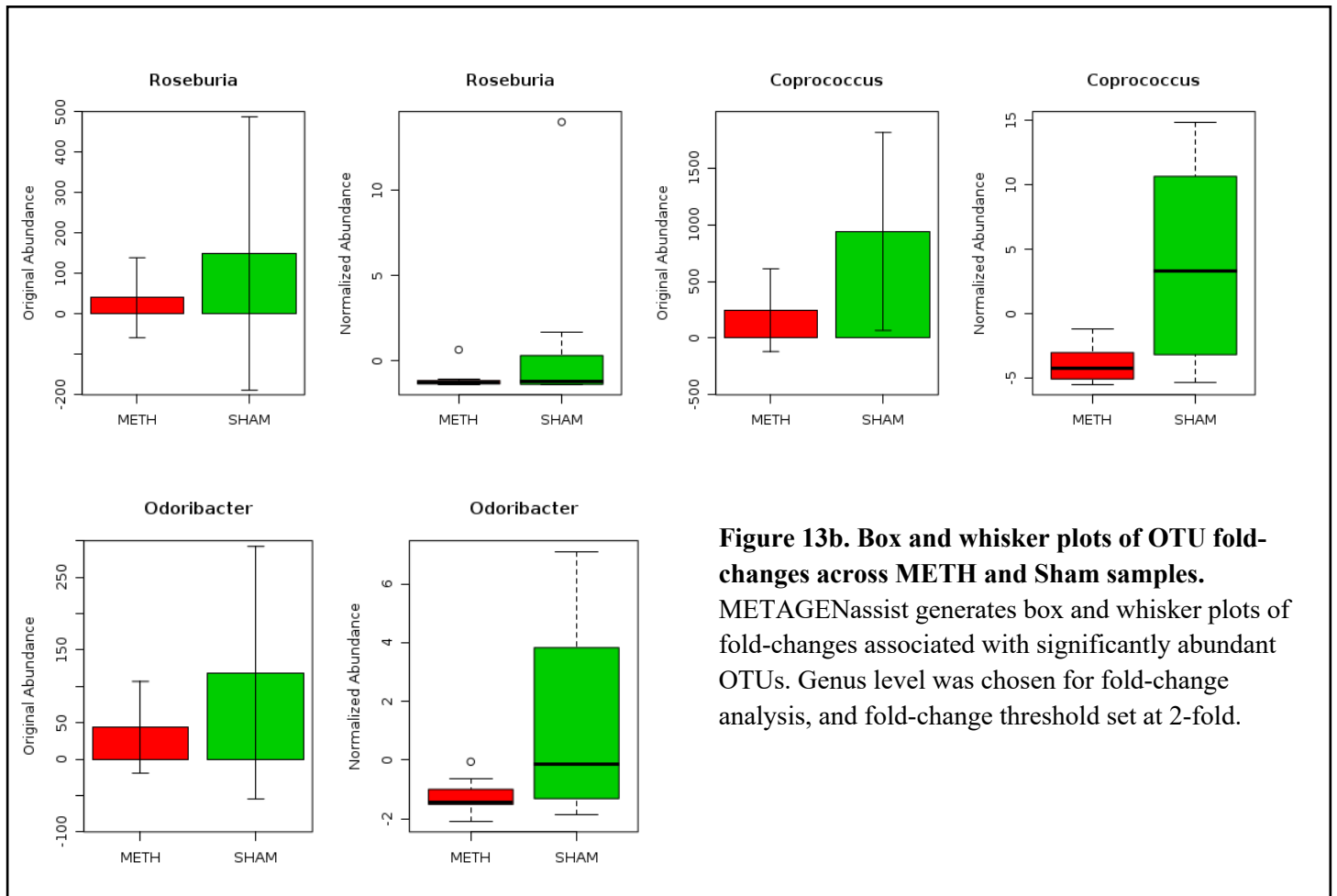
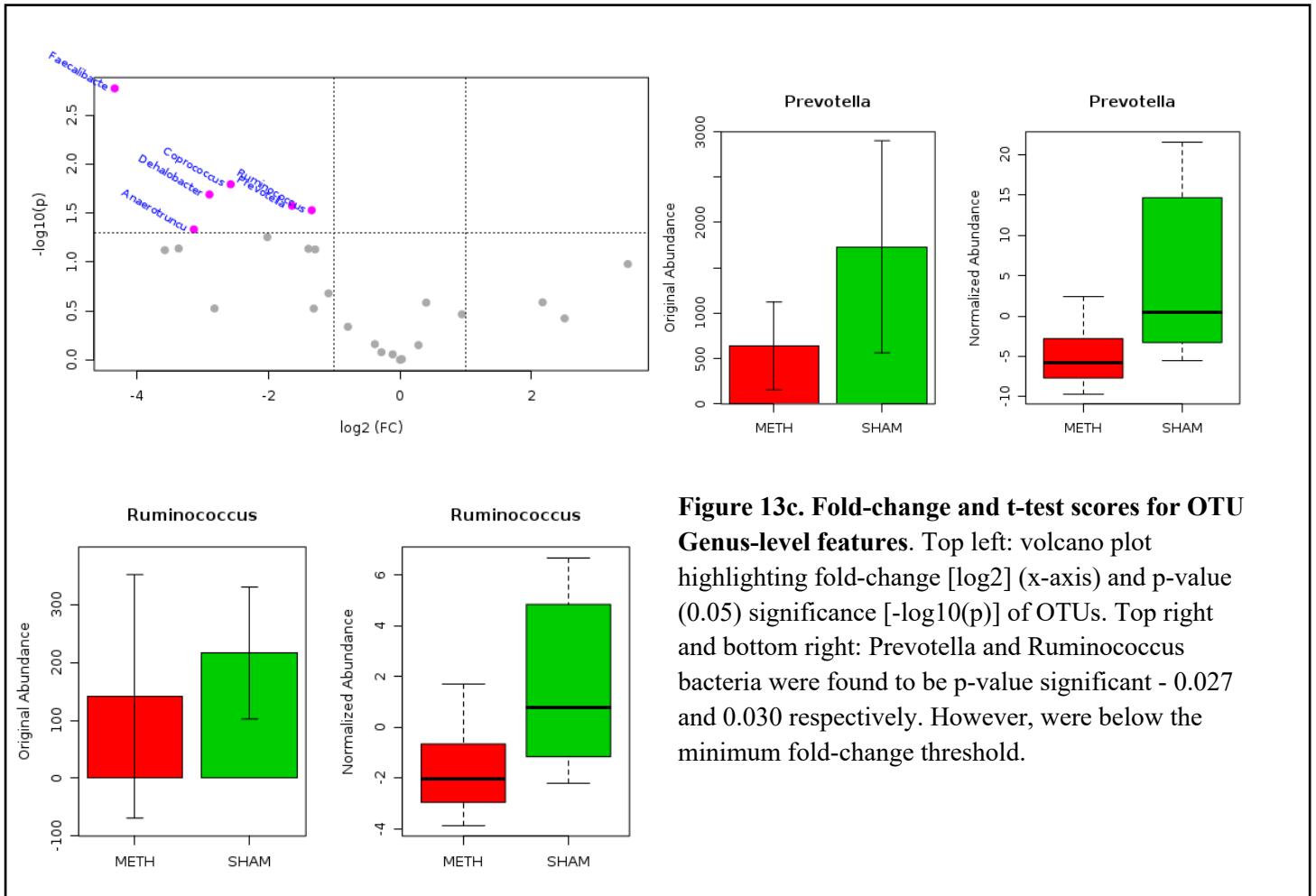


**Figure 13b. Box and whisker plots of OTU fold-changes across METH and Sham samples.** METAGENassist generates box and whisker plots of fold-changes associated with significantly abundant OTUs. Genus level was chosen for fold-change analysis, and fold-change threshold set at 2-fold.



Using MicrobiomeAnalyst, to confirm statistical significance, statistical analysis for sparse high-throughput sequencing data (MetagenomeSeq) was used to compute p-values. This algorithm uses the OTU features (or taxa level) to determine abundance of features between two groups. Moreover, it considers under-sampling and normalisation using a zero-inflated Gaussian fit model. Further, this statistical model determines features that are differentially abundant between two groups. Using this method found a total of 27 significant features (OTUs), at a p-value cut-off of 0.05. At the genus level, a total of 5 features were significantly ranked (Figure 14). In particular, *Desulfovibrio* ( $p=6.22 \times 10^{-10}$ ), *Ruminococcus* ( $p=6.22 \times 10^{-7}$ ), *Parabacteroides* ( $p=7.35 \times 10^{-7}$ ), *Coprococcus* ( $p=3.10 \times 10^{-4}$ ) and *Allobaculum* ( $p=0.02$ ) were among those with a p-value  $<0.05$ . This confirmed METAGENassist's p-value calculations (Figure 14); however, did not find *Faecalibacterium*, *Dehalobacterium*, *Prevotella* or *Anaerotruncus* to be significantly significant between METH and Sham groups.

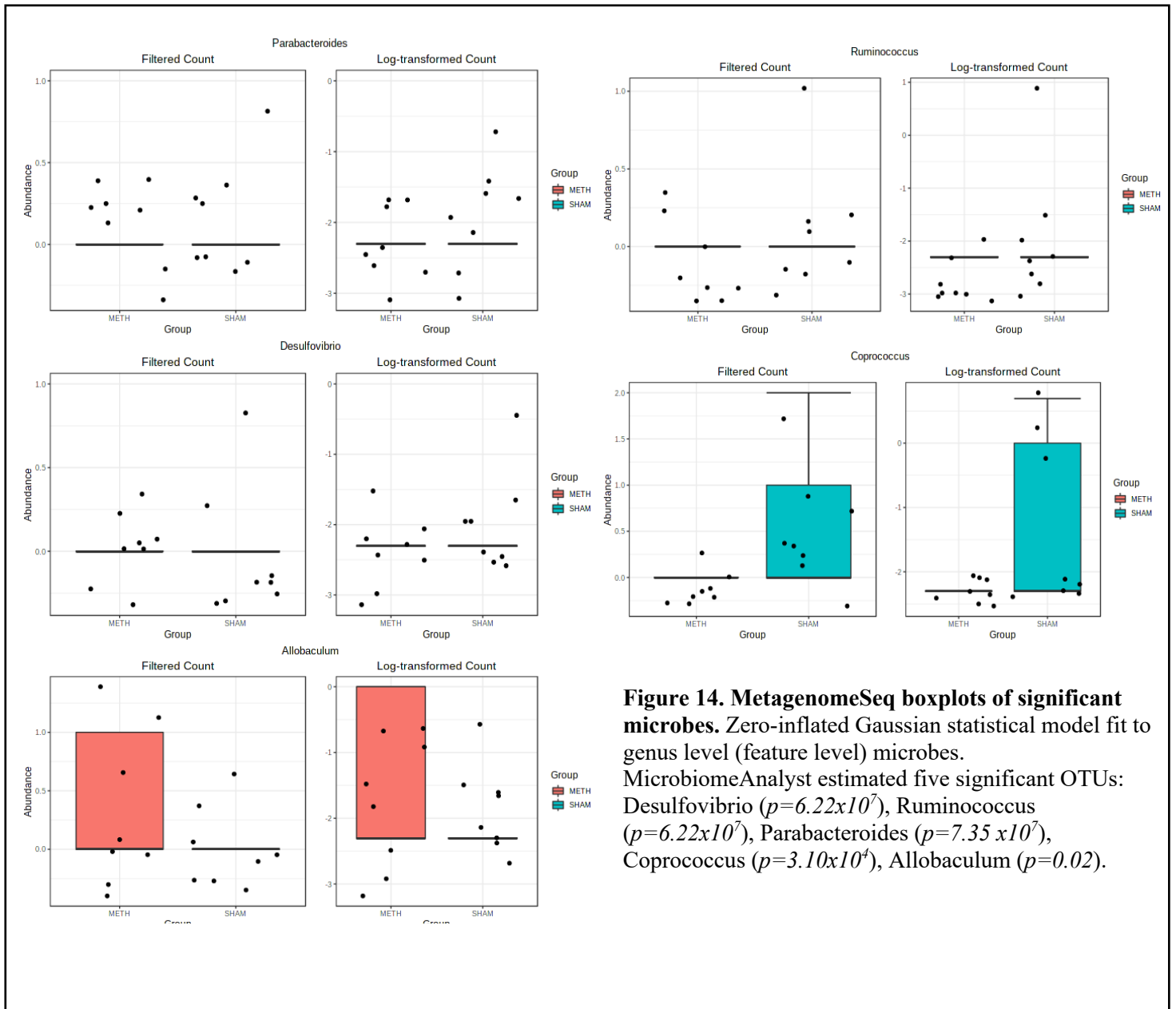


**Figure 14. MetagenomeSeq boxplots of significant microbes.** Zero-inflated Gaussian statistical model fit to genus level (feature level) microbes. MicrobiomeAnalyst estimated five significant OTUs: Desulfovibrio ( $p=6.22 \times 10^{-7}$ ), Ruminococcus ( $p=6.22 \times 10^{-7}$ ), Parabacteroides ( $p=7.35 \times 10^{-7}$ ), Coprococcus ( $p=3.10 \times 10^{-4}$ ), Allobaculum ( $p=0.02$ ).

### **3.5 Alpha diversity indices of METH and Sham samples**

Alpha diversity is described as the within-sample microbial diversity based on OTU richness and evenness was calculated using Chao1, abundance-based coverage estimators (ACE), Shannon and Simpson indices (Figure 15a, 15b). Alpha diversity calculates and measures sample richness and evenness. Richness considers unique species within a given community, and methods include Chao1 and ACE (both non-parametric methods) [Kim et al., 2017]. Evenness methods include Shannon and Simpson diversity metrics; Simpson method provides weight to more frequently occurring species; Shannon index method gives more weight to rare species in a given community. Alpha diversity (at the feature [OTU] and genus level) as calculated from MicrobiomeAnalyst resulted in an insignificant difference among samples belonging to both METH and Sham groups, as evidenced by p-value scores greater than 0.05 cut-off. Observed, Chao1 and ACE alpha diversity boxplots at the OTU (feature) level showed a greater abundance in the METH group compared with Sham group samples. Moreover, evenness alpha diversity metrics – Shannon and Simpson indices – found a greater microbial evenness within the METH group than the Sham group (Figure 15a). However, p-value significance between Chao1 and ACE, and between Shannon and Simpson did not reveal significant differences in diversity and evenness, respectively. At the genus level, METH and Sham alpha diversity methods also did not reveal any significant differences between microbial diversity and evenness. Attributions to this observed insignificant difference in both METH and Sham samples might be linked to several individual METH and Sham samples which seemed to contribute to variations in diversity.

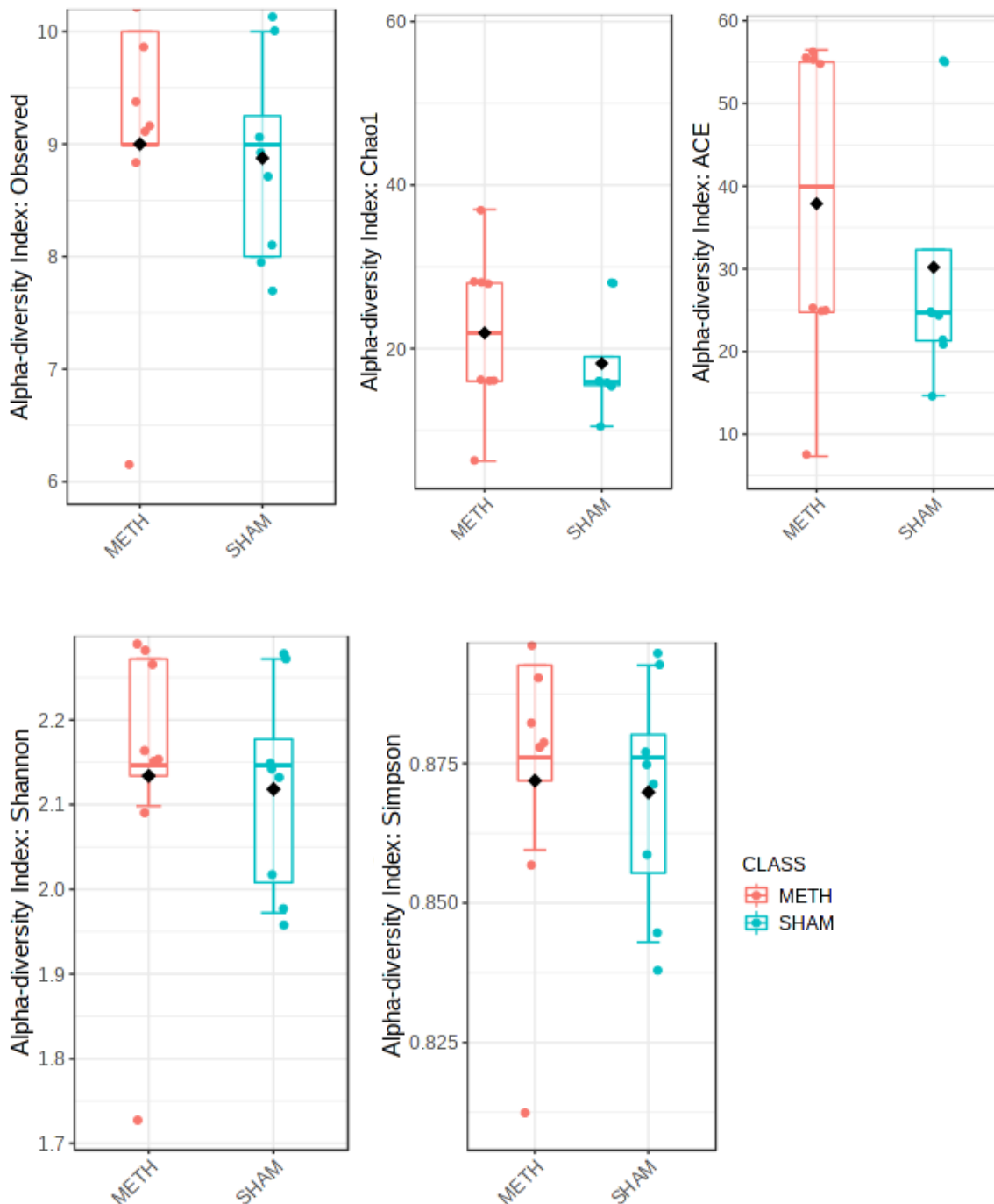


**Figure 15a. OTU-level alpha diversity boxplots of METH and Sham groups.** Observed, Chao1, ACE, Shannon and Simpson alpha diversity indices were used for METH and Sham calculations at the OTU level. Standard error (SE) was calculated for Chao1 and ACE, and were computed via MicrobiomeAnalyst's bootstrap procedure, which resamples observed data and recomputes estimators several times. For Chao1 and ACE, the greater the indices the higher the richness of the microbiome. Moreover, the smaller the Simpson index, and higher the Shannon index, the higher the diversity of the microbiome. P-values for Chao1 ( $p=0.27294$ [Mann-Whitney]), ACE ( $p=0.2794$ [Mann-Whitney]), Shannon ( $p=0.58358$ ), and Simpson ( $p=0.62149$ ) were calculated. Data and graphs of alpha indices for METH and Sham groups was obtained from MicrobiomeAnalyst. Boxplots: middle line is median; whiskers represent lowest and highest values within the interquartile range (IQR). All red (METH) and blue (Sham) dots represent individual samples in each group.

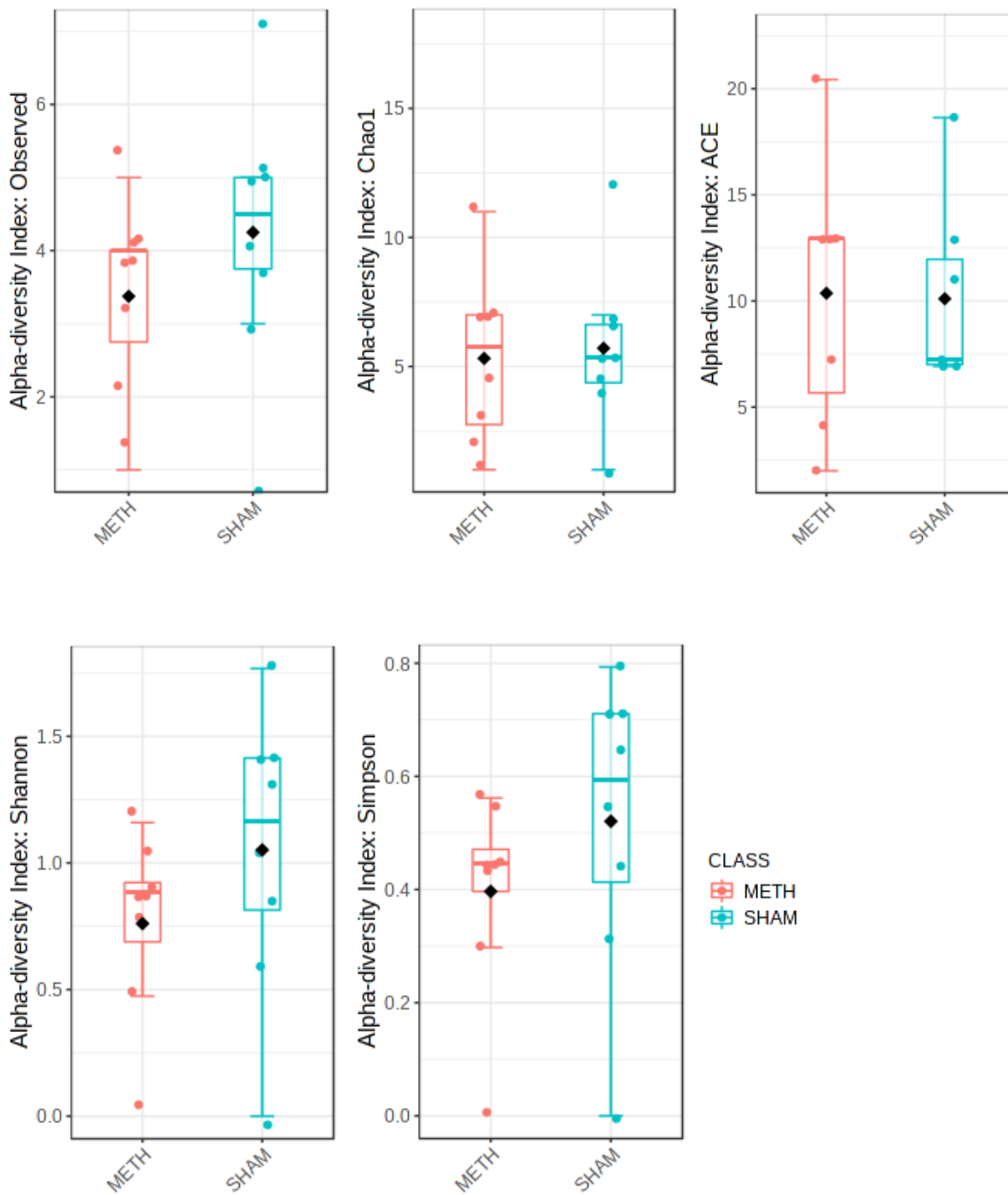
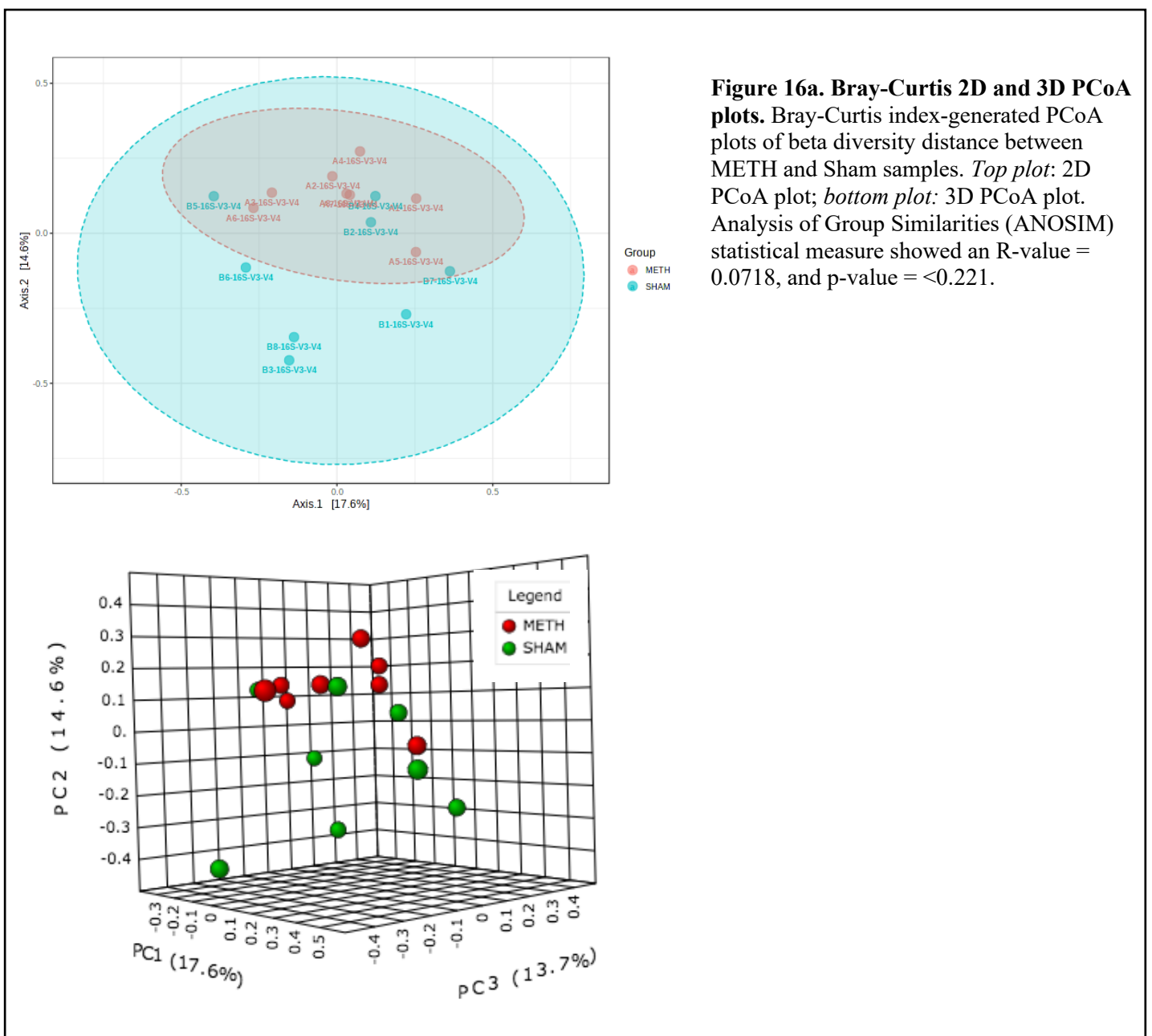


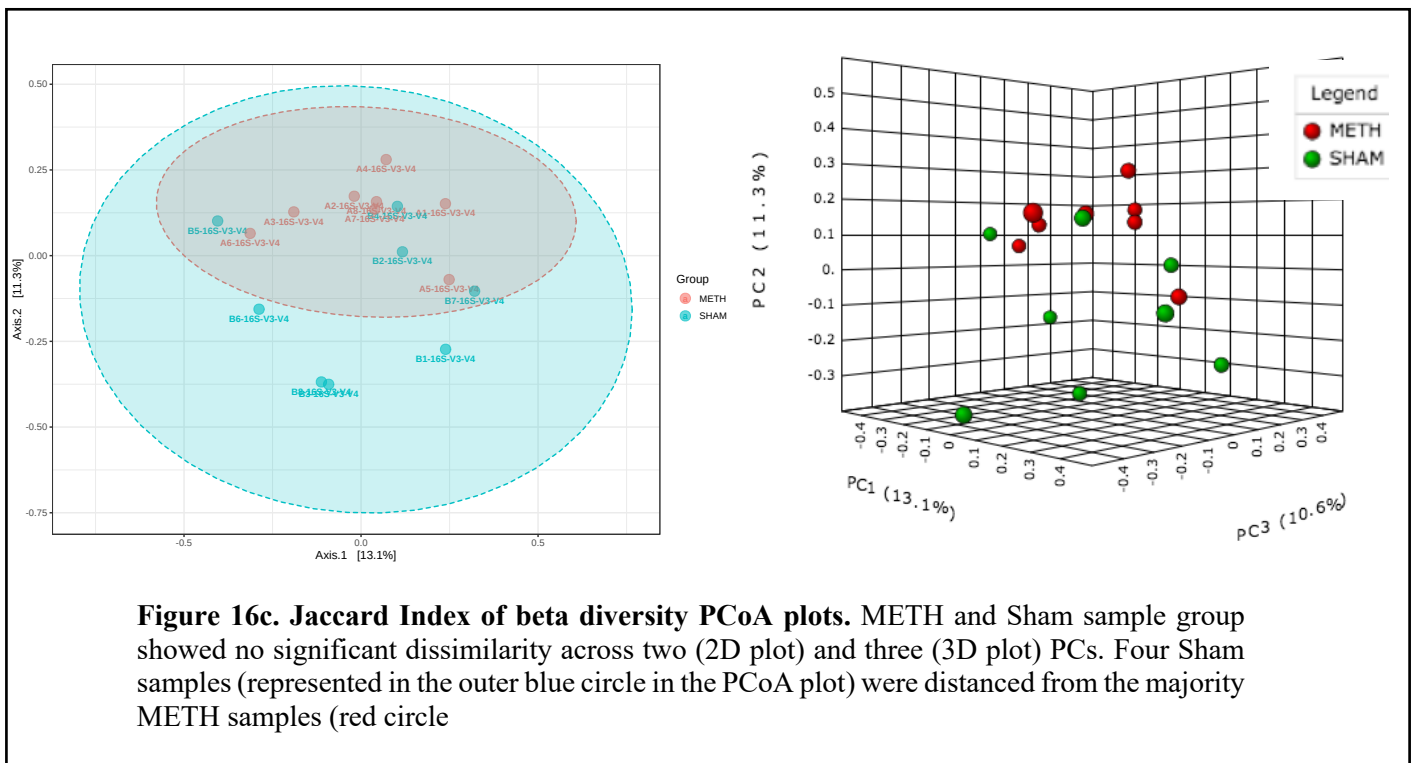
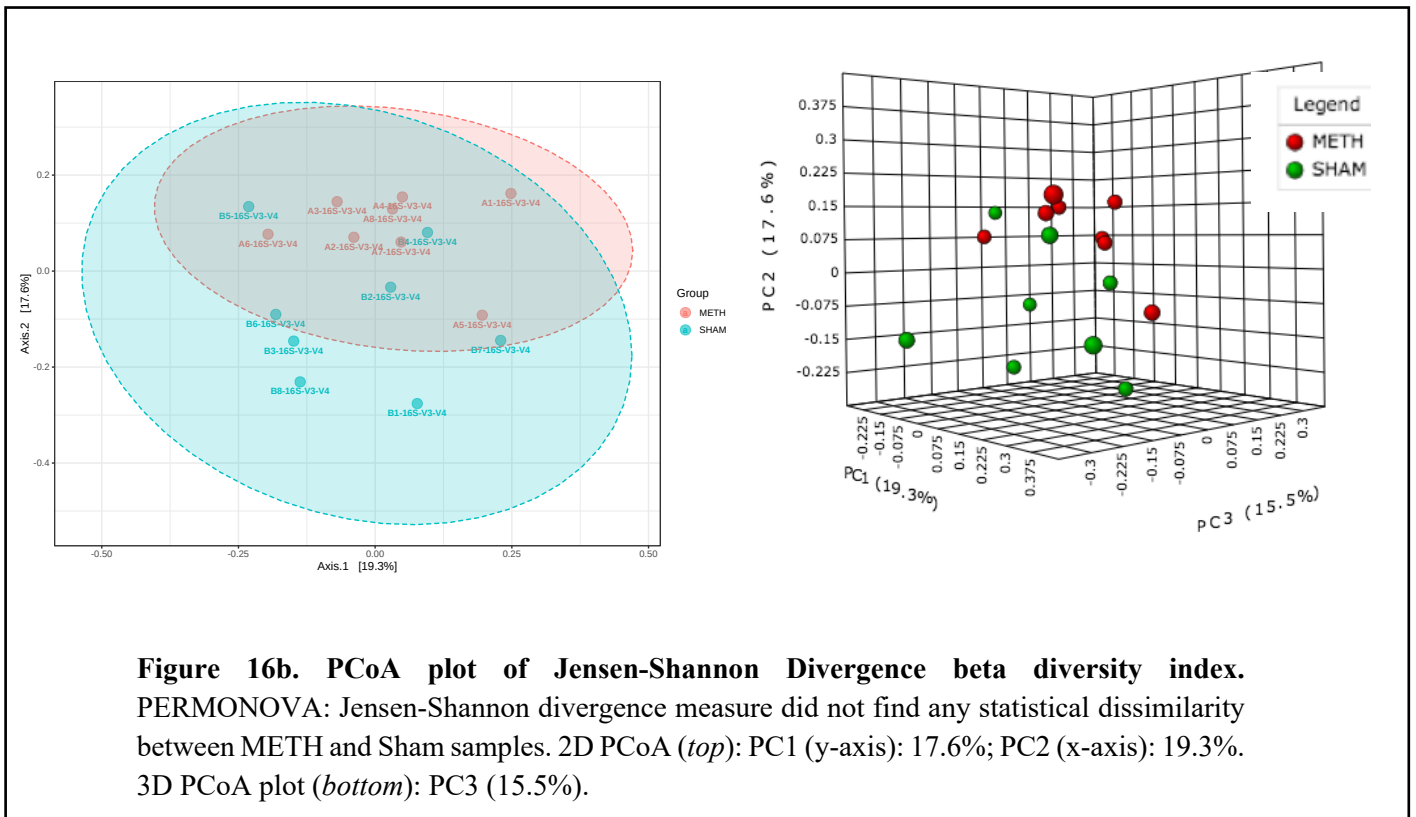
**Figure 15b. Genus-level alpha diversity boxplots of METH and Sham groups.** Observed, Chao1, ACE, Shannon and Simpson alpha diversity indices were used for METH and Sham calculations at the OTU level. Standard error (SE) was calculated for Chao1 and ACE, and were computed via MicrobiomeAnalysts’s bootstrap procedure, which resamples observed data and recomputes estimators several times. P-value calculations were produced using the Mann-Whitney statistic. Observed:  $p=0.231$ ; Chao1:  $p=1.00$ ; ACE:  $p=0.795$ ; Shannon:  $p=0.168$ ; Simpson:  $p=0.168$ . Boxplots: middle line is median; whiskers represent lowest and highest values within the interquartile range (IQR). All red (METH) and blue (Sham) dots represent individual samples in each group.

### 3.6 Beta diversity indices of METH and Sham groups

Beta diversity of between-METH and Sham samples was calculated using a series of distance methods, including Bray-Curtis index, Jensen-Shannon divergence, and Jaccard distance. In general, beta diversity compares microbial communities between samples, premised on the distance or dissimilarity between sample pairs. Ordination plots, notably PCoA allows visual illustration in a low-dimensional space of group distance/dissimilarity.



Bray-Curtis beta diversity dissimilarity index was calculated at  $R= 0.0718$ , based on the ANOSIM measure (Figure 16a). In general, an ANOSIM closer to 1 represents is sufficient to conclude dissimilarity between the METH and Sham groups. However, an R number closer to 0 was observed, representing no significant dissimilarity between both groups. In addition, 2D PCoA principal components (PCs) showed two PCs – PC1 (14.6%) and PC2 (17.6%), and 3D PCoA plot showed an additional – PC3 (13.7%). Besides the ANOSIM statistical measure, Permutational MANOVA (PERMANOVA) for beta diversity dissimilarity/distance computed as, F-value = 1.883,  $R^2 = 0.078$ , and p-value =  $<0.301$ . Homogeneity of Group Dispersions (PERMDISP) analyses multivariate homogeneity of group dispersions, and therefore focuses on any differences found in the spread/dispersion of groups. For PERMDISP, F-value = 1.1572, and a p-value = 0.300. Jensen-Shannon Divergence PCoA plots (Figure 16b) also found minimal dissimilarity between METH and Sham groups. For PERMONOVA statistics, F-value = 1.4536,  $R^2 = 0.094$ , and p-value =  $<0.14$ . As two main clusters were observed (as in Bray-Curtis PCoA plot), a minority of Sham samples, specifically B1, B3, and B8 were the most dissimilar compared to all METH (A1-A8) samples and were slightly dissimilar to B6 and B7; and, more dissimilar to B2, B4 and B5. ANOSIM statistical significance scores were, R-value = 0.079, and p-value =  $<0.187$ . PERMDISP scores were calculated as F-value = 1.0933, and p-value = 0.313. Jaccard index of beta diversity between METH and Sham groups (Figure16c). PERMANOVA statistical significance scores were F-value = 1.1018,  $R^2 = 0.073$ , p-value =  $<0.311$ . Two clusters were observed along the 2D PCoA plot, and an additional Sham sample (B6) was clustered with B1, B3 and B8 (Figure 16b). ANOSIM and PERMDISP statistics methods also revealed non-significant dissimilarity between METH and Sham sample groups – R= 0.05; p-value =  $<0.284$ , F-value = 1.0694; p-value=0.312, respectively.

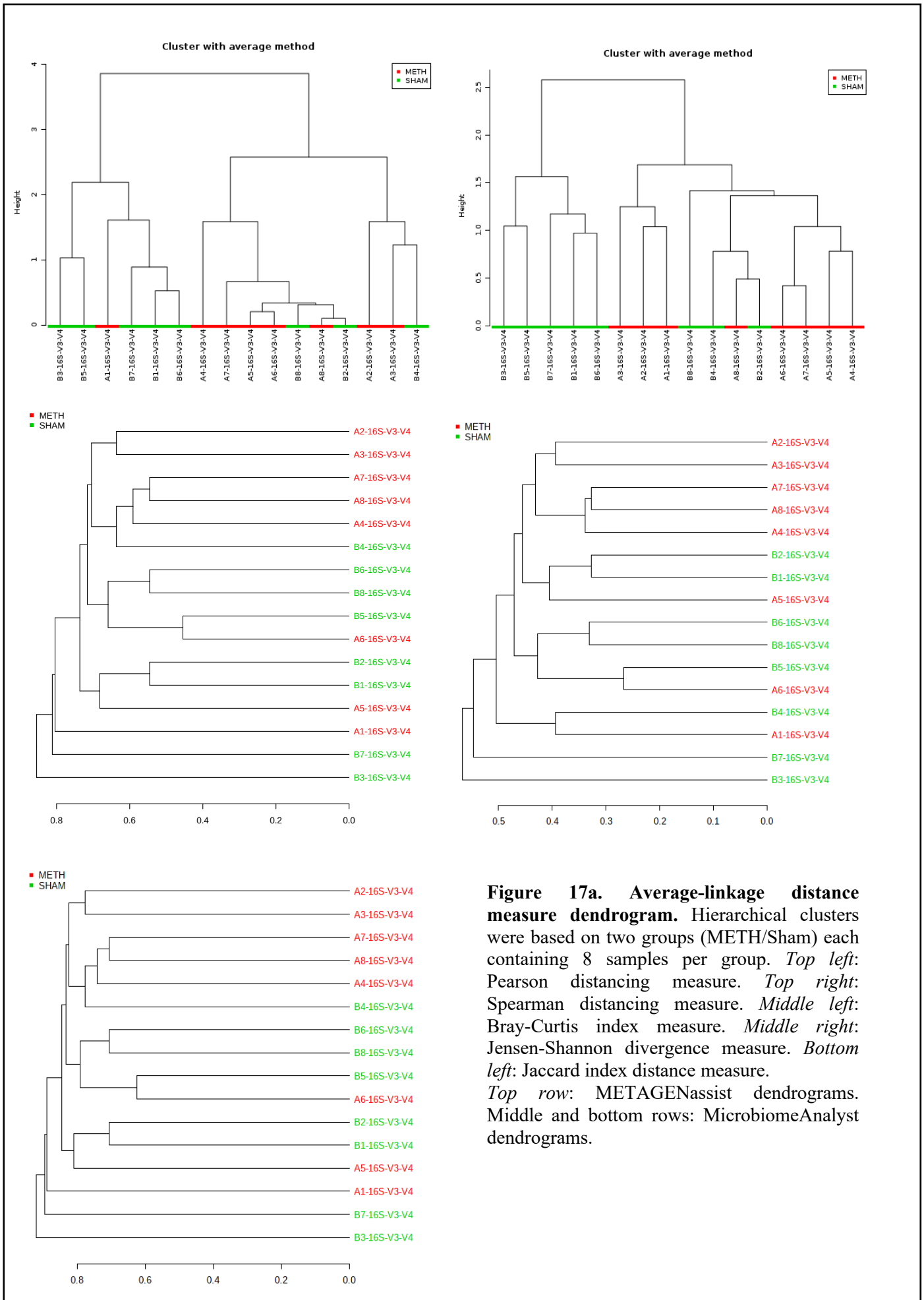


### **3.7 Hierarchical clustering revealed clusters based on distance measure methods.**

Clustering, in the context of microbiota data, represent a group of tools utilised to aggregate or group abundance profiles based on similar bacterial compositions. Two parameters, namely distance measure and clustering algorithm are used to initiate clustering of samples in a hierarchical manner. METAGENassist and MicrobiomeAnalyst contain hierarchical clustering and heatmap visualisation tools, that can be viewed at the feature (OTU) level, as well as across all phylogenetic branches. Pearson and Spearman distance measures (METAGENassist) were calculated for METH and Sham samples, and clustering methods based on average, complete, single and Ward were incorporated to assess sample clustering represented as a dendrogram. Bray-Curtis, Jensen-Shannon and Jaccard indices were used for dendrograms constructed in MicrobiomeAnalyst. Pearson and Spearman distance measures were used in combination with average/complete/single/Ward clustering (Figures 17a, 17b). All hierarchical agglomerative clustering dendrograms were constructed from feature-level taxa (OTU). Comparisons were made between the different distance measures and clustering methods to find consistent clusters across METH and Sham samples. Average, single and complete-linkage distance measures all operate on dissimilarities. Single-linkage measures the least dissimilar pair of points between two groups; complete-linkage measures the most dissimilar pair of points; average-linkage uses the average dissimilarity across all data pairs. Along the process of agglomerative clustering, each individual cluster is paired with similar clusters into a new single cluster. This is done until all steps belong to a single cluster ( $N$ ) [Kimes et al., 2017]. Each sample from METH and Sham was treated as a separate cluster. Dissimilarity is observed along the x-axis (MicrobiomeAnalyst), and y-axis (METAGENassist). Average-linkage function paired with Pearson dissimilarity function performed better than Spearman distance measure. Pearson/average,

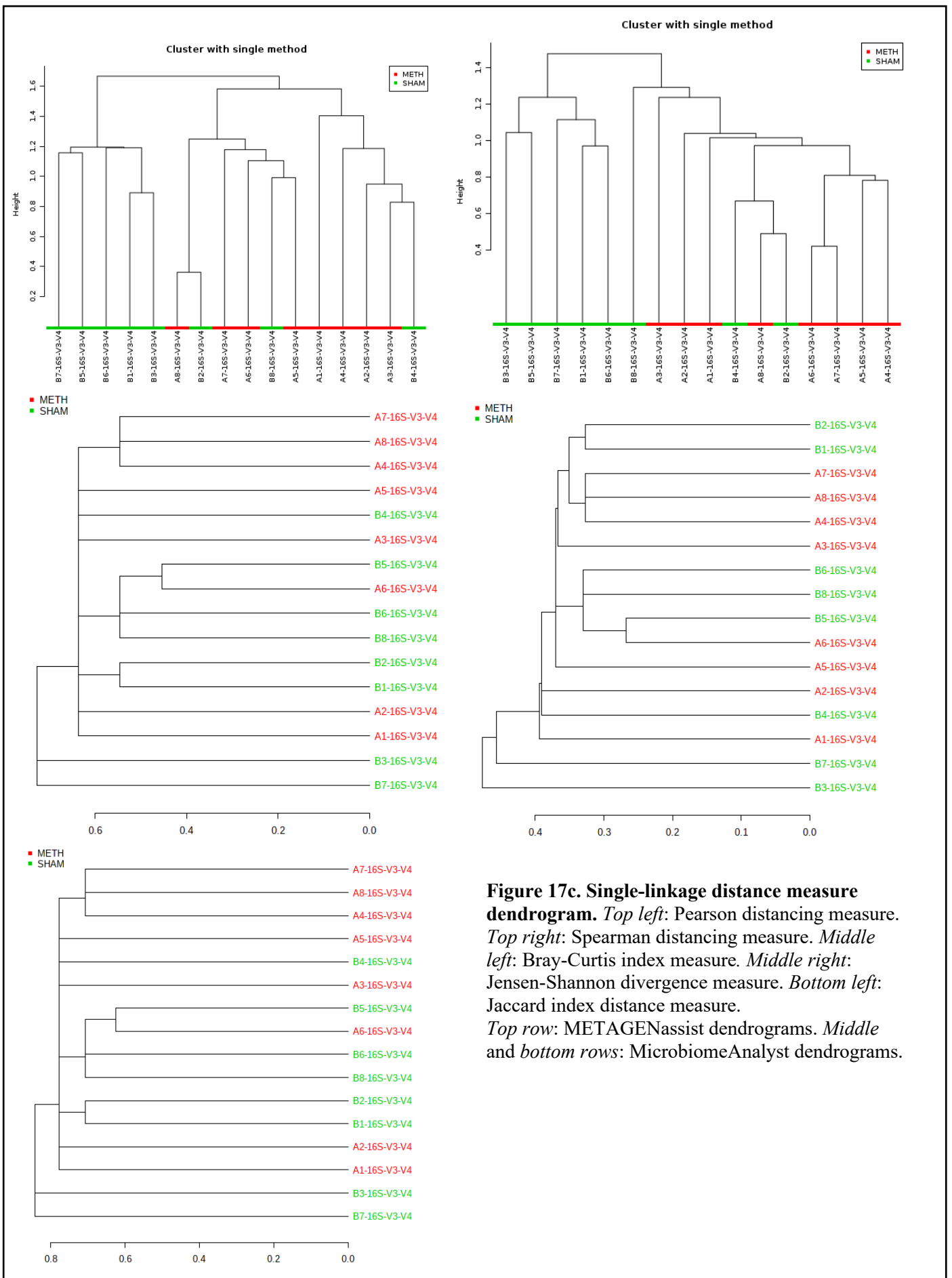
Spearman/average, Bray-Curtis/average, Jensen-Shannon/average and Jaccard/average clustering dendrograms (Figure 17c, 17d), showed a consistent similarity classification of METH samples A4, A7, A2, A7, A8 A5 and A6. Two main cluster nodes were observed in both Pearson and Spearman distance measures. Bray-Curtis/average, Jensen-Shannon/average and Jaccard/average distance measures revealed a consistent clustering of majority METH samples. Only METH samples A5, A6 and A1 were found to be clustered amongst Sham samples. For complete-linkage function, Pearson and Spearman distance measures found greater similarity (denoted by node cluster) across METH and Sham samples, with greater dissimilarity found between the METH and Sham groups. From MicrobiomeAnalyst, Jensen-Shannon performed well with computing distances between METH and Sham samples, with B1, B2, B3, B6 and B8 having greater similarity, and clustered to one node. In contrast, Jensen-Shannon/complete-linkage distancing mapped a cluster of METH samples – A4, A8, A7, A6, A3 and A2 – with A5, A4, A8 and A7 having greater similarity, compared with A6, A3 and A2, which formed a separate cluster with sample B5. Bray-Curtis/complete and Jaccard-linkage distance measures calculated Sham sample B7 as a singleton, yet found similar clusters belonging to Sham samples B8, B6, B1, and B2, with METH sample singleton A5 belonging to this cluster yet showing greater dissimilarity between aforementioned Sham samples. Single-linkage clustering from Pearson and Spearman distancing measures revealed two main hierarchical clusters, with majority Sham and METH samples being clustered in their respective groups. Overall, greater similarity was observed within Sham and METH samples, however similarity, based on cluster distance, was observed between some METH and Sham samples. In addition, single-linkage for bray-Curtis and Jaccard distance methods showed several outliers within their dendrograms – A5, A3, and B4 – which were largely dissimilar (based on height distance) from the main clusters. Ward-linkage clustering for Pearson and Spearman distance clustered Sham samples in a similar manner, with B1, B3, B5, B6 and B7

having less dissimilarity compared with METH samples. Bray-Curtis, Jensen-Shannon and Jaccard performed moderately well, and had very similar clustering dendrogram patterns. Across all three dissimilarity functions, B6, B8, B5 and B3 were clustered together. Moreover, METH samples A2, A3, A7, A8 and A4 were clustered similarly.

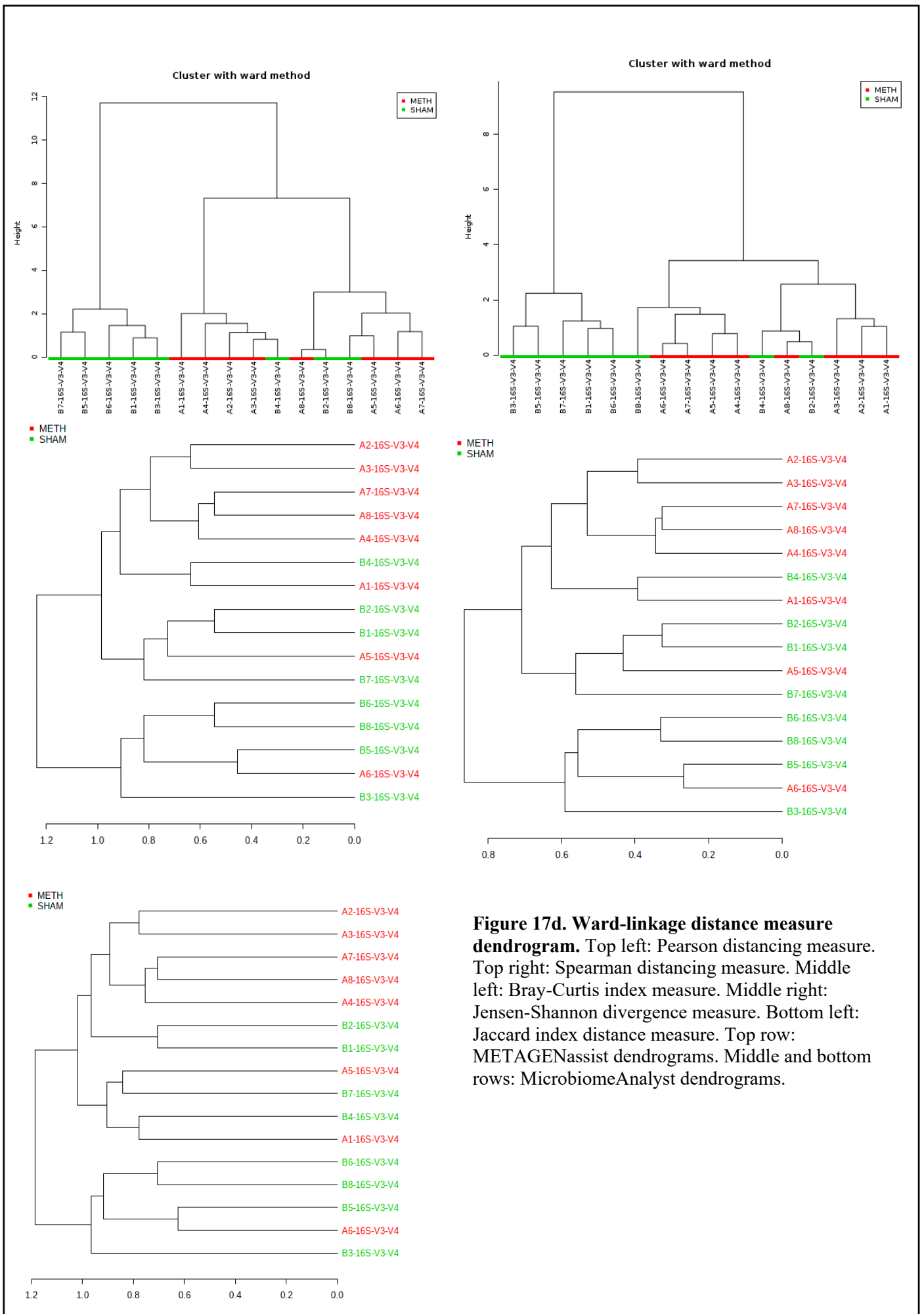


**Figure 17a. Average-linkage distance measure dendrogram.** Hierarchical clusters were based on two groups (METH/Sham) each containing 8 samples per group. *Top left:* Pearson distancing measure. *Top right:* Spearman distancing measure. *Middle left:* Bray-Curtis index measure. *Middle right:* Jensen-Shannon divergence measure. *Bottom left:* Jaccard index distance measure. *Top row:* METAGENassist dendrograms. *Middle and bottom rows:* MicrobiomeAnalyst dendrograms.





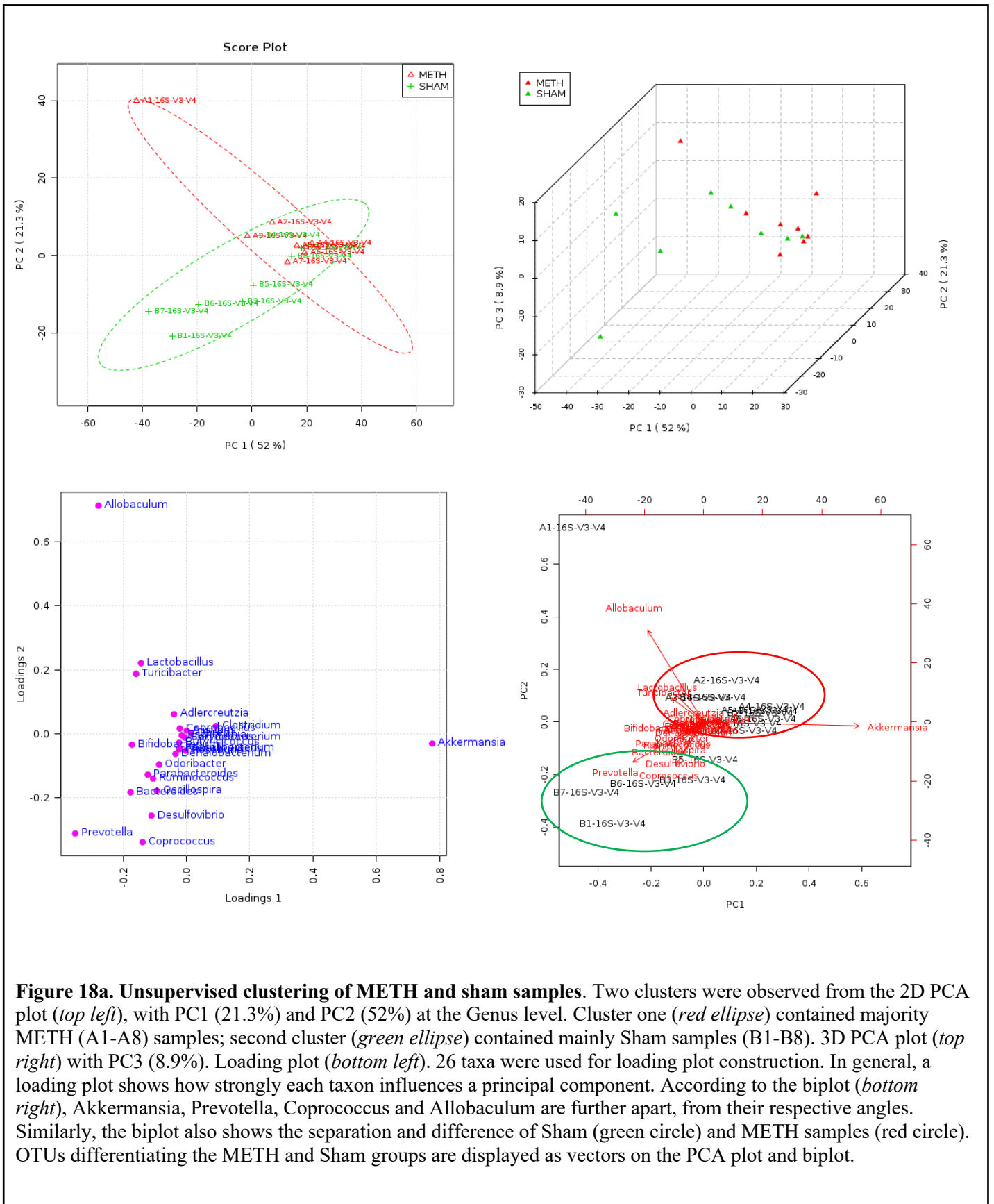
**Figure 17c. Single-linkage distance measure dendrogram.** *Top left:* Pearson distancing measure. *Top right:* Spearman distancing measure. *Middle left:* Bray-Curtis index measure. *Middle right:* Jensen-Shannon divergence measure. *Bottom left:* Jaccard index distance measure. *Top row:* METAGENassist dendrograms. *Middle and bottom rows:* MicrobiomeAnalyst dendrograms.



**Figure 17d. Ward-linkage distance measure dendrogram.** Top left: Pearson distancing measure. Top right: Spearman distancing measure. Middle left: Bray-Curtis index measure. Middle right: Jensen-Shannon divergence measure. Bottom left: Jaccard index distance measure. Top row: METAGENassist dendrograms. Middle and bottom rows: MicrobiomeAnalyst dendrograms.

### **3.8 Multivariate analysis revealed distinct clusters across METH and Sham samples.**

The high dimensionality of microbial diversity data requires dimension reduction and visualisation. PCA is an unsupervised method, which performs transformation of a complex collection of data points can be visualised on a 2D plane. Two main clusters were visualised from the PCA plot (genus level), along with incorporation of a loading plot, which mapped the most important features from the PCA plot. According to both the loading plot and biplot (Figure 18a), the most important features (taxon) contributing to the principal components (PCs) in the PCA plot, were Akkermansia, Allobaculum, Turicibacter, and Lactobacillus, Prevotella, Coprococcus, and Desulfovibrio. Moreover, loading plot values (denoted as Loading value 1 (LD1, and Loading value 2 (LD2) for important features were, Allobaculum (LD1: -0.28; LD2: 0.71), Akkermansia (LD1: 0.78; LD2: -0.03), Turicibacter (LD1: -0.16; LD2: 0.19), Lactobacillus (LD1: -0.14; LD2: 0.22), Prevotella (LD1: -0.35; LD2: -0.31), Coprococcus (LD1: -0.14; LD2: -0.34), and Desulfovibrio (LD1: -0.11; LD2: -0.27).



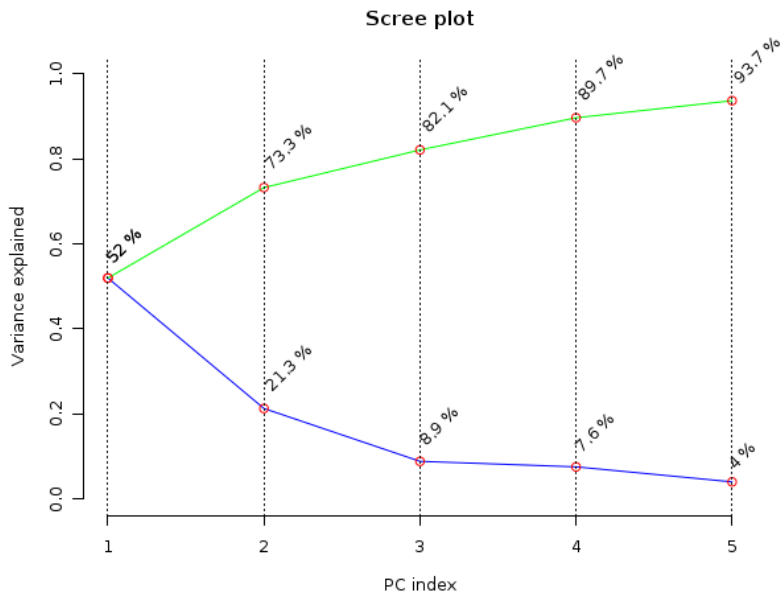


**Figure 18b. Scree plot of Principal Components.** The first PC1 contributed to 52% of the variance, with PC2 contributing to 21.3% of variance in the PCA plot. Top green line represents the accumulated variance of PCs; blue line represents individual PCs and their proportion to the variance. Majority of variance explained in the PCA plot could be attributed to the first two PCs.

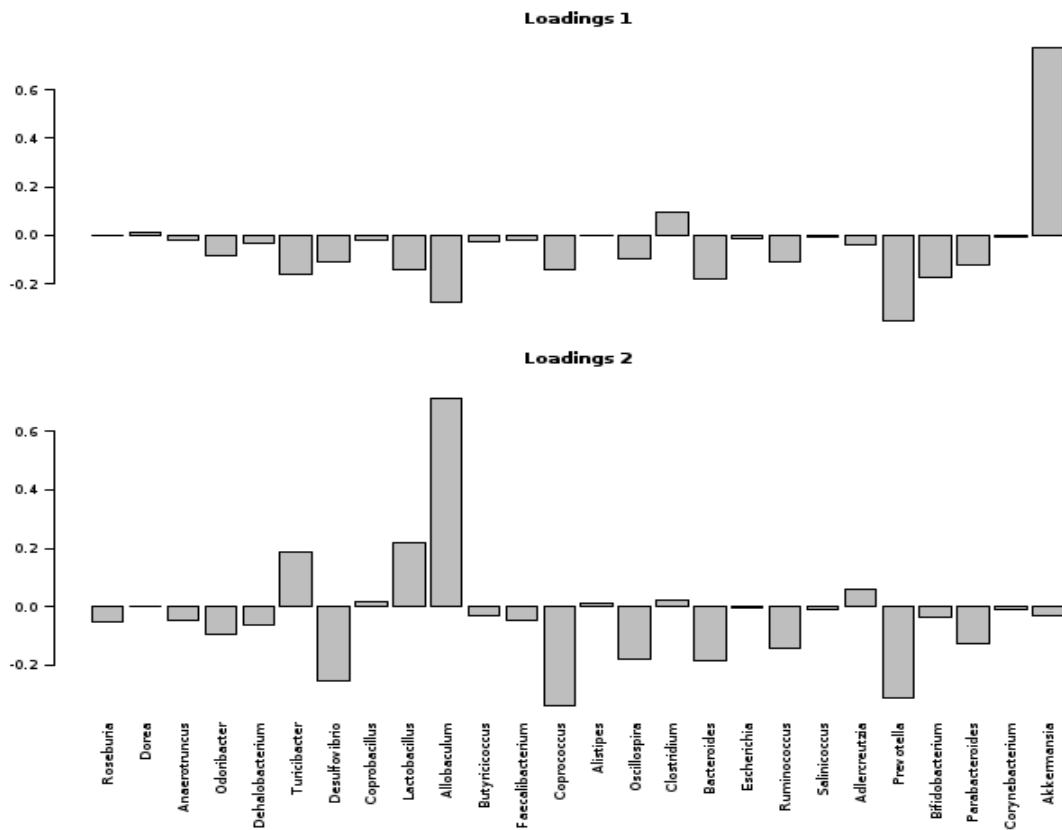


**Figure 18c. Bar chart of loading scores.** Loading scores were complementary to loadings plotted in Figure 18a.

K-means clustering was used, as a widely used non-hierarchical clustering method that seeks to minimise sum of squared error across all K clusters [Santos et al., 2018]. METAGENassist offers two popular clustering methods – k-means and self-organising maps (SOM). The operation of k-means creates k clusters where each sample is grouped to a cluster with the nearest mean value. SOM, a type of neural network, employs an iterative pipeline that maps non-linear statistical dependencies on a two-dimensional grid. Specifying two clusters, when selecting the ‘all ranks’ option for taxonomy analysis, two clusters were observed (Figure 19a). Cluster one contained 5 Sham samples only, whereas cluster two contained 11 samples: 8 METH, and 3 Sham samples. SOM clustering was also performed on samples. SOM is an unsupervised neural network algorithm, with the resulting plot indicating relative values of features in each cluster. Essentially, SOM converts complex, high-dimensional data features into a low-dimensional display. SOM plot of METH and Sham samples at the ‘All ranks’ level (with X dimension = 1, and Y dimension = 2) indicated two clusters (cluster 1: n=5 and cluster 2: n=11) (Figure 19b). As both K-means and SOM clustering are unsupervised methods of grouping similar features, both algorithms were able to group majority Sham and METH samples together (Figure 18a, 18b). For supervised learning algorithms, Random Forest was used from both METAGENassist and MicrobiomeAnalyst. Random Forest (RF) constructs a series of decision trees which is built upon a bootstrap training sample. Upon decision tree construction, around one-third of the features (instances) are excluded and then used as test samples. This test data is used to calculate the classification error (also known as out-of-bag (OOB) error). Importantly, the OOB error rate can be used to assess how efficient the performance of the RF was. Each built tree in a RF is premised on a random sample within the set of observations [Janitza et al., 2018]. In addition, RF utilises a variance of importance feature which is evaluated by the measured increase in the OOB error upon its permutation. The RF approach is further strengthened for its ability to detect outliers in

the data set; which can detect those samples which are considered outliers, according to the RF proximity measure. Based on RF as carried out by METAGENassist, RF classification of METH and sham samples found an OOB error of 0.188, with METH classification containing 0.125 class error; and, Sham group classification containing a class error of 0.25 (Figure 20a). Error appeared to reduce at approximately 100 trees (Figure 20a), as the RF was built from the original METH and Sham samples. For MicrobiomeAnalyst RF calculations, error seemed to reduce at around 150 trees, however error was also seen at approximately 380-390 trees, which then stabilised (Figure 20a). In addition, OOB error was computed as 0.5, with class error of METH classification of 0.375, and class error of Sham, 0.625. Mean decrease accuracy (MDA) calculates all OOB validated predictions and lists the most important variables/features are visualised as dots at the top of an MDA plot. Variables/features are listed along the y-axis, with importance of each plotted on the x-axis. By evaluating the RF MDA plot by METAGENassist (Figure 20b), it can be observed that the 15 most important features were: Faecalibacterium, Lachnospiraceae;gnavus, Clostridium;colinum, Butyrivicoccus;pullicaecorum, Anaerotruncus, Bacteria; F16, Bacteroides;acidifaciens, Bifobacterium;animalis, Salinicoccus, Rikenellaceae, Prevotella, Lachnospiraceae;saccharophila, Lachnospiraceae, Lactobacillus, and Ruminococcus. For RF MDA in MicrobiomeAnalyst, top features were: Bacteroidales, Rikenellaceae (Bacteroidales), Prevotella, Clostridiales (Firmicutes), Coprococcus, and Allobaculum.

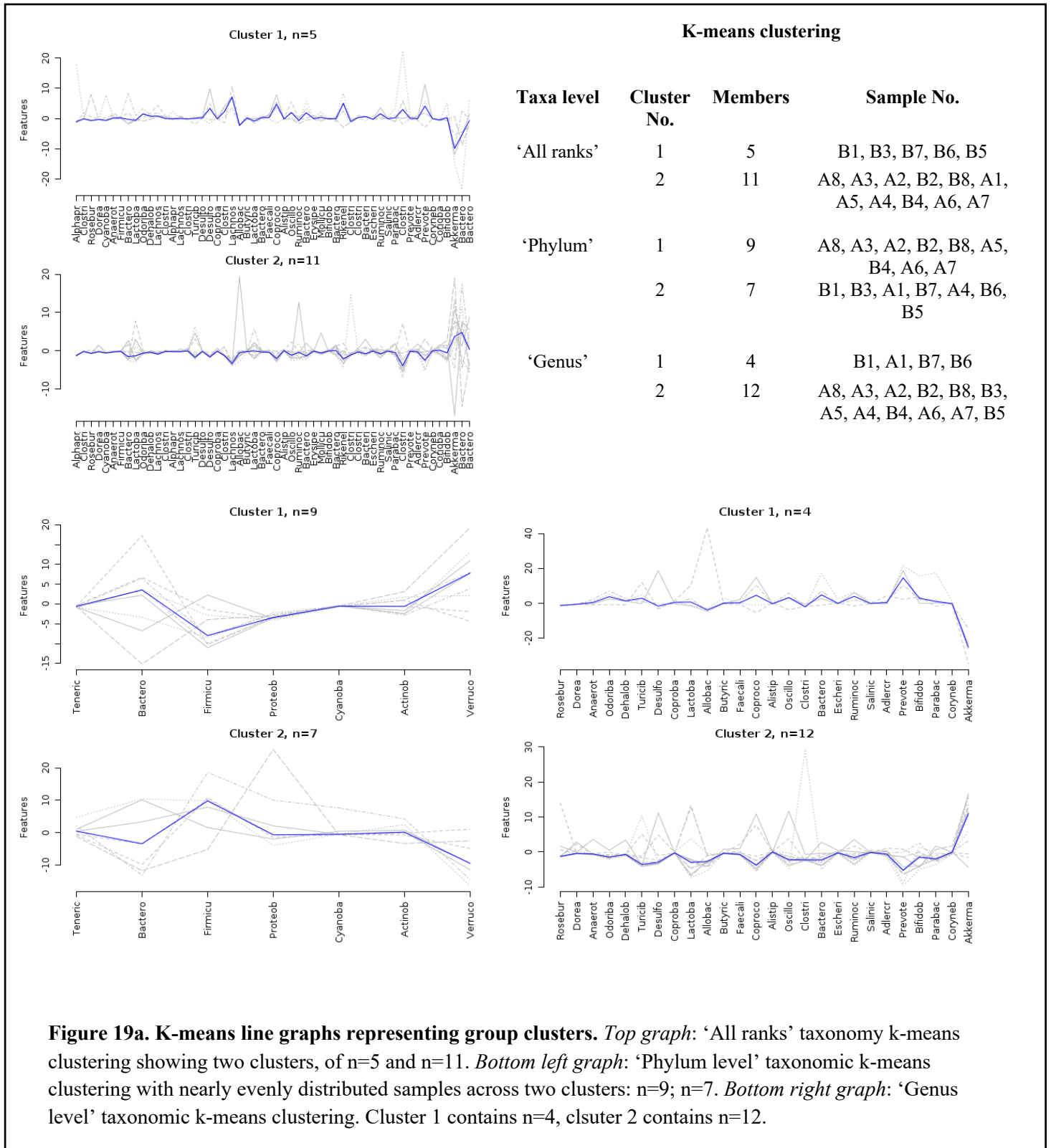
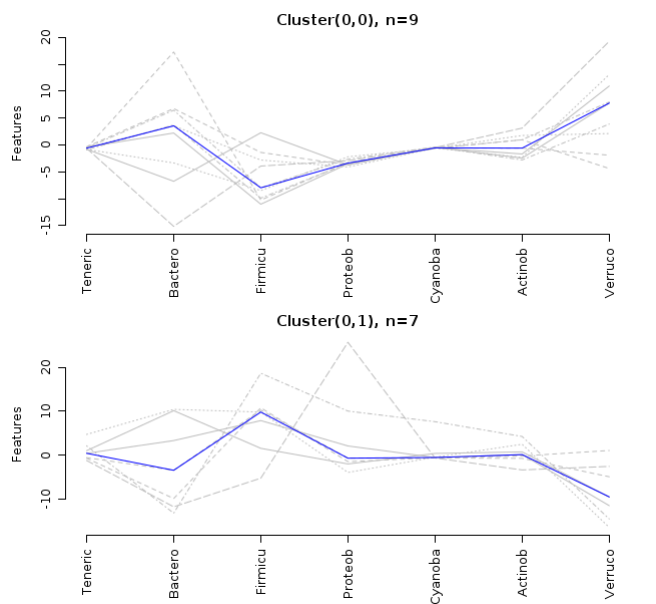
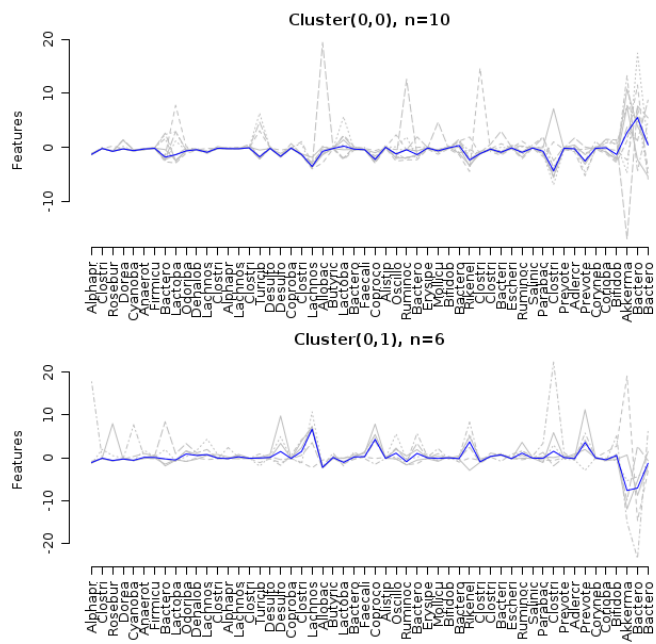


**Figure 19a. K-means line graphs representing group clusters.** *Top graph:* 'All ranks' taxonomy k-means clustering showing two clusters, of n=5 and n=11. *Bottom left graph:* 'Phylum level' taxonomic k-means clustering with nearly evenly distributed samples across two clusters: n=9; n=7. *Bottom right graph:* 'Genus level' taxonomic k-means clustering. Cluster 1 contains n=4, cluster 2 contains n=12.



**SOM clustering**

Taxa level	Cluster No.	Members	Sample No.
'All ranks'	1	10	A8, A3, A2, B2, A1, A5, A4, B4, A6, A7
	2	6	B1, B8, B3, B7, B6, B5
'Phylum'	1	9	A8, A3, A2, B2, B8, A5, B4, A6, A7
	2	7	B1, B3, A1, B7, A4, B6, B5
'Genus'	1	10	A8, A3, A2, B2, B8, A5, A4, B4, A6, A7
	2	6	B1, B3, A1, B7, B6, B5

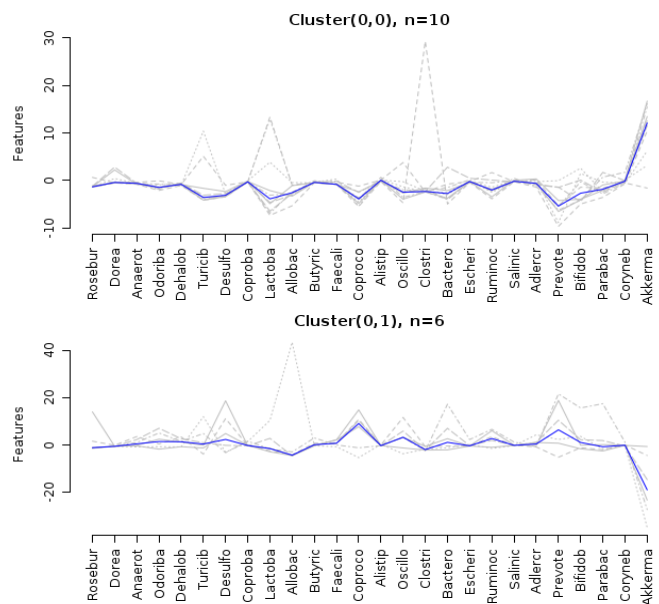


**Figure 19b. SOM clustering plots.** *Top:* 'All ranks' taxonomy level showing two main clusters: n=5 and n=11. *Bottom left:* Phylum level taxonomy SOM plot, with two clusters: n= 2 and n=14. *Bottom right:* Genus level SOM plot.

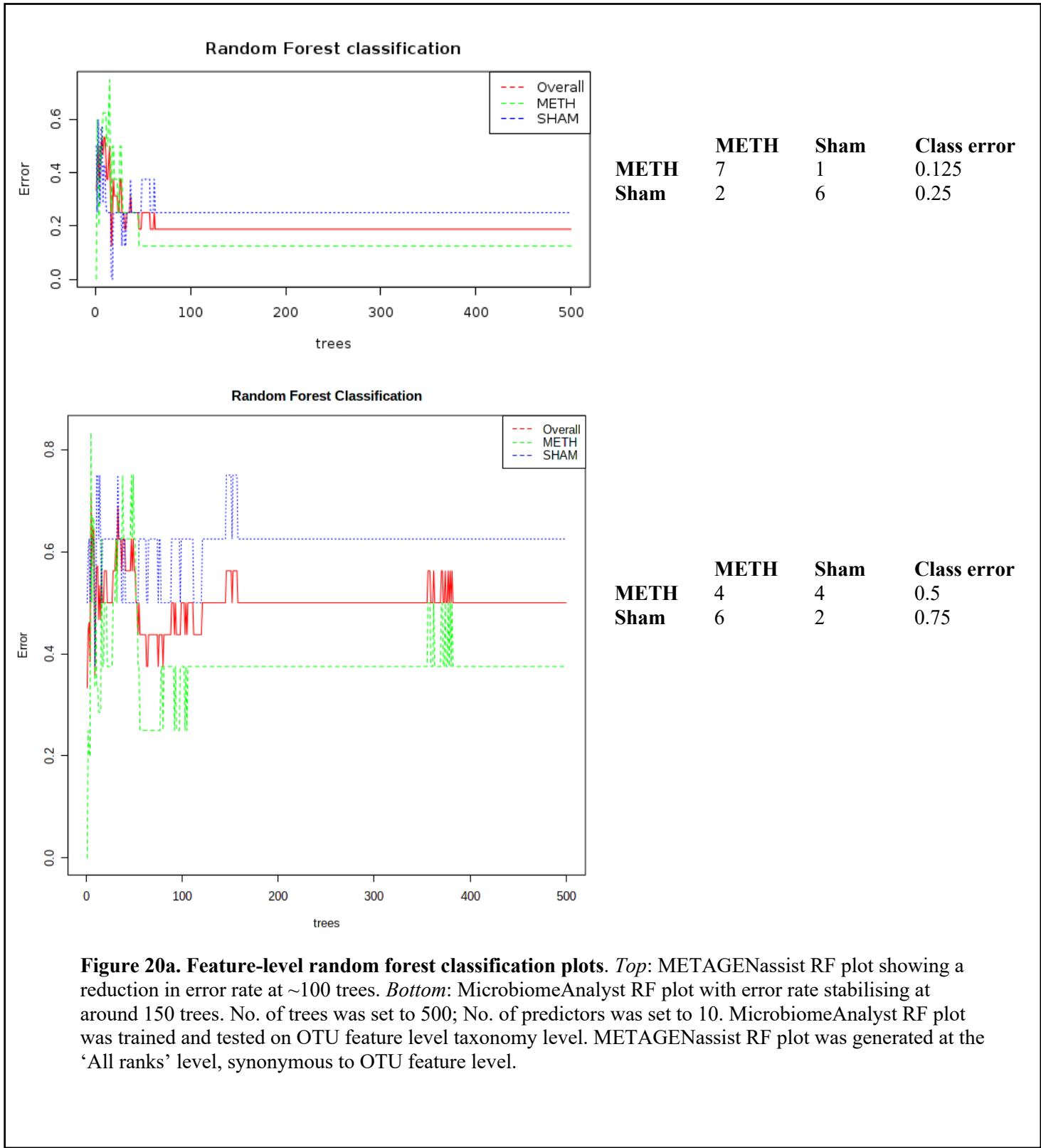


**Figure 20a. Feature-level random forest classification plots.** *Top:* METAGENassist RF plot showing a reduction in error rate at ~100 trees. *Bottom:* MicrobiomeAnalyst RF plot with error rate stabilising at around 150 trees. No. of trees was set to 500; No. of predictors was set to 10. MicrobiomeAnalyst RF plot was trained and tested on OTU feature level taxonomy level. METAGENassist RF plot was generated at the 'All ranks' level, synonymous to OTU feature level.

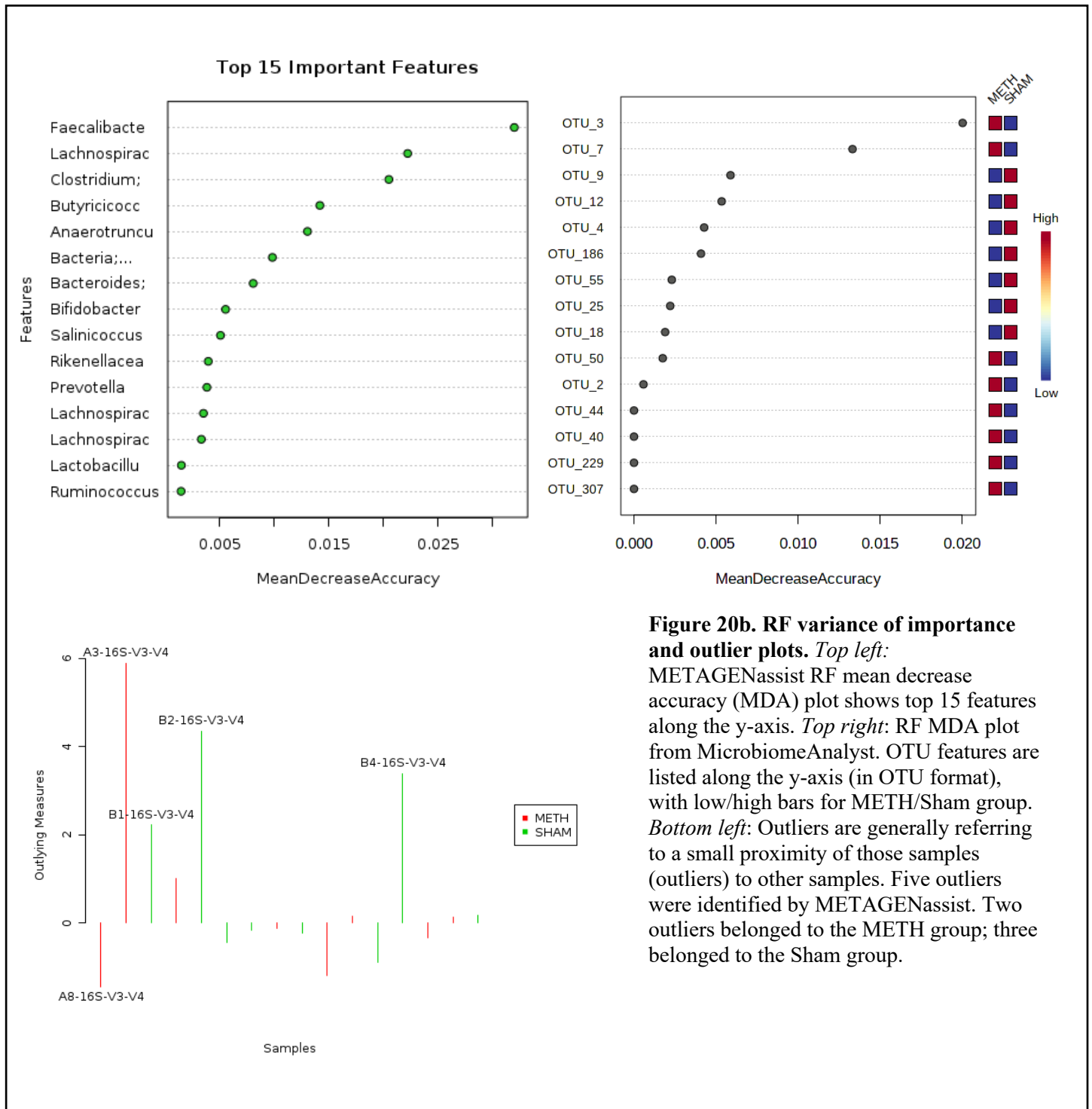


**Figure 20b. RF variance of importance and outlier plots.** *Top left:* METAGENassist RF mean decrease accuracy (MDA) plot shows top 15 features along the y-axis. *Top right:* RF MDA plot from MicrobiomeAnalyst. OTU features are listed along the y-axis (in OTU format), with low/high bars for METH/Sham group. *Bottom left:* Outliers are generally referring to a small proximity of those samples (outliers) to other samples. Five outliers were identified by METAGENassist. Two outliers belonged to the METH group; three belonged to the Sham group.

### **3.9 Heatmap visualisation and pattern search reveals taxonomic differences between METH and Sham groups.**

As a complement to dendrogram analysis, heatmaps were constructed using both METAGENassist and MicrobiomeAnalyst. Heat maps of Phylum, Genus and feature-level (OTU) were constructed and differences in abundances were visualised. From MicrobiomeAnalyst, the Bacteroidetes (Figure 21a) were more abundant in Sham samples B8, B3, B7, B6, B4 and B5. Similarly, METH samples A8, A3, A4 and A6 also showed higher abundances of Bacteroidetes. Only Sham sample B7 showed higher abundance of Cyanobacteria and Proteobacteria. All heat maps in MicrobiomeAnalyst were constructed by experimental factor (samples arranged in groups: METH vs. Sham). Heat maps constructed in METAGENassist used Pearson and Spearman distance measures, along with several clustering algorithms (Figure 21b, 21c). Comparisons were made between each distance and clustering method. In general, heatmaps tended to cluster the Sham samples (B1, B3, B5, B6 and B7) across all clustering algorithms (average, complete, single and Ward). For both Spearman and Pearson distance measures, a similar pattern was observed for Sham and METH samples; wherein predominantly two and clusters were generated across all four clustering algorithms. Sham sample B6, B7, B1, B5 and B3 were mainly clustered together, whereas METH samples A1 and A3; A5, A8 and A4 clustered together in the Spearman distance measure, across all four clustering algorithms. With Pearson distancing, METH samples A2 and A3 were clustered across the average, complete, and single clustering methods. Assessing both heatmap and pie charts for abundance, and explanation for these clusters, both sample A1 and A3 contained very similar abundances of Akkermansia (54.2% and 53.6%, respectively), which might owe to their clustering.

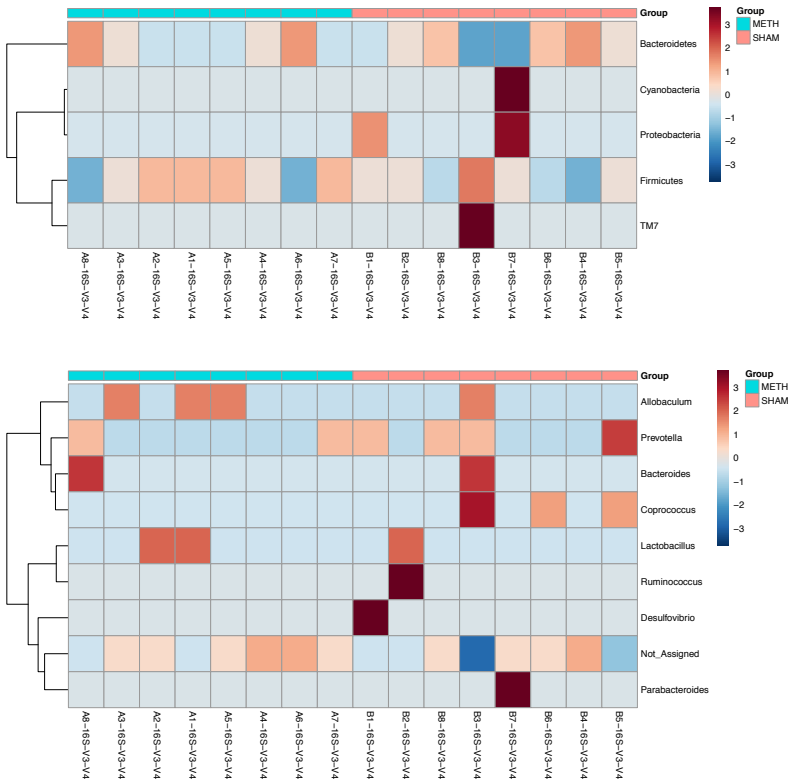


**Figure 21a. Heatmaps representation of taxonomic level abundance and clusters.** Phylum level (top) and Genus (bottom) heat maps indicate abundance variability across METH and Sham groups. Prevotella bacteria was markedly abundant in some Sham samples (B1, B3, B8 and B5); Allobaculum was more abundant in some METH samples (A3, A1 and A5).

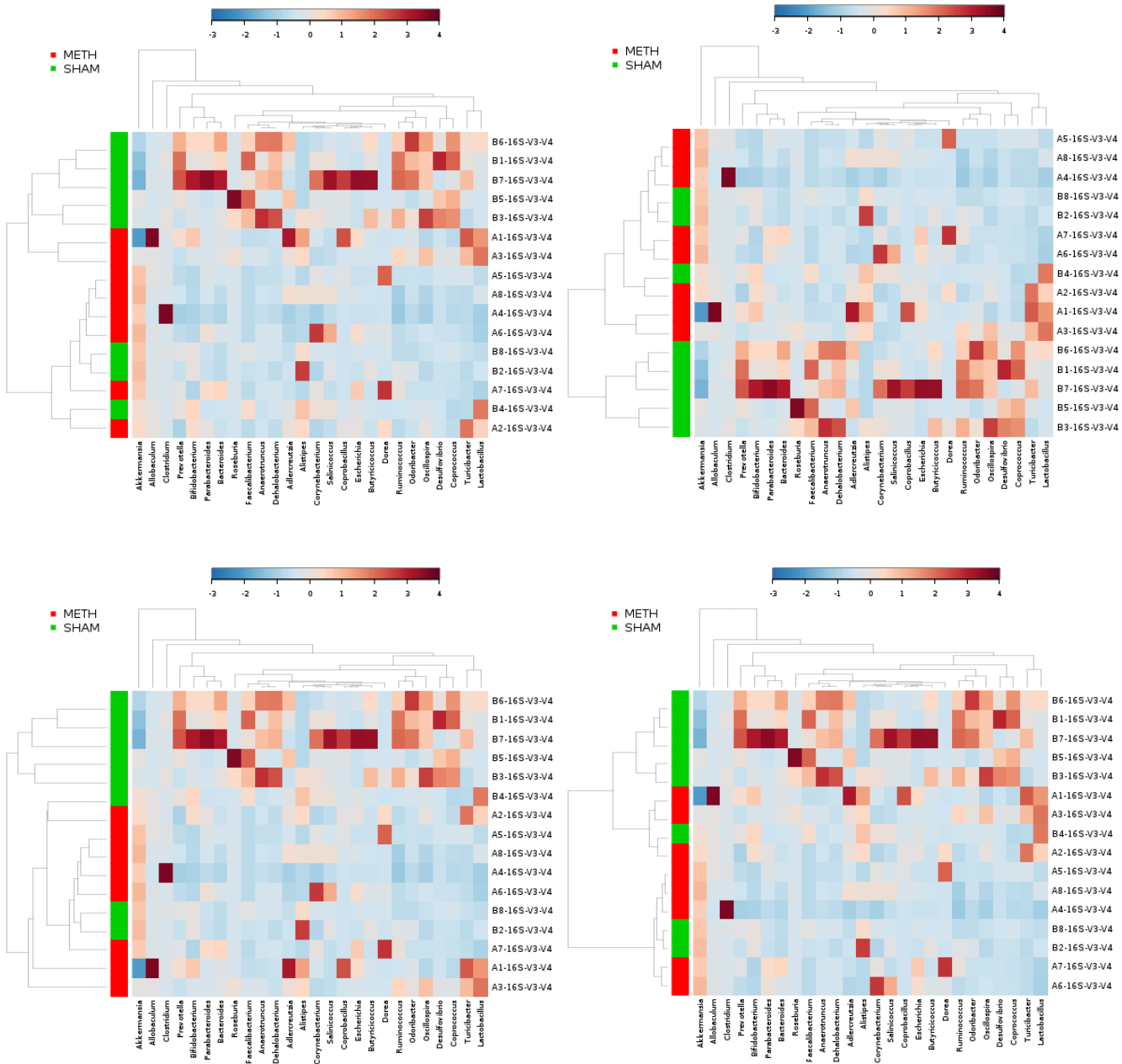


**Figure 21b. Spearman heat map visualisation of sample group clustering.** *Top row:* Spearman distance measure using average (left), and complete (right) clustering methods. *Bottom row:* single (left) and Ward (right) clustering methods.



### 3.10 Functional metabolic phenotype analysis of METH and Sham diversity

METAGENassist's Taxonomic-to-phenotype mapping method matches the input taxonomic data (OTUs), with its inbuilt phenotype database. Mapping is carried out via the use of a unique microbial phenotype database covering over 11,000 species, with 20 phenotype categories covered in each microbe. The advantage of this phenotype mapping is to examine bacteria across samples across variables such as preferred temperature range, and metabolism, in addition to comparing samples based on taxonomic distance. Moreover, this phenotype mapping tool is integrated into PCA and other clustering/classification plots, making data visualisation possible. Majority of metabolism phenotype bacteria (at Genus level) between METH and Sham groups were ammonia oxidizers, dehalogenation, nitrite reducers, sulfate reducers, and sulphide oxidizers (Figure 22). Univariate and multivariate statistical methods from METAGENassist software was used to calculate a number of tests in order to assess metabolic phenotype across both METH and Sham groups. Parametric (t-test), and non-parametric (Mann-Whitney test) was calculated for the significance ( $p < 0.05$ ) of metabolic phenotypes (Figure 23a, 23b). T-test (parametric testing) found three significant features (metabolic processes): cellulose degrader ( $p = 6.7 \times 10^{-3}$ ), sulphide oxidizer ( $p = 9.5 \times 10^{-3}$ ), and nitrogen fixation ( $p = 4.3 \times 10^{-2}$ ). Normalised abundance box plots revealed a higher abundance of cellulose degrader microbes in Sham compared to METH groups. Further, Sham group also had a higher normalised abundance of sulphide oxidizers, and nitrogen fixation microbes compared to METH group (Figure 23a). False discovery rates (FDRs), also commonly known as the error rate, is the proportion of the number of false (null) positives [Vidgen et al., 2016]. FDR values for p-value significant metabolic phenotype categories were cellulose degrader ( $FDR = 0.066$ ), sulphide oxidizer ( $FDR = 0.066$ ), and nitrogen fixation ( $FDR = 0.182$ ). For non-parametric methods, the Mann-Whitney – also known as the Wilcoxon rank-sum test – ignores group variance and can be referred to as the non-parametric equivalent of

the t-test. Metabolic phenotype categories for the Mann-Whitney non-parametric measure revealed the exact three categories as described by the student's t-test (Figure 23b). However, sulphide oxidizer was weighted with a higher significance ( $p=6.9 \times 10^3$ ) compared to cellulose degrader ( $p=1.5 \times 10^2$ ), and nitrogen fixation ( $p=3.8 \times 10^2$ ). Moreover, FDR scores for all three were slightly different than those derived from the parametric t-test, with sulphide oxidizer ( $FDR=0.09$ ), and cellulose degrader ( $FDR=1.10$ ), being higher, and nitrogen fixation (0.177) being lower than FDR calculated from the parametric t-test. Fold-change (FC) plots from METAGENassist highlighted the absolute value change between METH and Sham groups and calculates FC the ratio between both groups means using the data as it were prior to column-wise normalisation. Next, FC values are log transformed to induce symmetry of up- and down-regulated features (metabolic phenotype categories). Fold changes of metabolic phenotype found five significantly up- and down-regulated categories. Below 2-fold metabolic categories included – degrades aromatic hydrocarbons ( $\log_2(FC)=-3.24$ ), cellulose degrader ( $\log_2(FC)=-2.94$ ), and nitrogen fixation ( $\log_2(FC)=-2.65$ ). Non-significant FC categories were chitin degradation ( $\log_2(FC)=+1.76$ ), and sulphide oxidizer ( $\log_2(FC)=-1.51$ ).

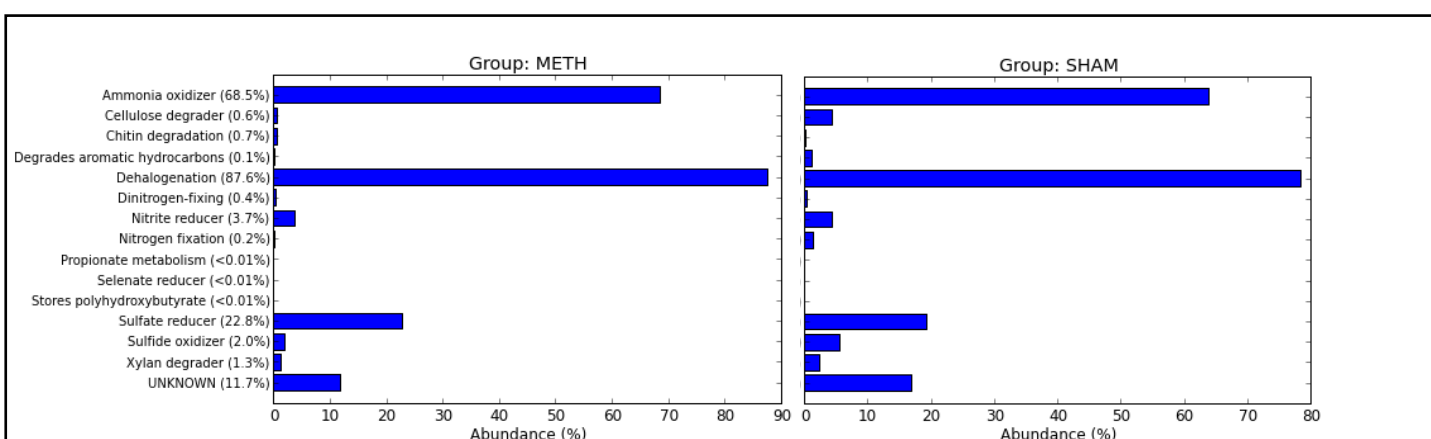


**Figure 22. METH and Sham metabolic phenotype profile of abundant bacteria.** Major metabolic phenotypes belonging to mapped taxa communities across METH and Sham samples included Ammonia oxidizers, Dehalogenation, Nitrite reducers, sulfate reducers, sulphide oxidizers, with a proportion of unknown. Sham samples showed a much higher proportion of cellulose degrader and Xylan degrader phenotype.

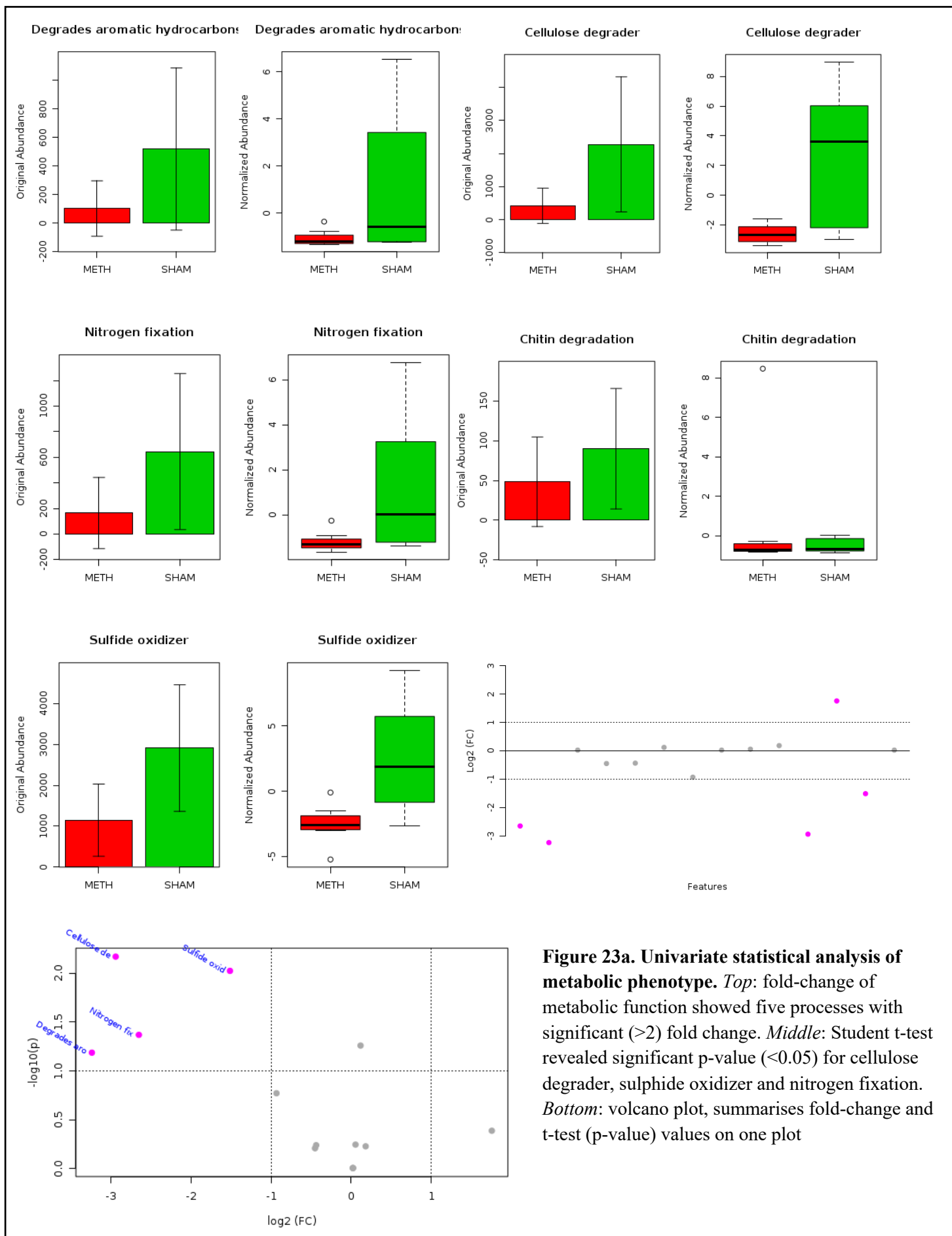


**Figure 23a. Univariate statistical analysis of metabolic phenotype.** *Top:* fold-change of metabolic function showed five processes with significant ( $>2$ ) fold change. *Middle:* Student t-test revealed significant p-value ( $<0.05$ ) for cellulose degrader, sulphide oxidizer and nitrogen fixation. *Bottom:* volcano plot, summarises fold-change and t-test (p-value) values on one plot

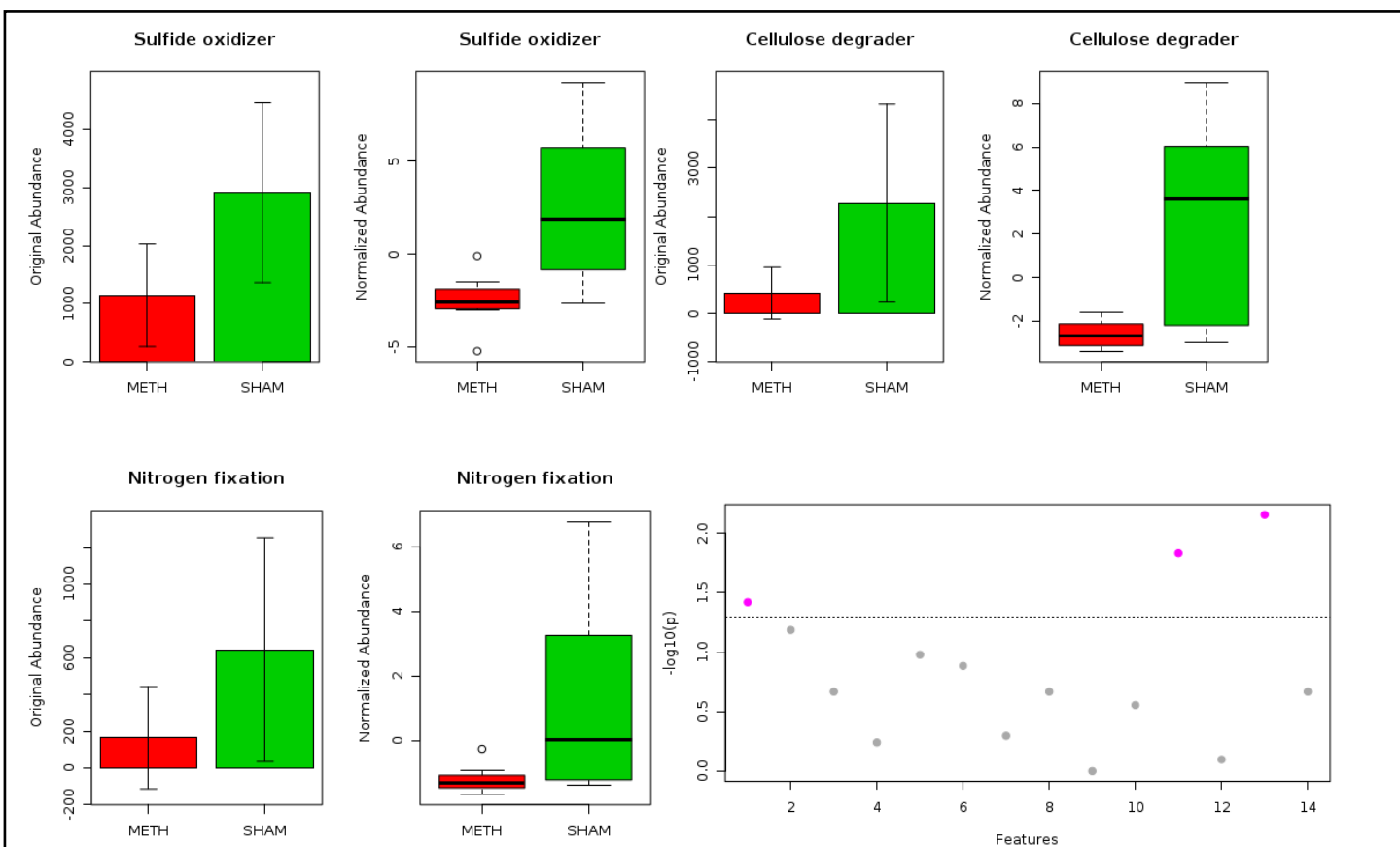
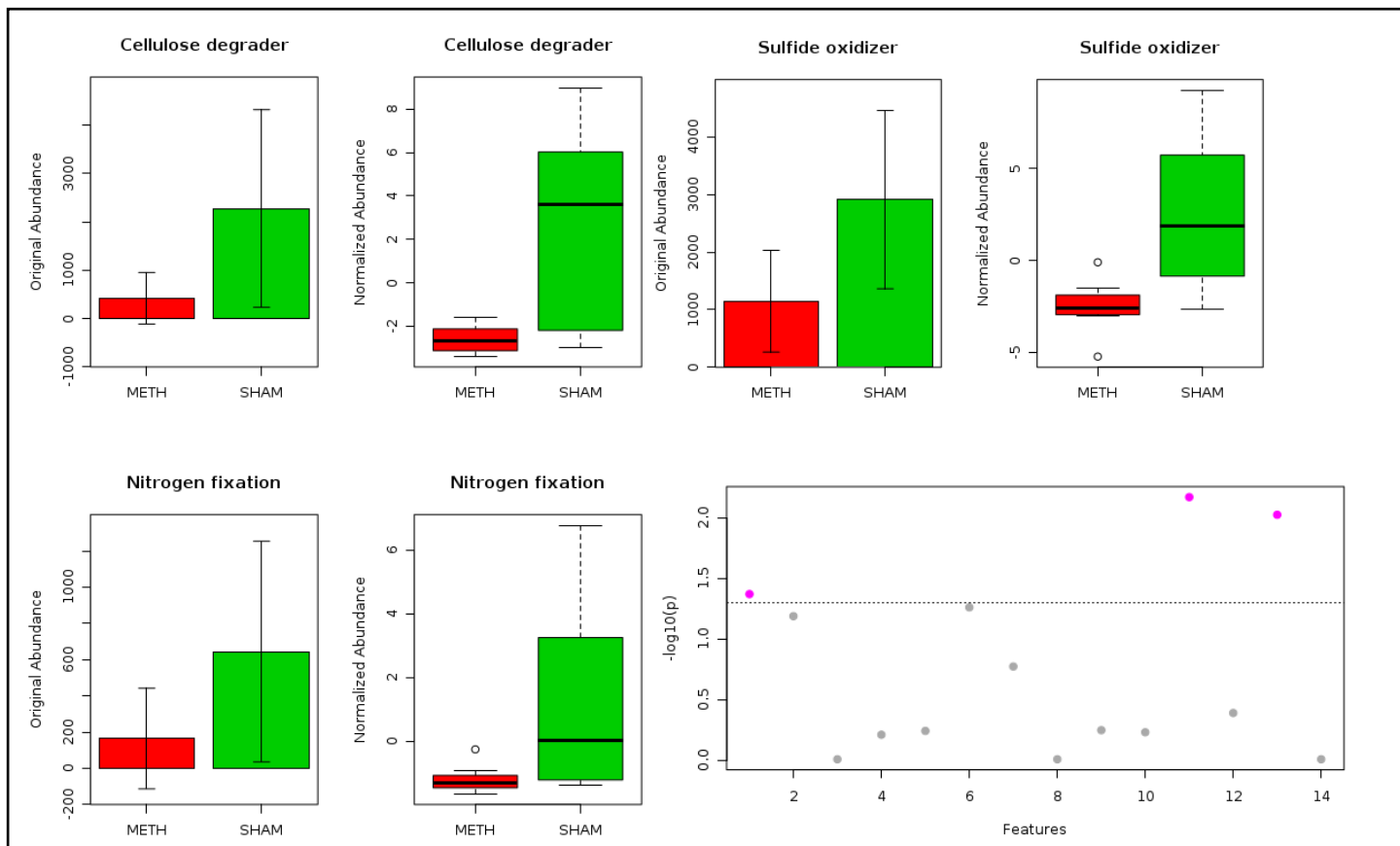
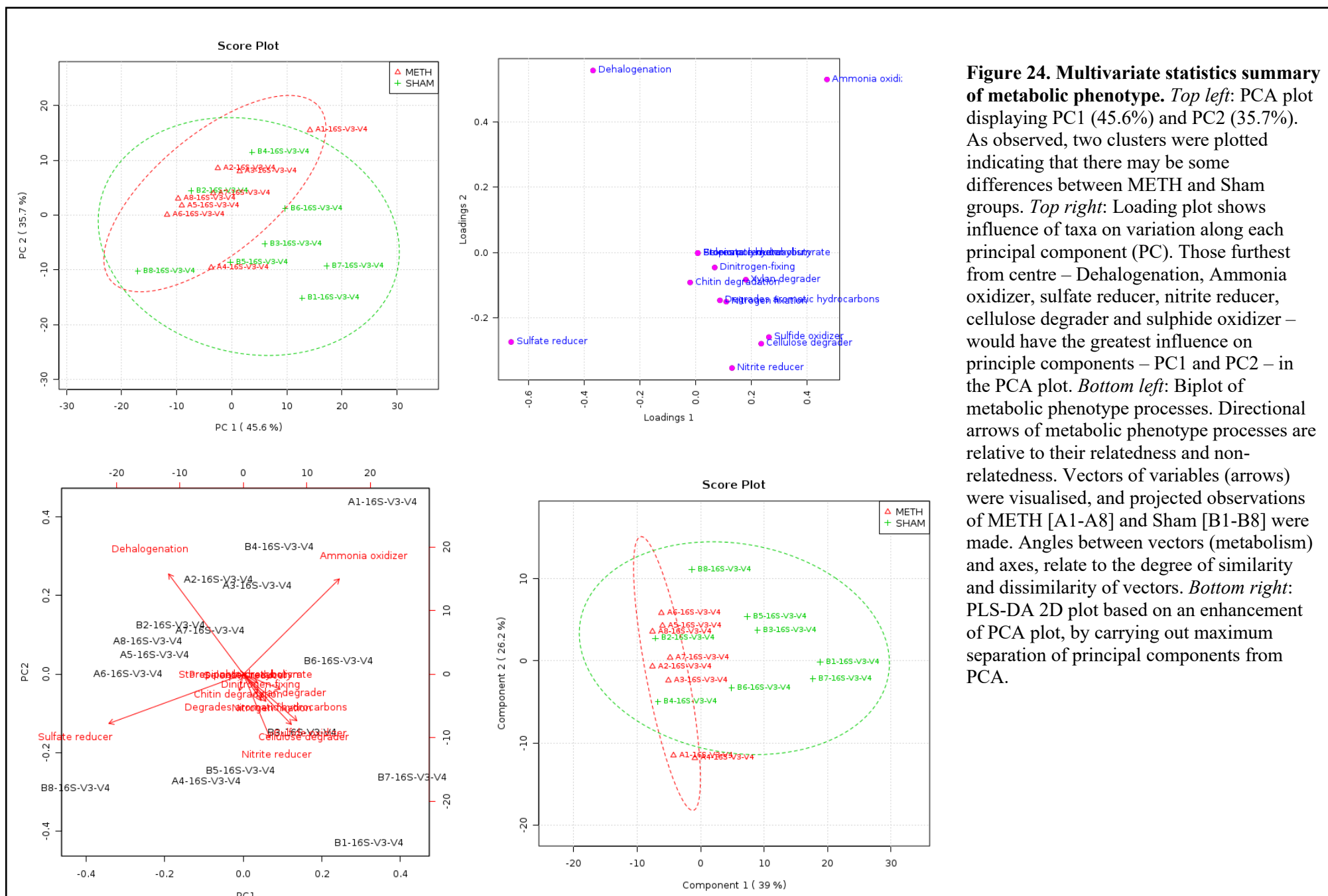


**Figure 23b. Loading score boxplots for metabolic phenotype categories.** *Top box:* Cellulose degrader, sulphide oxidizer, and nitrogen fixation boxplots, computed from parametric test (t-test). *Bottom box:* Wilcoxon rank-sum test plot (pink dots represent significant fold-change metabolic feature categories) and loading boxplots.  $p < 0.05$ .

PCA and PLS-DA plots were analysed based on loading scores across several metabolic phenotypes. Loading plot and biplot analysis was carried out for visualisation of most influential features (metabolic phenotypes) that could explain variation along each principal component axis (Figure 24). PCA loadings scores were also included to map the influence of metabolic phenotype and their contribution to principal components on PCA plots. Results indicated that dehalogenation, ammonia oxidizers, sulfate reducers, nitrite reducers, cellulose degraders and sulphide oxidizers contributed and influenced the most to principal components shown in the PCA, PLS-DA and biplots (Figure 24). Biplot of metabolic phenotypes showed several clusters of METH and Sham samples grouped according to metabolic phenotype principal components. Directional arrows in biplots, as found in this biplot, are related to the degree of relatedness and unrelatedness. METH samples seemed to be clustered between sulfate reducers and dehalogenators; whereas Sham samples tended to be scattered about the biplot with relatedness to most of the major metabolic phenotype categories. Shams samples B8, for example, was highly correlated to the sulfate reducer group, and B5 closely related to nitrate reducers. Overall, four main directional arrows representing dehalogenation, sulfate reducers, ammonia oxidizers, and nitrite reducers – with minor influences from sulphide oxidizers and cellulose degraders - confirmed loading plot results, and these metabolic phenotypes explained the majority variance observed across all METH and Sham microbial communities.



In addition to PLS-DA, other features that test accuracy and importance, including cross validation, and variable importance in projection (VIP). For importance measures, two methods are incorporated by METAGENassist. The first is VIP score; the second is coefficient score, which is the weighted sum of absolute regression coefficients. VIP scores of this study, with focus on metabolic phenotype categories and their influence on METH and Sham groups, found VIP scores  $>2$  with dehalogenation; and  $<2$  VIP scores associated with cellulose degrader, sulphide oxidiser and nitrogen fixation (Table 8). Cross-validation PLS-DA plots were generated for selection based on accuracy,  $Q^2$ , and  $R^2$  (Figure 25).  $R^2$ ,  $Q^2$  and accuracy for metabolic phenotype was calculated across five components (Table 7).  $R^2$  values relate to the predictive power of the model, and values between 0.67 and 0.19 indicate a strong-to-weak  $R^2$  values.  $R^2$  (coefficient of determination) was calculated as 0.381 (C1), 0.449 (C2), 0.476 (C3), 0.532 (C4), and 0.724 (C5). Traditionally,  $R^2$  values range between 0 and 1, with 1 representing highly confident predictive accuracy [Hair et al., 2014].  $Q^2$  values are used to evaluate the predictive relevance of the PLS-DA model, with  $Q^2$  values greater than 0 ( $Q^2 > 0$ ) deemed as predictively relevant [Peng et al., 2012]. In this study,  $Q^2$  values varied from 0.017 (C1), to -0.139 (C5) (Table 7).

**Table 7. Cross validation of metabolic phenotype (LOOCV).** Leave-one-out (LOOCV);  $R^2$ ,  $Q^2$  and accuracy for metabolic phenotype was calculated across five components

	<b>C1</b>	<b>C2</b>	<b>C3</b>	<b>C4</b>	<b>C5</b>
<b>Accuracy</b>	0.495	0.496	0.503	0.487	0.533
<b>R<sup>2</sup></b>	0.381	0.449	0.476	0.532	0.724
<b>Q<sup>2</sup></b>	0.017	0.013	-0.013	0.050	-0.139

**Table 8. VIP scores of PLS-DA across five components.** VIP scores for metabolic phenotype categories as computed by METAGENassist.

<b>Metabolic phenotype category</b>	<b>C1</b>	<b>C2</b>	<b>C3</b>	<b>C4</b>
Dehalogenation	2.074	1.981	1.935	1.831
Cellulose degrader	1.836	1.732	1.691	1.606
Sulfide oxidizer	1.764	1.647	1.608	1.525
Nitrogen fixation	0.839	0.777	0.755	0.7333

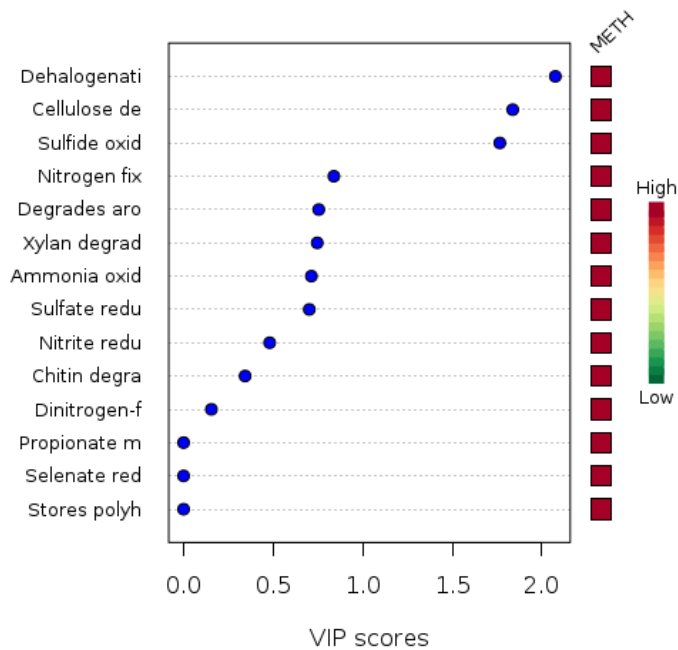
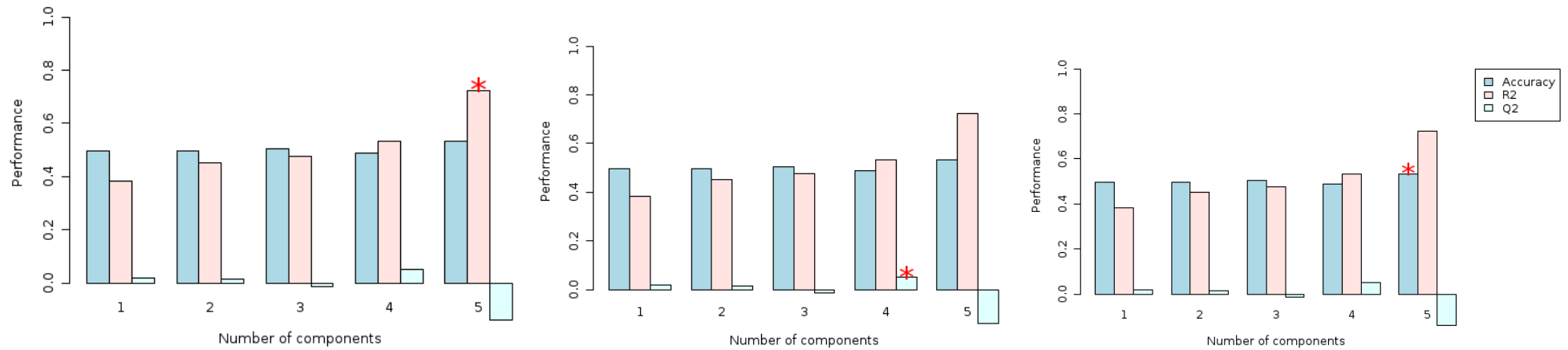


**Figure 25. PLS-DA model measures of accuracy and importance.** *Top left:* Cross validation plot of performance vs. no. of components. Five components (default) were selected. Cross validation method chosen was LOOC (leave one out). R2, Q2 and Accuracy scores were recorded across five components.

*Bottom left:* VIP plot. Top components (metabolic phenotypes) are plotted as determined by cross validation. *Bottom right:* weighted sum of PLS-regression coefficients. In both VIP and coeff. Scores, blue dots represent most significant feature/measure (metabolic phenotypes across OTUs).

## 4.0 Discussion

Metagenomics is a valuable tool that assists in describing and understanding the human gut microbiome [Wang et al., 2015]. Besides its function in producing enzymes to help break down food, the gut microbiome also helps in the development of the host immune system [Martin et al., 2018], along with serving functions in the gut epithelium and brain [Barko et al., 2018]. The most abundant, and therefore dominant phyla are the Firmicutes and Bacteroidetes species [Costea et al., 2018], which make up around 92% of the human microbiome [Shi et al., 2017]. The density of bacteria in the gastrointestinal tract (GI) is between  $10^{13}$ - $10^{14}$  cells per gram faecal matter, and 70% of total microorganisms reside in the colon [Wang et al., 2015]. In the colon, dense, highly anaerobic microbes exist [Sundin et al., 2017]. Diet and age are two factors which can influence the gut microbiota, along with stress, geography and drug intake [Noble et al., 2017; Kostic et al., 2014]. Importantly, understanding the gut microbiota ecosystem, in an unperturbed and perturbed state can help us understand the role of factors that may be associated with changes in gut composition and how this might impact human health [Costea et al., 2018]. Thus, the importance of investigating changes in microbial populations in the colon in a chronic drug model are crucial to adding new knowledge on the growing gut microbiome research and this might be related to drugs of abuse. Moreover, since diet, and dietary patterns, is one key factor in the development of a healthy gut microbiome, substance abuse with drugs such as METH may help in identifying how possible changes in the gut can influence the brain [Galland, 2014]. In this regard, the gut-brain axis (GBA), how microorganisms affect brain functioning, has yet to be fully clarified

[Wang et al., 2016]. However, gut microbiota impacts the brain through not only the nervous system, but also via the endocrine, immune and metabolic systems [Wang et al., 2016]. Interestingly, changes in how the gut and brain interact are believed to play a role in several brain disorders that alter mood and can cause Parkinson's disease [Martin et al., 2018], along with causing stress-related behaviours such as anxiety and depression [Bear et al., 2020; Logsdon et al., 2018]. Of equal relevance, gut microbes can reprogram immune cells, promote cytokine secretion and may even shift across the blood brain barrier (BBB) [Logsdon et al., 2018].

This work utilised a bioinformatics pipeline to classify bacterial community diversity, and microbial composition, in a chronic METH mouse model (Figure 3). Samples were taken across two conditions: mice exposed to a chronic METH dose, following a withdrawal period, and control mice (Sham). Sequencing and filtering of 16S data was performed on the Illumina platform, with cleaning steps to remove duplicate, and redundant reads. A series of pipelines were incorporated from METAGENassist, MicrobiomeAnalyst and MG-RAST (Figure 4, 5, 8) which allowed for metadata upload, sequence cleaning and normalisation and/or rarefaction (Figure 7, 9, 10) followed by graphical and statistical analyses. The choice of METAGENassist, MicrobiomeAnalyst and MG-RAST was chosen for both their user-friendly graphical interface, and also their ability to provide univariate and multivariate ordination analysis on metagenomic data. Many of the tools that are necessary for analysing abundance across OTU data are native to both METAGENassist, and MicrobiomeAnalyst, including composition, sequence quality, functional

analysis based on bacterial phenotype, and statistical inferences. Heat maps, principal coordinate analysis (PCoA), rarefaction and phylogenetic trees are features of both METAGENassist, MicrobiomeAnalyst and MG-RAST. MG-RAST and Galaxy (Table 6; Figure 4, 5) provide a complementary cleaning and analysis pipeline that allows for visual sequence analysis in the form of summary statistics (Figure 11a, 11b, 11c). Accurate data is required for all downstream statistical analysis with metagenomic data. Raw reads obtained from NGS Illumina sequencing can be further analysed in pre-processing steps, to check for adaptor presence, low quality nucleotides and GC content [Zhang et al., 2014]. MG-RAST allows raw sequences to be uploaded, and assessments of sequence quality along with visual representations [Keegan et al., 2016]. In this work, MG-RAST was used to process raw fastq raw reads, with subsequent Galaxy web application (Figure 5). This was done to ensure and confirm reads quality, prior to further ordination analysis. It was found that, upon pre-processing in MG-RAST, Galaxy application showed a good quality of reads across the sequence reads, with total sequence calculated as 215, 490. Galaxy allows for both exploratory and pipeline analysis of large datasets [Afgan et al., 2018]. Moreover, per sequence quality scores and adaptor content all passed quality checks as performed by the Galaxy web application (Figure 11a, 11b, 11c).

## **Distinct abundance differences exist between METH and Sham microbial communities**

Several microbial abundance fluctuations were observed in both the phylum and genus levels. In particular, the METH group was found to contain a lower abundance of Firmicutes (Figure 12a), and Verrucomicrobia (phylum level); and also, higher abundances of, Akkermansia, Turibacter and Allobaculum. Interestingly, Burkholderia (genus level) was not present in the Sham group (Figure 12b), but only in the METH group. The genera bacteria, Burkholderia is an intestinal microbe, and is considered a regulate innate immune responses against bacterial infections [Lankelma et al., 2017]. The most dominant phyla in the human gut are the Firmicutes, Actinobacteria, Proteobacteria, Bacteroidetes, Fusobacteria and Verrucomicrobia [Rinninella et al., 2019]. An *in-silico* study investigating microbial tryptophan metabolism found an enrichment of tryptophan metabolism pathways across Clostridium, Burkholderia, Streptomyces, Pseudomonas and Bacillus genera [Kaur et al., 2019]. Within the Firmicutes, Verrucomicrobia, Actinobacteria, Bacteroidetes and Proteobacteria phylum exist several genus examples (Figure 12b). These genus level bacteria are also represented across all phylum groups in both METH and Sham groups and can explain the variation at both the phylum and genus levels. Furthermore, significant fold changes were associated to these major phylum and genus microbiota (Figure 13a) from METAGENassists unique fold-change and significance scoring metrics. In particular, Dorea and Allobaculum were significantly higher in METH compared to Sham (Figure 13b). Dorea belongs to the family Lachnospiraceae. In addition, Dorea has been

associated with intestinal permeability (IP) in alcohol dependence (AD), in which gut dysbiosis is also associated [Leclercq et al., 2014]. High gut permeability was also associated with a dramatic decrease in bacteria belonging to the Ruminococcaceae family, in favour of increased abundance of Dorea [Leclercq et al., 2014]. Similarly, this work shows that Dorea was significantly abundant (>3-fold) (Figure 13b), and those bacteria belonging to the Ruminococcaceae family, which in this study was a significant decrease of abundance of Faecalibacterium (<4-fold). Gut dysbiosis from chronic METH withdrawal might explain the radical shift in abundances of these bacteria, observed in METH samples. Moreover, at the genus level, Ruminococcus was found to be significantly ( $p < 0.05$ ) less abundant in METH compared with Sham group (Figure 13c). 14 bacteria were significantly down-regulated, 3 were significantly up-regulated, and 6 bacteria were both significant at the fold-change and p-value level (Figure 13a). Specifically, these constituted, Faecalibacterium, Dehalobacterium, Coprococcus, Anaerotruncus, Ruminococcus and Prevotella. All 6 bacteria groups were observably higher in the Sham group, and lower in the METH group. Interestingly, reductions of Faecalibacterium, which belong to the Firmicutes phylum and Ruminococcaceae family, has been associated with intestinal disorders in humans [Lopez-Siles et al., 2017], and serve as a biomarker for intestinal health [Miquel et al., 2016]. *F. prausnitzii*, an obligate anaerobe, are the main butyrate-producing bacteria in the colon and play a role in gut homeostasis [Maier et al., 2017; Xu et al., 2020], and has anti-inflammatory properties [Savin et al., 2019; Martin et al., 2015]. An apparent significantly low abundance in the METH group of Faecalibacterium could be due to a dysregulation in anti-inflammatory function,

caused by METH. Moreover, a sudden shift in low abundant Faecalibacterium in the METH group, with conversely high abundance in the control group could be one indicator of the influence of METH, and subsequent METH withdrawal being potentially attributed to intestinal disorders specific to the colon. Furthermore, the presence of Faecalibacterium species has been shown to influence and enhance tight junction formation [Maier et al., 2017]. Control group abundance of Faecalibacterium might correlate with this tight junction regulation, which might also explain a healthy, unperturbed gut Faecalibacterium composition. Lastly, Faecalibacterium showed the strongest p-value and fold-change significance compared to other significantly down-regulated bacteria, which might suggest its predominant importance and relevance in METHs impact on the gut and colon. Moreover, Butyricoccus, found to be <3-fold abundance in the METH group (Figure 13b), is also a butyrate-producing bacterium [Eeckhaut et al., 2016]. Ning et al (2017) found that a high METH dose increased Ruminococcacea taxa, which plays a role in METH's negative impacts on cognition [Ning et al., 2017]. Cook et al (2019), investigating the association of microbiome composition between METH and non-METH users, found a reduction in both Faecalibacterium and Butyricoccus genera [Cook et al., 2019]. Importantly, their study included both HIV-positive and HIV-negative METH users, and alterations in microbial composition and abundance was found to be independent of HIV status [Cook et al., 2019]. These results, based on a significant reduction of Butyricoccus genera, coincide with these earlier results, however, cannot be conclusively permitted due to differences attributed to the drug model (human vs. mouse) in question. Dehalobacterium are anaerobic, dichloromethane-utilising bacteria

[Chen et al., 2017; Michalovich et al., 2019], which were shown to be significantly low in abundance in the METH group. In previous work, lower abundance of Dehalobacteria in the colon was attributed to atherosclerosis [Chan et al., 2016]. Little is known regarding the association between Dehalobacteria and METH use. However, one postulation to this observation is that a lowering of Dehalobacterium abundance in chronic METH use might suggest a microbial component to atherosclerosis. Indeed, it has been shown that among a group of five colonic genera, Dehalobacteria played a role in protecting against atherosclerosis via a high-fat (HF) diet replacement with LGG or Telmisartan [Chan et al., 2016]. Moreover, the pathogenesis of atherosclerosis, induced by chronic METH, has recently been attributed to immune and inflammatory responses via pro-inflammatory cytokine production [Zhu et al., 2017]. In line with this, the current observation of a significant reduction of Dehalobacteria by METH could have an association with a lessening of protective capabilities to atherosclerosis pathogenesis, and/or be a pre-cursor to a vulnerability caused by a chronic METH pattern in this mouse model. One other significant finding to support the hypothesis of colonic microbial associations to atherosclerosis is the co-occurring low abundance of Roseburia and Oscillospira, which were significantly down-regulated (<2-fold) in METH faecal microbiota, compared with Sham. This finding is in line with Chan et al (2016) who also found a similar pattern of low-abundant Roseburia and Oscillospira genera. [Chan et al., 2016].

Prevotella, Coprococcus, Anaerotruncus, Ruminococcus, and Odoribacter genera were notably, and significantly lower ( $p < 0.05$ ) in the METH group, compared to control group (Figures 13b and 13c). In addition, MicrobiomeAnalyst, using the MetagenomeSeq algorithm, found significant abundances - between METH and Sham groups - of Parabacteroides (Figure 14), with a lower abundance observed in the METH group. Parabacteroides, which belong to the Tannerellaceae family, and are also grouped as one of many SCFA-producing bacteria [Du et al., 2020]. The anaerobic Coprococcus, like Faecalibacterium is also a butyrate-producing bacterium, as well as a propionate-producing bacterium that is Gram-positive, and produce short-chain fatty acids (SCFA) from the fermentation of dietary fibers [Caspani et al., 2019]. One explanation of the observed low abundance Coprococcus, as well as Faecalibacterium, is that METH may impact tight junctions indirectly through an inductive drop in butyrate metabolites via the loss of important genera such as Coprococcus and Faecalibacterium. Butyrate, as a SCFA, is important for proper maintenance of intestinal barrier integrity, and influences expression of tight junction proteins [Kelly et al., 2015]. Furthermore, butyrate also functions as a neuro-hormonal signalling molecule, and is also produced by Clostridium, Roseburia, Bacteroides and Prevotella [Kelly et al., 2015]; and the majority of butyrate is utilised as an energy source by the colonic epithelium [Liu et al., 2018]. In this work, Bacteroides, Roseburia, and Prevotella were significantly reduced in the METH group. Along with butyrate production, Roseburia also produces propionate and serotonin [Caspani et al., 2019]. Gut-produced propionate has also been shown to protect the blood-brain barrier (BBB) against oxidative stress [Kaur et al., 2019]. Importantly, SCFAs can influence gut

serotonin levels and also influence mood disorders [Silva et al., 2020], which Jiang et al (2015) were able to confirm that Bacteroidetes, Actinobacteria and Proteobacteria were significantly more abundant in a major depressive disorder (MDD) patient group, with increased levels of Alistipes and Enterobacteriaceae, and reduced levels of Faecalibacterium [Jiang et al., 2015]. Moreover, Ning et al (2017) measured propionate and butyric acid in the faecal matter of METH and control groups and found a significant reduction in abundance of both [propionate and butyric] SCFAs [Ning et al., 2017]. The role of these gut-derived SCFAs could have a key role in regulating stress and depressive-like symptoms, and this has been shown with SCFA supplementation, in which acetate, butyrate and propionate alleviated psychosocial stress-induction brought on by reward-seeking behaviour [van de Wouw et al., 2018]. Further work would need to assess the loss of SCFA-producing bacteria in a chronic METH dose group context, which might solidify the role METH might play in influencing (through significant reduction) SCFAs such as butyrate and propionate. Furthermore, the possible interactions and/or influence of high METH doses on SCFA-producing bacteria might also suggest a pathway leading to a reduction in the protective capacity of SCFAs to prevent oxidative stress in the BBB. Collectively, METH may be responsible for reducing these colon-residing bacteria, which could subsequently lead to a decrease in metabolites, such as butyrate, responsible for maintaining energy homeostasis, along with providing communication via the gut-brain axis. Furthermore, a reduction in colon/gut barrier integrity from a reduction in barrier-maintaining bacteria, via bacterial metabolic production, could be a feature of chronic METH use over time. Also, METH (at significantly high doses) could

contribute to what is known as the ‘leaky gut’ hypothesis and be a significant ‘stressor’ or ‘stimulant’ that causes low-grade inflammation across many organs by not only perturbing healthy concentrations of colon bacteria – *Prevotella*, *Faecalibacterium*, *Coprococcus* - but by action of lessening the maintenance capabilities of microbial metabolites and their cross-communication along the gut-brain axis. Microbiota-to-brain bi-directional communication requires a clear pathway that can communicate any changes in SCFA, along with other important molecules, which would influence endocrine, neuronal, and immune cell signalling across multiple organs, including the brain [Parker et al., 2020]. METH does indeed disturb the body’s immunity [Papageorgiou et al., 2019], and specific changes to several microbial signalling processes from a marked shift and disruption in abundances might explain aspects of mental health disorders commonly seen in chronic METH abuse patients. In addition, the effects of exogenous chronic drug exposure, such as that of METH, to the colonic microbial communities may cause radical modulation on gut microbial composition, along with metabolic activity [Wilson et al., 2017]. When describing the gut microbial-depression connection, lower abundances in Firmicutes, *Akkermansia*, *Ruminococcus*, *Prevotella* and also *Lactobacillus* has been linked to depression-like behaviour [Li et al., 2020]. This study found a much less abundance in *Prevotella* and *Ruminococcus* bacteria in the METH group, which does indeed coincide with this observation.

## **Richness and evenness of bacteria composition in the colon may be influenced by METH**

Alpha and beta diversity estimates showed an insignificant alpha diversity – measured by Chao1, ACE, Shannon and Simpson measure metrics – yet, a significant beta diversity (Figure 15a and 15b), between the METH and Sham samples. Traditionally, Chao1 and ACE alpha diversity methods measure bacteria species richness, and are both non-parametric methods. Richness refers to the number of taxa/genera that are observed in the sample's community, which ignores frequency, whereas evenness is associated with the distribution of taxa/genera frequencies in a sample community [Wagner et al., 2018]. Non-parametric methods rely on the assumption that a set of data observations are not normally distributed, and this assumption of unequal distribution has an implicit advantage that data rarely follow normal distributions [Vickers, 2005]. For this reason, OTU reads were normalised and scaled in both METAGENassist and MicrobiomeAnalyst (Figure 7 and 10). Moreover, Shannon and Simpson alpha diversity methods, both which investigate evenness in a given group of samples, were applied to both METH and Sham group samples. Chao1 estimator of alpha diversity found a greater diversity of microbial composition (Figure 15a) in METH samples. Further, ACE alpha diversity measure also revealed greater microbial diversity amongst the METH group compared to Sham samples (Figure 15a). Shannon and Simpson alpha diversity – which reflect taxa/genera/OTU evenness – revealed several differences in evenness across METH and Sham samples as visualised by constructed boxplots (Figure 15a and 15b). However, overall alpha diversity

was not significant to conclude statistically significant differences. Further, box-plot representations as constructed by MicrobiomeAnalyst do not represent significance. To further support statistical significance, the Mann-Whitney statistical calculation showed no significance in diversity and evenness. From alpha diversity results, it could be suggested that chronic METH does not cause a greater shift in diversity of bacteria in the colon, however, results from this alpha diversity cannot rule out that several reductions and increases of certain bacteria in the METH and Sham groups are not present and unique to each group. By observing earlier fold-change and p-value significance scores (Figure 13a, 13b, 13c), as carried out by METAGENassist, it can be seen that several fold-changes exist across microbial genera between METH and Sham groups. As alpha diversity indices provide significance (p-value) scoring to denote at least one group that follows a different distribution, in this case, METH vs. Sham, the alpha diversity measures applied here should not be equated to a lack of relevance at the OTU or genera level, and the association of this relevance to aspects of colon physiology such as alterations to tight junction proteins. Beta diversity was calculated using several beta diversity methods, including Bray-Curtis, Jensen-Shannon divergence, and Jaccard index (Figure 16a, 16b, 16c). Beta diversity's strength lies in its ability to indicate differences or alterations in microbial composition across samples that belong to a particular group [Schroeder et al., 2018]. Beta diversity measures the dissimilarity of microbial composition between samples and can be visualised via principal coordination analysis (PCoA) plots and is usually complemented with dendrograms and heatmaps. Bray-Curtis PCoA showed two distinct groups, based on this dissimilarity measure (Figure 16a). The Bray-Curtis is premised on proportion

of the number of species observed at one site (group), and not another site [Ferrier et al., 2007]. Moreover, ANOSIM R values for Bray-Curtis dissimilarity methods was calculated as 0.0718, indicating a lack of clear dissimilarity between METH and Sham groups. This was also confirmed by a non-significant p-value. Five Sham samples (Figure 16a: blue cluster) had the most dissimilarity to METH samples (Figure 16a: red cluster), however four Sham samples grouped into this METH cluster. This lack of complete dissimilarity of microbial composition in both groups might be explained by the similar abundances of major phyla between several of the Sham and METH samples and the influence of these samples to group clustering algorithms. Similar to Bray-Curtis beta diversity, Jensen-Shannon and Jaccard indices also clustered two distinct groups based on dissimilarity (Figure 16b, 16c), however no significance was observed between both clusters across all beta diversity methods. The goal of constructing PCoA plots is to transform high-dimensional data to a low-dimensional plot that can also preserve distances between points (samples) across the plot relating to sample dissimilarity. Across all beta diversity PCoA plots, a characteristic overlap could be observed of METH and Sham samples. Whilst a certain degree of dissimilarity of roughly half of the Sham (control) samples was shown, and majority METH samples formed one unique cluster, this overlap could possibly explain the distinct dissimilarity of both groups. To visualise these PCoA plots along a dendrogram (agglomerative hierarchical dendrogram), beta diversity methods – Bray-Curtis, Pearson, Spearman, Jensen-Shannon, and Jaccard methods - were incorporated with four well-known distance measures – average, complete, single and Ward – to map the relationship of METH and Sham samples (Figure 17a, 17b, 17c, 17d).

Overall, most METH samples formed a distinct cluster of similarity, while a consistent group of Sham samples also clustered across all dendrograms. In general, the agglomerative clustering approach starts with two objects (samples) and merges them based on the extent of their similarity [Forina et al., 2002]. This continues until distinct clusters can be visualised. Specifically, it was observed that although there was a separation of METH samples across the dendrograms, there was more similarity share between all of the METH samples; and, distinct clusters were built which pooled majority control samples to the Sham group. This was observed notably on the Pearson, Spearman, and Jensen-Shannon dendrograms (Figure 17a, 17b, 17c). Collectively, beta diversity indices, although not significantly distinct, were able to cluster many of the METH samples within the METH group, and two main dendrogram nodes were observed which could help explain the relative similarities and dissimilarities across the samples. Some of this failure to capture a statistically significant dissimilarity between both groups might be attributed to a lack of sampling depth within each group. Rarefaction is often used (Figure 7) to account and adjust for differences in library size which can help in building more robust alpha and beta diversity plots [Willis, 2019]. Microbiome data analysed in MicrobiomeAnalyst was first rarefied prior to alpha and beta diversity methods were applied. This permits a fair analysis of microbial data, that can contrast one ecosystem to another without discrepancies in sample sizes, as rarefaction adjusts for these sample size differences.

## **Multivariate analysis displayed distinct clusters in METH and Sham groups**

PCA is an unsupervised method which takes data from a high dimension and transforms this data into one of low dimensionality. In this work two distinct clusters were observed across the PCA plot (Figure 18a). In addition, over half (52%) of all principal components (PC) contributed to the variance observed in the PCA plot, with a second PC contributing just over 21% of variance. Loading plot and biplot confirmed the weight of influence given to several genera (Figure 18a) on both METH and Sham samples. Loading plot values are usually interpretable when values are closer to +1 and/or -1. Moreover, biplots can feature both aspects of a loading plot and score plot. In this regard, it was found that *Allobaculum*, *Akkermansia*, *Coprococcus*, *Prevotella*, *Desulfovibrio*, and *Lactobacillus*, seemed to have the most influence on the clustering of both METH and Sham groups. Bi-plot results can clearly explain the influence of *Prevotella*, *Coprococcus*, *Desulfovibrio* varibales on Sham samples. Whereas *Allobaculum*, *Akkermansia*, *Lactobacillus*, and *Turicibacter*, seemed to have the most influence in separating METH samples along the PCA plot. Two principal components were displayed for construction of all plots, since it was found that PC1 and PC2 could explain 52% and 21.3% of variance across the complexity of both METH and Sham samples. After PC2, PC3 could capture and explain ~9% of the variance from the original samples. For this reason, PC1 and PC2 captured the most microbial variance (Figure 18b). Loading scores bar chart (Figure 18c) confirmed loading plots (Figure 18a) with higher scores for *Allobaculum* and *Akkermansia*. K-means (unsupervised learning clustering)

[Qu et al., 2019] and self-organising maps (SOM) are two clustering methods that are a feature of METAGENassist. In this study, clustering across OTU (feature), Phylum and Genus levels was computed by METAGENassist, using two cluster numbers (Figure 19a). K-means computes clusters based on objects that are closer to the mean of a particular cluster [Ramette, 2007]. It was found that k-means clustered samples into two distinct groups (figure 19a), however there was variation in the number of samples per group across OTU, Phylum and Genus levels. Overall, k-means served as a reliable unsupervised method to group similar samples based on no *a priori* knowledge of groupings. SOM clustering, also an unsupervised neural network algorithm [Weber et al., 2010], also grouped similar Sham and METH samples into two distinct clusters (Figure 19b). Strongest clustering was found at the OTU level, with SOM clustering 6 out of 8 Sham samples, and all METH samples into their respective groups. In addition to k-means and SOM clustering, random forest (RF) classification constructs a series of trees based on random sampling of OTU reads, and this method also incorporates an out-of-bag (OOB) error which is calculated by the RF algorithm using a subset of observations to predict the error of RF. This OOB (generalisation) error can then be used to assess the predictive power/performance of the RF [Janitza et al., 2018]. Class error rate was greater in MicrobiomeAnalyst than RF class error rate computed by METAGENassist (Figure 20a). Further, METAGENassist was able to classify a greater number of METH samples belonging to the true METH group, along with Sham samples into its actual group. RF as carried out by MicrobiomeAnalyst did not perform as well as METAGENassist's RF algorithm (Figure 20a). Comparing both METAGENassist and MicrobiomeAnalyst, random forest (RF) classification

plots and variance of importance plots were constructed to visualise genera. It was found that the majority of OTU features were also consistent with those features with a significant representation in fold-change and significance testing. In addition, outliers across METH and Sham samples were also computed by the RF algorithm (Figure 20b). Sham samples B2 and B4 were calculated as outliers, and these two samples were also clustered together amongst the METH cluster according to both k-means and SOM clustering methods. This ‘outlier effect’ contributed by these samples might explain the apparent non-uniform clustering found in the agglomerative hierarchical clustering dendrograms. This consistency of clustering and classification from employing several algorithmic methods and applying them to METH and Sham samples provides some confidence that not only the clustering methods are reliable; but also, that there are indeed distinct differences in both groups. K-means, SOM and RF (reference-free unsupervised) machine learning methods of clustering and classification, are able to recognise, classify, and predict patterns in data that are without pre-defined labels [Zhou et al., 2019]. This is an incredibly powerful approach to recognise [unbiased] patterns of clustering and classification otherwise apparent in supervised machine learning techniques. Heatmaps at the phylum level showed two main clusters, with similar patterns of Firmicutes and Bacteroidetes across Sham and METH groups (Figure 21a). At the genus level, some consistency of certain taxa was observed, including a lack of Ruminococcus, Desulfovibrio, Bacteroides and Coprococcus (Figure 21a). Conversely, control samples contained more Prevotella and Coprococcus compared to METH group. Several METAGENassist heatmaps were generated using four clustering methods – average, complete, single and

Ward – and, Spearman (Figure 21b), and Pearson (Figure 21c), distance methods. Coinciding with dendrogram results, heatmaps according to Spearman distancing found higher concentrations of Prevotella, Bifobacterium, Parabacteroides, Roseburia, Faecalibacterium, Anaerotruncus, Dehalobacterium, Corynebacterium, Ruminococcus, Odoribacter, Oscillospira, Desulfovibrio, Coprococcus, and Turibacter, across all four clustering algorithms using the Spearman distance metric (Figure 21b). Similar patterns across the Pearson heatmaps (Figure 21c) were also observed. These results confirmed the fold-change, significance scoring, and box-plot representations of microbial abundances in both METH and Sham groups. Clearly, from these results, the majority of Sham samples had a different abundance profile to the METH group samples.

### **Metabolic phenotype of microbial diversity revealed differences in METH and Sham groups**

A strong feature of METAGENassist rests in its ability to apply a functional analysis to microbial abundance data. In addition, this provides further support to traditional clustering methods, and can also be linked with the construction of ordination plots, such as PCA, and parametric/non-parametric statistical measures. Overall, significant fold-changes ( $\pm 2$ -fold) were seen with degrades aromatic hydrocarbons, cellulose degrader and nitrogen fixation (Figure 22). Further, chitin degradation and sulphide oxidizer metabolic processes held non-significant fold-changes yet were significant according to the constructed

volcano plot (Figure 23a). Across all metabolic process categories, the METH group had lower abundances of cellulose degradation, aromatic hydrocarbon degradation, nitrogen fixation, chitin degradation, and sulphide oxidation metabolic categories, compared to control group (Figure 23a, 23b). Multivariate analysis, using PCA and PLS-DA score plots found that the majority of variance between microbial abundances were accounted for by a handful of metabolic phenotype categories (Figure 24). Biplot of metabolic phenotypes (Figure 24) revealed several clusters of METH and Sham samples that were grouped according to metabolic phenotype principal components. Directional arrows within the biplot is related to the degree of relatedness and unrelatedness. Therefore, METH samples seemed to be clustered between sulfate reducers and dehalogenators; whereas Sham samples tended to be scattered about the biplot with relatedness to the majority of the major metabolic phenotype categories. In the [human] colon, sulfate-reducing bacteria belong predominantly to the genus *Desulfovibrio* [Rey et al., 2013]. Moreover, *Desulfovibrio* bacteria are the most well-studied sulfate-reducing bacteria and is the most abundant in the human gut [Ran et al., 2019]. In this study, the METH group had a significantly lower abundance of *Desulfovibrio*

Measures of accuracy and importance from PLS-DA plots (Figure 24) were calculated for metabolic phenotype categories. PLS-DA modelling is based on a relationship between microbial data (OTU reads), and some categorical variable (metabolic phenotype), and this model is constructed in a manner that metabolic categories can be predicted for OTU reads per sample. The  $Q^2$  statistic is a PLS-DA default diagnostic statistic measure that validates the PLS-

DA model [Szymanska et al., 2012]. Furthermore,  $R^2$  (coefficient of determination) and  $Q^2$  (cross-validation redundancy) values of the metabolic phenotype categories (class membership) and their relationship to the original variables were found to be strong ( $R^2 = 0.724$  (C5)), however, as a  $Q^2$  value greater than 0 ( $Q^2 > 0$ ) deemed as predictively relevant [Peng et al., 2012],  $Q^2$  – its application to the metabolic phenotype – was much lower than 0, with a reading of  $-0.139$  (C5) (Table 7). This suggested that although the PLS-DA model ( $R^2$ ) could predict the metabolic phenotype functional categories with good accuracy, the corresponding  $Q^2$  at C5 did not perform well with this model. One measure, the VIP score, assesses the importance of a variable by summarising the contribution that a particular variable has on the overall model. For this PLS-DA VIP score plot, it was observed that the most important metabolic phenotype categories were dehalogenators, cellulose degraders, and sulphide oxidisers (Figure 8). Overall, PLS-DA is a supervised method that is usually applied to microbial data to uncover any apparent microbial variation between groups, and can also be applied to functional group categories, such as metabolic phenotype of bacteria. In addition to PCA and PLS-DA multivariate ordination plots (Figure 25), VIP plots and scores were calculated to assess the contribution of each metabolism phenotype category. It was found that dehalogenators ( $VIP > 2$ ), cellulose degraders, sulphide oxidizers and nitrogen fixators ( $VIP < 2$ ) held the most significance for contributing to the variance observed across METH and Sham groups. (Figure 25; Table 8). This confirmed previous loading and biplot data which also found that METH and Sham groups seemed to be clustered towards these metabolic phenotype processes. Besides clustering and classification methods offered by METAGENassist and

MicrobiomeAnalyst, METAGENassist can offer a functional analysis of microbial datasets, which provides an additional layer of knowledge to traditional taxonomic clustering. From these results, it may be supportive that METH causes not only changes in microbial abundances in the colon, however that METH might also dampen or minimise several metabolic processes. PCA biplot confirmed that there was indeed a shift in metabolism phenotype between METH and control groups. Directional arrows assisted in this interpretation by the unrelatedness of opposite-directed arrows and their corresponding angle(s). Another postulation to this occurrence is that the majority of these metabolic processes - cellulose degradation, aromatic hydrocarbon degradation, nitrogen fixation, chitin degradation, and sulphide oxidation – belong to bacteria that were found to be in much lower abundances (as measured via fold-change and significance scores), in which METH may have a direct or indirect action on. One important consideration is related to understanding how these metabolic processes are required for normal gut function, in contrast to how perturbations in these metabolic processes, and subsequent shifts in homeostatic metabolism, could lead to greater downstream pathophysiology across multiple organs. In this respect, the metabolic potential of the gut/colon microbial communities can be partially explained by bacteria richness and diversity which correlates with proper metabolic function [Martin et al., 2019]. Moreover, gut bacteria can be profoundly influenced by diet, and xenobiotics [Guthrie et al., 2019]. The use of chronic METH, when applied to both a mouse model and human addict, constitutes as regular, and perhaps consistent/inconsistent dietary intake that the organism becomes habituated to encountering. From this chronic exposure, this then might lead to changes (over time) in gut microbial composition and

richness, which could shift the host towards particular immune characteristic(s) [Riedl et al., 2018]. This study indeed found changes in microbial abundance and differences in metabolic profiles between METH and control groups. Observing that microbial composition from mouse (METH) faecal samples had significant differences compared to normal, non-METH induced mice, METH might play a role in disturbing host energetics from this compositional/diversity/metabolic shift. Keeping in line with this hypothesis, METH can be perceived as a dietary component that reaches the distal colon, but where the parent compound is absorbed by in the upper gastrointestinal tract [Yip et al., 2015]; however, more evidence, and longitudinal studies would help unravel this possible connection. One popular area of current research is the effects of drugs on the gut-brain axis (GBA). Depending on the route of METH administration, along with dose exposure, perturbation of gut microbiota could have lasting effects on microbial composition which in turn may disrupt gut-brain communication. This disruption could be spear-headed by SCFA metabolite signals, immune system modulation and the enteric nervous system, which traverse and establish communications between the gut-brain. By considering the gut microbiota as an organ, that sits within the GI ecosystem, the role and influence of psychotropic drugs like METH on this component of a highly diverse ecosystem could assist in efforts to thoroughly unpack chronic, long-term METH addiction and its harmful effects on a range of systems and sub-systems that exist within the throughout gut microbes.

## Conclusion

Drugs of abuse, along with substance abuse disorders have been associated with a reduction in microbial diversity as well as modulation of metabolic processes. An increasing amount of interest in the effects of substances of abuse, such as METH, and gut health is beginning to unfold. Intertwined is the ongoing gut-brain axis theory which postulates that changes to gut microbiota can significantly impact the brain, leading to mood disorders such as depression. In this work, several significant alterations were observed across major and minor colon-residing bacteria. By applying supervised, and un-supervised ordination analysis to microbial populations in a chronic METH withdrawal mouse faecal group, in comparison to a control group, statistically significant alterations were observed between both treatment and control groups. Moreover, a clear difference in diversity, along with changes in metabolic phenotype, was also observed that may be attributed to by a chronic METH dose over an escalating model of administration. A lowering of colon microbial diversity may have dramatic impacts on health, and this could lead to dramatic and detrimental neurological events with lasting impacts for chronic METH users and those experiencing withdrawal. This study aimed to answer the question as to whether chronic METH causes changes to colon microbial diversity and composition. Major changes to several phyla and genus-level taxa, such as *Faecalibacterium*, *Dehalobacterium*, *Coprococcus*, *Anaerotruncus*, *Ruminococcus* and *Prevotella*. In addition, metabolism phenotypes: cellulose degradation, aromatic hydrocarbon degradation, nitrogen fixation, chitin degradation, and sulphide oxidation metabolic categories, were observably lower in the METH group. These results were confirmed with in-depth ordination analysis. Collectively,

chronic METH causes changes in abundance to not only particular microbes, but also shifts in microbial metabolism. This work represents a growing body of research with the objective of understanding how chronic METH impacts the gut microbial homeostasis, and how this might be linked to an impairment in brain function, in terms of memory, psychosis and long-term depression-like symptoms.

## References

- Afgan, E., Baker, D., Batut, B., van den Beek, M., Bouvier, D., Cech, M., Chilton, J., Clements, D., Coraor, N., Grüning, B. A., Guerler, A., Hillman-Jackson, J., Hiltemann, S., Jalili, V., Rasche, H., Soranzo, N., Goecks, J., Taylor, J., Nekrutenko, A., & Blankenberg, D. (2018). The Galaxy platform for accessible, reproducible and collaborative biomedical analyses: 2018 update. *Nucleic acids research*, 46(W1), W537–W544. <https://doi.org/10.1093/nar/gky379>
- Arndt, D., Xia, J., Liu, Y., Zhou, Y., Guo, A. C., Cruz, J. A., Snelnikov, I., Budwill, K., Nesbø, C. L., & Wishart, D. S. (2012). METAGENassist: a comprehensive web server for comparative metagenomics. *Nucleic acids research*, 40(Web Server issue), W88–W95. <https://doi.org/10.1093/nar/gks497> Arndt et al., 2012
- Barko, P. C., McMichael, M. A., Swanson, K. S., & Williams, D. A. (2018). The Gastrointestinal Microbiome: A Review. *Journal of veterinary internal medicine*, 32(1), 9–25. doi:10.1111/jvim.14875
- Bear, Tracey & Dalziel, Julie & Coad, Jane & Roy, Nicole & Butts, Christine & Gopal, Pramod. (2020). The Role of the Gut Microbiota in Dietary Interventions for Depression and Anxiety. *Advances in nutrition* (Bethesda, Md.). 11. 10.1093/advances/nmaa016.
- Caspani, G., Kennedy, S., Foster, J. A., & Swann, J. (2019). Gut microbial metabolites in depression: understanding the biochemical mechanisms. *Microbial*
- Chan, Y. K., Brar, M. S., Kirjavainen, P. V., Chen, Y., Peng, J., Li, D., Leung, F. C., & El-Nezami, H. (2016). High fat diet induced atherosclerosis is accompanied with low colonic bacterial diversity and altered abundances that correlates with plaque size, plasma A-FABP and cholesterol: a pilot study of high fat diet and its intervention with *Lactobacillus rhamnosus* GG (LGG) or telmisartan in ApoE<sup>-/-</sup> mice. *BMC microbiology*, 16(1), 264. <https://doi.org/10.1186/s12866-016-0883-4>
- Chen, G., Murdoch, R. W., Mack, E. E., Seger, E. S., & Löffler, F. E. (2017). Complete Genome Sequence of *Dehalobacterium formicoaceticum* Strain DMC, a Strictly Anaerobic Dichloromethane-Degrading Bacterium. *Genome announcements*, 5(37), e00897-17. <https://doi.org/10.1128/genomeA.00897-17>
- Chénard T, Prévost K, Dubé J, Massé E. Immune System Modulations by Products of the Gut Microbiota. *Vaccines (Basel)*. 2020;8(3):E461. Published 2020 Aug 21. doi:10.3390/vaccines8030461

- Chivero, E. T., Ahmad, R., Thangaraj, A., Periyasamy, P., Kumar, B., Kroeger, E., ... Buch, S. (2019). Cocaine Induces Inflammatory Gut Milieu by Compromising the Mucosal Barrier Integrity and Altering the Gut Microbiota Colonization. *Scientific reports*, 9(1), 12187. doi:10.1038/s41598-019-48428-
- Cook, Ryan & Fulcher, Jennifer & Tobin, Nicole & Li, Fan & Lee, David & Woodward, Cora & Javanbakht, Marjan & Brookmeyer, Ron & Shoptaw, Steve & Bolan, Robert & Aldrovandi, Grace & Gorbach, Pamina. (2019). Alterations to the Gastrointestinal Microbiome Associated with Methamphetamine Use among Young Men who have Sex with Men. *Scientific Reports*. 9. 10.1038/s41598-019-51142-8.
- Costea, P. I., Hildebrand, F., Arumugam, M., Bäckhed, F., Blaser, M. J., Bushman, F. D., ... Bork, P. (2018). Enterotypes in the landscape of gut microbial community composition. *Nature microbiology*, 3(1), 8–16. doi:10.1038/s41564-017-0072-8
- Courtney, K. E., & Ray, L. A. (2014). Methamphetamine: an update on epidemiology, pharmacology, clinical phenomenology, and treatment literature. *Drug and alcohol dependence*, 143, 11–21. doi:10.1016/j.drugalcdep.2014.08.003
- Dhariwal, A., Chong, J., Habib, S., King, I. L., Agellon, L. B., & Xia, J. (2017). MicrobiomeAnalyst: a web-based tool for comprehensive statistical, visual and meta-analysis of microbiome data. *Nucleic acids research*, 45(W1), W180–W188. <https://doi.org/10.1093/nar/gkx295>
- Du, X., Xiang, Y., Lou, F., Tu, P., Zhang, X., Hu, X., Lyu, W., & Xiao, Y. (2020). Microbial Community and Short-Chain Fatty Acid Mapping in the Intestinal Tract of Quail. *Animals : an open access journal from MDPI*, 10(6), 1006. <https://doi.org/10.3390/ani10061006>
- Dudhagara, P., Bhavsar, S., Bhagat, C., Ghelani, A., Bhatt, S., & Patel, R. (2015). Web Resources for Metagenomics Studies. *Genomics, proteomics & bioinformatics*, 13(5), 296–303. <https://doi.org/10.1016/j.gpb.2015.10.003>
- Eeckhaut, V., Wang, J., Van Parys, A., Haesebrouck, F., Joossens, M., Falony, G., Raes, J., Ducatelle, R., & Van Immerseel, F. (2016). The Probiotic *Butyrivibrio* *pullicaeorum* Reduces Feed Conversion and Protects from Potentially Harmful Intestinal Microorganisms and Necrotic Enteritis in Broilers. *Frontiers in microbiology*, 7, 1416. <https://doi.org/10.3389/fmicb.2016.01416>

- F. Hair Jr, J., Sarstedt, M., Hopkins, L. and G. Kuppelwieser, V. (2014), "Partial least squares structural equation modeling (PLS-SEM): An emerging tool in business research", *European Business Review*, Vol. 26 No. 2, pp. 106-121. <https://doi.org/10.1108/EBR-10-2013-0128>
- Ferrier, Simon & Manion, Glenn & Elith, Jane & Richardson, K.. (2006). Using generalised dissimilarity modelling to analyse and predict patterns of beta diversity in regional biodiversity assessment. *Diversity and Distributions*. 13. 252-264.
- Forina, Michele & Armanino, C & Raggio, V. (2002). Clustering with dendograms on interpretation variables. *Analytica Chimica Acta - ANAL CHIM ACTA*. 454. 13-19. 10.1016/S0003-2670(01)01517-3.
- Galland L. (2014). The gut microbiome and the brain. *Journal of medicinal food*, 17(12), 1261–1272. <https://doi.org/10.1089/jmf.2014.7000>
- Garrido-Cardenas JA, Manzano-Agugliaro F. The metagenomics worldwide research. *Curr Genet*. 2017;63(5):819-829. doi:10.1007/s00294-017-0693-8
- Ghurye, J. S., Cepeda-Espinoza, V., & Pop, M. (2016). Metagenomic Assembly: Overview, Challenges and Applications. *The Yale journal of biology and medicine*, 89(3), 353–362.
- Guthrie, L., Wolfson, S., & Kelly, L. (2019). The human gut chemical landscape predicts microbe-mediated biotransformation of foods and drugs. *eLife*, 8, e42866. <https://doi.org/10.7554/eLife.42866>
- Hart, C. L., Marvin, C. B., Silver, R., & Smith, E. E. (2012). Is cognitive functioning impaired in methamphetamine users? A critical review. *Neuropsychopharmacology : official publication of the American College of Neuropsychopharmacology*, 37(3), 586–608. doi:10.1038/npp.2011.276
- Huang, X., Chen, Y. Y., Shen, Y., Cao, X., Li, A., Liu, Q., ... Yuan, T. F. (2017). Methamphetamine abuse impairs motor cortical plasticity and function. *Molecular psychiatry*, 22(9), 1274–1281. doi:10.1038/mp.2017.143
- Janitza S, Hornung R. On the overestimation of random forest's out-of-bag error. *PLoS One*. 2018;13(8):e0201904. Published 2018 Aug 6. doi:10.1371/journal.pone.0201904
- Jiang H, Ling Z, Zhang Y, et al. Altered fecal microbiota composition in patients with major depressive disorder. *Brain Behav Immun*. 2015;48:186-194. doi:10.1016/j.bbi.2015.03.016

- Kaur, H., Bose, C., & Mande, S. S. (2019). Tryptophan Metabolism by Gut Microbiome and Gut-Brain-Axis: An in silico Analysis. *Frontiers in neuroscience*, 13, 1365. <https://doi.org/10.3389/fnins.2019.01365>
- Keegan, Kevin & Glass, Elizabeth & Meyer, Folker. (2016). MG-RAST, a Metagenomics Service for Analysis of Microbial Community Structure and Function. 10.1007/978-1-4939-3369-3\_13.
- Kelly, J. R., Kennedy, P. J., Cryan, J. F., Dinan, T. G., Clarke, G., & Hyland, N. P. (2015). Breaking down the barriers: the gut microbiome, intestinal permeability and stress-related psychiatric disorders. *Frontiers in cellular neuroscience*, 9, 392. <https://doi.org/10.3389/fncel.2015.00392>
- Kim BR, Shin J, Guevarra R, et al. Deciphering Diversity Indices for a Better Understanding of Microbial Communities. *J Microbiol Biotechnol*. 2017;27(12):2089-2093. doi:10.4014/jmb.1709.09027
- Kimes, P. K., Liu, Y., Neil Hayes, D., & Marron, J. S. (2017). Statistical significance for hierarchical clustering. *Biometrics*, 73(3), 811–821. <https://doi.org/10.1111/biom.12647>
- Kish, S. J., Boileau, I., Callaghan, R. C., & Tong, J. (2017). Brain dopamine neurone 'damage': methamphetamine users vs. Parkinson's disease - a critical assessment of the evidence. *The European journal of neuroscience*, 45(1), 58–66. doi:10.1111/ejn.13363
- Kostic, A. D., Xavier, R. J., & Gevers, D. (2014). The microbiome in inflammatory bowel disease: current status and the future ahead. *Gastroenterology*, 146(6), 1489–1499. doi:10.1053/j.gastro.2014.02.009
- Lankelma JM, Birnie E, Weehuizen TAF, et al. The gut microbiota as a modulator of innate immunity during melioidosis. *PLoS Negl Trop Dis*. 2017;11(4):e0005548. Published 2017 Apr 19. doi:10.1371/journal.pntd.0005548
- Lê Cao K-A, Costello M-E, Lakis VA, Bartolo F, Chua X-Y, Brazeilles R, et al. (2016) MixMC: A Multivariate Statistical Framework to Gain Insight into Microbial Communities. *PLoS ONE* 11(8): e0160169. doi:10.1371/journal.pone.0160169
- Leclercq S, Matamoros S, Cani PD, et al. Intestinal permeability, gut-bacterial dysbiosis, and behavioral markers of alcohol-dependence severity. *Proc Natl Acad Sci U S A*. 2014;111(42):E4485-E4493. doi:10.1073/pnas.141517411
- Li Q, Han Y, Dy ABC and Hagerman RJ (2017) The Gut Microbiota and Autism Spectrum Disorders. *Front. Cell. Neurosci*. 11:120. doi: 10.3389/fncel.2017.00120
- Li, S., Hua, D., Wang, Q., Yang, L., Wang, X., Luo, A., & Yang, C. (2020). The Role of Bacteria and Its Derived Metabolites in Chronic Pain and Depression: Recent Findings and

Research Progress. *The international journal of neuropsychopharmacology*, 23(1), 26–41.  
<https://doi.org/10.1093/ijnp/pyz061>

- Liu H, Wang J, He T, et al. Butyrate: A Double-Edged Sword for Health?. *Adv Nutr*. 2018;9(1):21-29. doi:10.1093/advances/nmx009
- Logsdon AF, Erickson MA, Rhea EM, Salameh TS, Banks WA. Gut reactions: How the blood-brain barrier connects the microbiome and the brain. *Exp Biol Med (Maywood)*. 2018;243(2):159-165. doi:10.1177/1535370217743766
- Lopez-Siles, M., Duncan, S. H., Garcia-Gil, L. J., & Martinez-Medina, M. (2017). Faecalibacterium prausnitzii: from microbiology to diagnostics and prognostics. *The ISME journal*, 11(4), 841–852. <https://doi.org/10.1038/ismej.2016.176>
- Luo, Y. L., Bian, J. W., Zheng, Z. J., Zhao, L., Han, S., Sun, X. H., ... Ni, G. X. (2018). Effects of methamphetamine abuse on spatial cognitive function. *Scientific reports*, 8(1), 5502. doi:10.1038/s41598-018-23828-y
- Lyoo IK, Yoon S, Kim TS, et al. Predisposition to and effects of methamphetamine use on the adolescent brain. *Mol Psychiatry*. 2015;20(12):1516-1524. doi:10.1038/mp.2014.191
- Maier, E., Anderson, R. C., & Roy, N. C. (2017). Live Faecalibacterium prausnitzii Does Not Enhance Epithelial Barrier Integrity in an Apical Anaerobic Co-Culture Model of the Large Intestine. *Nutrients*, 9(12), 1349. <https://doi.org/10.3390/nu9121349>
- Marshall, J. F., & O'Dell, S. J. (2012). Methamphetamine influences on brain and behavior: unsafe at any speed? *Trends in neurosciences*, 35(9), 536–545. doi:10.1016/j.tins.2012.05.006
- Martin AM, Sun EW, Rogers GB, Keating DJ. The Influence of the Gut Microbiome on Host Metabolism Through the Regulation of Gut Hormone Release. *Front Physiol*. 2019;10:428. Published 2019 Apr 16. doi:10.3389/fphys.2019.00428
- Martin, C. R., Osadchiy, V., Kalani, A., & Mayer, E. A. (2018). The Brain-Gut-Microbiome Axis. *Cellular and molecular gastroenterology and hepatology*, 6(2), 133–148. <https://doi.org/10.1016/j.jcmgh.2018.04.003>
- Martín, R., Miquel, S., Chain, F., Natividad, J. M., Jury, J., Lu, J., Sokol, H., Theodorou, V., Bercik, P., Verdu, E. F., Langella, P., & Bermúdez-Humarán, L. G. (2015). Faecalibacterium prausnitzii prevents physiological damages in a chronic low-grade inflammation murine model. *BMC microbiology*, 15, 67. <https://doi.org/10.1186/s12866-015-0400-1>

- Martin, T. C., Visconti, A., Spector, T. D., & Falchi, M. (2018). Conducting metagenomic studies in microbiology and clinical research. *Applied microbiology and biotechnology*, 102(20), 8629–8646. doi:10.1007/s00253-018-9209-9
- Matsumoto, R. R., Seminerio, M. J., Turner, R. C., Robson, M. J., Nguyen, L., Miller, D. B., & O'Callaghan, J. P. (2014). Methamphetamine-induced toxicity: an updated review on issues related to hyperthermia. *Pharmacology & therapeutics*, 144(1), 28–40. <https://doi.org/10.1016/j.pharmthera.2014.05.001>
- Michalovich D, Rodriguez-Perez N, Smolinska S, et al. Obesity and disease severity magnify disturbed microbiome-immune interactions in asthma patients. *Nat Commun*. 2019;10(1):5711. Published 2019 Dec 13. doi:10.1038/s41467-019-13751-9
- Miquel, S., Martín, R., Lashermes, A., Gillet, M., Meleine, M., Gelot, A., Eschalier, A., Ardid, D., Bermúdez-Humarán, L. G., Sokol, H., Thomas, M., Theodorou, V., Langella, P., & Carvalho, F. A. (2016). Anti-nociceptive effect of *Faecalibacterium prausnitzii* in non-inflammatory IBS-like models. *Scientific reports*, 6, 19399. <https://doi.org/10.1038/srep19399>
- Ning, T., Gong, X., Xie, L., & Ma, B. (2017). Gut Microbiota Analysis in Rats with Methamphetamine-Induced Conditioned Place Preference. *Frontiers in microbiology*, 8, 1620. <https://doi.org/10.3389/fmicb.2017.01620>
- Nipperess, D. A. (2016). The rarefaction of phylogenetic diversity: formulation, extension and application. In R. Pellens, & P. Grandcolas (Eds.), *Biodiversity conservation and phylogenetic systematics: preserving our evolutionary heritage in an extinction crisis* (pp. 197-218). (Topics in Biodiversity and Conservation; Vol. 14). Switzerland: Springer, Springer Nature. [https://doi.org/10.1007/978-3-319-22461-9\\_10](https://doi.org/10.1007/978-3-319-22461-9_10)
- Noble, E. E., Hsu, T. M., & Kanoski, S. E. (2017). Gut to Brain Dysbiosis: Mechanisms Linking Western Diet Consumption, the Microbiome, and Cognitive Impairment. *Frontiers in behavioral neuroscience*, 11, 9. doi:10.3389/fnbeh.2017.00009
- Papageorgiou M, Raza A, Fraser S, Nurgali K, Apostolopoulos V. Methamphetamine and its immune-modulating effects. *Maturitas*. 2019;121:13-21. doi:10.1016/j.maturitas.2018.12.003
- Parker, A., Fonseca, S., & Carding, S. R. (2020). Gut microbes and metabolites as modulators of blood-brain barrier integrity and brain health. *Gut microbes*, 11(2), 135–157. <https://doi.org/10.1080/19490976.2019.1638722>
- Peng, Xiaosong & Lai, Fujun. (2012). Using Partial Least Squares in Operations Management Research: A Practical Guideline and Summary of Past Research. *Journal of Operations Management*. 30. 10.1016/j.jom.2012.06.002.

- Qu, K., Guo, F., Liu, X., Lin, Y., & Zou, Q. (2019). Application of Machine Learning in Microbiology. *Frontiers in microbiology*, 10, 827.  
<https://doi.org/10.3389/fmicb.2019.00827>
- Ramette A. (2007). Multivariate analyses in microbial ecology. *FEMS microbiology ecology*, 62(2), 142–160. <https://doi.org/10.1111/j.1574-6941.2007.00375.x>
- Ran, Shuwen & Mu, Chunlong & Zhu, Wei-Yun. (2019). Diversity and community pattern of sulfate-reducing bacteria in piglet gut. *Journal of Animal Science and Biotechnology*. 10. 40. 10.1186/s40104-019-0346-5.
- Rey, F. E., Gonzalez, M. D., Cheng, J., Wu, M., Ahern, P. P., & Gordon, J. I. (2013). Metabolic niche of a prominent sulfate-reducing human gut bacterium. *Proceedings of the National Academy of Sciences of the United States of America*, 110(33), 13582–13587.  
<https://doi.org/10.1073/pnas.1312524110>
- Riedl, R. A., Atkinson, S. N., Burnett, C., Grobe, J. L., & Kirby, J. R. (2017). The Gut Microbiome, Energy Homeostasis, and Implications for Hypertension. *Current hypertension reports*, 19(4), 27. <https://doi.org/10.1007/s11906-017-0721-6>
- Rinninella, E., Raoul, P., Cintoni, M., Franceschi, F., Miggiano, G., Gasbarrini, A., & Mele, M. C. (2019). What is the Healthy Gut Microbiota Composition? A Changing Ecosystem across Age, Environment, Diet, and Diseases. *Microorganisms*, 7(1), 14.  
<https://doi.org/10.3390/microorganisms7010014>
- Santos, Vitor & Corrêa, Leandro & Meiguins, Bianchi & Oliveira, Guilherme & Alves, Ronnie. (2018). Metagenomics-based signature clustering and interactive visualization analysis. 1-8. 10.1109/IJCNN.2018.8489165.
- Savin, K. W., Zawadzki, J., Auld, M. J., Wang, J., Ram, D., Rochfort, S., & Cocks, B. G. (2019). Faecalibacterium diversity in dairy cow milk. *PloS one*, 14(8), e0221055.  
<https://doi.org/10.1371/journal.pone.0221055>
- Schroeder, P. & Jenkins, David. (2018). How robust are popular beta diversity indices to sampling error?. *Ecosphere*. 9. 10.1002/ecs2.2100.
- Shi, N., Li, N., Duan, X., & Niu, H. (2017). Interaction between the gut microbiome and mucosal immune system. *Military Medical Research*, 4, 14. doi:10.1186/s40779-017-0122-9
- Shin, H. E., Kwak, S. E., Lee, J. H., Zhang, D., Bae, J. H., & Song, W. (2019). Exercise, the Gut Microbiome, and Frailty. *Annals of geriatric medicine and research*, 23(3), 105–114.  
<https://doi.org/10.4235/agmr.19.0014>

- Silva, Y. P., Bernardi, A., & Frozza, R. L. (2020). The Role of Short-Chain Fatty Acids From Gut Microbiota in Gut-Brain Communication. *Frontiers in endocrinology*, *11*, 25. <https://doi.org/10.3389/fendo.2020.00025>
- Skonieczna-Żydecka, K., Grochans, E., Maciejewska, D., Szkup, M., Schneider-Matyka, D., Jurczak, A., Łoniewski, I., Kaczmarczyk, M., Marlicz, W., Czerwińska-Rogowska, M., Pełka-Wysiecka, J., Dec, K., & Stachowska, E. (2018). Faecal Short Chain Fatty Acids Profile is Changed in Polish Depressive Women. *Nutrients*, *10*(12), 1939. <https://doi.org/10.3390/nu10121939>
- Sundin, O. H., Mendoza-Ladd, A., Zeng, M., Diaz-Arévalo, D., Morales, E., Fagan, B. M., ... McCallum, R. W. (2017). The human jejunum has an endogenous microbiota that differs from those in the oral cavity and colon. *BMC microbiology*, *17*(1), 160. doi:10.1186/s12866-017-1059-6
- Szumliński, K. K., Lominac, K. D., Campbell, R. R., Cohen, M., Fultz, E. K., Brown, C. N., Miller, B. W., Quadir, S. G., Martin, D., Thompson, A. B., von Jonquieres, G., Klugmann, M., Phillips, T. J., & Kippin, T. E. (2017). Methamphetamine Addiction Vulnerability: The Glutamate, the Bad, and the Ugly. *Biological psychiatry*, *81*(11), 959–970. <https://doi.org/10.1016/j.biopsych.2016.10.005>
- Szymańska, E., Saccenti, E., Smilde, A. K., & Westerhuis, J. A. (2012). Double-check: validation of diagnostic statistics for PLS-DA models in metabolomics studies. *Metabolomics : Official journal of the Metabolomic Society*, *8*(Suppl 1), 3–16. <https://doi.org/10.1007/s11306-011-0330-3>
- Thanos, Panayotis & Kim, Ronald & Delis, Foteini & Ananth, Mala & Chachati, George & Rocco, Mark & Masad, Ihssan & Muniz, Jose & Grant, Samuel & Gold, Mark & Cadet, Jean Lud & Volkow, Nora. (2017). Correction: Chronic Methamphetamine Effects on Brain Structure and Function in Rats. *PLOS ONE*. *12*. e0172080. 10.1371/journal.pone.0172080.
- van de Wouw M, Boehme M, Lyte JM, et al. Short-chain fatty acids: microbial metabolites that alleviate stress-induced brain-gut axis alterations. *J Physiol*. 2018;596(20):4923-4944. doi:10.1113/JP276431
- van den Berg, R. A., Hoefsloot, H. C., Westerhuis, J. A., Smilde, A. K., & van der Werf, M. J. (2006). Centering, scaling, and transformations: improving the biological information content of metabolomics data. *BMC genomics*, *7*, 142. <https://doi.org/10.1186/1471-2164-7-142>
- Vickers AJ. Parametric versus non-parametric statistics in the analysis of randomized trials with non-normally distributed data. *BMC Med Res Methodol*. 2005;5:35. Published 2005 Nov 3. doi:10.1186/1471-2288-5-35

- Vidgen, Bertram & Yasserli, Taha. (2016). P-Values: Misunderstood and Misused. *Frontiers in Physics*, 4. 10.3389/fphy.2016.00006.
- Wagner, B. D., Grunwald, G. K., Zerbe, G. O., Mikulich-Gilbertson, S. K., Robertson, C. E., Zemanick, E. T., & Harris, J. K. (2018). On the Use of Diversity Measures in Longitudinal Sequencing Studies of Microbial Communities. *Frontiers in microbiology*, 9, 1037. <https://doi.org/10.3389/fmicb.2018.01037>
- Wang, H. X., & Wang, Y. P. (2016). Gut Microbiota-brain Axis. *Chinese medical journal*, 129(19), 2373–2380. <https://doi.org/10.4103/0366-6999.190667>
- Wang, W. L., Xu, S. Y., Ren, Z. G., Tao, L., Jiang, J. W., & Zheng, S. S. (2015). Application of metagenomics in the human gut microbiome. *World journal of gastroenterology*, 21(3), 803–814. <https://doi.org/10.3748/wjg.v21.i3.803>
- Weber, M., Teeling, H., Huang, S. et al. Practical application of self-organizing maps to interrelate biodiversity and functional data in NGS-based metagenomics. *ISME J* 5, 918–928 (2011). <https://doi.org/10.1038/ismej.2010.180>
- Wilke, A., Bischof, J., Harrison, T., Brettin, T., D'Souza, M., Gerlach, W., Matthews, H., Paczian, T., Wilkening, J., Glass, E. M., Desai, N., & Meyer, F. (2015). A RESTful API for accessing microbial community data for MG-RAST. *PLoS computational biology*, 11(1), e1004008. <https://doi.org/10.1371/journal.pcbi.100400>
- Willis A. D. (2019). Rarefaction, Alpha Diversity, and Statistics. *Frontiers in microbiology*, 10, 2407. <https://doi.org/10.3389/fmicb.2019.02407>
- Wilson, I. D., & Nicholson, J. K. (2017). Gut microbiome interactions with drug metabolism, efficacy, and toxicity. *Translational research : the journal of laboratory and clinical medicine*, 179, 204–222. <https://doi.org/10.1016/j.trsl.2016.08.002>
- Worley B, Halouska S, Powers R. Utilities for quantifying separation in PCA/PLS-DA scores plots. *Anal Biochem*. 2013;433(2):102-104. doi:10.1016/j.ab.2012.10.011
- Worley, B., & Powers, R. (2013). Multivariate Analysis in Metabolomics. *Current Metabolomics*, 1(1), 92–107. <https://doi.org/10.2174/2213235X11301010092>
- Xu, J., Liang, R., Zhang, W., Tian, K., Li, J., Chen, X., Yu, T., & Chen, Q. (2020). *Faecalibacterium prausnitzii*-derived microbial anti-inflammatory molecule regulates intestinal integrity in diabetes mellitus mice via modulating tight junction protein expression. *Journal of diabetes*, 12(3), 224–236. <https://doi.org/10.1111/1753-0407.12986>

- Yip LY, Chan EC. Investigation of Host-Gut Microbiota Modulation of Therapeutic Outcome. *Drug Metab Dispos.* 2015;43(10):1619-1631.  
doi:10.1124/dmd.115.063750
- Zarrabi, H., Khalkhali, M., Hamidi, A., Ahmadi, R., & Zavarmousavi, M. (2016). Clinical features, course and treatment of methamphetamine-induced psychosis in psychiatric inpatients. *BMC psychiatry*, 16, 44.  
doi:10.1186/s12888-016-0745-5
- Zhang S, Dogan B, Guo C, et al. Short Chain Fatty Acids Modulate the Growth and Virulence of Pathosymbiont *Escherichia coli* and Host Response. *Antibiotics (Basel)*. 2020;9(8):E462. Published 2020 Jul 30.  
doi:10.3390/antibiotics9080462
- Zhang, M., Sun, H., Fei, Z., Zhan, F., Gong, X., & Gao, S. (2014). Fastq\_clean: An optimized pipeline to clean the Illumina sequencing data with quality control. 2014 IEEE International Conference on Bioinformatics and Biomedicine (BIBM), 44-48.
- Zhou, Y. H., & Gallins, P. (2019). A Review and Tutorial of Machine Learning Methods for Microbiome Host Trait Prediction. *Frontiers in genetics*, 10, 579.  
<https://doi.org/10.3389/fgene.2019.00579>
- Zhu, P., Li, L., Gao, B., Zhang, M., Wang, Y., Gu, Y., & Hu, L. (2017). Impact of chronic methamphetamine treatment on the atherosclerosis formation in ApoE<sup>-/-</sup> mice fed a high cholesterol diet. *Oncotarget*, 8(33), 55064–55072.  
<https://doi.org/10.18632/oncotarget.19020>

## Chapter 4

### ***In vitro* investigation of the effects of METH on the human lung using a U937 cell line.**

---

#### **Abstract**

Methamphetamine, METH, is a highly addictive psychoactive compound that is widespread in many parts of the world. METH is known to cause responses in microglia and astrocytes, along with causing neurotoxic effects. The aim of this study was to determine how a high METH dose (500 $\mu$ M) impacted an *in vitro*, differentiated (vitamin D) and undifferentiated U937 pro-monocytic cell line. RNA analysis of METH-stimulated U937 cells was carried out using Qiagen immune and adaptive immune response gene arrays. Results showed no significant changes in gene expression in differentiated U937 cells, upon addition of 500 $\mu$ M. However, undifferentiated U937 cells showed changes to IFN $\beta$ 1, IL4, TLR1 and TLR3. Furthermore, toxicity studies, using MTT assay showed that a 500 $\mu$ M dose was toxic to U937 cells after 3 days incubation with MTT. Thus, these results confirm the effects of METH on a pro-monocytic cell line, in which METH does not significantly impact gene expression in differentiated U937 cells, however METH may impact on gene expression in an undifferentiated cell line.

## Table of contents

<b>1.0 Introduction</b> .....	226-227
<b>2.0 Methods</b> .....	228-236
2.1 Cell culturing .....	228
2.2 Methamphetamine (METH) .....	228
2.3 MTT METH concentration calculations.....	229
2.4 MTT Assay.....	230
2.5 FACS staining.....	231
2.6 RNA extraction.....	232
2.7 Gene array preparation and analysis.....	233
2.7.1 cDNA synthesis .....	233
2.7.2 Real-Time PCR for RT <sup>2</sup> Profiler PCR Array .....	234
<b>3.0 Results</b> .....	237-246
3.1 MTT analysis of undifferentiated U937 cells stimulated with METH.....	237
3.2 RT <sup>2</sup> PCR Innate & Adaptive Immunity Gene Array .....	238
3.2.1 U937 Differentiated gene array results.....	238
3.2.2 U937 Undifferentiated gene array results.....	240
3.3 FACS data analysis.....	243
3.3.1 Differentiated U937 stimulated with METH.....	243
3.3.2 Differentiated U937 without METH addition .....	244
3.3.3 Undifferentiated U937 +/- METH stimulation.....	245
<b>4.0 Discussion</b> .....	247-251
4.1 METH inhibits cell growth at high concentrations .....	247
4.2 FACS revealed insignificant differences across cell subsets.....	247
4.3 METH does not cause changes to genes in – differentiated U937 monocyte-like cells .....	248
4.4 METH caused gene expression changes to - undifferentiated U937 cells .....	250
<b>Conclusion(s)</b> .....	251
<b>References</b> .....	253-256

## List of tables and figures

**Table 1.** Time-course absorbance readings (570nm) of 0-1000 $\mu$ M METH.

**Table 2.** RIN of extracted RNA from cultured U937 cells incubated with 500 $\mu$ M

**Table 3.** Volumes of reagents used for cDNA synthesis

**Table 4.** Reverse transcription reaction

**Table 5.** Master-mix addition to cDNA prior to real-time PCR

**Table 6.** PCR cycles.

**Figure 1.** Time-course (3-day) MTT absorbance readings across a U937 cell line incubated with 500 $\mu$ M methamphetamine (METH).

**Figure 2.** Scatterplot of treatment and control differentiated U937 cell groups.

**Figure 3.** Heat map of treatment and control differentiated U937 cell groups.

**Figure 4.** Clustergram of genes expressed in treatment and control differentiated U937 groups.

**Figure 5.** Scatterplot of undifferentiated U937 cells and gene expression.

**Figure 6.** Heatmap of gene expression in undifferentiated U937 cells.

**Figure 7.** Fold change comparison between METH-treated and control undifferentiated U937 cells

**Figure 8.** FACS analysis of differentiated U937 cells stimulated with METH.

**Figure 9.** FACS analysis of differentiated U937 cells unstimulated.

**Figure 10.** FACS analysis of undifferentiated U937 cells stimulated with METH.

**Figure 11.** FACS analysis of undifferentiated U937 cells unstimulated

## 1.0 Introduction

Methamphetamine, METH, is a popular illegal psychostimulant drug which is abused worldwide [Badisa et al., 2019]. METHs mechanism involves the regulation of dopamine (DA) neurotransmission, by, competing with DA uptake, decreasing tyrosine hydroxylase (TH) activity, along with reducing DA and vesicular monoamine transporter levels [Lin et al., 2016]. Moreover, METH abuse and addiction impairs hippocampal function leading to changes to brain structure and function, remodelling the neurobiological circuitry related to the propensity of METH relapse [Takashima et al., 2018]. In addition, METH can also lead to neuronal damage which can have serious implications in causing apoptotic and necrotic cell death in long-time METH users [Gold et al., 2009]. METH is typically administered orally, intravenously or nasally, and its effects include those associated with feelings of euphoria, a reduction in appetite, arousal post-administration and hyperactivity [Harms et al., 2012]. The immune-modulating and immune-suppressing effects of METH are evident [Papageorgiou et al., 2018; Peerzada et al., 2013], with exposure producing several proinflammatory cytokines and chemokines [Fernandes et al., 2016]. Moreover, METH compromises the blood brain barrier (BBB) which can further lead to peripheral invasion of HIV and HCV into the brain [Loftis, 2015]. Indeed, in a chronic lymphocytic choriomeningitis virus (LCMV) infection model, METH was shown to have significant effects on CD4 and CD8 T cells [Sriram et al., 2015]. In a rodent model that investigated the self-administration of METH over a 14-day period, spleen samples were assessed for their CD4+ and CD8+ frequencies [Mata et al., 2015]. Self-administration of METH resulted in lower frequencies of CD4+ T cells, however the majority of these

cells produced IFN- $\gamma$ . Furthermore, serum levels of IFN- $\gamma$ , TNF- $\alpha$  and IL-6 were unchanged [Mata et al., 2015]. METH also has effect on peripheral blood mononuclear cells (PBMCs) such as dendritic cells, macrophages, and monocytes [Liu et al., 2012]. Lastly, METH has the capacity to cause immune dysregulation in the CNS in large part due to the dependence of METH [Loftis et al., 2011].

This study sought to investigate, assess and evaluate the effects of a high METH dose (500 $\mu$ M) on a pro-monocytic cell line (U937). To investigate changes to genes belonging to host cell immunity, a commercially available gene array kit was used that could pinpoint changes to specific genes in the adaptive and/or innate immune response. Results of this work can help understand the changes at the gene level METH has on a monocytic-like cell line. This can further unravel the possible impacts METH has on cells of the innate immune system.

## **2.0 Methods**

### **2.1 Cell culturing**

U937 cells (ATCC CRL-1593.2) were cultured according to culturing guidelines specified by ATCC CRL-1593.2. U937 cells were cultured using T75 flasks in RPMI media (10% FCS, 1% antibiotics: Streptomycin-Penicillin, and 0.1% L-Glutamine). Cells were incubated at 37°C. Cells were maintained between a density of  $1 \times 10^5$  and  $2 \times 10^6$  cells/mL and media changed to maintain healthy and proliferating cells every 3-4 days. For media change, cells were transferred into 15mL falcon tubes and centrifuged for 5 minutes at 1000RPM. Media was then removed and supplemented with fresh RPMI complete media. Cells were then transferred into sterile T75 flasks at a final volume of 15mL and incubated at 37°C. To assess cell viability, approximately 20uL cells was mixed with 20uL 0.4% Trypan blue and live/dead cells were assessed using a light microscope at a magnification of 40x. For differentiation, U937 cells were exposed to Vitamin D3 for 72 hours. For U937 cells (undifferentiated), these cells were maintained throughout until the addition of methamphetamine 500  $\mu$ M (METH).

### **2.2 Methamphetamine (METH)**

Based on MTT results, METH was added to U937 cells – differentiated and undifferentiated – at a final concentration of 500 $\mu$ M. This concentration was chosen as previously reported cell culturing has indicated that a METH concentration of 500 $\mu$ M does not cause cell toxicity. METH (500 $\mu$ M) concentration was determined based on calculations from METH stock of 167.522mM.

### 2.3 MTT METH concentration calculations

400µL of METH from a 25mg/mL stock (167.522mM) was aliquoted and transferred into 1.6ml of sterilised water. 5mg/mL stock METH solution was used for downstream experiments. METH concentrations were calculated (table 1) from 100-1000µM.

**Table 1.** Summary of calculations of METH concentrations. A range of concentrations (100-1000µM) were used to conduct the MTT assay, in order to ascertain a high METH concentration that would impact U937 cell respiration.

100µM	250µM	500µM	750µM	1000µM
Convert 200µl to mL = 0.200 Stock conc. = 33.5 Conc. Needed = 100uM	Convert 200ul to mL = 0.200 Stock conc. = 33.5 Conc. Needed = 250uM	Convert 200ul to mL = 0.200 Stock conc. = 33.5 Conc. Needed = 500uM	Convert 200ul to mL = 0.200 Stock conc. = 33.5 Conc. Needed = 750uM	Convert 200ul to mL = 0.200 Stock conc. = 33.5 Conc. Needed = 1000uM
$\frac{0.200 \times 0.100mM}{33.5}$ 0.00059 (x 1000) = 0.59uL = 1.18	$\frac{0.200 \times 0.250mM}{33.5}$ 0.00149 (x1000) = 1.49uL = 2.98	$\frac{0.200 \times 0.500mM}{33.5}$ 0.00298 (x 1000) = 2.98uL = 5.96	$\frac{0.200 \times 0.750mM}{33.5}$ 0.00447 (x 1000) = 4.47uL 8.94	$\frac{0.200 \times 1.0mM}{33.5}$ 0.00597 (x 1000) = 5.97uL = 11.94

## 2.4 MTT Assay

Undifferentiated U937 cells were assessed for their viability using the MTT assay. The MTT (3-[4,5-dimethylthiazol-2-yl]-2,5 diphenyl tetrazolium bromide) assay involves the conversion of MTT into formazan crystals by living cells – determining the mitochondrial activity [Meerlo et al., 2011]. Moreover, the [MTT] assay is designed to measure viable cells without the inconvenience of cell counting. Principally, the MTT assay exploits a cells' mitochondrial activity – viable cells hold constant mitochondrial activity – in which this mitochondrial activity is a function of the conversion of tetrazolium salt MTT into formazan crystals. Effectively, formazan concentration can be measured via its optical density at a wavelength adjusted to 540nm – 720nm: changes in absorbance reflect an increase or decrease in cell viability [Meerlo et al., 2011]. U937 cells in this experiment – with the addition of METH (100-500 $\mu$ M) - showed that cell viability lowered at 500 $\mu$ M over a 3-day period. Based on this absorbance, METH was concluded to effectively inhibit cell growth at 500 $\mu$ M and this dose was used for remaining cell culturing and gene array assays. Absorbance readings over the 3-day incubation period.

## **2.5 FACS staining**

U937 cells were harvested and cell suspension was adjusted to reach a final concentration of  $2 \times 10^5$  cells/mL, using cold (4°C) PBS buffer. 100µl of U937 cells was added to a total of 11 1.5mL eppendorf tubes. Primary antibody, at a 1:100 dilution, was added to each reaction tube. Cells were pipetted up and down and incubated at room temperature for at least 30 minutes, avoiding direct sunlight. After incubation, cells were washed with 2mL of cold (4°C) PBS buffer, and cells were then centrifuged at 400xg for 5 minutes, at 4°C. Afterwards, the supernatant was discarded. Cells were then resuspended in 200µl of cold (4°C) PBS. Cells were transferred to FACS tubes and analysed for surface markers within 24 hours. Markers analysed were, CD14, CD16, CD86, CD40, CD80, CD83, CD206, CD209, MHC I, MHC II and CD11b. Appropriate controls, cells with no antibodies and only fluorescence markers were also prepared for FACS analysis.

## 2.6 RNA extraction

Differentiated and undifferentiated U937 cells were harvested at a concentration of  $\sim 1 \times 10^6$  cells/mL. To ensure cell concentration was consistent, dilutions were made across cultured cells to achieve a final concentration of  $10^6$  cells/mL. Cells were transferred to clean 15mL falcon tubes and centrifuged at 1000RPM for 5 minutes. Supernatant was removed, and cells were placed on ice prior to RNA extraction experiment. RNA extraction was carried following the manufacturer's specifications (Qiagen RNeasy Mini Kit). DNase was passed through all cell samples (differentiated cell sets and undifferentiated cell sets) to remove DNA contamination. RNA absorbance was measured using a benchtop spectrophotometer and all A260/280 ratios were within RNA quality limits. Furthermore, RNA concentrations were assessed using a bioanalyser instrument. RNA Integrity numbers (RINs) are shown in table 3.

**Table 2. RIN of extracted RNA from cultured U937 cells incubated with 500 $\mu$ M.** RNA integrity number (RIN) is a vital assessment algorithm which determines the quality of RNA in a sample.

Differentiated U937 cells		Undifferentiated U937 cells	
Treatment (METH)	Control (No METH)	Treatment (METH)	Control (No METH)
9.8/10	9.9/10	9.8/10	9.7/10
9.7/10	9.7/10		
9.7/10	9.7/10		

## 2.7 Gene array preparation and analysis

### 2.7.1 cDNA synthesis

First Strand RT2 reagents were thawed on ice, and briefly pulse centrifuged for 10 seconds to bring contents to bottom of tubes. Next, genomic DNA elimination mix was prepared according to the following volumes indicated in table 3.

**Table 3. Volumes of reagents used for cDNA synthesis.** A total volume of 10 $\mu$ L was prepared for each sample.

Component	Amount
RNA (samples)	25ng – 5ug
GE buffer	2 $\mu$ l
RNase-free water	Variable
<b>Total volume</b>	10uL

Genomic DNA elimination mix was incubated for 5 minutes at 42°C, and then tubes were placed on ice for 1 minute. Reverse transcription mix was prepared according to table 4.

**Table 4. Reverse transcription reaction.** Steps carried out according to manufacturer's volume specifications.

<b>Component</b>	<b>Reaction volumes (<math>\mu\text{L}</math>)</b>
5x buffer BC3	4
Control P2	1
RE3 Reverse Transcriptase mix	2
RNase-free water	3
<b>Total volume</b>	<b>10</b>

10uL reverse transcription mix was added to each tube (containing 10uL genomic DNA elimination mix). Contents were mixed by pipetting up/down. Then, tubes were incubated at 42°C for 15 minutes, followed by incubation at 95°C for 5 minutes. 91uL of RNase-free water was then added to each reaction tube. Contents were mixed by pipetting up/down. Reaction tubes were then placed on ice (or stored in a -20°C freezer until real-time PCR step).

### **2.6.2 Real-Time PCR for RT<sup>2</sup> Profiler PCR Array.**

RT2 SYBR Green Mastermix was briefly centrifuged (at room temperature: 15-25°C) to bring contents to bottom of tube. PCR components were prepared in a sterile 5mL tube, according to table 5.

**Table 5. Mastermix addition to cDNA prior to real-time PCR.** Aliquots of reagents were prepared per sample.

Reagents	96-well array (volumes: uL)
2x RT2 SYBR Green Mastermix	1350
cDNA synthesis reaction	102
RNase-free water	1248
<b>Total volume</b>	2700

Total volume (above) was dispensed into a sterile disposable well. The RT2 Profiler PCR Array was removed from its storage bag, and gene array was placed in a well holder to reduce any unwanted movement during the dispensing of PCR mix to each 96-well. 25uL of PCR mix was then added to each well using a multi-channel pipette. The RT2 PCR Array was carefully sealed using optical thin-wall 8-cap strips. The RT2 Array was then centrifuged for 1 minute at 1000g at room temperature (15-25°C) to remove any bubbles present in any of the 96 wells. The removal of bubbles was also checked by inspecting the underside of the RT2 Array plate. Before PCR cycling, the array was placed upon ice. Real-time cycling for Roche LightCycler 480 was adjusted according to parameters in table 6.

**Table 6. PCR cycles.** Cycle number according to manufacturer's recommendation.

<b>Cycles</b>	<b>Duration</b>	<b>Temperature</b>
1	10 minutes	95°C
45	15 seconds	95°C
	1 minute	60°C

After the PCR programme was adjusted, the RT2 PCR Array was placed into the real-time cycler. The Array was allowed to run for its estimated time until cycling was complete. Upon full completion of cycles, data was exported as csv. Excel sheets and saved to an external drive for further analysis. Qiagen's Sample to Insight software tool was employed for data analysis. Moreover, housekeeping genes, fold-change threshold and CT cut-off were predefined. Results from all RT2 PCR Innate & Adaptive Gene Arrays were exported in a single PDF document.

### 3.0 Results

#### 3.1 MTT analysis of undifferentiated U937 cells stimulated with METH

MTT measures the metabolic activity of cells [Grela et al., 2018]. MTT analysis of undifferentiated U937 cells showed an overall increase in cell growth over a three-day period (Figure 1). Previous work using MTT assay and METH has observed ER-stress and its role in apoptosis in astrocytes [Shah et al., 2016]. Other work has used a smaller METH dose of 1 $\mu$ M over a 24-72-hour period in human brain microvascular endothelial cells (HBMECs) [Ma et al., 2014]. This work used a range of METH doses, from 0-1000 $\mu$ M over a three-day period. METH, at a high concentration of between 500-1000 $\mu$ M seemed to decrease OD values compared to 0-250 $\mu$ M (Figure 1).

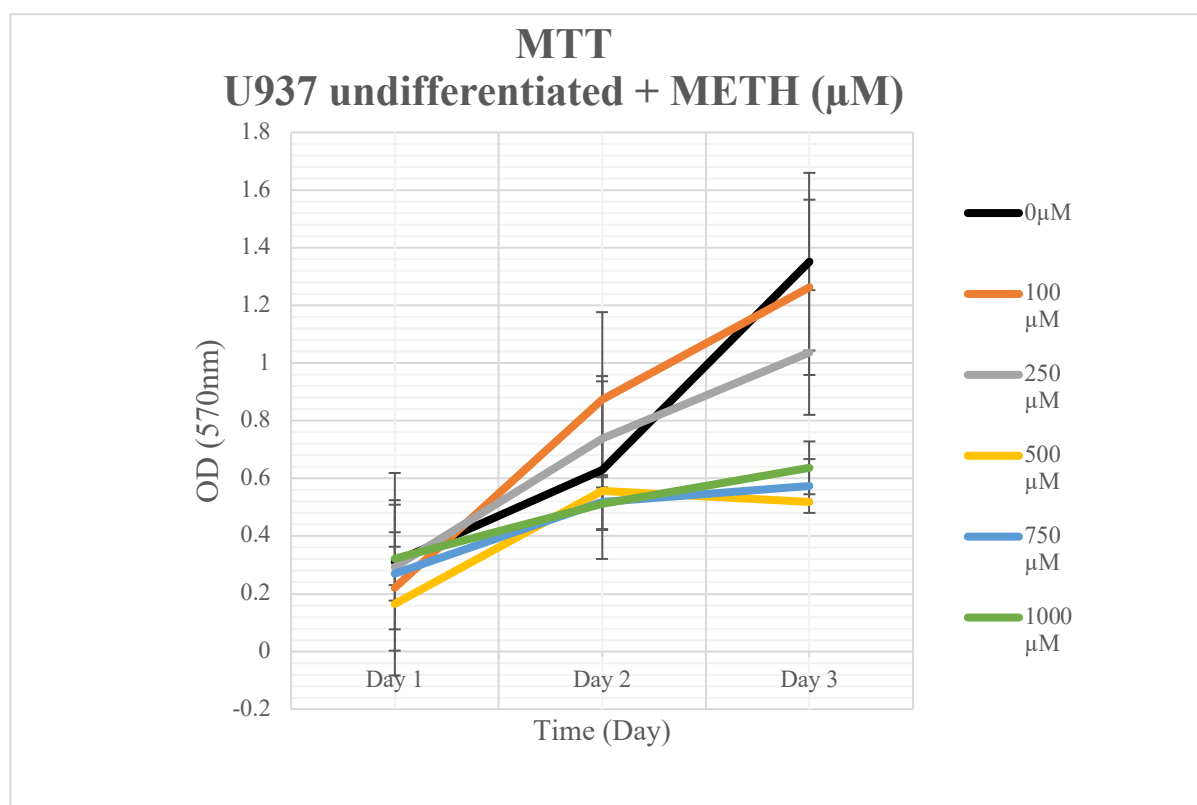


**Figure 1. Time-course (3-day) MTT absorbance readings across a U937 cell line incubated with 500 $\mu$ M methamphetamine (METH).** Formation of formazan crystals (precipitate) indicating mitochondrial activity of U937 cells across different METH concentrations.

## 3.2 RT<sup>2</sup> PCR Innate & Adaptive Immunity Gene Array

### 3.2.1 U937 Differentiated gene array results

Genes relating to the innate and adaptive immune response in humans were analysed in U937 cells. Gene arrays were carried out in triplicates, and reproducibility and efficiency quality checks were performed on the data using Qiagen's Data quality control (QC) software interface. Data was then normalised using the automated selection from HKG panel genes. Calculations comprised geometric mean and average geometric mean of both control and METH groups. Gene fold cut-off scores were set to 2, with a p-value cut-off score of 0.05. Fold change was calculated based on the normalised gene expression ( $2^{(\Delta \text{CT})}$  in the test sample (METH) divided by the normalised gene expression in the control sample (No Meth). No genes were significantly up or downregulated in this gene array. Scatter plot (Figure 2), and heat map (Figure 3) were chosen since a scatterplot compares normalised expression of all genes across the array between both groups. This can efficiently visualise expression changes, via two dotted lines which indicate a particular gene being under or over-expressed. Similarly, a heat map in this data set can help understand and visualise gene expression in the context of the array layout.

By assessing the scatterplot, the majority of genes were expressed at 1-fold relative to unchanged expression (central line). The most upregulated of these (although below 2-fold) were, CD86 (+1.88), LY96 (+1.62), TLR1 (+1.46), TLR8 (+1.72) and TLR9 (-1.66). In general, CD86, along with CD80

represent co-stimulatory receptors on innate immune cells [Nolan et al., 2009]. Lymphocyte antigen 96 (LY96) is known to bind bacterial lipopolysaccharide (LPS), and also collaborate with TLR2. Toll-like receptors (TLR) are that sit on a cell surface function to recognise bacterial products and by-products, whereas TLRs residing intracellularly play a role in viral and nucleic acid detection [Parker et al., 2007]. In this work, TLR1, 8 and 9 were expressed roughly >1.5 fold. TLR1, a cell surface bound TLR, interacts with TLR2 and therefore function as a complex to recognise antigens. TLR8 and TLR9, which are both localised in the endosome, respond to viral and bacterial RNA and DNA nucleic acid material, respectively [Kawasaki et al., 2014]. Apart from their expression in dendritic cells and macrophages, TLRs are also expressed in non-immune cells of the body, including fibroblasts and epithelial cells [Kawasaki et al., 2014].

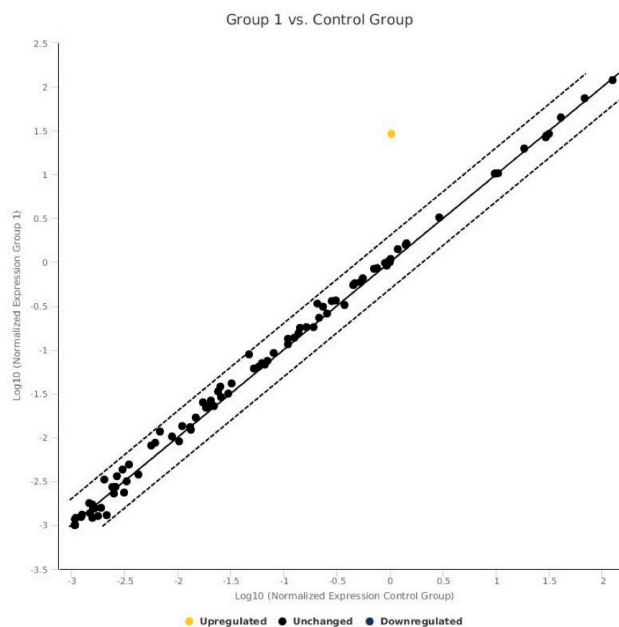
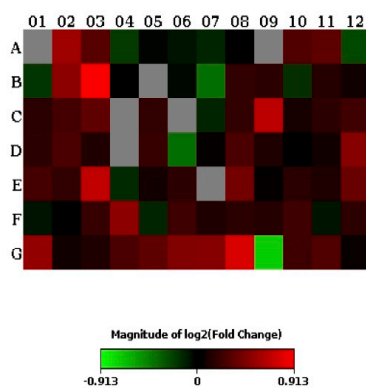


**Figure 2. Scatterplot of treatment and control differentiated U937 cell groups.** Qiagen software Log10 scatter plot expression of genes upon exposure of 500 $\mu$ M METH to differentiated U937 cells. Central line indicates unchanged gene expression.



Layout	01	02	03	04	05	06	07	08	09	10	11	12
A	APCS -1.08 C	C3 1.49 A	CASP1 1.25	CCL2 -1.16	CCL5 -1.03	CCR4 -1.05 B	CCR5 -1.09 B	CCR6 1.00 B	CCR8 -1.08 C	CD14 1.23	CD4 1.27 A	CD40 -1.20 B
B	CD40LG -1.14 B	CD80 1.43 B	CDB6 1.88	CD8A -1.00 B	CRP -1.08 C	CSF2 -1.04 B	CXCL10 -1.33 B	CXCR3 1.14 B	DDX58 1.13	FASLG -1.13 B	FOXP3 1.10	GATA3 1.06 B
C	HLA-A 1.11	HLA-E 1.19	ICAM1 1.27	IFNA1 -1.08 C	IFNAR1 1.13	IFNB1 -1.08 C	IFNG -1.10 B	IFNGR1 1.14	IL10 1.60 B	IL13 1.06	IL17A 1.13 B	IL18 1.17
D	IL1A 1.12 B	IL18 1.21 B	IL1R1 1.09 B	IL2 -1.08 C	IL23A 1.15 B	IL4 -1.31 B	IL5 1.04 B	IL6 1.21 B	CXCL8 1.08	IRAK1 1.01	IRF3 1.06	IRF7 1.41 B
E	ITGAM 1.19	JAK2 1.14	LY96 1.62	LYZ -1.11	MAPK1 1.05	MAPK8 1.12	MBL2 -1.08 C	MPO 1.33 B	MX1 1.02 B	MYD88 1.11	NFKB1 1.07	NFKBIA 1.31
F	NLRP3 -1.05	NOD1 1.02	NOD2 1.15 B	RAG1 1.43 B	RORC -1.10 B	SLC11A1 1.17	STAT1 1.08	STAT3 1.11	STAT4 1.10 B	STAT6 1.18	TBX21 -1.06 B	TICAM1 1.12
G	TLR1 1.46 B	TLR2 1.05 B	TLR3 1.08 B	TLR4 1.21	TLR5 1.27 B	TLR6 1.39 A	TLR7 1.40 B	TLR8 1.72 B	TLR9 -1.66 B	TNF 1.17 B	TRAF6 1.22	TYK2 1.04

**Figure 3. Heat map of treatment and control differentiated U937 cell groups.** Qiagen software analysis heat map of differentiated U937 cells upon ~8-hour exposure to 500µM METH.

### 3.2.2 U937 Undifferentiated gene array results

Gene array data from undifferentiated U937 cells showed significant gene expression (downregulation) of four genes: IFNβ1 (-2.15), IL4 (-2.59), TLR1 (-2.05), and TLR3 (-2.09). In this gene analysis, and by visualising the scatterplot, the majority of genes in undifferentiated U937 cells, based on this array, were downregulated (Figure 5). IFNβ1, known as interferon beta 1, fibroblast, is expressed in a range of innate immune cells, including macrophages, as well as non-immune cells, such as epithelial cells [Bolivar et al., 2018]. Type I Interferons, such as IFNβ1, function in response to bacterial

and viral infections, and also play a role in responding to immunomodulatory stimuli [Henig et al., 2013]. IL4, often produced by T-cells, mast cells, basophils and eosinophils, and is characterised by its ability to determine the Th2 appearance of lymphocytes [Luzina et al., 2012]. Moreover, IL4 signalling can bind to either type I or type II signalling complexes to initiate a downstream cascade leading to sustained survival and mitogenesis, and binding of transcription factors to DNA in the nucleus [Gadani et al., 2012]. TLR3 (-2.09) is involved in double-stranded RNA recognition and can be expression both on the cell surface and intracellularly [Parker et al., 2007].

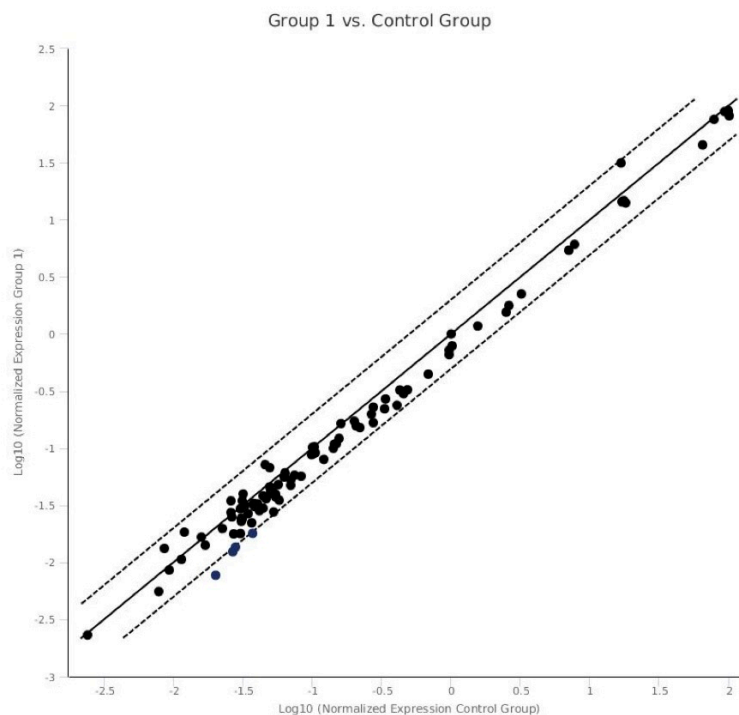
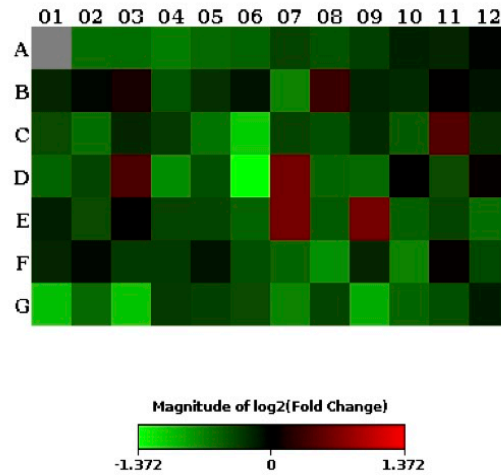


**Figure 4. Scatterplot of undifferentiated U937 cells and gene expression.** Qiagen software Log10 scatter plot expression of genes upon exposure of 500 $\mu$ M METH to undifferentiated U937 cells for ~8 hours. Central line represents unchanged gene expression levels.



Layout	01	02	03	04	05	06	07	08	09	10	11	12
A	APCS	C3	CASP1	CCL2	CCL5	CCR4	CCR5	CCR6	CCR8	CD14	CD4	CD40
	-1.04	-1.53	-1.51	-1.60	-1.49	-1.45	-1.29	-1.36	-1.27	-1.14	-1.16	-1.04
	C	B				B	B	B	B	B	B	B
B	CD40LG	CD80	CD86	CD8A	CRP	CSF2	CXCL10	CXCR3	DDX58	FASLG	FOXP3	GATA3
	-1.16	-1.05	1.10	-1.37	-1.21	-1.08	-1.65	1.25	-1.14	-1.18	1.02	-1.08
	B	B	B	B	B	B	B	B		B		B
C	HLA-A	HLA-E	ICAM1	IFNA1	IFNAR1	IFNB1	IFNG	IFNGR1	IL10	IL13	IL17A	IL18
	-1.33	-1.53	-1.16	-1.25	-1.54	-2.15	-1.29	-1.34	-1.18	-1.42	1.37	-1.20
			B	B	B	B	B	B	B	B	B	B
D	IL1A	IL1B	IL1R1	IL2	IL23A	IL4	IL5	IL6	CXCL8	IRAK1	IRF3	IRF7
	-1.46	-1.30	1.34	-1.70	-1.34	-2.59	1.54	-1.47	-1.50	-1.00	-1.32	1.06
	A	B	B	B	B	B	B	B				B
E	ITGAM	JAK2	LY96	LYZ	MAPK1	MAPK8	MBL2	MPO	MX1	MYD88	NFKB1	NFKBIA
	-1.13	-1.33	1.02	-1.29	-1.30	-1.45	1.55	-1.40	1.56	-1.43	-1.29	-1.53
		B					B	B	B			
F	NLRP3	NOD1	NOD2	RAG1	RORC	SLC11A1	STAT1	STAT3	STAT4	STAT6	TBX21	TICAM1
	-1.16	-1.05	-1.24	-1.25	-1.08	-1.35	-1.46	-1.72	-1.16	-1.65	1.05	-1.32
		B	B	B	B				B		B	
G	TLR1	TLR2	TLR3	TLR4	TLR5	TLR6	TLR7	TLR8	TLR9	TNF	TRAF6	TYK2
	-2.05	-1.49	-2.09	-1.25	-1.28	-1.33	-1.66	-1.30	-1.91	-1.47	-1.36	-1.12
	B	B	B		B		B	B	B	B		B

**Figure 5.** Qiagen software heat map and gene table comparing treated and non-treated undifferentiated U937 cells upon exposure with 500 $\mu$ M METH for ~8 hours. Significantly expressed genes in the undifferentiated U937 cells were found to be, IL4, TLR1, TLR3 and IFN $\beta$ 1.

### 3.3 FACS data analysis

#### 3.3.1 Differentiated U937 stimulated with METH

Differentiated U937 cells were analysed for their expression of surface markers upon an ~8-hour exposure of a high 500  $\mu$ M METH dose. U937 cells were stained with a series of monocytic markers (Figure 7). FITC (fluorescein) fluorophore, PE, and BV421 channels were used to visualise cell events.

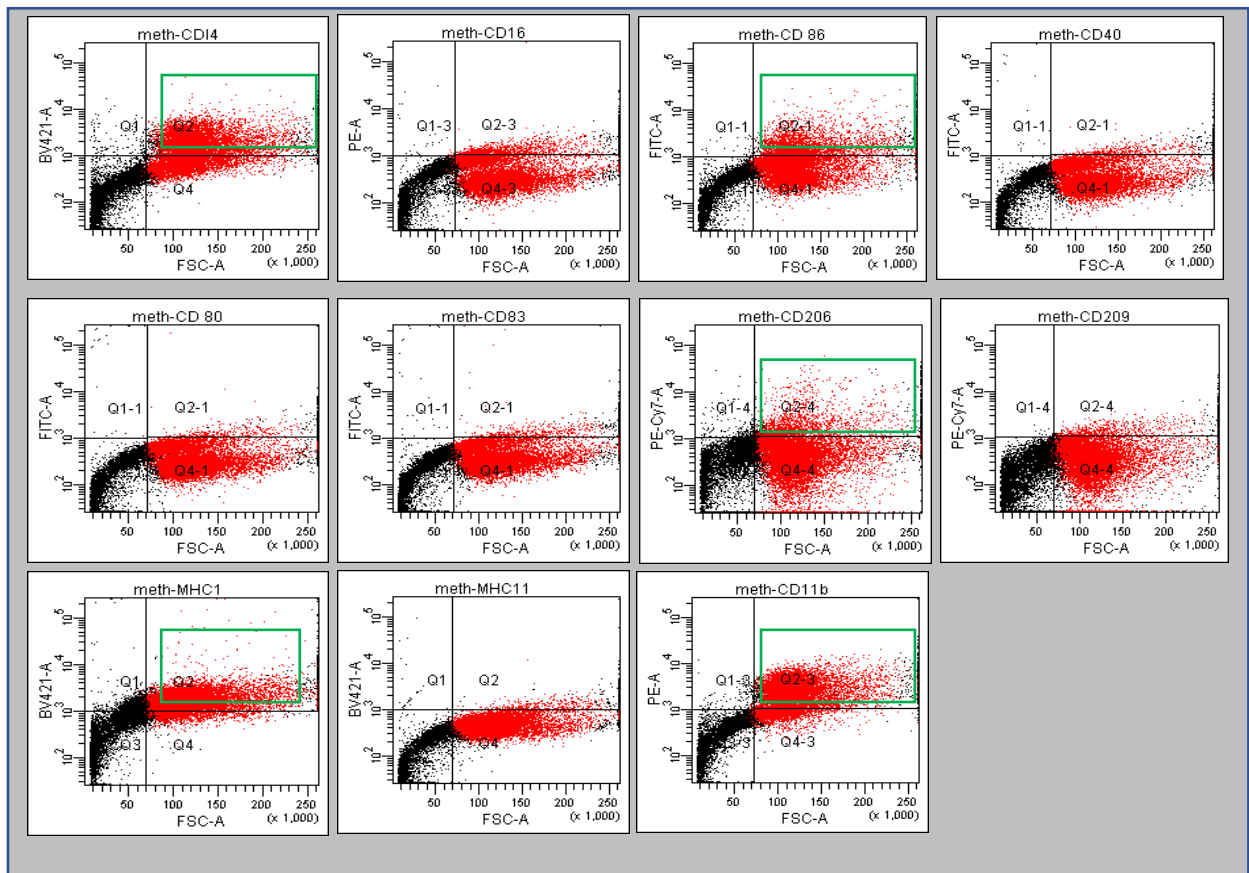


**Figure 6A. FACS summary of differentiated U937 cells stimulated by METH for 24 hours.** Green boxes are shown for those markers which showed significant events during forward light scattering. Markers CD14, CD86, CD206, MHC1 and CD11b were shown as positive cell populations.

### 3.3.2 Differentiated U937 without METH addition

Differentiated U937 cells were analysed for their surface marker expression, without the addition of a high 500  $\mu$ M METH dose.

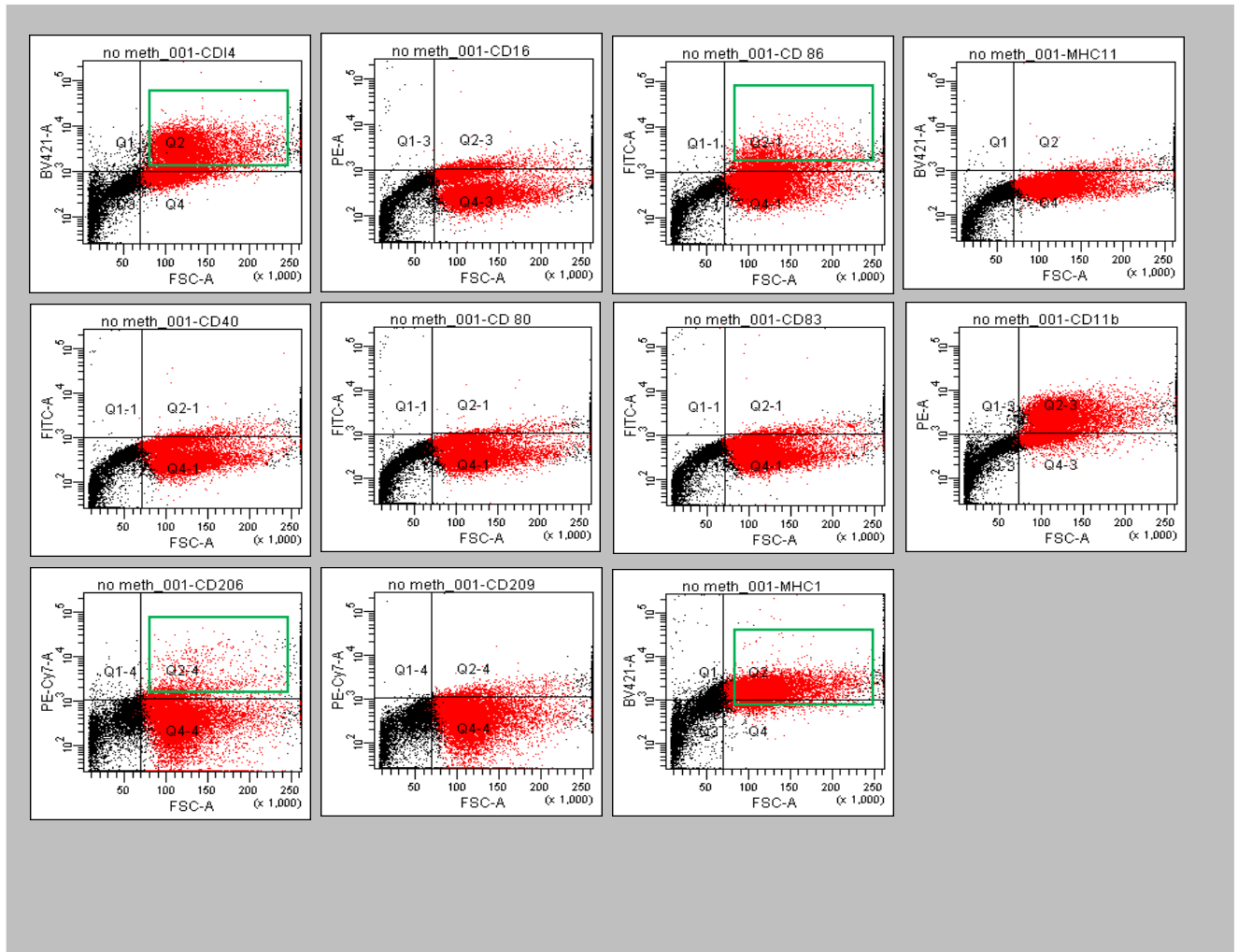


**Figure 6B. FACS analysis of differentiated U937 cells unstimulated.** FACS surface marker analysis results of undifferentiated U937 cells unstimulated.

### 3.3.3 Undifferentiated U937 +/- METH stimulation

Undifferentiated U937 cells were analysed by FACS for their surface marker expression with the addition of a 500  $\mu$ M METH concentration. No significant changes were observed of the forward light scattering, however MHCII revealed some higher expression (see panel below).

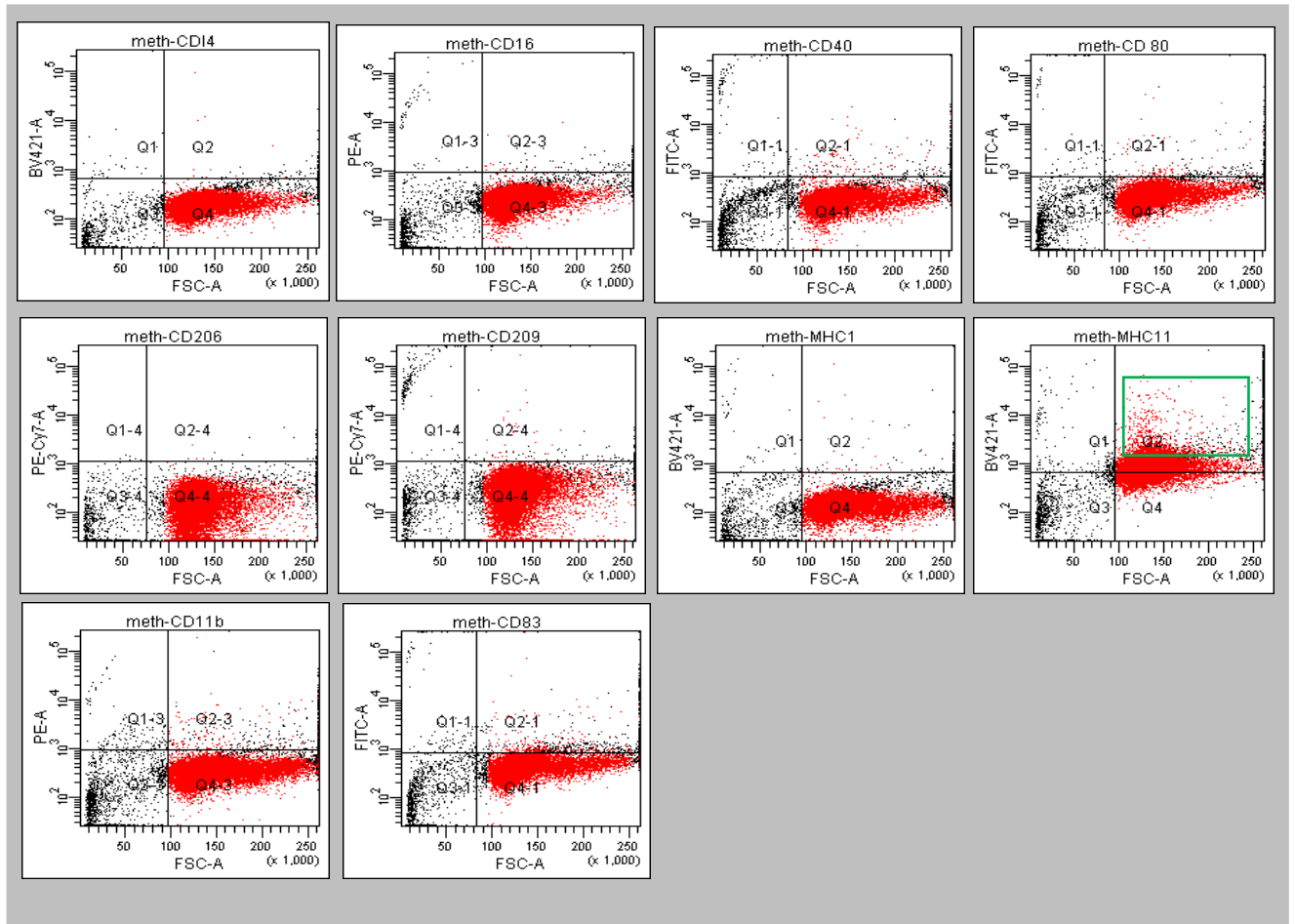


**Figure 7A. FACS analysis of undifferentiated U937 cells stimulated with METH.** FACS surface marker analysis results of undifferentiated U937 stimulated by 500  $\mu$ M METH.

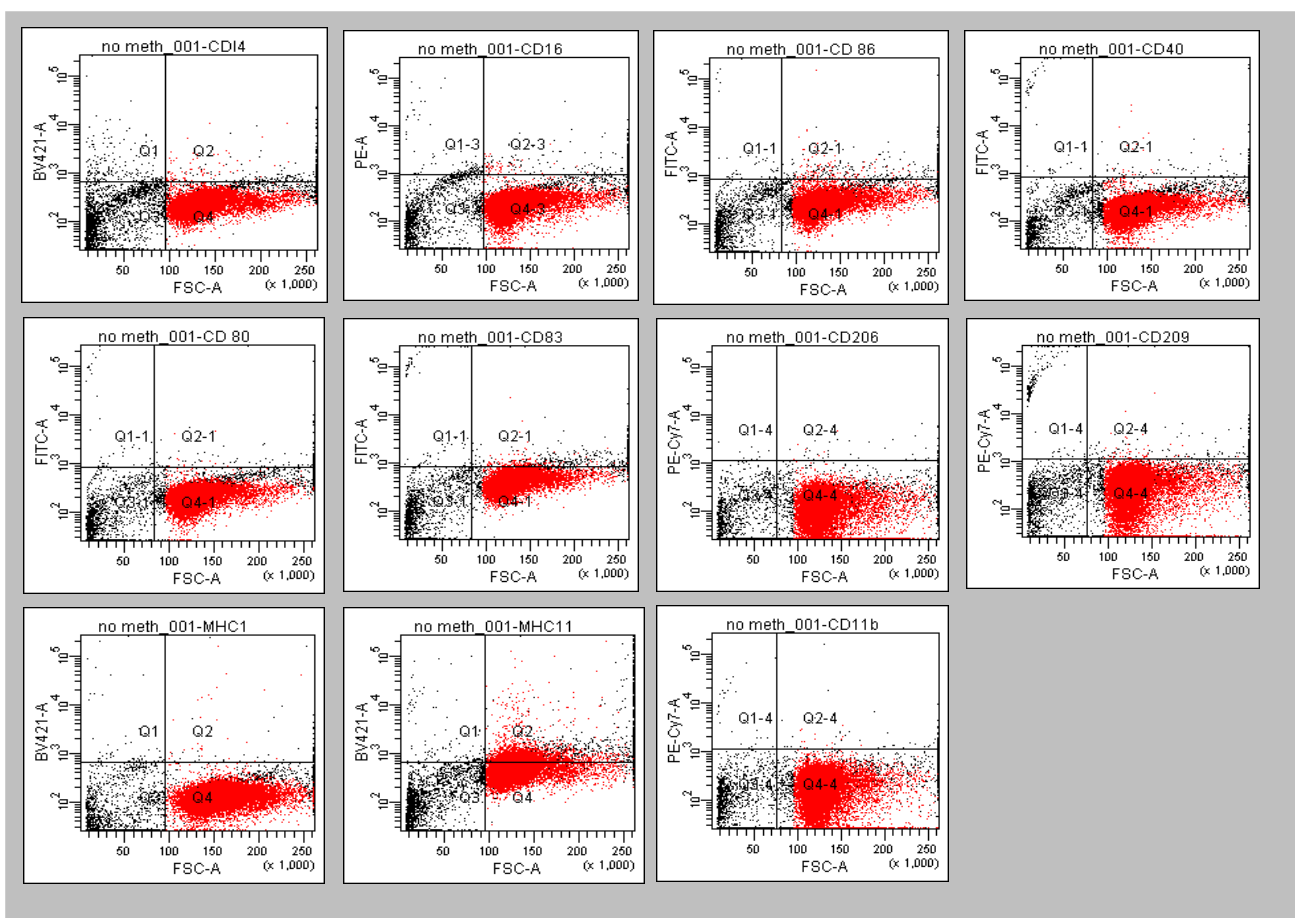


**Figure 7B. FACS analysis of undifferentiated U937 cells unstimulated.**  
 FACS surface marker analysis results of undifferentiated U937 unstimulated.

## **4.0 Discussion**

### **4.1 METH inhibits cell growth at high concentrations**

MTT data revealed inhibition of cell respiration of U937 cells across a three-day period. On the first day of incubation, METH, at concentrations between 250 and 1000 $\mu$ M, showed little changes in absorbance (measured at 570nm). However, by day 2 and 3, conversion of tetrazolium salt MTT into formazan crystals was much denser (Appendix 2). Moreover, METH, at much higher doses, was able to inhibit U937 respiration; however, at lower concentrations METH did not seem to inhibit, or effect, cell viability. This study chose 500  $\mu$ M as an intermediate, high dose of METH, as it has been described in previous studies.

### **4.2 FACS revealed insignificant differences across cell subsets.**

Overall, FACS data showed METH-treated U937 cells had little differences compared to non-METH treated cells. METH did not cause surface marker changes to U937 cells treated with vitamin D3. Likewise, METH caused no significant changes to U937 cell markers in cells not treated (differentiated) with vitamin D3. Only one marker (MHCII) showed a slightly different expression profile between control and treated cells. In U937 cells, MHCII is expressed at detectable levels [Barbaro et al., 2005]. Expression of MHCII in this FACS analysis might be attributed to basal expression of this marker, independent of METH. However, control (- METH) showed an apparent lower MHCII marker expression on differentiated U937 cells. Little data exists for the involvement of MHCII in METH studies. Talloczy et al (2008) showed that pharmacological

doses of METH had immunosuppressive effects on dendritic cells and macrophages. Moreover, their work also described the inhibition of MHC class II antigen processing via the endosomal-lysosomal pathway [Talloczy et al., 2008]. More work is required to understand the role of MHCII in chronic and acute METH in vitro and animal studies.

#### **4.3 METH does not cause changes to genes in differentiated U937 monocyte-like cells.**

The addition of a high - 500 $\mu$ M – METH dose did not cause any significant changes to genes associated with the Innate & Adaptive Immune Response. Furthermore, METH, compared to control samples, showed no significant gene expression changes in the following categories of immunity: Innate immunity, adaptive immunity, humoral immunity, inflammatory response, defence response to bacteria and defence response to viruses. Previous reports have shown that METH caused gene expression changes to primary, rat, cortical-derived astrocytes in vitro [Bortell et al., 2017]. Moreover, these expression changes involved: MAP2K5, GPR65 and CXCL5, which showed strong overexpression [Bortell et al., 2017]. Overall, this study reported that METH at concentrations of 10 or 100 $\mu$ M increased 411 genes in in vitro, cortical-derived astrocytes compared to controls; additionally, 1 $\mu$ M METH caused an increased expression in 180 genes [Bortell et al., 2017]. In comparison to monocytes, astrocytes are readily activated in the brain of METH users and associated gene expression changes perturb the central nervous system.

Using a differentiated THP-1 monocyte cell line – to macrophages, Burns and Ciborowski, 2017, profiled cytokine and chemokine expression using the Human cytokines and chemokines RNA PCR array [Burns and Ciborowski, 2017]. Across a times series (2, 6, or 24 hours), and using a METH dose of 100µM, results indicated 58 differentially expressed genes. Specifically, METH caused a strong up-regulation of CXCL16 and CXCL2; a moderate (between 5 and 10-fold) up-regulation gene expression of IL7, CCL20, CXCL1, CCL24 and IL8; and, a strong down-regulation of CCL7 [Burns and Ciborowski, 2017]. Results of this study also suggested that across a 2- and 6-hour time point, the majority of immune mediators that were up-regulated were in fact pro-inflammatory cytokines [Burns and Ciborowski, 2017].

In the present study, METH – at a chronic dose – did not show significant changes to any of the 84 genes. Discrepancies between this data and that of previously reported data using a similar cell line (THP-1) could be associated with technical error and/or cell behaviour during culture period. Moreover, one limitation of this cell culturing model is the absence of time points. Since only a single timepoint to harvest cells upon METH exposure was used – 8 hours – during this time an irregular gene expression pattern may have occurred, resulting in a baseline gene expression during/or toward the end of the 24-hour incubation period.

#### **4.4 METH caused gene expression changes to undifferentiated U937 cells**

U937 cells not treated with VitD3 – undifferentiated U937 cells – showed changes to several genes. Genes under-expressed in METH-treated U937 cells included, IL4, IFNB1, TLR3 and TLR1. IL4 has yet to be fully associated with METH. IL4 plays a role in promoting the proliferation and differentiation of antigen-presenting cells (APCs) [Dhanda et al., 2013], and is known as a T-helper cytokine [Bhattacharjee et al., 2013]. Moreover, IL4 is an anti-inflammatory molecule [Bhattacharjee et al., 2013]. In undifferentiated U937 cells, METH may lower the expression of IL4, thus lowering its overall anti-inflammatory response in monocytes. This possible action of METH on IL4 could also be attributed to METHs ability to cause inflammation. TLR3 was shown to be significantly lowered in its expression in undifferentiated U937 cells. Toll-like receptors (TLRs) recognise pattern associated molecular patterns (PAMPs) and serve a special purpose in the innate immunity by directing immune responses towards microbial pathogens [Allhorn et al., 2008]. In addition, TLR3 primes the appropriate immune response as it senses DNA and RNA viral infections in the host [Pan et al., 2011; Huik et al., 2013]. METH dependence has been previously ascribed as a major risk factor for HIV infection [Blackstone et al., 2013]. The apparent down-regulation of TLR3 in this study could be to the effects METH has on lowering TLR3 signalling, which in turn leads to the activation of interferon-regulatory factor-3 and NF- $\kappa$ B, following activation of pro-inflammatory cytokines [Huik et al., 2013]. Importantly, activation of TLR3 inhibits HIV [Dai et al., 2015]. TLR3, in this study, may contribute to better understanding the role of TLR3 in a high METH

dose context. The cytokine interferon beta 1 (IFNB1) was shown to be downregulated in undifferentiated U937 cells. IFNB1 is secreted in the innate immune system's response to pathogens. Furthermore, type I interferons, such as IFNB1, are manufactured in most cells and respond to viral infections [Marckmann et al., 2004]. Interestingly, IFN $\beta$ 1 type 1 interferons protect cells from apoptosis and METH is known to cause cell death along with autophagy [Yu et al., 2015]. The apparent decrease in gene expression of IFNB1 could be a consequence of METH's role in cell injury. In this study, TLR1 was observed as having a significantly lower gene expression (-2.05-fold). TLR1 cooperates with TLR2 and both serve to mediate the innate immune response to bacterial pathogens. Since TLR3 was also shown to be downregulated in this study, the concurrent downregulation of TLR1 might also be due to a high METH dose having the ability to disarm the innate immune response and allow for pathogens and viruses to spread.

## **Conclusion(s)**

Together, cultured U937 cells exposed to a high METH dose did not display significant changes in gene expression across the innate and adaptive immune system. However, undifferentiated U937 cells showed some changes in gene expression to genes pertaining to TLR signalling and inflammatory responses. Further, significantly downregulated gene expression, namely IL4, TLR1, TLR3 and IFN $\beta$ 1, was observed in undifferentiated U937 cells. These genes are mainly active and play roles in pathogen and virus sensing, where they in turn contribute to the innate immune response. Although more work is needed to fully determine the role of METH on this cell line, a high concentration of METH seems to downregulate TLR signalling, which may possibly interfere with normal functioning of TLR signalling and IL4, and IFN $\beta$ 1 response. METH may impact these genes, however further *in vitro* and animal studies are required to fully determine the role METH plays on TLRs and inflammatory cytokines.

## References

- Allhorn, S., Böing, C., Koch, A. A., Kimmig, R., & Gashaw, I. (2008). TLR3 and TLR4 expression in healthy and diseased human endometrium. *Reproductive biology and endocrinology : RB&E*, 6, 40. doi:10.1186/1477-7827-6-40
- Badisa, R. B., Wiley, C., Randell, K., Darling-Reed, S. F., Latinwo, L. M., Agharahimi, M., ... Goodman, C. B. (2019). Identification of cytotoxic markers in methamphetamine treated rat C6 astroglia-like cells. *Scientific reports*, 9(1), 9412. doi:10.1038/s41598-019-45845-1
- Bhattacharjee, A., Shukla, M., Yakubenko, V. P., Mulya, A., Kundu, S., & Cathcart, M. K. (2013). IL-4 and IL-13 employ discrete signaling pathways for target gene expression in alternatively activated monocytes/macrophages. *Free radical biology & medicine*, 54, 1–16. doi:10.1016/j.freeradbiomed.2012.10.553
- Bolívar S, Anfossi R, Humeres C, et al. IFN- $\beta$  Plays Both Pro- and Anti-inflammatory Roles in the Rat Cardiac Fibroblast Through Differential STAT Protein Activation. *Front Pharmacol*. 2018;9:1368. Published 2018 Nov 28. doi:10.3389/fphar.2018.01368
- Bortell, N., Basova, L., Semenova, S., Fox, H. S., Ravasi, T., & Marcondes, M. C. (2017). Astrocyte-specific overexpressed gene signatures in response to methamphetamine exposure in vitro. *Journal of neuroinflammation*, 14(1), 49. doi:10.1186/s12974-017-0825-6
- Burns, A., & Ciborowski, P. (2016). Acute exposure to methamphetamine alters TLR9-mediated cytokine expression in human macrophage. *Immunobiology*, 221(2), 199–207. doi:10.1016/j.imbio.2015.09.006
- Dai, M., Wang, X., Li, J. L., Zhou, Y., Sang, M., Liu, J. B., ... Ho, W. Z. (2015). Activation of TLR3/interferon signaling pathway by bluetongue virus results in HIV inhibition in macrophages. *FASEB journal : official publication of the Federation of American Societies for Experimental Biology*, 29(12), 4978–4988. doi:10.1096/fj.15-273128
- De Lerma Barbaro, Andrea & Procopio, Francesco & Mortara, Lorenzo & Tosi, Giovanna & Accolla, Roberto. (2005). The MHC class II transactivator (CIITA) mRNA stability is critical for the HLA class II gene expression in myelomonocytic cells. *European journal of immunology*. 35. 603-11. 10.1002/eji.200425378.
- Dhanda, S. K., Gupta, S., Vir, P., & Raghava, G. P. (2013). Prediction of IL4 inducing peptides. *Clinical & developmental immunology*, 2013, 263952. doi:10.1155/2013/263952

- Fernandes, N. C., Sriram, U., Gofman, L., Cenna, J. M., Ramirez, S. H., & Potula, R. (2016). Methamphetamine alters microglial immune function through P2X7R signaling. *Journal of neuroinflammation*, *13*(1), 91. doi:10.1186/s12974-016-0553-3
- Gadani, S. P., Cronk, J. C., Norris, G. T., & Kipnis, J. (2012). IL-4 in the brain: a cytokine to remember. *Journal of immunology (Baltimore, Md. : 1950)*, *189*(9), 4213–4219. <https://doi.org/10.4049/jimmunol.1202246>
- Gold, M. S., Kobeissy, F. H., Wang, K. K., Merlo, L. J., Bruijnzeel, A. W., Krasnova, I. N., & Cadet, J. L. (2009). Methamphetamine- and trauma-induced brain injuries: comparative cellular and molecular neurobiological substrates. *Biological psychiatry*, *66*(2), 118–127. doi:10.1016/j.biopsych.2009.02.021
- Grela E, Kozłowska J, Grabowiecka A. Current methodology of MTT assay in bacteria - A review. *Acta Histochem.* 2018;120(4):303-311. doi:10.1016/j.acthis.2018.03.007
- Harms, R., Morsey, B., Boyer, C. W., Fox, H. S., & Sarvetnick, N. (2012). Methamphetamine administration targets multiple immune subsets and induces phenotypic alterations suggestive of immunosuppression. *PloS one*, *7*(12), e49897. doi:10.1371/journal.pone.0049897
- Henig, N., Avidan, N., Mandel, I., Staun-Ram, E., Ginzburg, E., Paperna, T., Pinter, R. Y., & Miller, A. (2013). Interferon-beta induces distinct gene expression response patterns in human monocytes versus T cells. *PloS one*, *8*(4), e62366. <https://doi.org/10.1371/journal.pone.0062366>
- Huik, K., Avi, R., Pauskar, M., Kallas, E., Jõgeda, E. L., Karki, T., ... Lutsar, I. (2013). Association between TLR3 rs3775291 and resistance to HIV among highly exposed Caucasian intravenous drug users. *Infection, genetics and evolution : journal of molecular epidemiology and evolutionary genetics in infectious diseases*, *20*, 78–82. doi:10.1016/j.meegid.2013.08.008
- Kawasaki, T., & Kawai, T. (2014). Toll-like receptor signaling pathways. *Frontiers in immunology*, *5*, 461. <https://doi.org/10.3389/fimmu.2014.00461>
- Lin, M., Sambo, D., & Khoshbouei, H. (2016). Methamphetamine Regulation of Firing Activity of Dopamine Neurons. *The Journal of neuroscience: the official journal of the Society for Neuroscience*, *36*(40), 10376–10391. doi:10.1523/JNEUROSCI.1392-16.2016
- Liu, X., Silverstein, P. S., Singh, V., Shah, A., Qureshi, N., & Kumar, A. (2012). Methamphetamine increases LPS-mediated expression of IL-8, TNF- $\alpha$  and IL-1 $\beta$  in human macrophages through common signaling pathways. *PloS one*, *7*(3), e33822. doi:10.1371/journal.pone.0033822

- Loftis J. M. (2015). Commentary: Methamphetamine mediates immune dysregulation in a murine model of chronic viral infection. *Frontiers in microbiology*, 6, 1473. doi:10.3389/fmicb.2015.01473
- Loftis, J. M., Choi, D., Hoffman, W., & Huckans, M. S. (2011). Methamphetamine causes persistent immune dysregulation: a cross-species, translational report. *Neurotoxicity research*, 20(1), 59–68. doi:10.1007/s12640-010-9223-x
- Luzina, I. G., Keegan, A. D., Heller, N. M., Rook, G. A., Shea-Donohue, T., & Atamas, S. P. (2012). Regulation of inflammation by interleukin-4: a review of "alternatives". *Journal of leukocyte biology*, 92(4), 753–764. <https://doi.org/10.1189/jlb.0412214>
- Ma, J., Wan, J., Meng, J., Banerjee, S., Ramakrishnan, S., & Roy, S. (2014). Methamphetamine induces autophagy as a pro-survival response against apoptotic endothelial cell death through the Kappa opioid receptor. *Cell death & disease*, 5(3), e1099. <https://doi.org/10.1038/cddis.2014.64>
- Marckmann, S., Wiesemann, E., Hilde, R., Trebst, C., Stangel, M., & Windhagen, A. (2004). Interferon-beta up-regulates the expression of co-stimulatory molecules CD80, CD86 and CD40 on monocytes: significance for treatment of multiple sclerosis. *Clinical and experimental immunology*, 138(3), 499–506. doi:10.1111/j.1365-2249.2004.02624.x
- Mata, M. M., Napier, T. C., Graves, S. M., Mahmood, F., Raeisi, S., & Baum, L. L. (2015). Methamphetamine decreases CD4 T cell frequency and alters pro-inflammatory cytokine production in a model of drug abuse. *European journal of pharmacology*, 752, 26–33. doi:10.1016/j.ejphar.2015.02.002
- Nolan A, Kobayashi H, Naveed B, Kelly A, Hoshino Y, Hoshino S, et al. (2009) Differential Role for CD80 and CD86 in the Regulation of the Innate Immune Response in Murine Polymicrobial Sepsis. *PLoS ONE* 4(8): e6600. <https://doi.org/10.1371/journal.pone.0006600>
- Pan, Z. K., Fisher, C., Li, J. D., Jiang, Y., Huang, S., & Chen, L. Y. (2011). Bacterial LPS up-regulated TLR3 expression is critical for antiviral response in human monocytes: evidence for negative regulation by CYLD. *International immunology*, 23(6), 357–364. doi:10.1093/intimm/dxr019
- Papageorgiou, Marco & Raza, Ali & Fraser, Sarah & Nurgali, Kulmira & Apostolopoulos, Vasso. (2018). Methamphetamine and its immune-modulating effects. *Maturitas*. 121. 10.1016/j.maturitas.2018.12.003.
- Parker, L. C., Prince, L. R., & Sabroe, I. (2007). Translational mini-review series on Toll-like receptors: networks regulated by Toll-like receptors mediate innate and adaptive immunity. *Clinical and experimental immunology*, 147(2), 199–207. <https://doi.org/10.1111/j.1365-2249.2006.03203.x>

- Peerzada, H., Gandhi, J. A., Guimaraes, A. J., Nosanchuk, J. D., & Martinez, L. R. (2013). Methamphetamine administration modifies leukocyte proliferation and cytokine production in murine tissues. *Immunobiology*, 218(8), 1063–1068. doi:10.1016/j.imbio.2013.02.001
- Shah, A., & Kumar, A. (2016). Methamphetamine-mediated endoplasmic reticulum (ER) stress induces type-1 programmed cell death in astrocytes via ATF6, IRE1 $\alpha$  and PERK pathways. *Oncotarget*, 7(29), 46100–46119. <https://doi.org/10.18632/oncotarget.10025>
- Sriram, U., Haldar, B., Cenna, J. M., Gofman, L., & Potula, R. (2015). Methamphetamine mediates immune dysregulation in a murine model of chronic viral infection. *Frontiers in microbiology*, 6, 793. doi:10.3389/fmicb.2015.00793
- Takashima, Y., & Mandyam, C. D. (2018). The role of hippocampal adult neurogenesis in methamphetamine addiction. *Brain plasticity (Amsterdam, Netherlands)*, 3(2), 157–168. doi:10.3233/BPL-170058
- Tallóczy, Z., Martinez, J., Joset, D., Ray, Y., Gácsér, A., Toussi, S., ... Santambrogio, L. (2008). Methamphetamine inhibits antigen processing, presentation, and phagocytosis. *PLoS pathogens*, 4(2), e28. doi:10.1371/journal.ppat.0040028
- Van Meerloo, Johan & Kaspers, Gertjan & Cloos, Jacqueline. (2011). Cell sensitivity assays: The MTT assay. *Methods in molecular biology (Clifton, N.J.)*. 731. 237-45. 10.1007/978-1-61779-080-5\_20.
- Yu, S., Zhu, L., Shen, Q., Bai, X., & Di, X. (2015). Recent advances in methamphetamine neurotoxicity mechanisms and its molecular pathophysiology. *Behavioural neurology*, 2015, 103969. doi:10.1155/2015/103969

## **Chapter 5**

### **General discussion**

#### **Introduction**

The broad themes of this thesis encompass the overall effects of METH on cellular immunity, along with how METH causes changes to regions of the gastrointestinal tract (GI) (chapter 3). Moreover, the thesis expounds the relationship between chronic METH, and the implications (including withdrawal) which may be apparent in changes to gene expression in mouse models (chapter 2). Gene expression, in this context of METH (or exposure of biological and molecular systems and processes to METH), is represented as fold-changes across one or more genes involved in regulating or maintaining the homeostasis of a cell's proper functioning (chapter 4). Proper cellular immunity, including the proper functioning of molecular patterns, is necessary for a system to resist and/or evade any incoming foreign insults which might potentially – significantly or non-significantly – impact a host's ability to mount an adequate immune response upon infection. Furthermore, drugs of abuse, such as METH and cocaine, not only harm and present dangers to physiological aspects of an organism; they also pose long-term threats to psychological features that may lead to significant mal-behavioural adaptations.

## Chapter 5

### General discussion

#### Introduction

The broad themes of this thesis encompass the overall effects of a chronic METH dose, and how this impacts cellular immunity, along with causing changes to regions of the gastrointestinal tract (GI) (chapter 3). Specifically, chronic METH dose was investigated in a mouse model where several postulations were made regarding the relationship between METH dose (high/escalating), and internal systems (colon gene expression/microbiota composition/abundance), and how these aspects of chronic METH use might help explain the downstream impacts leading to changes in brain functioning. Internal systems, within this purview, translates to the microbiota homeostasis and abundance/composition profile that could be disturbed in the colon upon a chronic METH dose infiltration (chapter 3). This internal system of diverse microbiota communicates with the brain (gut-brain axis) and can influence several brain processes embedded within the human psyche – such as those associated with major depression, anxiety, stress, appetite and psychosis. Further, changes in colon physiology, across both the gene expression and microbiota composition/abundance perspectives, may have profound effects on both innate and adaptive immunity (chapter 3; chapter 4). Proper innate and adaptive immunity, including the proper functioning of molecular patterns, is necessary for any internal system to recognize, resist and/or evade any incoming foreign insults which might potentially impact a host's ability to mount an adequate immune response upon infection or disturbance from an exogenous

stimulus. In METH studies, this aspect of immunity is often observed with METH users susceptible of HIV and *staphylococcus aureus* infection. An important feature of chronic and/or acute METH use is its ability to interfere with decision making and learning (chapter 1). Since METH can cause significant alterations to the brain's neurochemistry, this can lead to severe cognitive decline which can manifest out later as stroke, cardiovascular pathologies and other forms of neurological diseases such as Alzheimer's Disease and Parkinson's Disease (chapter 1). Collectively, initial postulations made across all four chapters can be summarized as key findings:

- Chronic METH [ab]use may follow similar inflammatory, immune-metabolomic, and immune-modulatory patterns to those also associated to psychiatric disorders, including depression, and neurodegenerative disorders.
- Chronic METH [ab]use in an animal model provides some evidence that a high METH dose could have significant impacts on several gene ontological categories: including cytokine signaling, tight junctions, placental and blood vessel development, neuropeptide signaling. Enrichment of significant differentially expressed genes (DEG) across these genes ontologies provides evidence that, compared to control group gene expression, chronic METH could impact many developmental and regulatory systems in the body.
- Chronic METH and withdrawal (mouse model) could cause major shifts in common colon microbiota. In addition, these alterations of microbial composition and abundance may also have significant impacts on

several metabolic phenotype categories, which are important for correct colon homeostasis.

- An *in vitro* Chronic METH model suggests several changes in genes related to the innate and adaptive immunity. These significant fold-changes in several genes were observed in an undifferentiated U937 [pre-monocytic] cell line, however insignificant gene expression was observed in the differentiated U937 cell line.

## **Discussion**

### **Neurodegeneration and microbial dysbiosis**

Drugs of abuse, such as METH, lead to brain dysfunction through the deterioration of synapses over time. METH is beginning to be increasingly associated with the slow degeneration of mental health – depression, Alzheimer’s Disease (AD) and Parkinson’s Disease (PD), to name a few neurodegenerative disorders. More evidence is mounting regarding the correlations between gut health and brain health, the so-called ‘gut-brain axis’ model of mental health. This theory posits the idea that gut health, symbolised by diet, age, and other variables, has a profound effect on brain development or degeneration over time. METH, as a psychostimulant invades an individual’s perceptions through hallucinatory and auditory modifications. METH may also alter other tissues, and their specific cellular contents. In the colon, epithelial cells maintain barrier integrity; a visible ascertainment between ‘inside’ and ‘outside’ the colon is properly distinguished. This separation must function as to keep microbes residing inside the colon away from other molecules in the bloodstream. METHs effect on tight junctions (chapter 2) could be a reason why several microbial species were seen to shift (chapter 3) under the stimulation of METH (or, more specifically, shifts in microbial species in mouse faecal samples upon DNA extraction). What was not studied further or analysed in-depth in this thesis was the connection of the gut and brain. Anxiety, depression and suicidal thoughts are brought on by chronic, long-term METH use. Over time, the bidirectional combination of the constant bombardment of METH upon the brain, with concurrent insults made to the gut might be a key in

uncovering why METH addicts suffer from mild to severe forms of mental dysregulation and health.

### **Colon microbial dysbiosis and tight junction compromise**

The colon is home to millions of bacterial species, where the majority of bacteria reside in this segment of the gastrointestinal (GI) tract. The colon must maintain a proper barrier between the luminal environment and the internal part of the body. Failure to do so is usually based on the theory of the ‘leaky gut’ phenomena, where spaces between epithelial cells, held together, in close proximity by tight junction proteins, are damaged and cannot sustain cell-cell interactions/adhesion. Moreover, compromise of these tight junctions can lead to an influx of immune cells, leading to a cascade of proinflammatory molecules. Chapter 2 of this thesis investigated a vast array of differentially expressed gene expression data via the assessment of gene ontology groupings and categories. Several differentially expressed genes (DEGs) belonged to those associated to the tight junction complex. The apparent downregulation of several tight junction genes, along with closely related genes belonging to the leukocyte trans-endothelial migration (LTM) pathway (chapter 2) could suggest a relationship between chronic METH and epithelial cell disruption, through the interference of tight junction genes. Interestingly, tight junctions and adherens – claudin-15, claudin-1, ZO-1, and  $\alpha$ -T-catenin – were found to be involved in significant up and down regulation in this chronic METH mouse model. Both tight junctions and adherens are described as two modes of cell-to-cell adhesion that are crucial for maintaining epithelial cell adhesion. Adherens serve several

functions, including regulating the actin cytoskeleton, intracellular signalling and regulating transcription. ZO-1, members of the membrane-associated guanylate kinase homologs (MAGUK) family, has been found to play a role in scaffolding between transmembrane and cytoplasmic proteins; and might form a link between the tight junctions and adherens. Ontological pathway analysis enrichment of these particular genes – claudins, occludins and adherens – in the leukocyte trans-endothelial migration (LTM) ontology. This could suggest that METH, either directly or indirectly, influences one or more of these genes and leads to physiological changes to the endothelial cells of the colon. Implications of this tight junction and adherens perturbation could also explain the inflammatory imbalance often seen in METH users – both acute and chronic.

### **Colon Microbiota is altered in chronic METH**

Chapter 3 postulated and discussed the microbial diversity, abundance and alterations in faecal samples collected from a chronic METH withdrawal group of mice and compared to with a control group. The hypotheses made here were: (1) chronic METH causes changes in the microbial composition and diversity in the gut, and (2) changes to the gut microbiota from a disturbance caused by METH, has downstream impacts on microbial metabolism and subsequent signalling processes. Several bacteria were found to be significantly lower in the chronic METH group, compared to the control, such as, *Faecalibacterium*, *Dehalobacterium*, *Coprococcus*, *Anaerotruncus*, *Ruminococcus* and *Prevotella* (chapter 3). These bacteria were found to be significantly down-regulated in the

METH group, suggesting that perhaps METH has a crucial role – and capacity - in dampening or suppressing these bacteria during chronic use of the drug. Robust statistical analyses, aided by available metagenomic analysis programs and tools, further explored these observed differences, and found strong statistical evidence that suggests there are indeed microbial changes between a normal gut, undisturbed by METH, and a gut influenced by METH. These results give some indication and provide preliminary evidence that chronic METH use is related to a dysbiosis of the gut flora, and also that these shifts in microbial communities could also influence bacterial metabolism. This metabolic aspect of bacteria was further assessed in a robust web-page program (METAGENassist) which besides providing stringent clustering and classification tools, also performs functional studies on a set of microbial data. Metabolic phenotype categories that were found to be significantly correlated with the METH group were, cellulose degradation, aromatic hydrocarbon degradation, nitrogen fixation, chitin degradation, and sulphide oxidation metabolic categories. In this case, it can be suggested that there may be a relationship between the initial microbial communities dampened by METH, and the further dampening effect on several metabolic processes assessed via functional analysis. This then can provide some utility for further investigating whether or not prolonged chronic METH use (addiction), creates an imbalance and disturbance in the production of signalling molecules (microbiota-derived metabolites), such as short-chain fatty acids (SCFAs) which might otherwise regulate aspects of human immunity and metabolism that originate from a healthy gut microbiota. Gut-brain axis communication might also be altered in chronic METH use, as part of METHs downstream impacts. As SCFA

metabolites, such as butyrate and propionate - are also known to be signalling molecules that traverse and establish communication between the gut and brain; if METH does indeed cause a reduction in microbial abundance in bacteria such as *Faecalibacterium*, *Dehalobacterium*, *Coprococcus*, *Anaerotruncus*, *Ruminococcus* and *Prevotella*, then perhaps a significant reduction in these SCFAs might account for dramatic changes in neurophysiology. It is to be acknowledged that *Faecalibacterium* and *Ruminococcus* are a major SCFA-producing bacterium, and the observed reduction in this bacterium could also impact the production of these metabolites, however this is yet to be fully known. Further, SCFAs are important homeostatic regulators in the gut, and butyrate is also known to promote epithelial barrier function, as well as being a major energy source of colonocytes. Chronic METH use could serve as one dietary factor that disrupts not only the homeostatic signalling between the gut and brain, but also through disturbances to SCFA metabolites and anti-inflammatory molecules that are necessary requirements for balancing intestinal homeostasis.

Indeed, further research on the specific effects of chronic METH on SCFAs, based on the investigation of particular SCFA-producing bacteria (as those detailed in this thesis), would uncover much important new knowledge on the potentially observable importance of SCFAs and how these metabolites could offer some insight into their therapeutic use in chronic METH users experiencing short- or long-term neurological impacts such as depression, and psychosis. This larger picture of gut-brain therapy for chronic drug addiction should be commensurate with complementary evidence that supports the role of chronic METH use on the gut microbial populations.

## **Innate immunity perturbations**

The innate immune response must safeguard the host – human, mouse, rat, etc. – from foreign attack. The innate immunity takes on a first line of defense approach which must constantly be active and alert for it to appropriately buffer the various systems from infection. Drugs of abuse lower the body's overall immunity. Furthermore, once immunity has been compromised infections can be greatly exacerbated leading to short and/or long-term illness, as in the case for HIV infection and METH abuse. Chapter 4 of this thesis describes the impacts of a high METH dose on cells of the innate immune system – notably monocytes (differentiated U937 cells) and pre-monocytes (undifferentiated U937 cells). Chapter 4, along with previously published studies, serves to describe how specific changes in innate and adaptive gene expression, if any, in monocytes is brought about by METH. Genes belonging to the toll-like receptor (TLR) signaling family were shown to be significantly impacted by METH in monocytes (chapter 4). These included changes to IL-4, TLR1, TLR3 and IFN $\beta$ 1. These results suggest that a high METH dose could lower the immune response through a perturbation in genes that offer protection against cell death (apoptosis) and through the mediation of the innate immunity.

TLR signaling is a crucial component of innate immune responses as activation of these pathways subsequently lead to activation of a range of transcription factors which further guide the outcome of the innate immune response. The success of TLR signaling in innate immunity is nested in the ability of the innate immune system to mobilize specific pattern-recognition receptors (PRRs). These recognition patterns activate downstream signalling,

subsequently leading to the production of inflammatory cytokines, along with other mediators of the innate immune response. METH may serve as a disruptor of these pattern-recognition receptors (PRRs) which can further inhibit successful innate immunity against infection. Moreover, more specifically, PRRs such as pathogen-associated molecular patterns (PAMPs) and damage-associated molecular patterns (DAMPs) are responsible for responding to cellular stress and tissue injury and induce potent inflammatory responses which activate the innate immune system. METH, as a potential disruptor of regular PAMPs and DAMPs activity could explain the likelihood of increased infection amongst METH users. DAMPs are also beginning to be recognised as playing roles in human diseases, such as Alzheimer's Disease (AD) and Parkinson's Disease (PD). As more evidence is mounting regarding the connection(s) between illicit drug use and neurodegenerative diseases, such as AD and PD, METH could, over time, and under chronic use (abuse), cause severe disruptions to DAMPs through toll-like receptor signalling. This model of neurodegeneration is currently being investigated, and this thesis provides insight into the role(s) of monocyte [innate and adaptive] gene expression which should be further unravelled by considering the expression patterns of major DAMPs and PAMPs in a METH – *in vitro* and *in vivo* – context.

## **Conclusions**

METH, at high chronic doses, carries out a range of alterations within the human body over time. This study incorporated several gene ontology, and metagenomic software programs to describe impacts of METH on cellular, molecular, biological, and microbial processes. The utilization of gene ontologies is a powerful tool that can provide insights into differentially expressed genes (DEGs) and how enrichment in certain pathways and processes provides some evidence of changes in a diseased/perturbed state. Further, the growing capacity of openly available metagenomic platforms is aiding in the in-depth analysis of microbial data taken from a range of environments, including the gut. Moreover, as bioinformational analysis of genetic and bacterial data becomes more widely available and communicated, genes and gene sets, and their corresponding metabolic pathways, will have a significantly greater role to play in understanding METH addiction. Importantly, pharmaco-epigenetics, defined as the interplay between epigenetic mechanisms and individual drug responses, has recently emerged as a crucial aspect of influencing drug absorption, distribution, metabolism and excretion (ADME) genes. Epigenetic gene ontology analysis might one day help bridge chronic drug use to epigenetic alterations across genes, via shifts in the homeostatic balance of the gut-brain axis, along with neurobiological effects as a result. Without doubt, new knowledge about how METH abuse affects individuals will require a deeper insight into genetic and epigenetic factors, that span multiple systems associated with the gut-brain landscape that will more thoroughly and precisely guide decision-making on personalised medicine for those suffering from METH abuse, withdrawal and long-term mental health disorders.

**Appendix 1. Genes associated with METH are enriched across several ontological terms in Gorilla.**

**Table 1:** Response to bacterium.

<b>GO: 0009617</b> <b>p-value: 4.56x10<sup>-4</sup></b>	
<b>Gene</b>	<b>Fold change</b>
Ang4	+12.4
Thrsp	+2.5
Adipoq	+5.3
Cxcl9	+3.0
Cyp2e1	+5.1
Gpm6a	+4.1
Fabp4	+2.5
Serpine1	+3.1
Hist1h2be	+2.3
Retnlb	+6.9
Upk1b	+5.8
Gdap10	+2.8
Cfd	+3.3

**Table 2:** Fatty acid metabolism.

<b>GO: 0006631</b> <b>p-value: 1.42x10<sup>-4</sup></b>	
<b>Gene</b>	<b>Fold change</b>
Hao2	+2.4
Cyp2d12	+2.2
Cyp2c69	+3.3
Cyp4f14	+2.1
Adipoq	+5.3
Abcd2	+2.1
Cyp2e1	+5.1
Lep	+7.6

Pnpla3	+2.7
Fabp4	+2.5
Lpl	+2.1
Fabp2	+2.5
Ces1f	+2.6
Ggt1	+5.9
Cyp2c44	+2.4

**Table 3.** Neuropeptide signalling pathway.

<b>GO: 0007218</b> <b>p-value: 6.47x10<sup>-4</sup></b>	
<b>Gene</b>	<b>Fold change</b>
Gal	+2.6
Ppy	+3.0
Galr2	+2.3
Grp	+3.6
Sstr1	+2.4

**Table 4.** Monocarboxylic acid metabolic process.

<b>GO: 0032787</b> <b>p-value: 9.44x10<sup>-4</sup></b>	
<b>Gene</b>	<b>Fold change</b>
Hao2	+2.4
Cyp2d12	+2.2
Cyp2c69	+3.3
Cyp4f14	+2.1
Adipoq	+5.3
Abcd2	+2.1
Cyp2d9	+2.6
Cyp2e1	+5.1
Lep	+7.6
Aldh1a2	+2.5
Pnpla3	+2.7
Cyp2c55	+2.1
Fabp4	+2.5
Lpl	+2.1
Fabp2	+2.5
Rdh9	+2.2
Ces1f	+2.6
Ggt1	+5.9
Cyp2c44	+2.4
Ccbl1	+2.0

**Table 5:** Blood vessel development.

<b>GO: 0001568</b> <b>p-value: 9.72x10<sup>-5</sup></b>	
<b>Gene</b>	<b>Fold change</b>
Cdx2	10.2
Wt1	6.2
Lep	7.6

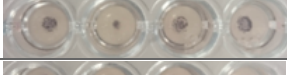
**Table 6:** Placenta development

<b>GO: 0001890</b> <b>p-value: 5.12x10<sup>-4</sup></b>	
<b>Gene</b>	<b>Fold change</b>
Cdx2	10.2
Lep	7.6

**Table 7:** Exogenous drug catabolic process

<b>GO: 0042738</b> <b>p-value: 9.58x10<sup>-4</sup></b>	
<b>Gene</b>	<b>Fold change</b>
Cyp2c55	+2.1
Cyp2d12	+2.2
Cyp2c69	+3.3
Cyp2c44	+2.4
Cyp2d9	+2.6
Cyp2e1	+5.1

**Appendix 2. Time-course absorbance readings (570nm) of 0-1000 $\mu$ M METH.** Formazan crystals were noticed after 3 days of incubation of METH-stimulate U937 cells.

Time (day)	Absorbance (570nm)	Concentration( $\mu$ M)	Figure
<b>1</b>	0.311	0	
	0.221	100	
	0.293	250	
	0.165	500	
	0.270	750	
	0.322	1000	
<b>2</b>	0.629	0	
	0.873	100	
	0.739	250	
	0.557	500	
	0.518	750	
	0.513	1000	
<b>3</b>	1.352	0	
	1.263	100	
	1.037	250	
	0.518	500	
	0.574	750	
	0.637	1000	

**End of thesis**